School of Doctoral Studies in Biological Sciences

University of South Bohemia in České Budějovice

Faculty of Science

Analysis of cyanobacterial protein complexes by advanced techniques of mass spectrometry

PhD thesis

Mgr. Peter Koník

Supervisor: Prof. Ing. Roman Sobotka, PhD

Institute of Microbiology, Academy of Sciences of the Czech Republic

Faculty of Science, University of South Bohemia, České Budějovice

České Budějovice 2024

This thesis should be cited as:

Koník P. 2023: Analysis of cyanobacterial protein complexes by advanced techniques of mass spectrometry. PhD thesis, University of South Bohemia, Faculty of Science, School of Doctoral Studies in Biological Sciences, České Budějovice, Czech Republic, 152 pp.

Annotation

For the last two decades, mass spectrometry (MS) is a method of choice for the identification of proteins involved in the formation of photosynthetic complexes in cyanobacteria. The aim of this thesis was to optimize and utilize MS methods beyond a simple protein identification for the model cyanobacterium *Synechocystis* sp. PCC 6803. Specifically, I focused on label free protein quantification, both in cell extracts and in isolated proteins, and structural proteomics by crosslinking (XL-MS). To this thesis I however included also my publications where I contributed by identification of proteins, that were co-isolated with tagged Photosystem II assembly factors CyanoP, Psb27, Psb28, Psb29 and Pam68. This research significantly broadened the knowledge about PSII biogenesis and connected the Psb29 protein with formation of heterocomplexes of FtsH proteases.

In order to identify substrates of *Synechocystis* FtsH4 protease, I employed quantitative proteomic analysis of proteins co-eluted with catalytically-inactivated $FtsH4^{trap}$ enzyme. This work led to discovery of several Photosystem I assembly factors and Photosystem I-related protein such is IsiA, as FtsH4 substrates. Other group of identified proteins (substrates) seems to be specifically involved in CO_2 uptake. Quantitative proteomics was further used to clarify the role of High-light inducible proteins (Hlips). A detail analysis of HliA and HliB pulldowns prepared from wild type and Δ*hliC* backgrounds mapped protein-protein interactions involved in photoprotection of Photosystem II biogenesis. Utilizing XL-MS, I probed the structure of the ArgD-Gun4 protein complex that regulatory connects nitrogen metabolism and the biosynthesis of tetrapyrroles. The formation of the ArgD-Gun4 complex is promoted by ornithine, an intermediate of arginine biosynthesis.

Declaration

I hereby declare that I am the author of this dissertation and that I have used only those sources and literature detailed in the list of references.

Mgr. Peter Koník, České Budějovice, 8. 1. 2024

This thesis originated from a partnership of the **Faculty of Science, University of South Bohemia**, and **Institute of Microbiology, CAS, Centre Algatech**, supporting doctoral studies in the **Molecular and Cell Biology and Genetics** study programme.

Financial support

This work was financially supported by European Research Council Synergy Award “Redesigning the Photosynthetic Light Reactions” (854126), Czech Science Foundation grant “Intertwined biogenesis of photosystems I and II: born together to work together” (19-29225X), Czech Science Foundation "The role of FtsH proteases in biogenesis of thylakoid membranes and photosynthetic complexes in cyanobacteria” (19-08900Y) and the Czech Ministry of Education, Youth and Sport grant “Mechanisms and dynamics of macromolecular complexes: from single molecules to cells” (CZ.02.1.01/0.0/0.0/15_003/0000441).

Acknowledgements

First and foremost, I would like to thank Roman Sobotka, for unwavering support, patience, optimism and friendship. You are an inspiring person and talking to you is always a delight, regardless of topic, be it photosynthesis, proteins, history or good music.

For the opportunity to be a part of her team, and introducing me to quantitative proteomics, I would like to thank Vendula Krynická. Many thanks to all my great collaborators: Martina Bečková, Lenka ‘Agnes’ Bučinská, Éva Kiss, Jana Knoppová, Minna Konert Petra Skotnicová and Jana Talbot. Working with you was not only scientifically inspiring, it was also great fun, and I hope there will be more in the future. I am grateful to the whole team at Algatech in Třeboň, for their acceptance of me as a ‘guest’ collaborator, for their advice, direction, help and invitation to their legendary parties. For the opportunity to consult topics ranging from profound to banal, I would like to thank Josef Komenda and Roman Tůma. Many thanks to Filip Dyčka, my ally in the endless quest of keeping the MS instrumentation in working order. My gratitude extends to the whole ‘Makrokomplex’ group in České Budějovice, a wild bunch of incredibly creative people.

Many thanks to Nir Kalisman and his team at the Hebrew University in Jerusalem, for welcoming me in their laboratory and introducing me to the methods of protein crosslinking.

I feel a great debt to my family, for support, for love, for always being a place to go back to. To my patient wife and sons who never fail to surprise me. To my parents who have thought me the value of knowledge and curiosity. To my friends, with whom I could always share my trouble and my thirst.

Thanks to you all, I would not be who I am without you.

List of publications and author's contributions

The thesis is based on the following publications and my unpublished data:

i) Knoppová J, Yu J, Koník P, Nixon P.J Komenda J: CyanoP is Involved in the early steps of Photosystem II assembly in the cyanobacterium Synechocystis sp. PCC 6803. Plant and Cell Physiology, 57:1921–1931, 2016; doi: 10.1093/pcp/pcw115.

P.K. performed MS identification of proteins cut from the stained gel after 2D electrophoresis.

ii) Bečková M, Gardian Z, Yu J, Koník P, Nixon P.J, and Komenda J: Association of Psb28 and Psb27 proteins with PSII-PSI supercomplexes upon exposure of *Synechocystis* sp. PCC 6803 to high light. Mol. Plant. 10:62-72, 2017; doi: 10.1016/j.molp.2016.08.001

P.K. performed MS identification of proteins cut from the stained gel after 2D electrophoresis.

iii) Bečková M, Yu J, Krynická V, Kozlo A, Shao S, Koník P, Komenda J, Murray J.W.and Nixon P.J: Structure of Psb29/Thf1 and its association with the FtsH protease complex involved in photosystem II repair in cyanobacteria. *Philos Trans R Soc Lond B Biol Sci*. 372:20160394, 2017; doi: 10.1098/rstb.2016.0394.

P.K. performed MS identification of proteins cut from the stained gel after 2D electrophoresis.

iv) Bučinská L, Kiss É, Koník P, Knoppová J, Komenda J, Sobotka R: The ribosome-bound protein Pam68 promotes insertion of chlorophyll into the CP47 Subunit of Photosystem II. *Plant Physiology*, 176:2931–2942, 2018; doi:10.1104/pp.18.00061

P.K. performed MS identification of proteins cut from the stained gel after 1D and 2D electrophoresis and the analysis of proteins co-eluted with the purified CP47

assembly module.

v) Konert MM, Wysocka A, Koník P, Sobotka R: High-light-inducible proteins HliA and HliB: pigment binding and protein–protein interactions. Photosynth Res 152:317–332, 2022; doi: 10.1007/s11120-022-00904-z

P.K. performed quantitative MS analysis of the purified membrane protein complexes containing Hli proteins. P.K. participated in data processing, the interpretation of obtained values and writing the manuscript.

vi) Koník P, Skotnicová P, Gupta S, Tichý M. Sharma S, Komenda J, Sobotka R, Krynická V: The cyanobacterial FtsH4 protease controls accumulation of protein factors involved in the biogenesis of photosystem I. BBA – Bioenergetics 1865:149017, 2023; doi: 10.1016/j.bbabio.2023.149017.

P.K. contributed to experiment design and the preparation of cell cultures. P.K. performed the quantitative MS analysis of all obtained eluates with statistical data interpretation and participated in the preparation of manuscript. In addition, P.K. designed and performed the whole cell proteomic analysis (see unpublished results), data processing and interpretation.

vii) Kiss É, Talbot J, Adams NBP, Opekar S, Moos M, Pilný J, Kvasov T, Schneider E, Koník P, Šimek P, Sobotka R: Chlorophyll biosynthesis under the control of arginine metabolism. *Cell Reports* 42:113265, 2023;
doi: 10.1016/j.celrep.2023.113265.

P.K. performed MS identification of proteins cut from the stained gel after 1D and 2D electrophoresis. P.K. prepared recombinant ArgD and Gun4 proteins in E. coli cells, designed and performed the crosslinking analysis of the ArgD-Gun4 complex, MS analysis and data processing, interpretation and visualization (see unpublished results).

Roman Sobotka, Peter Nixon, Josef Komenda and Vendula Krynická, the corresponding authors of the listed publications, approve the contribution of Peter Koník as described above:

.....

Prof. Roman Sobotka Prof. Peter Nixon

.....

Prof. Josef Komenda Dr. Vendula Krynická

Table of Contents

List of abbreviations

CAB	Chlorophyll a/b binding
DDA	Data-dependent or Data-directed analysis
DIA	Data independent analysis
ESI	Electro-spray ionization
FT ICR	Fourier transform ion cyclotron resonance
HDX	Hydrogen/Deuterium exchange
Hlip	High light inducible protein
iBAQ	Intensity based absolute quantification
IMS	Ion mobility mass spectrometry
LC	Liquid chromatography
LFQ	Label free quantification
LHC	Light harvesting complex
LMM	Low molecular mass (protein)
MALDI	Matrix assisted laser desorption / ionization
MS	Mass spectrometry
Ni-NTA	Nickel- nitrille triacetic acid
n/s	Not specified
NPQ	Non-photochemical quenching
OEC	Oxygen evolving complex
PASEF	Parallel accumulation / Serial fragmentation
PMF	Peptide mass fingerprint
PSI	Photosystem I
PSII	Photosystem II
PTM	Post-translational modification
RC	Reaction centre

ROS	Reactive oxygen species
SP	Stationary phase
TIMS	Trapped ion mobility mass spectrometry
TMT	Tandem mass tag
ToF	Time of flight
XL-MS	Crossllnking / mass spectrometry

1. Preface

1.1 Oxygenic photosynthesis

It could be argued that oxygenic photosynthesis is the most important biological process on our planet. Molecular oxygen, the by-product of this type of photosynthesis, is the main acceptor of electrons in cellular respiration in the majority of living organisms and in all multicellular organisms. The carbon fixed by phototrophs is the single most important source of organic carbon for the planetary biosphere. Thus, virtually all life on Earth, including extremophile bacteria and archeans, depend directly or indirectly on photosynthesis.

Oxygenic photosynthesis has evolved in cyanobacteria - Gramm-negative prokaryotes fixing CO_2 using Rubisco enzyme, with a fossil record 3.5 billion years old (Schopf *et al.,* 2006). As the photosynthetic apparatus of algae and plants is of the cyanobacterial origin (reviewed in Sánchez-Baracaldo and Cardona, 2020), photosynthetic complexes in chloroplast are highly similar to cyanobacteria. From a methodological point of view, it is just another benefit of cyanobacteria as a tool to study molecular aspects of oxygenic photosynthesis. These organisms offer all advantages to work with bacteria, which includes fast life cycle, easy phenotyping and small and well characterized genomes.

The most used cyanobacterium model organism is *Synechocystis* sp. PCC 6803 (hereafter *Synechocystis*), a unicellular, non-diazotrophic strain isolated in late sixties in California. In contrast to higher plants and algae, but also to many cyanobacterial species, gene inactivation, modification and regulation became routine in *Synechocystis* due to natural transformation and efficient homologous recombination. *Synechocystis* can be easily transformed by either plasmid vectors or linear PCR fragments (Koksharova and Volk, 2002). Indeed, the cyanobacterium was the first photosynthetic organism to have the genome sequenced (Kaneko *et al.,* 1996). Currently, the UNIPROT database of *Synechocystis* proteins contains 3562 entries. Genetic manipulations of cyanobacteria are not just in the realm of science - there are many biotechnological applications to bioengineer *Synechocystis* and other species as a

producers of valuable bio-products, while sequestering atmospheric CO_2 (Liu *et al.*, 2012).

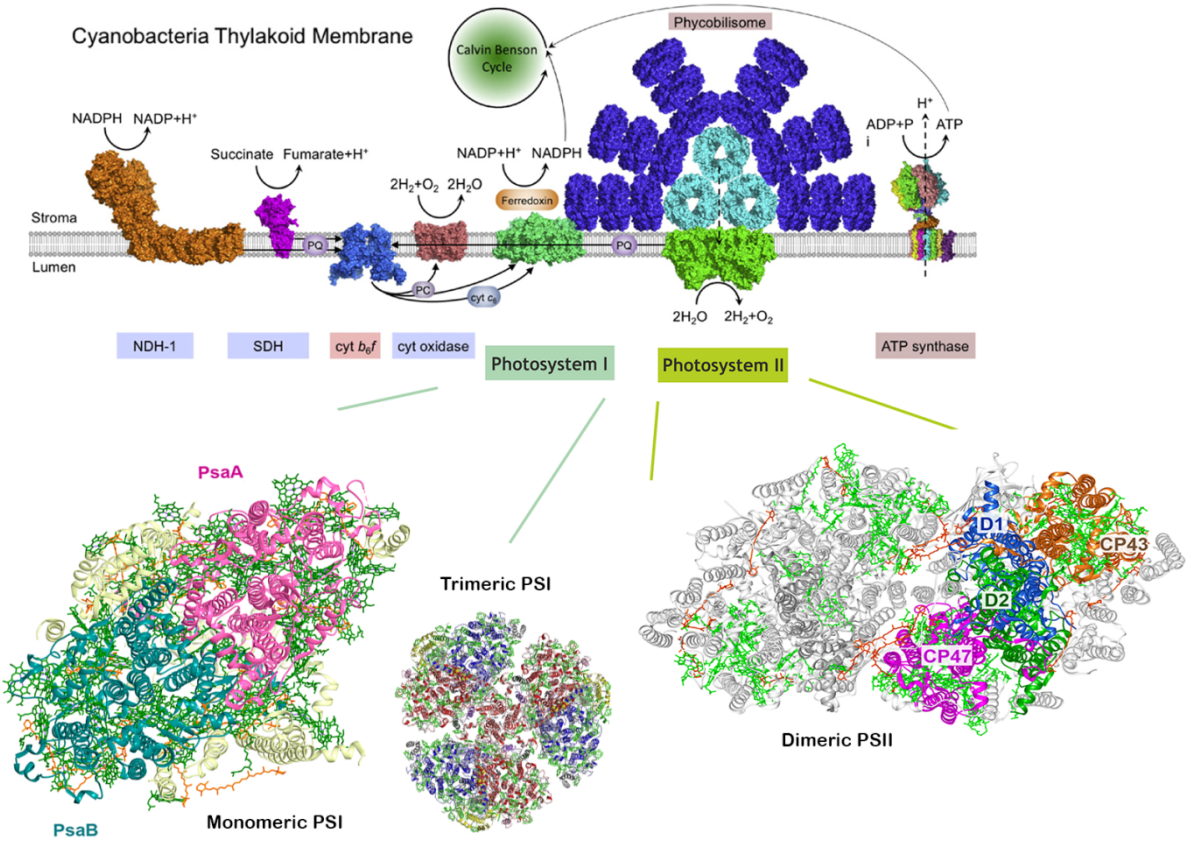

***Figure 1**: Cyanobacterial thylakoid membranes harbour the elements of both photosynthetic and respiratory electron transfer chain. This schematic model shows photosynthetic complexes with extrinsic phycobilisomes as well as respiratory membrane complexes from a side view (top; modified from Liu, 2016). Crystal structures of trimeric PSI (Jordan et al., 2001) and dimeric PSII (Umena et al., 2011) are shown from stromal side (below). A detailed view of a (monomeric) PSI unit is also shown (left). Individual Chl-binding subunits (PsaA/B, D1, D2, CP47 CP43) of both photosystems are highlighted by different colours. In cyanobacteria almost all Chl molecules (~95%) are bound to these five proteins (Xu et al., 2004).*

1.2 Photosynthetic apparatus in cyanobacteria

The first step of oxygenic photosynthesis is executed by photosystem II (PSII), a complicated enzyme that uses energy of four captured photons to oxidize two molecules of water into two protons, four electrons and two molecules of oxygen (see Figure 1). The enzymatic function of PSII can be described as light driven water:plastoquinone oxidoreductase. PSII complex is embedded in a specialized (thylakoid) membrane system and, apart from about 20 known protein subunits,

it includes several types of pigment cofactors (chlorophylls, heme, carotenoids and pheophytins), lipids, ions and a unique Mn_4CaO_5 inorganic metal cluster. (Barber and Kühlbrandt 1999; Blankenship 2002; Umena *et al.,* 2011). The reaction centre core of PSII consists of two chlorophyll-binding subunits D1 and D2, flanked by two internal light harvesting proteins CP47 and CP43, cytochrome c_{559} and a score of low molecular mass (LMM) membrane spanning subunits (Tang *et al.,* 1990; Bricker and Frenkel 2002; Terentyev 2022). In cyanobacteria these include PsbH (Komenda *et al.,* 2005), PsbJ (Nowaczyk *et al.,* 2012), PsbK (Iwai *et al*., 2010), PsbL (Anbudurai and Pakrasi 1993), PsbM (Kawakami *et al.,* 2011), PsbN (Torabi *et al*., 2014), PsbX (Shi *et al*., 1999, Funk 2000), PsbY (Meetam *et al*., 1999) and PsbZ (Swiatek *et al*., 2001). On the lumenal side, the water splitting/oxygen evolving Mn cluster is bound, protected by extrinsic lumenal subunits: PsbO (Murakami *et al*., 2002), PsbV and PsbU. In addition, CyanoQ protein has been reported in cryo-EM map of cyanobacterial PSII complex (Gisriel *et al.,* 2022) and it is likely that CyanoQ is a weakly-associates but regular subunit of PSII. On the stromal side, the cyanobacterial PSII is attached to the huge, light harvesting phycobilisome (Figure 1).

The protons, produced by PSII, generate proton gradient (powering ATP synthase), while electrons are sequentially transferred to plastoquinone. This lipid-like molecule is oxidized by cytochrome b_6f and the released energy is used to pump more protons from stroma to the lumen. Electrons are further passed to plastocyanin that is finally oxidized by Photosystem I (PSI). PSI employs light energy to reduce the cytoplasmic ferredoxin.

The core of PSI is structurally similar to PSII as both complexes have the same evolutionary origin (reviewed in Sánchez-Baracaldo and Cardona, 2020). PSI core reaction centre consists of the PsaA and PsaB subunits binding together 79 chlorophyll molecules; stromal subunits PsaC, containing two terminal FeS clusters; PsaD facilitating attachment of ferredoxin and PsaE, further helping the docking of ferredoxin. In cyanobacteria, PSI is mostly present in trimeric form (Figure 1), but the monomeric form is also relatively abundant, with various ratios between the two, depending on conditions (Kłodawska *et al*., 2015). Under high light conditions, tetrameric PSI has been observed in some cyanobacteria (Li *et al*., 2019). Six small membrane subunits PsaI, PsaL and PsaM are oriented to the

inside of the PSI trimer and PsaF, PsaJ and PsaK positioned on the outside of the trimer (Fromme, 2001). PsaL is considered the contact site between PSI monomers enabling trimerisation (Chitnis & Chitnis, 1993). In total, PSI trimer in *Synechocystis* contains 33 protein subunits, 72 carotenoids, 285 chlorophylls, 51 lipids, 9 iron-sulphur clusters, 6 phylloquinones, and 6 putative calcium ions (Katayama, 2022).

1.3 Photosynthetic pigments

Photosynthetic pigments are a chemically diverse group of molecules capable to absorb light at a specific wavelength, transfer to another pigments or proceed photochemistry as chlorophylls do in the core of photosystems. Chlorophyll-*a*, that serves in cyanobacteria as cofactors of photosystems, consists of a tetrapyrrole ring chelating magnesium atom in its centre and possessing various aliphatic sidechains. Based on protein environment chlorophyll-*a* absorbs visible light wavelengths in the blue (435–445 nm) and red (630–675 nm) range (Masojídek *et al.,* 2013).

Another tetrapyrrole pigments are phycobilins that serve in cyanobacteria specifically as chromophores in phycobilisomes. Phycobilins are linear tetrapyroles with a broad absorption range from blue-green to orange, 500-650 nm (Masojídek *et al.,* 2013). Unlike chlorophylls, they are covalently bound to phycobiliproteins, which together with colourless linker polypeptides form several rods that are attached to the core, forming the phycobilisome antenna system (Liu *et al.,* 2005, Domínguez-Martín *et al*., 2022).

Carotenoid molecules function as accessory light harvesting molecules in photosystems, but they have a structural role during photosystem assembly and play a crucial role in protection against harmful oxygen radicals. Carotenoids are able to quench both singlet and triplet chlorophylls and can be oxidized by reactive oxygen species (ROS), protecting other cellular components against oxidation (Masojídek *et al.,* 2013). Generally, carotenoids contain two hexacarbon rings with a 18-carbon conjugated chain between them and absorb light in range between 400 and 550 nm (violet to yellow-green). Xanthophylls such is zeaxanthin or myxoxanthophyll contain oxygen atoms and are also very

abundant in cyanobacterial cells.

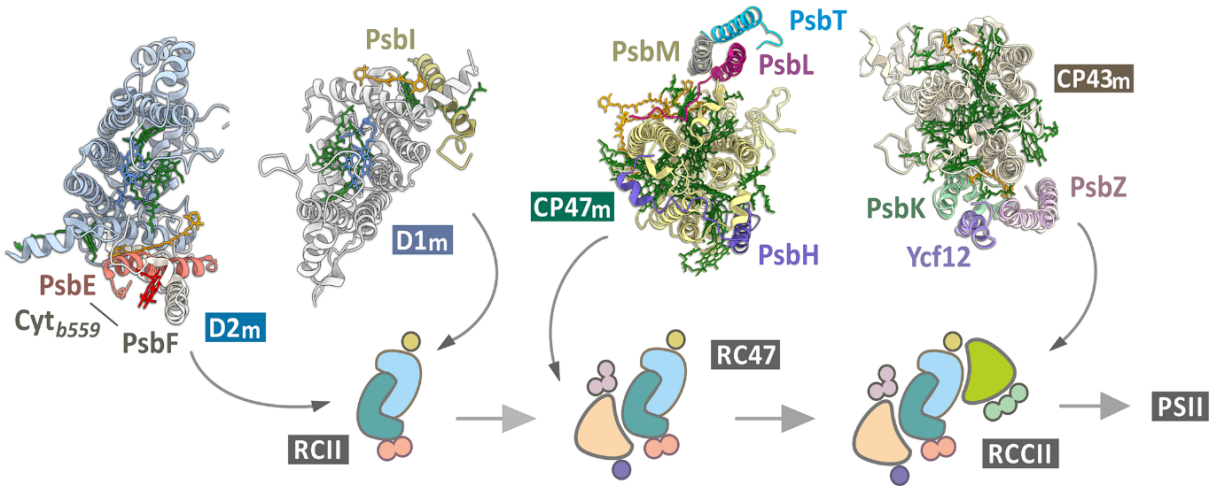

***Figure 2**: Modular de novo assembly of PSII. According to the current model in ref PSII is built from four pre-assembled modules (D1m, D2m, CP47m and CP43m) in a step-wise manner. Each module contains one core chlorophyll-binding subunit of PSII already associated with a set of small subunits (as indicated) and with pigment cofactors. D1m and D2m combine first to produce the RCII reaction center assembly complex which associates with CP47m to form the RC47 assembly complex which is converted to the RCCII non-oxygen-evolving PSII intermediate by binding CP43m. The final steps of assembly to produce oxygen-evolving PSII involve light-driven assembly of the Mn4CaO5 cluster and attachment of the lumenal subunits and dimerization. The picture was prepared using the cryo-EM structure of Synechocystis PSII (PDB = 7N8O) (Gisriel et al., 2022).*

1.4 Biogenesis of photosystems

The intricate structure of photosystem complexes and phototoxicity of chlorophyll provides a challenge for the photosystem biosynthesis and precise assembly in the cell. According to current model, the assembly of the PSII reaction core occurs in a stepwise manner starting from four pre-assembled smaller subcomplexes called modules (Komenda *et al.,* 2012). Each module consists of one large chlorophyll-binding subunit mentioned above (D1, D2, CP47, CP43) and several neighbouring low molecular mass polypeptides (Figure 2). Moreover, a number of auxiliary factors were identified (see below) that are not present in fully functional complex but thought to support in the process of PSII assembly (see below, Komenda *et al.,* 2012). The later steps PSII assembly includes attachment of the Mn cluster and the lumenal subunits PsbO, PsbU and PsbV and the dimeriz-

ation of the whole complex (reviewed in Nixon *et al.,* 2010, Komenda *et al.,* 2012).

Additionally, light-induced damage accumulates over time; particularly the D1 subunit is susceptible to photo-oxidation, even in low-light conditions (Keren *et al.,* 1997). It has been shown that the damaged D1 subunit is always replaced, while the other subunits can be recycled to form a new complex (Aro *et al.,* 1993, Komenda *et al.,* 2008, Komenda *et al.,* 2012). The damaged D1 subunit is recognized and degraded by the FtsH 2/3 Zn-metalloprotease complex (Nixon *et al.,* 2005). A new D1 subunit is introduced at the same time to the partially de-assembled (so called RC47) complex; CP43 is then re-attached and the final step of the D1 replacement is same as the *de-novo* PSII assembly (reviewed in Nixon *et al.,* 2010). D2 subunit is also relatively short-lived during stress conditions, while inner antenna subunits CP43 and CP47 have usually slower turnover. PSIIs are thus typically assembled from a mixture of newly-synthesized subunits (particularly D1 and D2) and the 'recycled' antenna assembly modules (Komenda and Sobotka, 2019). The biogenesis of PSII, either from completely newly-synthesized subunits or from a mixture of new and recycled subunits, requires a number of 'assembly' factors - proteins that facilitate or protect the whole process. By definition, these factors are not themselves incorporated into the final PSII structure. Many of these factors have been first characterized in *Synechocystis*, which became an especially useful model organism for studies focused on the biogenesis of photosynthetic complexes. A good example is Ycf48 protein known to bind to nascent D1 and to promote the formation of RCII. Although this factor has been first described in plants as HCF136, most of details about its function has been later elucidated using *Synechocystis* mutants (Komenda *et al.,* 2008). Recently, a structure of *Synechocystis* Ycf48 in complex with D1/D2 assembly intermediate (RCII complex; see Figure 2) has been solved (Zhao *et al.,* 2023). Another such example it the lumenal Psb27 protein that probably binds and stabilizes CP43m before its attachment to the PSII assembly intermediate RC47 (Komenda *et al.,* 2012b).

Special care is given to chlorophylls during PSII biosynthesis, since unbound chlorophylls can produce toxic ROS (reviewed in Apel and Hirt 2004). Chlorophyll production should be therefore synchronized with photosynthesis of the

chlorophyll-binding proteins (Kopečná *et al.,* 2012). An important role in the process of PSII biogenesis and repair is played by High light induced proteins (Hlips). These one-helix proteins associate with different PSII assembly intermediates (Konert *et al.,* 2022) and probably photoprotect these subcomplexes by dissipating exciton energy (reviewed in Komenda and Sobotka 2016). Indeed, also enzymes catalysing the last steps of chlorophyll biosynthesis are presumed to be closely connected to the site of PSII assembly (reviewed in Komenda and Sobotka 2019). The terminal enzyme of chlorophyll synthesis, chlorophyll synthase, associates with the translocon apparatus (YidC insertase and the SecY translocase), but also with Hlips (Chidgey *et al.,* 2014). The work of Knoppová *et al.,* (2014) described and characterized another complex participating in early steps of PSII biogenesis that includes assembly factor Ycf39 (Slr0399) and, again, Hlips. The Ycf39-Hlip sub-complex associates with D1 assembly module early in the process of PSII assembly and probably photoprotects the formation of RCII complex (Knoppová *et. al*., 2014). A possible role of Hlips in chlorophyll delivery to PSII subunits has been also discussed (reviewed in Komenda and Sobotka 2016).

In contrast to PSII, much less is known about the assembly of the PSI complex. It is apparently a rapid process, starting with the core PsaA and PsaB subunits forming a heterooligomer together with assembly factors Ycf3 and oligomeric Ycf4 (Nellaepalli *et al.,* 2018). After the stromal subunits PsaC, PsaD and PsaE are attached, the assembly factors dissociate and PsaF, PsaJ, PsaH, PsaI, PsaL join the complex (reviewed in Komenda and Sobotka, 2019). For long time, the attachment of PsaK subunit has been considered as the last step starting the trimerisation of PSI, (Dühring *et al.,* 2007); however new data of the Josef Komenda’s group show that the PsaK associates with PsaA/B core early, prior to the stromal subunits (Komenda J, Gupta S, unpublished data).

2. Introduction

2.1 Isolation of PSI and PSII assembly complexes

To obtain this fairly comprehensive, yet still incomplete image of the structure and function of the photosynthetic machinery, many different methods have been used. Analysis of assembly intermediates of photosystems presents an extra challenge – their very low abundance. One method of circumventing this limitation is targeted mutagenesis of individual protein subunits, impairing the PSII/PSI assembly at a particular step, thus leading to an over-accumulation of an assembly intermediate, which can be isolated in higher yields (reviewed in Chiu & Chu, 2022). Complexes can be then isolated using non-targeted or semi-targeted biochemical methods, exploiting differences in biochemical properties, such as size/mass (size exclusion chromatography, gel electrophoresis, ultrafiltration, ultracentrifugation in sucrose gradient); charge (ion exchange chromatography, native gel electrophoresis); solubility (hydrophobic or hydrophilic chromatography, reverse phase chromatography); affinity to metallic ions or specific ligands (immobilized metal chromatography, affinity chromatography) and many variations thereof (reviewed in Liu *et al.,* 2020). Optimal results are obtained by combining two or more methods, however yields usually decrease with each separation step and the amount of source material has to be increased.

Targeted methods are variations of affinity chromatography, with the specificity and yield greatly increased by affinity tags on modified proteins. For example, a FLAG-tagged protein has a specific sequence attached on the N-terminus or C-terminus, which has high affinity to a FLAG-specific antibody. An agarose column with immobilized anti-FLAG antibody can be used to separate (purify) the protein from a mixture, e.g. a cell lysate (reviewed in Terpe *et al.,* 2003). Alternatively, the shorter His-tag consists only of a series of (at least 6) histidine residues, which have a high affinity to nickel. Tagged proteins are then purified using chromatography column with nickel immobilized by nitrilotriacetic acid (Ni-NTA), washed and then eluted by imidazole (Spriestersbach *et al., 2015*). The tag can be located either on the N-terminus or the C-terminus, whichever has the lesser negative effect on the function of the protein. With some optimization, interaction

partners of the tagged protein will be still bound to the protein bait and can later be visualized by gel electrophoresis methods or identified by protein mass spectrometry (Simpson, 2003).

Information about the function of a protein can be obtained by reverse genetics – elimination or modification of the protein of interest by mutagenesis or insertion of an antibiotic resistance factor into its gene sequence. The function then reveals itself by a detectable lack in a biochemical function, missing or defective structure or aberrant behaviour. The mutation can then be complemented by inserting of an additional copy of the gene, which can verify the suspected protein function. Indeed, the extra copy can be modified by adding an affinity tag, enabling its purification and further analysis.

2.2 Mass spectrometry as a tool for protein identification

Although analysed proteins (e.g. in the isolated protein complexes) can be identified by specific antibodies (if they are available) or N-terminal sequencing, identification of an unknown protein by mass spectrometry (MS) is now very common and extremely useful. Protein identification can be based on two basic MS approaches - bottom-up and top-down. The bottom-up method starts by **digestion** of the protein by a specific (with predictable cleavage sites) proteolytic enzyme (e.g. porcine or bovine trypsin, chymotrypsin), a semi-specific enzyme (pepsin) or a chemical agent such as cyanogen bromide (CNBr; Chapman 2000, Simpson 2003). The analysed protein in solution can be pure (e.g. an isolated recombinant protein), semi-pure (e.g. isolated by affinity chromatography as a part of a complex) or part of a complex protein mixture, such as a cell lysate (sometimes called shotgun proteomics).

To combine the powerful method of gel electrophoresis with MS, trypsin can be also used for in-gel digests, where a gel slice, or 2D gel spot is destained, dried, re-soaked in buffer containing the protease and incubated; peptides diffuse from the gel piece and can be isolated from the buffer (Rosenfeld *et al.,* 1991; Shevchenko *et al.,* 1996; Shevchenko *et al.,* 2006). Desalting and **isolation** of peptides is performed by one of a plethora of methods based on the affinity of peptides to C-18 alkyl group, which can be immobilized on commercially available

magnetic beads or microcolumns, or lab made StageTips (Rappsilber *et al.,* 2007). De-salting is necessary to avoid adducts, which would make the interpretation of spectra difficult. MS analysis is usually preceded by a **liquid chromatography separation** of peptides. A popular option is reverse phase Nano-liquid chromatography (nano-LC) separation (flow rates of 200-500 nL/minute), separating peptides according to their hydrophobicity in C-18 columns, using a water:acetonitrile gradient. Nano-LC equipment can be on-line coupled to MS analysers (eluate form the column flows directly into the ion source) or deposited for a later MS analysis of the fractions. This combination is abbreviated LC/MS or LC/MS-MS (Ducret *et al.,* 1998).

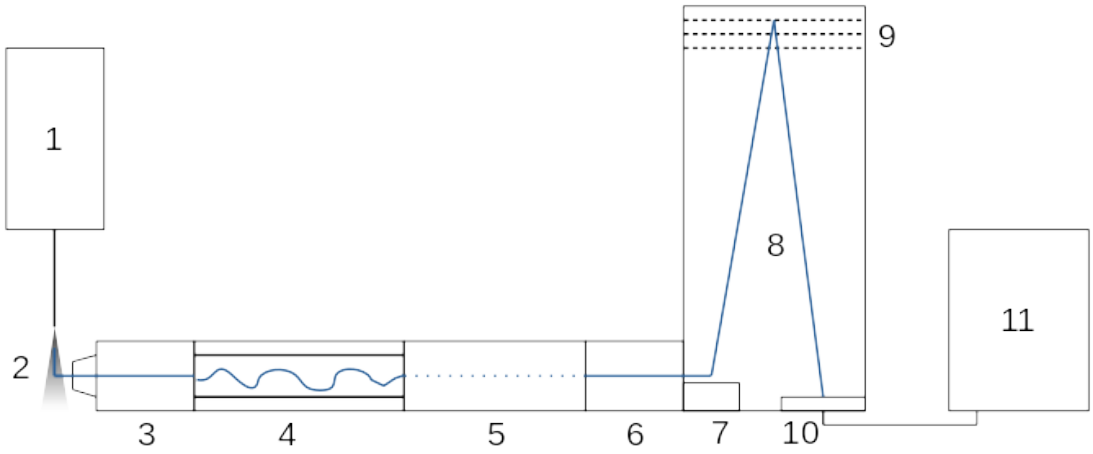

***Figure 3**: Schematic of a ESI-ToF mass spectrometer: 1 – LC device; 2 – electrospray ion source; 3 – (optional) ion mobility mass selector; 4 – quadrupole; 5 – collision chamber; 6 – (optional) analytical ion mobility chamber; 7 – orthogonal acceleration pusher; 8 – ToF flight tube; 9 – reflectron; 10 – ion detector; 11 – controlling and data acquiring PC. The ion flight path is represented by the blue line.*

Ionization of the analyte is necessary, so that the mass spectrometer can manipulate, focus or even stop the ion flows through the device using tuned electromagnetic fields, all under high vacuum conditions inside the machine. In positive mode, a proton is attached to the peptide; in negative mode, an electron. Ionization of peptides is most commonly achieved by electrospray (ESI) or, after mixing with a UV-light absorbing matrix and crystallizing, by matrix-assisted laser desorption ionization (MALDI). ESI sources often produce multiply charged

peptides – carrying 2, 3 or even more protons. Various mass analysers can be used to measure the mass of the peptides. Time of Flight (ToF) analysers exploit the fact that lighter ions are accelerated through a flight chamber to higher speed than heavier ones, when the accelerating energy is constant. After they are registered by the detector (e.g. a multi-channel plate, essentially a signal multiplier), the mass is deductible from the time they spent crossing the length of the flight tube. In multipole mass analysers, the ionized particles are deflected from their direct path through the analyser by electromagnetic fields, and the frequency of switching of the poles from positive to negative tunes the ion paths in such fashion, that only an ion of specific mass is allowed to hit the detector. By scanning the whole mass range of interest, signals will register in the mass spectrum according to the mass of the ion.

Alternatively, multipoles such as quadrupoles can be used as a pre-selection device, only transmitting ions of a select mass (such as a single peptide) and de-ionizing the rest, greatly simplifying the analyte ion flow and allowing a more detailed analysis in combination with collision chambers and mass analysers of any type. This function is designated by the letter “Q” in the identification of the instrument, e.g. ESI-Q-ToF MS/MS. Ion traps work in similar fashion, with the distinction that the ions are trapped on a circular path inside a chamber by electromagnetic fields instead of flying through – ion cyclotron resonance (ICR). Mass measurement is then deduced form the voltage needed to release them from this path and hitting a detector, or is calculated from the electromagnetic changes the particles induce in the detector electrodes, by Fourier transformation (Ekman *et al.,* 2009). For a simple schematic of a ESI Q ToF mass spectrometer, see Figure 3.

From any of these mass analysers, the resulting **mass spectrum** (Figure 4) has two dimensions: the mass (m/z; mass divided by charge state of the ion) and intensity of the peptide. Since a specific protease or chemical agent was used, the masses of the resulting peptides can be predicted and searched for in databases, translated from DNA sequences (Chapman 2000). The protein can be identified by comparing the measured peptide masses with the database, obtaining an identification based on a peptide mass fingerprint (PMF). Higher confidence of identification is provided by peptide amino-acid sequencing, done

by breaking of the peptide bonds within the analysed peptide. This disruption can be facilitated most commonly by collision with a neutral gas molecule (collision induced dissociation, CID); by reaction with radical anions (electron transfer dissociation, ETD); by bombardment with low energy electrons (electron capture dissociation, ECD) inside a specific part of the ion path of the mass spectrometer called the collision cell (Ekman *et al.,* 2009). In CID, with the right tuning of the energy of the collisions, peptides are ideally broken in exactly one peptide bond within the chain of the peptide. After collecting fragment data from many such breaks, differences between masses of the fragments in the mass spectrum then correspond to the mass of a single amino-acid. The sequence of amino-acids in the peptide can be then read by assigning the amino-acid code to the mass difference in the peptide spectra (Simpson, 2002).

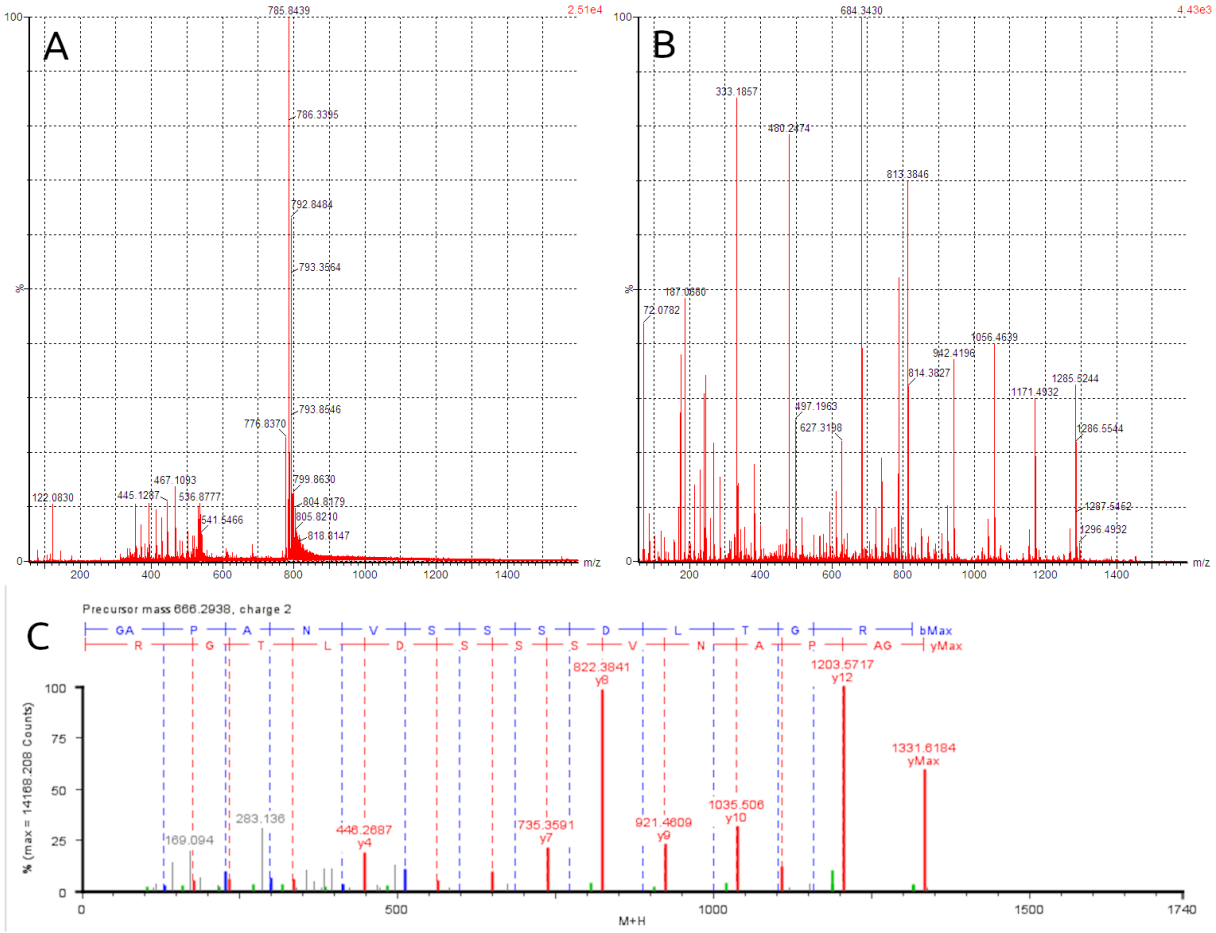

Figure 4*: Mass spectra. Top left: Precursor (parent) MS mass spectrum of a petide with a m/z of 785.84 Da; Top right: fragment (product) MSMS mass spectrum of the same peptide; Bottom: a fragment mass spectrum of a peptide with m/z 666.29 Da interpreted by the PLGS 3.0 software (Waters).*

2.3 MS data acquisition and processing

Mass spectrometer can acquire spectral data in two basic modes of action. The standard mode is data-dependent analysis (DDA), where the machine first performs a full scan - the multipole is transmitting all ions – the mass analyser acquires the spectra, identifies interesting signals and feeds back the masses of the interesting ions back to the multipole. The multipole then sequentially transmits only the selected ions, which are fragmented in the collision cell and the mass analyser acquires their fragment masses. Interesting ions are selected based on: i) the ion intensity being above the level of noise; ii) ion charge state being equal or higher than two (which indicates peptides); iii) the mass shows a pre-programmed indicator fragment; iv) masses are included in a pre-programmed list of targets (reviewed in Mann *et al.,* 2001).

DDA mode produces clear sets of fragments matched to their parent ion, with low demands on processing power and allowing detailed analysis of the peptide, such as search for post translational modifications (PTM). Hand in hand with those advantages come the limitations of the DDA method. During detailed analysis of one peptide, the rest of the ion flow is lost for any further analysis. The selection process is pre-programmed and can be biased, tending to favour higher intensity ions and losing low intensity ones. It altogether reduces the reproducibility between measurements. Various technical, computational and methodical solutions are used to counteract these limitations (Batemann *et al.,* 2004; Hu *et al.,* 2016).

An alternative to DDA is the data-independent analysis (DIA), where the collision chamber switches between low energy (producing no fragments) and high energy (producing fragments) in alternating full-spectrum scans (Batemann *et al.,* 2002; Batemann *et al.,* 2004). In the Identity^{E} (Waters) algorithm, precursor (peptide) spectra and fragment spectra are processed and fragments are matched to their precursors by multiple parameters following a theoretical model. It includes mass accuracy of precursors and fragments; total product ion intensity; consecutive and complementary b and y ions and their intensities, intensities of precursors and fragments; retention time model compliance; neutral losses conformance with amino-acid composition and multiplicity of charge states (Identity^{E} marketing presentation, Waters, 2007).

DIA is highly multiplexed, essentially free of bias and its sensitivity is limited only by the dynamic range of the instrument itself. This analysis offers a wider dynamic range, requires almost no prior knowledge of the sample and allows very high repeatability. All those characteristics provide greater confidence in quantitative proteomics. On the other hand, it produces vast amounts of raw data and its processing requires greater computational resources. The imperfect matching of precursors and fragments makes search for PTMs more challenging and can be prone to false positives. Some of these limitations are addressed by sequential window acquisition of all theoretical mass spectra (SWATH) (Gillet *et al.,* 2012) and the use of spectral libraries (reviewed in Hu *et al.*. 2016). Recently, a hybrid of the DDA and DIA methods named DDIA has been proposed (Guan *et al.,* 2020). In DDIA, fast full spectrum (survey), DDA and DIA scans alternate. DDA data is then used to identify peptides, create a spectral library and match it to DIA data.

Raw data processing includes separation of signal from noise, de-isotoping the raw spectra, deconvolution of multiply charged ions and centroiding of the peaks. As a following step, the processed spectra are matched to theoretical peptides produced *in silico* from sequence databases by dedicated software. Optionally, the database search can be omitted to obtain *de novo* sequences (Bartels, 1990). Since that process is extremely processor time consuming and prone to errors, it is used only in special circumstances; for instance, in cases where a protein database is missing or incomplete. The progress of MS-based protein identification was dramatically facilitated by the availability of public protein databases (reviewed in Henzel *et al.,* 2003), advances in computer hardware, search algorithm development and the advent of neural networks (Demichev *et al.,* 2020).

2.4 Ion mobility – the 3rd dimension of the mass spectrum

Ions moving through the mass spectrometer device are manipulated by electromagnetic fields and in specific areas, gas is used to focus or to disrupt the structure. However, when the electromagnetic fields push the ions against the flow of inert gas, usually N_2, but He or CO_2 are also used, ions start to separate according to their collisional cross section (CCS), basically the shape of the ion

(Schroeder *et al.,* 2020). This feature is utilized in travelling wave ion mobility (IMS) Synapt instruments produced by the Waters company (Giles *et al.,* 2004; Shvartsburg *et al.,* 2008). IMS can be analytically used to distinguish between ions of the same mass, but different structure. Specifically, in proteomics, this approach is able to differentiate between isomeric peptides (e.g. containing a D-amino-acid within the chain), while in native MS, it can distinguish between active and denaturated forms of a protein. IMS can also be used to decrease the complexity of the peptide mixture in shotgun proteomics. The principle is a sequential transmission of ions based on their CCS to the mass analyser, placed between the multipole and the mass analyser, basically an extension of the collision cell (reviewed in Uetrecht *et al.,* 2010; Lapthorn *et al.,* 2012; see Figure 3).

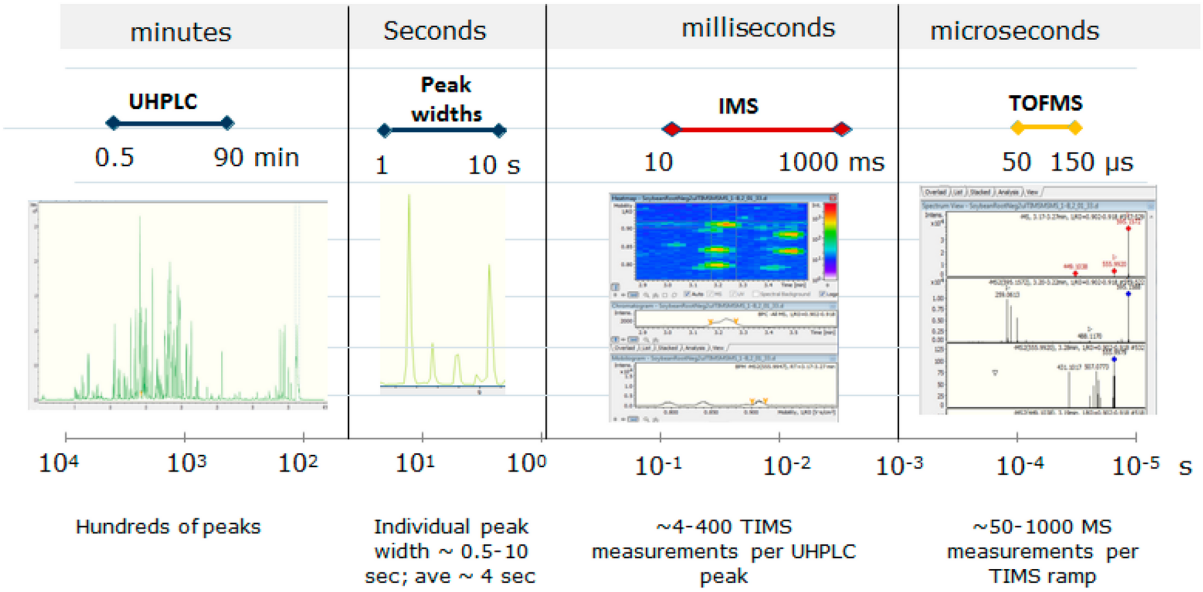

Figure 5*: Duty cycle comparison between components of an LC-MSMS system; the X axis represents time resolution in seconds for each level of an LC-MS analysis. Each LC-MS analysis takes between a few minutes to hours and can be represented by a chromatogram (far left); a chromatogram consists of individual peptide peaks (center left); each peak can be separated into several TIMS measurements (center right); each TIMS measurement can yield numerous MS fragment spectra (far right) (from Schroeder et al., 2020).*

The mobility cell of Trapped Ion Mobility MS (TIMS) device from Bruker is constructed in opposite way to Synapt instruments. The cell is placed right after the ion source, where the gas pressure difference between the ion source and the inner environment of the MS device pushes the ions against a trapping

electromagnetic field. This way ions are concentrated allowing parallel accumulation and serial fragmentation (PASEF) of peptides. In this setting the ion mobility cell is divided into two separate cells: the first acting as a trap, where ions are accumulated, while the second cell uses an energy gradient to separate ions according to their CCS. Higher CCSs are released first. The success of IMS can also be attributed to the fact, that its duty cycle fits well between the LC separating peptides into seconds wide peaks and the ToF, acting in microsecond range (Figure 5).

2.5 Quantitative proteomics

Living systems are dynamic - they react to changes in environment and their internal state. Many of those changes manifest themselves as changes in the level of individual proteins. Some proteins are freshly synthesized, others are recycled. It is not enough to know what proteins are in the sample, increasingly, there is demand to know the ratios of the proteins present and how their levels change in different conditions. As mentioned earlier, the height of the mass spectrum signal peak is proportional to the number of ions captured by the detector, thus allowing quantitative analysis. The intensity of the peptide in a spectrum *per se* is however not a direct indicator of its concentration, because of differential ionization ability of different peptides, suppression effects and other parameters (reviewed in Urban, 2016). However, it can be used to compare the relative abundance of the same peptide in different samples.

There are two basic approaches for quantitative proteomics – the analysis based on labels or tags and a label free quantification. **Quantitative labels**, also called tandem mass tags (TMT) are based on stable isotopes, heavy metals or isobars. The last types of tags have the same overall mass, but varying in distribution of heavy isotopes. Each sample is labelled by a different mass tag – a chemical agent that attached itself to the peptide after digestion. The samples are then mixed and analysed by MS. During fragmentation, a splinter of the tag with a sample-specific mass is split form the peptide and appears in the resulting mass spectrum. The intensity of the tag in the fragment spectra then directly corresponds to the amount of that specific peptide in the sample. Since samples were mixed together, the fragment spectrum contains ideally specific tags from

all samples, allowing their direct comparison (Wiese *et al.,* 2007). Meanwhile, there are enough isobaric tags to allow comparison of up to 11 samples in one experiment (reviewed in Pappireddi *et al.,* 2019). In a variant of the method known as 'stable isotope labelling with amino-acids in cell culture (SILAC)', isobarically-tagged amino-acids are introduced to the growth medium, allowing tracking the expression of proteins as they are produced in a cell culture (Ong *et al.,* 2002).

Label free quantification (LFQ) relies solely on the comparison of peptide intensities (area under peak) or spectral counts and robust statistical methods for validation. Multiple strategies were introduced to obtain the best possible results (Bantscheff *et al.,* 2007, Al Shweiki et al., *2017*). By definition, the basic methods offer only relative quantification; absolute quantification can be achieved by spiking the sample by a standard alien protein with a known concentration.

An interesting hybrid between the labelled and label free strategies is the Q-conCAT, where up to 50 proteins of interest are selected, 3 tryptic peptides of each are picked and concatenated to form an artificial polypeptide. These proteins are typically produced in *E. coli* cells grown in media containing an isotopically labelled amino-acid precursor. Labelled polypeptides are then isolated, purified and added to the sample prior to digestion in known quantity and the sample is processed. The proteins of interest are absolutely quantified by comparing intensities of their peptides with their labelled counterparts from the Q-conCAT polypeptide (Beynon *et al.,* 2005).

Crucial for the successful quantification are reproducibility of LC separation, stability of the electrospray ion source, the computational algorithms for comparison, retention time alignment, and statistical evaluation of several LC-MS datasets (Rozanova *et al.,* 2021). The absolute protein expression (APEX) method uses spectral counts representing the number of detected tryptic peptides and their corresponding MS spectra as a ground for the quantification. Indeed, it circumvents the fact that each peptide has a different detection probability due to the variability of its physicochemical properties severely affecting its MS detection (Braisted *et al.,* 2008).

Other methods are based on the area under the curve (peak), which has a wider

dynamic range and high precision, but is even more dependent on repeatability, especially of the LC separation (Rozanova *et al.,* 2021). The Top3 (or Top N) algorithm quantifies proteins by averaging the intensity of three (or N) peptides with the highest intensity from one protein. Another approach, the intensity-based absolute quantitation (iBAQ), sums intensities of peptides that map to a protein and divides it by the number of theoretical peptides suited for the successful MS identification - between 6 and 30 amino acids in length. Software packages specialized in protein quantification, such as Progenesis QI (Nonlinear Dynamics/Waters) or MaxQuant (Cox and Mann 2008; Cox *et al.,* 2011; Tyanova *et al.,* 2016a) offer a range of quantification methods, normalization and statistical options for the experiment (reviewed in Al Shweiki et al., *2017)*. MaxQuant iBAQ algorithm is convenient for the analysis of protein levels within a sample, its LFQ module is focused on the comparison of protein levels between samples.

An interesting combination of quantitative proteomic methods and structural proteomics is the limited proteolysis method (Schopper *et al.,* 2017). In this method, the sample is first partially digested by a non-specific protease for various time periods but shorter than needed for a complete digestion. Then, each of the partially digested sub-samples is subjected to a complete proteolysis with a specific enzyme, e.g. trypsin and analysed by MS. In the resulting dataset, the variability in identification of select peptides in the different sub-samples suggests that there were differences in the availability of the cleavage sites to the protease, thus pointing to a possible structural change in the protein. Structural changes often reflect the functional state of the protein. This can add valuable insight into the state of the cell, especially when pathways are not regulated by the protein expression level, but by conformational changes (Feng *et al.,* 2014).

2.5 MS analysis of protein complexes after crosslinking (XL-MS)

The protein amino-acid sequence determines the protein structure, which determines the protein function. The majority of known protein structures are elucidated by X-ray crystallography, however other methods like NMR spectroscopy and cryo-electron microscopy (cryo-EM) are also frequently used.

The PSII structure has been solved by both X-ray crystallography and cryo-EM with very high resolution (Umena *et al.,* 2011; Gisriel *et al.,* 2022). However, probing transient or heterologous protein structures, for instance interactions between PSII subunits and PSII assembly factors, by co-crystalization is challenging (Chichili *et al.,* 2013). The small size of many complexes also make their structure inaccessible by cryo-EM.

An alternative method to map the structure of interacting proteins is based on chemical crosslinking combined with MS (XL-MS). Proteins are crosslinked by using a chemical agent with two reactive groups connected by an alkyl chain (Chapman 2000). The active groups can be amino-, sulfhydryl- or carboxy-reactive, homo-bifunctional or hetero-bifunctional and can be active simultaneously or sequentially. Crosslinkers can be further sorted based on their origin, either natural (e.g. genipin, nordihydroguaiaretic acid, tannic acid, citric acid, procynaidins) and synthetic (carbodiimide agents, epoxides, N-hydroxysulfosuccinimide and aryl sulphonyl fluoride; reviewed in Jayachandran *et al.,* 2022). The advantage of natural crosslinkers is their non-toxicity, yet their very narrow specificity, often only a single type of protein, e.g. collagen, makes their utilization in protein research very limited. The chain connecting the active groups can be of various length, which defines the “reach” of the crosslinker.

Table 1: *Overview of selected synthetic crosslinkers (from Crosslinkers Technical Handbook, Thermo Fischer Scientific 2012)*

Crosslinker	**Specificity**	**Link length**
Disuccinimidyl suberate (DSS)	Primary amine (K, N-term)	6-carbon
Disuccinimydil glutarate (DSG)	Primary amine (K, N-term)	3-carbon
Bis(sulfosuccinimydil) suberate (BS^3)	Primary amine (K, N-term)	8-carbon
1-Ethyl-3-(3-dimethylaminopropyl) carbodiimide (EDC)	Carboxyl group (D, E, C-term) to primary amine (K, N-term)	Peptidic bond
Bismaleimide-activated polyethylene glycol (BM-PEG2)	Sulfhydryl (C)	2-carbon

Crosslinks between peptides are of covalent nature, so they persist isolation, purification and proteolytic cleavage. After MS measurement, proximity of the linked peptides can be mapped to structural models of the involved proteins, allowing better understanding of their interaction (Chapman 2000). However, crosslinks between the two involved proteins are discovered only in the ideal case. Common are intra-peptide links, or loops, and inter-peptide links within the same protein (monolinks). Frequent are also type-0 modifications, where only a single active group of the crosslinker has reacted with the peptide, with the other active site vacant. Occasionally, a combination of various crosslink types produces a networked concatenate, which is more-less impossible to interpret. In any case, the number of possible crosslinks between proteins is enormous and made the technique impractical for a long time since its inception (reviewed in Leitner *et al.,* 2010; Rappsilber 2011; Yılmaz *et al.,* 2018).

With the advent of available high precision MS, the interest in XL-MS inspired the development of algorithms that sift through high throughput proteomic MS data and identify crosslinks. Such algorithms are bundled into xQuest (Rinner *et al.,* 2008) or StavroX/MeroX (Götze *et al.,* 2012) software packages, both available to use free of charge. A limitation in both mentioned programs is that they require input in open file formats, such as *.mgf. This format is available as optional output of most MS data processing programs, however conversion to *.mgf is leads to loss of fidelity and there can be differences in the conversion process, e.g. output of one retains charge state, other is deconvoluted into monoisotopic form. An exception is the upgraded version of MaxQuant, containing MaxLynx plug-in (Yılmaz *et al.,* 2022), which combines raw data processing, database search and crosslink detection.

Even so, the analysis of XL-MS data is not straightforward, mainly due to a high amount of non-crosslinked peptides exceeding the signal of the crosslinked ones. Various methods are tested to enrich the crosslinked peptides in the mixture, or to specifically detect the crosslinks and disregard non-crosslinks. By using LC-MS, the crosslinked peptides elute separated from their non-crosslinked variants. The crosslinkers can be labelled radioisotopically, usually using deuterium. Another possibility is digestion in $H_2{}^{18}O$ water, where the enzymatic hydrolysis adds the heavy oxygen to the C-termini of both crosslinked peptides. The isotopic mass

shift is then detected by MS, and labelled peptides are analysed preferentially. Affinity labelled crosslinkers (with e.g. biotin) have also been proposed, but the bulkiness of the affinity tag can make the crosslinking process sterically disadvantageous and their usage is limited (reviewed in Leitner *et al.,* 2010). Generally, detection of crosslinks can be improved by:

i) using recombinant proteins reacting *in vitro* instead of a cell lysate or purified protein complexes

ii) optimizing the ratio between proteins/protein complexes and the crosslinking agent

iii) using a strong cation exchanger to enrich crosslinked peptides after digestion (Chen *et al.,* 2017).

iv) reducing the size of the protein database used for matching of peptides to relevant proteins

3. Aims of the thesis

Although MS methods, such as protein identification, are used quite routinely for cyanobacteria, the analyses of photosynthetic complexes are not trivial. These protein assemblies are very hydrophobic, isolated in detergent and containing small proteins that are difficult to detect. The same is true for the whole-cell proteomics or the analysis of total membrane proteins. Although the Laboratory of Photosynthesis in Třeboň has developed a unique workflow how to isolate very low-abundance assembly complexes of photosystems (combining mutagenesis and affinity chromatography), still the abundance of many proteins is limited and the identification is even more challenging after separation of protein complexes on 2D gel electrophoresis followed by the analysis of protein spots.

The aims of the thesis are:

- To optimize MS methods for the analysis of membrane protein complexes isolated from the cyanobacterium *Synechocystis*.
- To develop advanced MS approaches such are crosslinks and whole-cell protein profiling for this model cyanobacterium.
- To explore the role of FtsH4 protease in the biogenesis of photosynthetic complexes in *Synechocystis* using quantitative proteomics.

4. Published results

4.1 Publication I

Knoppová J, Yu J, Koník, Nixon PJ, Komenda J: CyanoP is involved in the early steps of Photosystem II assembly in the cyanobacterium *Synechocystis* sp. PCC 6803. *Plant and Cell Physiology*, **57**:1921–1931, 2016; doi: 10.1093/pcp/pcw115

CyanoP is a distant cyanobacterial homolog of the PsbP – the chloroplast PSII lumenal subunit and a lipoprotein of hitherto unknown function that was previously co-isolated with the RCII* assembly intermediate. In this study, we used FLAG-tagged CyanoP to isolate and identify its interaction partners by a combination of 2D clear native/SDS - PAGE and MS. The tagged protein was expressed in strains of *Synechocystis* lacking either the D1 or the D2+CP43 subunits. In the resulting isolations, CyanoP was identified as a member of the D2 assembly module ($D2_m$). The $D1_m$ and $D2_m$, respectively, are present in the early stages of PSII biogenesis, as the newly synthesized D1 and D2 core subunits exit the ribosome and are inserted into the thylakoid membrane by SecY translocon and YidC insertase complex. In the proposed model, CyanoP is present on the lumenal side of the assembled complex, together with the assembly factor Ycf48 and the PsbO subunit. where they facilitate association of the $D1_m$ and $D2_m$ into the RCII assembly intermediate.

4.2 Publication II

Bečková M, Yu J, Krynická V, Kozlo A, Shao S, Koník P, Komenda J, Murray JW and Nixon PJ: Structure of Psb29/Thf1 and its association with the FtsH protease complex involved in Photosystem II repair in cyanobacteria. *Philos Trans R Soc Lond B Biol Sci*. **372**:20160394, 2017
doi: 10.1098/rstb.2016.0394

FtsHs are membrane-bound ATP-dependent metalloproteases found in prokaryotes, as well as in plastids and mitochondria of eukaryotes. In *Synechocystis*, four homologs are organized as heterohexamers (FtsH1/3 or FtsH2/3) or homo-hexamers (FtsH4) to perform quality control and turnover of

PSII and PSI subunits. Here, we discovered that expression of FtsH2/3 heterohexamers dependents on Psb29. This protein factor with a C-terminal 3xFLAG-tag was purified and the obtained pulldown contained both FtsH1/3 and FtsH2/3. It implies that Psb29 binds both types of heterooligomers. In addition, two different prohibitins (Phb1 and phb3) belonging to the Band7 superfamily were co-isolated with Psb29. The exact function of prohibitins and the significance of the association to the FtsHs is still unknown.

4.3 Publication III

Bečková M., Gardian Z., Yu J., Koník P., Nixon PJ., Komenda J: Association of Psb28 and Psb27 proteins with PSII-PSI supercomplexes upon exposure of *Synechocystis* sp. PCC 6803 to high light. *Mol. Plant*. **10**:62-72, 2017, doi: 10.1016/j.molp.2016.08.001.

Psb28-1 and Psb28-2 are homologous assembly factors of PSII with slightly different binding preferences. For this publication, both Psb28 proteins were FLAG-tagged and used to isolate their binding partners, which were identified by MS. Whereas dimeric Psb28-1 binds exclusively to the assembly intermediate RC47, monomeric Psb28-2 binds to RC47 and the RCCII complex. Under high light conditions, both Psb28 homologs associate with oligomeric PSII and the PSII-PSI supercomplex consisting of trimeric PSI and two PSII monomers, together with another assembly factor, Psb27. PSI likely protects assembling PSII complexes form light damage.

4.4 Publication IV

Bučinská L, Kiss É, Koník P, Knoppová J, Komenda J, Sobotka R: The ribosome-bound protein Pam68 promotes insertion of chlorophyll into the CP47 subunit of Photosystem II. *Plant Physiology*, **176**:2931–2942, 2018
doi: 10.1104/pp.18.00061.

The photosynthesis-affected mutant 68 (Pam68) protein has been known to be important for PSII assembly, however its exact role remained unclear. In this article, we used FLAG-tagged Pam68 as a bait for isolating its interaction partners by immunoaffinity chromatography. After visualization by 2D clear native/SDS-

PAGE, subsequent MS analysis of the spots identified CP47, a collection of both large and small ribosomal subunits, the SecY/YidC translocase/ insertase, Ycf48, FtsH2/3, light repressed protein A (LrtA) and two unknown proteins. In the proposed model, the N-terminus of Pam68 is attached to the ribosome, while its C-terminus binds the stromal loops of the nascent CP47, facilitating insertion of chlorophylls into its structure. CP47 is then joined by PsbH, and chlorophyll-binding Hlips making up the CP47 module.

4.4.1 Additional experiments

The proteins co-isolated with the 3xFLAG-tagged Pam68 were submitted to cross-linking with BS3 agent. BS3 was added to 100 µL of the Pam68 elution to a final concentration of 2 µg/mL and incubated on ice. For further details on the method, please refer to published results, Kiss *et al.,* 2023 (chapter 4.7). The identified crosslinked peptides belonged to the Pam68 protein and other proteins. However, the crosslinked amino-acid residues in Pam68 were located in the N-terminal 3xFLAG-tag used to isolate the protein, and the 3xFLAG peptide used for the competitive elution of the bound protein from the resin. These results were not included in the publication.

4.5 Publication V

Konert MM, Wysocka A, Koník P, Sobotka R: High-light-inducible proteins HliA and HliB: pigment binding and protein–protein interactions. *Photosynth Res.* **152**:317–332, 2022, doi: 10.1007/s11120-022-00904-z.

Hlips are small (45-70 amino-acid residues), trans-membrane helix proteins with chlorophyll and -carotene binding motifs; these proteins are essential for survival of cyanobacteria even under moderate light stress conditions. In *Synechocystis,* four Hlips were identified. While HliC/D heterodimer is known to bind to the PSII assembly factor Ycf39 and photoprotect RCII assembly intermediate, the role of HliA/B remained obscure. Here, we used quantitative proteomics to compare Hlip pulldowns from solubilized membranes of different *Synechocystis* Hlip mutant together with the control strain after shift to high light. In none of the pulldowns, oxygen evolving complex proteins were identified, suggesting that HliA/B bind

only to PSII assembly intermediates. HliC was the preferred partner for HliA/B and novel interaction partners were identified. In absence of HliC, significantly less proteins were identified and a small amount of HliB appeared to interact with HliA (and vice versa), together with HliD and two of its known interaction partners (ChlG and Ycf39). On the other hand, some PSII core subunits were missing in the Δ*hliC* isolations. Altogether, HliC seems to be the “central” Hli protein, binding all other Hlips. In the absence of HliC, the other Hlips show a weak affinity to each other but the resulting complexes are probably non-functional.

4.6 Publication VI

Koník P, Skotnicová P, Gupta S, Tichý M, Sharma S, Komenda J, Sobotka R, Krynická V: The cyanobacterial FtsH4 protease controls accumulation of protein factors involved in the biogenesis of photosystem I. *Biochim Biophys Acta Bioenerg*. **1865(1)**:149017, 2024, doi: 10.1016/j.bbabio.2023.14901.

FtsH4 is a membrane bound ATP-dependent metalloprotease. While the other *Synechocystis* FtsH homologs (FtsH1-3) are organized as hetero-hexamers, FtsH4 is present as a homo-hexamer. In this study, we used quantitative proteomics to distinguish binding partners from substrates, when comparing proteins co-eluted with the active form (FtsH4-His) and the proteolysis deficient ^{trap}FtsH4-His. We identified several proteins related to PSI biogenesis as probable substrates of FtsH4. Specifically, it includes PSI subunit PsaB, assembly factors Ycf4 and Ycf37 and chlorophyll-binding protein IsiA forming oligomeric rings around PSI under iron stress conditions.

4.6.1 Unpublished results – proteomic profiling of FtsH4 mutants

To obtain a global view on the role of FtsH4, we performed quantitative proteomic experiments with cells grown under various light conditions and growth phase. WT, and strains lacking FtsH4 (°FtsH4), (over)expressing *ftsH4* gene (F4O) and an additional control strain lacking *psbAI* and *psbAII* genes (A3), were grown under different regimes. We expected that the proteins identified as substrates will be enriched in cells lacking FtsH4 and/or depleted in cells overexpressing FtsH4. Additionally, the aim was to analyse in what phase of the growth cycle the FtsH4

protease has the strongest impact on the proteome. Proteomic analysis of the samples identified 2323 proteins form the Cyanobase and Uniprot *Synechocystis* databases, which represents about 65% of the entries. Comparisons between the experimental strain (H4 and F4O) and their corresponding controls (WT and A3) are shown represented as volcano plots in Figure 6.

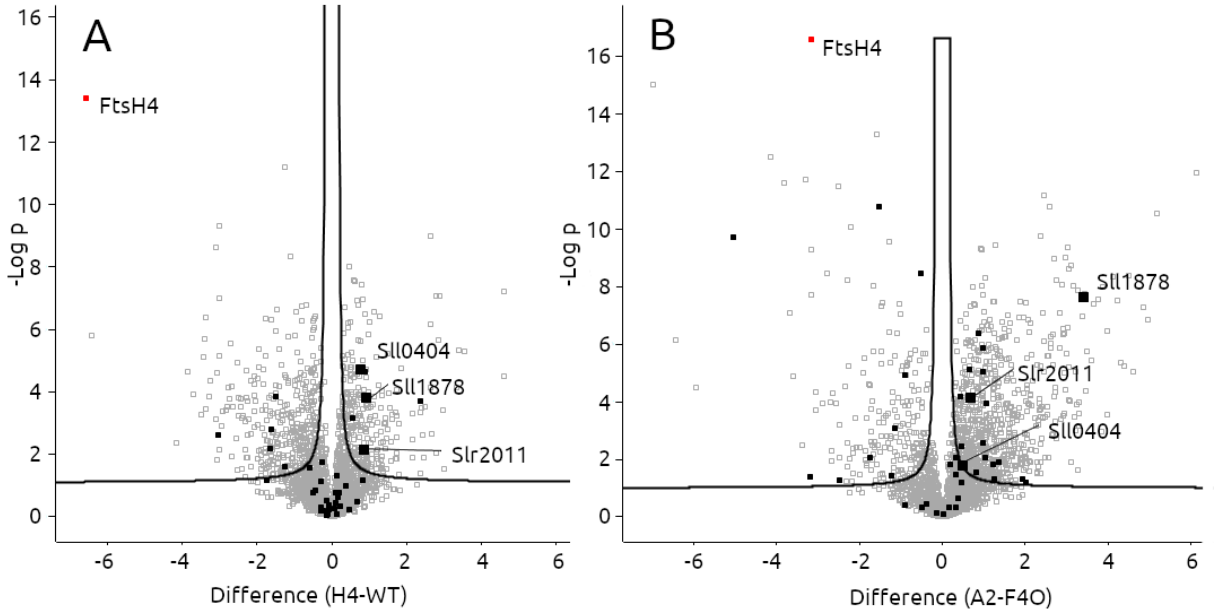

Figure 6*: Volcano plot comparison between protein expression in A: H4 and WT B: A2 and F4O cells. Identified proteins are represented by gray squares. FtsH4 is represented by a red box. Substrates recognized as substrates in the trap-FtsH4 experiment are represented as black boxes. Bigger black boxes represent proteins, which are enriched in H4 cells, depleted in F4O cells and were recognized by the FtsH4 trap assay as substrates: Sll0404, Sll1878, Slr2011. In volcano plots, difference between protein expression is plotted on the x-axis; -Log p value on the y-axis. Curved black line represents threshold of statistical significance: points above the line show T-test significant difference between samples.*

4.6.2 Materials and methods

Liquid *Synechocystis* cultures were grown in 100 mL of BG-11 medium in Erlenmeyer flasks at 28°C on a rotary shaker (120 rpm). Illumination conditions were 40 µmol photons m^{-2} s^{-1} (NL), 500 µmol photons m^{-2} s^{-1} (HL) or 5 µmol photons m^{-2} s^{-1} (LL). For the stationary phase experiment, the cultures were grown photoautotrophically without any dilution for 14 days at NL. For the recovery back to exponential phase, 1mL from the stationary phase culture was diluted in fresh BG11 medium and grown for additional 24 hours under HL. Cells were harvested at an OD750nm of ~0.8 by centrifugation at 6000 × *g* for 10 min, 5 µL of the pellet was resuspended in 45µL of 0.1% Rapigest RSF 30

(Waters) in 50 mM ammonium bicarbonate. The mixture was sonicated by 10 pulses at 50% intensity and 50% amplitude with a needle sonicator (Heischler Ultrasonic) on ice, then incubated at 60°C for 45 minutes, while shaking gently. The mixture was then left to cool down, proteomic grade trypsin (Pierce) was added to a final concentration of 10 ng/µL and incubated at 37C for 12 hours.

Digested peptides were isolated using the StageTip protocol (Rappsilber et al., 2007) and subjected to MS analysis on a TimsTOF pro (Bruker) on-line coupled to a UltiMate3000 UHPLC (ThermoFisherr) device. Peptides were trapped in C18 PepMap 100 µ-Precolumn (5µm, 100 Å; Thermo Fisher Scientific) by perfusion by 0.1% formic acid in water (mobile phase A) and then separated by a 30 minutes gradient of acetonitrile with 0.1% formic acid (mobile phase B) on a Acclaim PepMap RSLC column (75 µm × 15 cm, C18, 2 µm, 100 Å; Thermo Fisher Scientific). Separated peptides from the column were fed directly into the Captive Spray ion source of the MS. Spectra were acquired in data dependent PASEF regime with an accuracy of 0.2 ppm for precursors and 0.5 ppm for fragments. 3 technical replicates were acquired for each of the 3 biological replicates for each sample. Raw data were processed by the MaxQuant/Andromeda software, statistical analysis was performed in Perseus (Tyanova *et al*., 2016b). Data was curated, contaminants, random hits and low quality hits were removed, the intensities were normalized by dividing each protein intensity by the sum of all intensities in the sample and 2(x)log transformed. Gene ontology annotations from the PFAM (Mistry *et al.,* 2020) and KEGG (Kanehisa *et al.,* 2021) databases were associated with proteins to aid data interpretation. T-test, ANOVA, post hoc Tukey HSD test for one-way ANOVA and the Fisher exact test were used to assess significant differences and enrichment of GO annotations among protein subgroups, Pearson correlation was used to match protein expression profiles to an expected reference profile.

Next page: ***Figure 7****: Profile plots of proteins quantified from Synechocystis cells grown under various light conditions; gray line represents expression level of individual proteins, the y-axis is 2(x)log of protein intensity divided by sum of all protein intensities. Only proteins with T-test significant differences in expression are shown. Highlighted are protein by gene ontology association: A) photosynthetic proteins in green, antenna proteins in blue; B) ribosomal proteins; C) FtsH1, FtsH2 and FtsH3 proteins in brown, FtsH4 protein in red.*

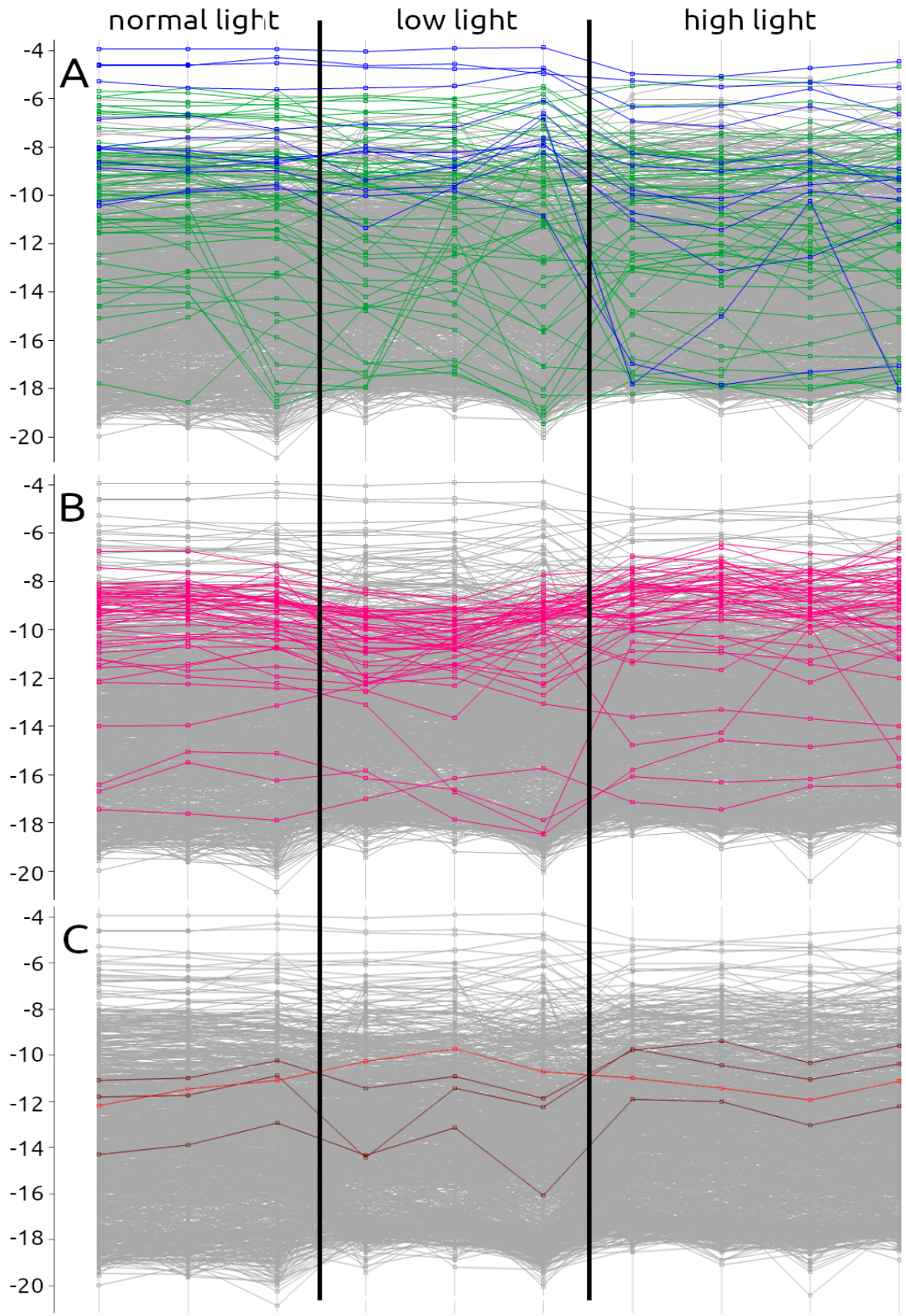
normal light
low light
high light
A
B
C
-4
-6
-8
-10
-12
-14
-16
-18
-20

4.7 Publication VII

Kiss E, Talbot J, Adams NBP, Opekar S, Moos M, Pilný J, Kvasov T, Schneider E, Koník P, Šimek P, Sobotka R: Chlorophyll biosynthesis under the control of arginine metabolism. *Cell Reports* **42**:113265, 2023,
doi: 10.1016/j.celrep.2023.113265.

ArgD (N-acetylornithine aminotransferase) is an essential enzyme involved in the biosynthesis of arginine and this arginine biosynthetic pathway plays a crucial role in the regulation of nitrogen metabolism. Gun4 (Genomes uncoupled 4) is an indispensable member in the chlorophyll biosynthesis pathway enhancing the activity of magnesium chelatase complex. In this article, we show that the binding of ArgD to Gun4 leads to the inhibition of the tetrapyrrole biosynthesis. Interestingly, the formation of ArgD-Gun4 complex is stimulated by ornithine, an intermediate of the Arg biosynthesis.

4.7.1 Unpublished results – XL-MS analysis of the Gun4-ArgD complex

ArgD binds to Gun4 most likely in a 2:1 ratio, however the exact interface is still unknown. Cross-linking was performed to elucidate the topology of the interaction and positioning it into the overall context of the involved protein complexes. We prepared recombinant *Synechocystis* ArgD and Gun4 proteins in *E. coli*, purified them using His-tag and mixed them in various ratios. The expected ArgD-Gun4 complex was then submitted to BS3 crosslinking.

In the MS analysis of the samples, 29 different crosslinked peptide pairs were identified. Specifically, 24 crosslinks were identified within and between the ArgD molecules of the complex, 3 within the Gun4 molecule and 2 between ArgD and Gun4. The majority (22 pairs within/between the ArgD protein) came from the reaction with the molar ratio between ArgD and Gun4 being 20:1. The reaction with the molar ratio of 2:10 yielded the most interesting peptide pairs between the ArgD and GUN4 proteins, as well as 2 within/between ArgD molecules and 3 within the GUN4 molecule. Crosslinks between peptides were mapped onto the polypeptide chains (Figure 8) by xiNET (Combe *et al.,* 2015).

The crosslinked peptides were fitted to a structural model of the ArgD-Gun4

complex calculated in Alphafold multimer 2.3 (Figure 9A). According to *b*-factor value and PAE data of the model, the prediction of ArgD dimer and Gun4 proteins are of high confidence, which is however expected as structures of these proteins are available. On the other hand, even the Alphafold model with highest score shows very low confidence for Gun4-ArgD interaction (Figure 9B). The possibility that the model is not correct is further supported by our XL-MS results indicating that the Gun4 binds to ArgD via N-terminal domain and not the porphyrin-binding C-terminal part as proposed by Alphafold (see Discussion).

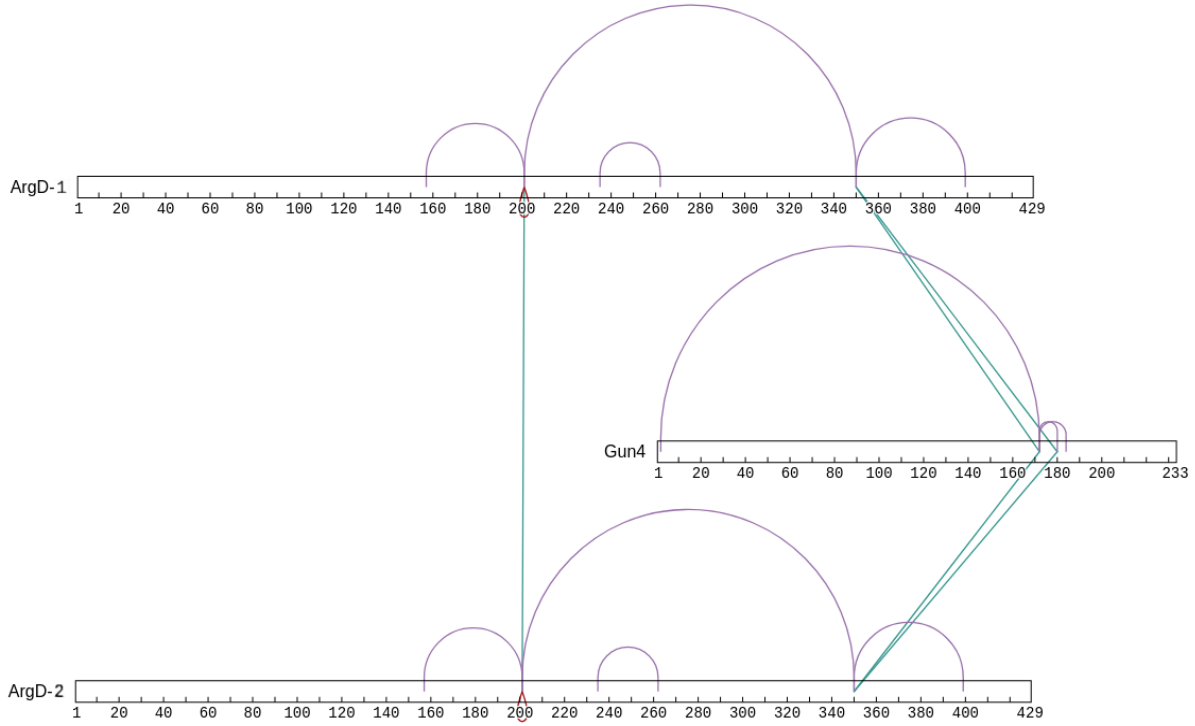

***Figure 8**: Crosslinks mapped onto the ArgD-Gun4 complex. Inter-molecular links are represented in green, intra-molecular in violet, link between same peptides is represented as red loop. Black rectangles represent the length of the polypeptide chains, where the N-terminus is on the left side and C-terminus on the right. Numbers below signify the amino-acid residue.*

4.7.2 Preparation of recombinant His-ArgD and His-Gun4

Synechocystis *argD* and *gun4* gene sequences containing an C-terminal hexahistidine tag were cloned into pET21a plasmid (Novagen) and the constructs were used to transform BL21(DE3; Invitrogen) *E. coli* cells. The transformed cells were grown in LB medium (Roth) supplemented with 50 μg/mL of ampicilin (Serva) at 37°C overnight. The production of the recombinant protein was

triggered by adding IPTG to a final concentration of 0.4 mM. After 4 hours, cells were harvested, resuspended in 50 mM HEPES buffer containing 5 mM of $MgCl_2$, 5 mM of $CaCl_2$, pH 7.2, and Sigma protease inhibitor cocktail without EDTA, Cells were disrupted with LM20 Microfluidizer (Microfluidics) using six breaking cycles. The cell debris was centrifuged for 1 h at 40 000 x g at 4°C and the filtrated supernatant was loaded into Äkta pure 25 M2 (GE Healthcare) liquid chromatography device.

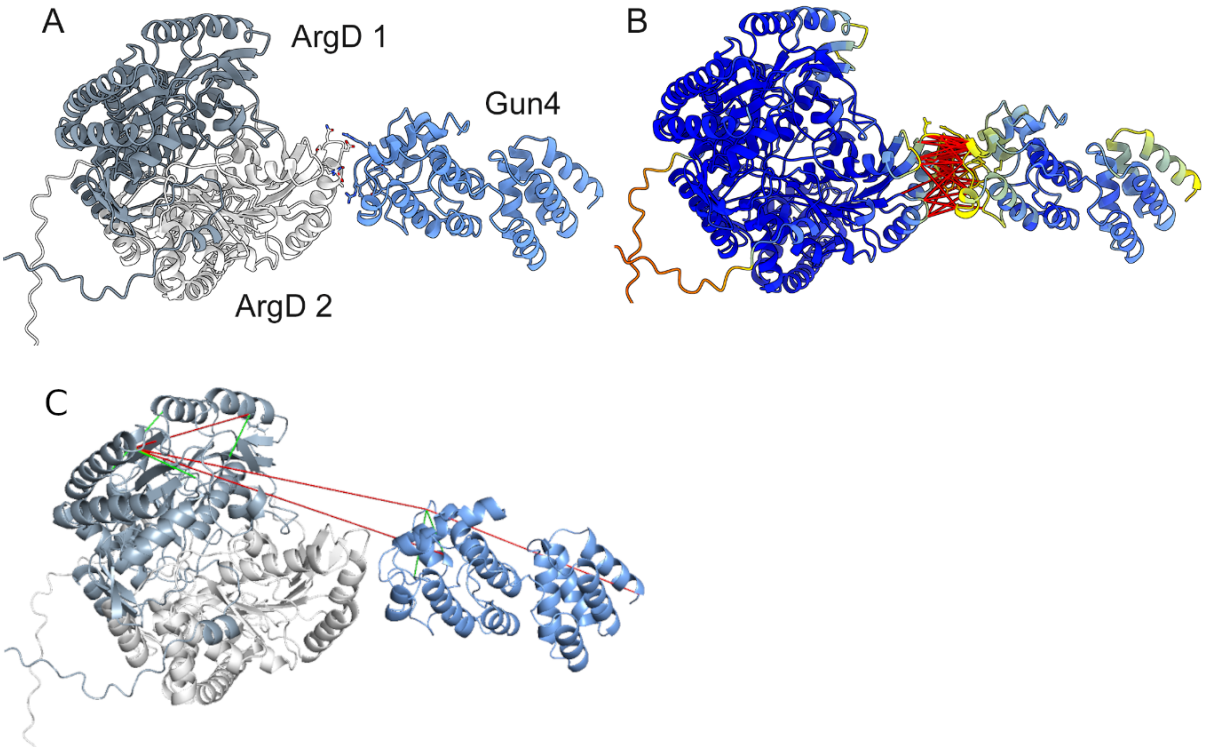

***Figure 9**: Alphafold model of the ArgD-Gun4 complex and the quality score of the ArgD and Gun4 interaction. A) A model calculated in Alphafold multimer 2.3. Dimeric structure of the ArgD aminotransferase is in grey, Gun4 in light blue. The Gun4 binds one copy of the ArgD by its conserved, porphyrin binding C-terminal domain. B) b-factor of the Alphafold model demonstrates a high probability of ArgD and Gun4 structures but very low (minimal) score for the ArgD-Gun4 interaction. This figure was calculated in ChimeraX using Alphafold predicted aligned error (PAE) data. Blue color represents high confidence, red very low. C) PYMOL visualization of the ArgD-Gun4 complex (Alphafold model) visualizing the crosslinked peptides. Satisfied crosslinks are shown in green, violated in red.*

His-tagged proteins were isolated using a His-trap High Performance column (Cytiva/Merck) and eluted by a 20 minutes gradient (10% to 100%) against the HEPES buffer supplemented with 500 mM Imidazole. 1 mL fractions were collected during the gradient and analyzed by SDS-PAGE followed by

immunodetection with Monoclonal Anti-polyHistidine from mouse (Sigma-Aldrich). Highest yield fractions were re-purified using an Äkta pure 25 M2 (GE Healthcare) on a Superdex 75 10/300 GL Increase gel column (Cytiva/Merck). Protein concentrations were measured using NanoDrop One (Thermo Scientific) and the protein solutions were stored on ice until crosslinking.

4.7.3 Crosslinking, peptide enrichment, isolation and MS analysis

The recombinant ArgD and Gun4 were mixed in 3 different molar ratios of 2:1; 20:1 and 2:10 in 30 µL of 50 mM HEPES buffer at pH 7.2 and kept on ice. After 30 min, BS3 (Sigma-Aldrich) cross-linker was added to a final concentration of 2 µg/mL and the mixture was kept on ice. After 2 hours, the reaction was quenched by adding 40 µL of 100 mM ammonium bicarbonate and left on ice for another 30 minutes. For the precipitation, 500 µL of ice-cold acetone was added and the solution was placed for 30 min to 20°C, then pelleted by centrifugation for 30 min at 20 000 x g. The supernatant was carefully aspirated and the residual acetone was left to evaporate at room temperature. After 15 min, 10 ng/µL of proteomic grade trypsin (Pierce) in 50 mM ammonium bicarbonate was added and incubated at 37°C for 12 h.

Digested peptides were separated by SCX in similar fashion to the StageTip isolation method, just with Cation 47 mm Extraction disks (Empore) instead of Octadecyl C18 disks (Empore). After loading the sample into the prepared tip, fractions were eluted by an elution buffers containing 50mM, 150mM, 300mM ammonium acetate (Sigma-Aldrich) in 20% acetonitrile, and finally by 5% NH_4OH v/v (Fluka Analytical) in 80% acetonitrile, respectively. Peptides from fractions were isolated using the StageTip protocol (Rappsilber *et al.,* 2007) and subjected to MS analysis on a TimsTOF pro (Bruker Daltonics) on-line coupled to a UltiMate3000 UHPLC (ThermoFisher) device. Peptides were trapped in C18 PepMap 100 µ-Precolumn (5µm, 100 Å; Thermo Fisher Scientific) by perfusion by 0.1% formic acid in water (mobile phase A) and then separated by a 30 minutes gradient of acetonitrile with 0.1% formic acid (mobile phase B) on a Acclaim PepMap RSLC column (75 µm × 15 cm, C18, 2 µm, 100 Å; Thermo Fisher Scientific). Separated peptides from the column were injected directly into the Captive Spray ion source of the MS. Spectra were acquired in data dependent

PASEF regime with an accuracy of 0.2 ppm for precursors and 0.5 ppm for fragments. Additionally, raw data were processed by the MaxQuant2 software, and searched against a database with only the 2 proteins of interest. Crosslinked peptides were visualized in PYMOL (Delano 2002).

5. Discussion

The *Synechocystis* genome has been first published by Kaneko *et al.,* in 1996. A year after that, the first proteomic study was published, where 2D electrophoresis was used in combination with N-terminal Edmann degradation, identifying about a hundred *Synechocystis* proteins (Sazuka & Ohara, 1997). The initial studies utilizing MS for protein identification from 2D electrophoresis gel spots came after the year 2000, but soon reached the limits of the approach, mainly the dynamic range of both methods and LC-MS became the method of choice for shotgun proteomics (Gao *et al.,* 2015). However, this does not mean that 2D electrophoresis is no longer used. The first dimension is usually native electrophoresis, where, under ideal conditions, protein complexes travel intact and their subunits only separate in the second, denaturing dimension. Untargeted shotgun proteomics cannot provide this type of insight.

In the last decade, the purification of protein complexes from mutant *Synechocystis* strains followed by MS analyses of 2D gel spots and whole pulldowns was the (methodological) driving force pushing further our understanding of PSII biogenesis. Most of ‘new’ protein factors involved in PSII assembly has been identified by this approach. For instance, the work of Knoppová *et al.,* 2016 and Bučinská *et al.,* 2018, described CyanoP as a component of D2 assembly module (D2m) or the interaction of Pam68 with nascent CP47. In the publication of Kiss *et al.,* 2019, the RubA protein with a rubredoxin domain, was connected to RCII assembly complex. Several new factors have been discovered by a detail MS analysis of purified D1m, D2m and RCII complexes (Knoppová *et al.,* 2022). Apart from discoveries of assembly factors, this methodology also revealed an important role of PSI in PSII assembly. PSI complex is probably protecting the unfinished PSII from light damage (Bečková *et al.,* 2017b).

In publications listed above and also in most of other publications from Laboratory of Photosynthesis, Třeboň, the analysed proteins are typically very hydrophobic membrane proteins. The MS data acquisition method therefore needed some optimization. To obtain the highest sequence coverage, I tried multiple approaches: increasing the end point of the acetonitrile gradient from 40

% to 50 % and higher; a gradient that increases steeper to reach 20 % of acetonitrile and then more flat to reach 40 %; various gradient curves instead of a linear gradient (data not shown). At the end, a slight increase in the length of the gradient, from 30 to 40 minutes, produced the best results and I used this modification in for all studies that are included in my thesis.

A limitation of the 2D-gel/MS analysis is that is can analyse only quite abundant proteins that are visible after gel staining. An alternative approach, the analysis of the whole pulldown, results typically in hundreds of hits, and the list can be sorted based on different parameters (intensity, coverage). However, it is difficult to decide what is still a significant hit. We therefore started to use statistically-supported quantitative MS techniques. In Konert *et al.,* 2022, small, single helix transmembrane Hlips were used as His-tagged baits, therefore the isolation of adequate quantities and their identification was not especially challenging. However, identification of interacting proteins of individual Hlips was possible only by comparing enrichment of proteins in comparison to the control, and each other.

By this approach, known interaction partners of HliD were identified (ChlG and Ycf39), and also new interactors: translocon proteins SecD and SecF. The presence of those proteins, together with the absence of PSII oxygen evolving complex proteins suggests that HliA/B only bind to PSII intermediates, not to active PSII. The paper also focused on the question of what types of Hlips homodimers and heterodimers can be found in the cell. Apart from the protein partners of Hlips, the mechanism of Hlip dimerization has been addressed. We demonstrated that the HliC is a ‘universal’ Hli partner, which associates with all other Hlips (HliA/B/D) at various stages of photosystem biogenesis and repair. Again, it needs to be stressed that these findings would not be possible without a quantitative MS analysis.

Similarly, in Koník *et al.,* (2024), HliD was enriched in the FtsH4 trap assay, although not meeting the stringent criteria for significance, while HliA, HliB and HliC were not found. This absence could be explained by their low abundance in cells growing in conditions, which do not induce their accumulation, while HliD is expressed constitutively (He *et al.,* 2001). In contrast, Krynická *et al.,* (2023)

observed degradation of Hlips in the presence of active FtsH4 and their accumulation in the ΔFtsH4 cells. Interestingly, both Krynická *et al.,* (2023) and Koník *et al.,* (2024) describe the uncharacterised protein Sll1106 as a binding partner of FtsH4, not a substrate. The protein is currently subject to follow-up experiments – the analysis of ^{rap}FtsH4-His pulldown obtained from cells lacking the Sll1106 protein.

Quantitative proteomic analysis was used in Koník *et al.,* (2024) with the goal of identifying substrates of the FtsH4 protease. Two his-tagged versions were used to pull-down partnering proteins: the protease deficient ^{trap}FtsH4 and the active control FtsH4. Both substrates and binding partners were identified by MS analysis of pulldowns; substrates were enriched in the ^{trap}FtsH4-his in comparison with ^{wt}FtsH-his pulldown, while binding partners were expected to stay at the same level. This way, PSI subunit PsaB was identified as substrate of the FtsH4 protease, together with Ycf4, a PSI assembly factor, and Ycf37, which is also associated with PSI biogenesis and stability (Dühring *et al.,* 2006). This would point to the role of FtsH4 as a regulator of PSI biogenesis in the early stages of PSI assembly.

In *Synechocystis,* the biogenesis of PSI is inhibited for several hours when light conditions change from normal light (NL) to high light (HL; Kopečná *et al.,* 2013). To explore the role of FtsH4 in this process, I performed quantitative proteomic analysis of cells growing under NL, HL, and low light (LL). By using label free quantification I identified 2323 proteins in extract from cells that were grown under NL (see chapter 4.6.1). As mentioned before, *Synechocystis* has 3562 entries in the current UNIPROT and 3672 entries in the older, but still much used Cyanobase protein databases. Out of those, about 80 % can be identified by MS (Gao *et al.,* 2015; Jackson *et al.,* 2022). The highest number of identified and TMT quantified proteins, as reported, was 2367 (Ge *et al.,* 2017), which is comparable to our result.

In cyanobacterial research, label free quantification is slowly gaining popularity, due to a simpler sample preparation protocol, while producing a comparable proteome insight (Battchikova *et al.,* 2018). In our case, both LFQ and iBAQ were tested, however the LFQ data was plagued with artefacts, most probably due to

the fact that more than half of the identified proteins showed differential expression between the samples. Therefore, for further analysis, iBAQ quantification was used. The primary objective of this experiment was to observe the changes in the *Synechocystis* proteome in various stages of growth and under different light regimes, in WT cells and in mutants lacking (ΔFtsH4) or over-accumulating FtsH4 (F4O strain). Indeed, quantification results show high levels of FtsH4 in the F4O strain. Although a low presence of FtsH4 can be detected in the FtsH4 knocked-out strain, it is possibly due to miss-attributing peptides belonging to other FtsH proteases; there is about 50% sequence similarity and some tryptic peptides are identical.

Out of the 2323 proteins identified, 1840 proteins showed significant differential expression between the samples using ANOVA. From those, 56 proteins were recognized as enriched in ΔFtsH4 cells, and in the same time depleted in F4O sample (see Figure 6). However, only 3 proteins from this group matched the substrates established in the ^{trap}FtsH4 (Koník *et al.,* 2024; Fig. 1): Sll0404, Sll1878 and Slr2011. Sll0404 is the D subunit of the glycolate oxidase complex, essential for the 2-phposphoglycerate metabolism (Eisenhut et al 2008). Sll1878 (FutC), is a membrane associated protein involved in ferric iron uptake and transport (Katoh *et al.,* 2001; reviewed in Fresenborg, *et al* 2020). The function of Slr2011 is not known, but it has 3 transmembrane helices and is characterised as “putative multicomponent Na^+:H^+ antiporter subunit B” in KEGG database (Kanehisa *et al.,* 2021). The Fisher exact test did not identify any enrichment in GO terms among the subset of 56 proteins matching the expected profile. However, in proteins matching the profile best, as established by Pearson correlation, 3 proteins associated with iron transport were detected: Sll1878, Ssl2667 and Slr0513. This could point to the IsiA protein, which level strongly responses to low-iron stress and is identified as the FtsH4 substrate (Koník *et al.,* 2024).

The discrepancy between the whole cell proteomic experiments and the ^{trap}FtsH4 is probably caused by high demands on repeatability of the proteomic quantification, where very slight differences in cell culturing, e.g. minute differences in exact timing of the sampling, or unpredictable stress effects. Other possibility is that the whole cell proteomic analysis observes second or third order effects of the experimentally altered expression of FtsH4, while the expression of

substrates identified by the ^{trap}FtsH4 experiments is recovered by redundancy of the cellular interaction network. Another explanation would be imperfect lysis of the membranes and solubilisation of transmembrane proteins by sonication combined with use of the Rapigest (Waters) surfactant. In follow-up experiments, we plan to use membranes solubilized by either β-DDM or SDS.

An interesting by-product of these measurements, is a collection of WT *Synechocystis* quantitative proteomes from various stages of growth and light regimes. In the data, we can observe the expression profiles of groups of proteins based on their gene ontology classification. For example, expression levels of antenna proteins and proteins belonging to photosynthetic complexes are upregulated in stationary phase cells under LL conditions and downregulated under HL conditions in the exponential phase of growth (see Figure 7). On the contrary, ribosomal proteins have the opposite profile with a lower expression in stationary phase and high in exponential phase. Expression profiles of individual proteins can also be useful to clarify the function of a protein. We plan to publish these and other datasets as a searchable web application, where the expression of any identified protein of interest can be inspected under various experimental growth conditions.

A similar atlas of 2176 *Synechocystis* proteins including their detailed subcellular localization and their quantities was published recently (Wang *et al.,* 2022). In addition, Jackson *et al.,* (2022) quantified 1081 proteins, with special emphasis on processes related to photosynthesis – biogenesis of photosystems, chlorophyll, carotenoid and bilin biosynthesis; membrane assembly, carbon dioxide fixation and metabolism of nitrogen, hydrogen and sulphur. The mentioned datasets describe *Synechocystis* cells growing under NL, while we analysed three different light conditions and growth phases. Additionally, we plan to include more growth regimes later, such as nutrient stress, heat/cold stress and presence of environmental toxins.

Right now, our data is missing information about the subcellular localization, but pre-fractionation is a plan for the future work. Separating the soluble cytoplasmic fraction of proteins form the membranes, allows following different sample preparation and MS data acquisition methods, optimized for the specifics of the

sample. Preparation steps involve detergents, which are not always MS-compatible. SDS, deemed the “perfect” denaturing agent, is not directly MS-compatible and needs to be removed during sample preparation (reviewed in Santoni *et al.,* 2000). Removal of SDS can be done by acetone precipitation or using specialized kits, followed by the FASP protocol (Wiśniewski *et al.,* 2009). While ideal for protein identification, this approach brings the risk of subsequent partial aggregation of proteins or their adsorption to filter, making quantitative analysis undependable. In-gel digestion of cut-of 2D spots avoids the risks, since any residual detergent is washed off during preparation steps. Another possibility is treatment with a MS- compatible detergent, such as β-DDM to isolate membrane proteins from the phospholipid bi-layer. Such a step is completely unnecessary for the proteins in the soluble fraction, yet has to be performed when working with whole cell lysate.

In studies dealing with PSII, XL-MS has been repeatedly employed to obtain insight on the organization of the complicated protein complex. For instance, PsbE, the cytochrome b_{559} alpha subunit and PsbP has been localized, and the structure of the Cl^- binding site has been clarified by this way (Ido *et al.,* 2012). The binding of lumenal CyanoQ subunit to CP47 and PsbO has been first revealed by XL-MS (Liu *et al.,* 2014) and confirmed later by cryo-EM (Gisriel *et al.,* 2022). The binding of CyanoQ to cyanobacterial PSII is either transient, or very weak, since other studies (Opatíková *et al.,* 2023) did not find this elusive subunit in cryo-EM. XL-MS experiments have further shown that Psb28 binds on the cytosolic surface of RC47, where it shares an interface with PsbE, PsbF, CP47, PsbX, and PsbY. possibly protecting the assembly intermediate from redox stress (Weisz *et al.,* 2017).

It needs to be however noted, that there are discrepancies between the XL-MS models and other structural methods such as cryo- EM. A model showing the binding interface between CP43 and Psb27 in the PSII as described by XL-MS (Liu *et al.,* 2011) is supported by one cryo-EM study (Huang *et al.,* 2021), but challenged by another (Zabret *et al.,* 2021). Although the XL-MS study was performed on S*ynechocystis* and the cryo-EM experiments used *Thermo-synechococcus vulcanus* and *Thermosynechococcus elongatus,* it is very unlikely that these complexes are structurally different, given the highly conserved

mechanism of PSII biogenesis.

As a follow-up on our experiments to Bučinská *et al.,* (2018), I have cross-linked the purified Pam68 complex with BS3. However, all identified crosslinks were located in the N-terminal 3xFLAG-tag used for the affinity isolation of Pam68 and probably also with the FLAG peptide used for eluting the isolated proteins. The 3xFLAG-tag is relatively long, contains several lysine residues and presumably has no secondary structure. It is therefore especially prone to attract the crosslinker molecule and randomly attach to anything in close vicinity. It can be concluded that 3xFLAG-tagged complexes are not ideal for XL-MS studies, particularly when eluted with 3xFLAG peptide.

For further crosslinking experiments, I worked with protein complexes isolated using His-tag and nickel-affinity chromatography. It needs to be stressed, that this experiment was performed on *ex-vivo* isolated proteins, which adds to the challenge. Main difficulty is the presence of contaminating proteins, even in concentrations comparable to the proteins of interest. In contrast to FLAG-tag affinity purification, the isolations using metal-affinity chromatography are much less pure, and indeed, contaminants are also subject of crosslinking. Perhaps, the best solution would be to use StrepII-tag and Strep-tactin resin (Schmidt & Skerra, 2007). Proteins isolated by StrepII-tag are typically highly pure, despite its short length, and eluted with a small compound that does not interfere with crosslinking.

In an attempt to study the interaction between Ycf39, the Hli protein HliD and core D1and D2 subunits of PSII (Chidgey *et al.,* 2014) by XL-MS (BS3), the RCII* complex was isolated using His-tagged D2. After MS analysis, no crosslinks were identified between Ycf39 and HliD, however a single crosslink was identified between Ycf48 (Slr2034) and Ycf39 (Slr0399) (data not shown). Since Ycf48 is a distinctly lumenal protein (Knoppová *et al.*, 2016), while Ycf39 is bound on the stromal side of the RCII* (Knoppová *et al.*, 2014), this crosslink must be an artefact, possibly due to aggregation of the complexes in solution, and the data is not to be trusted (data not shown). Regarding the very hydrophobic nature of PSII subunits, including of size-exclusion chromatography or sucrose gradient just prior to XL-MS (to remove aggregates and broken complexes) might be essential

and need to be tested in the future.

Due to this failure to obtain reliable crosslinks on native complexes purified from *Synechocystis*, we worked later with recombinant proteins produced in *E. coli*. This is also the case of analysing the ArgD-Gun4 complex (Kiss *et al.,* 2023). Preparation of recombinant proteins enabled mixing the crosslinking reaction in exact molar ratios, while increasing the concentration of Gun4 ten times yielded the best results. To enrich crosslinked peptides, SCX chromatography was performed, where the most crosslinked peptides were detected in the final fraction, eluted by 5% NH_4OH. The MS data acquisition was also modified to preferentially target heavier peptides with higher charges, by changing the shape of the PASEF selection window – crosslinked peptides both tend to carry protons, doubling the usual charges to states of 4x and 6x charged ions.

Among the resulting crosslinks, there is one self-link between identical peptides of ArgD, which is only possible when the protein forms a homodimer. Indeed, ArgD is a stable homodimer (Kiss *et al*., 2023). Mapping to the 3D model shows that some crosslinks within the ArgD molecules and within the Gun4 satisfy the criterion of maximum distance between BS3 crosslinked peptide pairs, but crosslinks between the ArgD and Gun4 molecules violate the maximum distance of 25Å. It is very likely that the Alphafold2 model is not accurate, which indicates also the analysis of the PAE output (pkl file; see Figure 9). A possible scenario is that the Gun4 interacts with ArgD dimer via the cyanobacteria-specific N-terminal domain. It will be interesting to employ a tool like Alphalink and generate models of Gun4-ArgD supported by XL-MS data. The interpretation is further obstructed by the fact that the two molecules of ArgD involved in the complex cannot be distinguished from each other under the current conditions. It is unclear, if the crosslinked peptides both pairs belong to the same molecule (crosslinks within one ArgD molecule) or each to one of the ArgD molecules in the pair. This problem could be addressed by producing a separate recombinant ArgD in *E. coli* cells grown in presence of an isotope labelled protein precursors in the growth medium, then mixing the 3 different proteins prior to crosslinking and considering the crosslink pairs between labelled and unlabelled ArgD as inter-pair crosslinks, between labelled and labelled or unlabelled and unlabelled as intra-ArgD crosslinks.

6. Conclusion

In my thesis, I introduced advanced methods of protein MS such is analysis of hydrophobic transmembrane complexes, label-free protein quantification and protein crosslinking to study physiology of cyanobacteria, mostly biogenesis of photosystems. The thesis consists of one first-author publication, six co-author publications and unpublished data.

The main conclusions are as follows:

- Lumenal CyanoP proteins associates with D2m and together with Ycf48 facilitates the combining of the D1m and D2m into the RCII assembly intermediate.
- Pam68 protein associates with ribosome, aids the insertion of newly synthesized internal antenna CP47 into the thylakoid membrane and probably promotes the insertion of chlorophylls into the nascent CP47. This process occurs at the beginning of the formation of CP47m.
- Psb28-1 and Psb28-2 protein factors bind to the RC47 assembly intermediate; however the role of these proteins remain unclear. Interestingly, the RC47 associated with Psb28 can apparently attach to PSI trimers, likely protecting the assembling PSII from photodamage during severe conditions.
- Ornithine, an intermediate of the Arg biosynthesis, induces the accumulation of the ArgD-Gun4 complex, which leads to the inhibition of the tetrapyrrole biosynthesis, closely linking both pathways.
- HliC is the smallest Hlip in *Synechocystis* and its only interacting partners are other Hlips (HliA, HliB, HliD) proteins. Hlips need to dimerize to bind pigments and to serve their photoprotection role. While HliA/B/D interact with PSII subunits and PSII assembly factors, the role of HliC is to provide the second helix. HliA/C, HliB/C and HliD/C heterodimers are thus most likely the functional units. Interestingly, this work showed that Hlips also interact with translocon proteins SecD and SecF.
- The formation of hetero-hexamers of FtsH1/3 and FtsH2/3 proteases depends

on the PSII assembly factor Psb29, which also partners with these complexes. All four FtsH proteases are probably also involved in quality control and turnover of photosystems in *Synechocystis*.

- FtsH4 is a membrane bound metalloprotease that digests proteins related to PSI biogenesis and assembly factors, as well as proteins involved in CO_2 uptake.

7. References

Al Shweiki MHDR, Mönchgesang S, Majovsky P, Thieme D, Trutschel D, Hoehenwarter W: Assessment of Label-Free Quantification in Discovery Proteomics and Impact of Technological Factors and Natural Variability of Protein Abundance. *Journal of Proteome Research* **16(4)**: 1410-1424, 2017

Anbudurai PR, Pakrasi HB.: Mutational Analysis of the PsbL Protein of Photosystem II in the Cyanobacterium *Synechocystis* sp. PCC 6803. *Z. Naturforsch C*. **48c**: 267-274, 1993

Apel K, Hirt K.: Reactive oxygen species: Metabolism, Oxidative Stress, and Signal Transduction. *Annu. Rev. Plant Biol*. **55**:373–99, 2004

Aro EM, Virgin I, Andersson B.: Photoinhibition of Photosystem II. Inactivation, protein damage and turnover. *Biochimica et Biophysica Acta – Bioenergetics*, **1143(2)**: 113-134, 1993

Barber J, Kühlbrandt W. Photosystem II: *Curr Opin Struct Biol*. **9(4)**:469-75, 1999

Bartels, C.: Fast algorithm for peptide sequencing by mass spectroscopy. *Biological Mass Spectrometry*, **19(6)**: 363–368, 1990

Bateman RH, Carruthers R, Hoyes JB, Jones C, Langridge JI, Millar A, Vissers JP: A novel precursor ion discovery method on a hybrid quadrupole orthogonal acceleration time-of-flight (Q-TOF) mass spectrometer for studying protein phosphorylation. *J Am Soc Mass Spectrom*. **13(7)**:792-803, 2002

Batemann RH, Hoyes JB, Clayton EJ: Methods and apparatus for mass spectrometry. US patent no. US6717130B2, United States Patents and Trademarks Organisation, 2004

Battchikova N, Muth-Pawlak D, Aro EM. Proteomics of cyanobacteria: current horizons. *Curr Opin Biotechnol.* **54**:65-71, 2018

Bečková M, Yu J, Krynická V, Kozlo A, Shao S, Koník P, Komenda J, Murray JW, Nixon PJ: Structure of Psb29/Thf1 and its association with the FtsH protease complex involved in photosystem II repair in cyanobacteria. *Philos Trans R Soc Lond B Biol Sci*. **372(1730)**:20160394, 2017b

Bečková M, Gardian Z, Yu J, Konik P, Nixon PJ, Komenda J. Association of Psb28 and Psb27 Proteins with PSII-PSI Supercomplexes upon Exposure of *Synechocystis* sp. PCC 6803 to High Light. *Mol Plant*. **10(1)**:62-72, 2017a

Beynon RJ, Doherty MK, Pratt JM, Gaskell SJ.: Multiplexed absolute quantification In proteomics using artificial QCAT proteins of concatenated signature peptides. *Nature Methods,* **2(8)**: 587-589, 2005

Bantscheff M, Schirle M, Sweetman G. Rick J, Kuster B*:* Quantitative mass spectrometry in proteomics: a critical review. *Anal Bioanal Chem* **389**, 1017–1031, 2007

Blankenship RE.: Molecular Mechanisms of Photosynthesis. Blackwell Science Ltd, MPG Books Ltd, Bodmin, Cornwall, 2002

Braisted JC, Kuntumalla S, Vogel C, Marcotte EM, Rodrigues AR, Wang R, Huang ST, Ferlanti ES, Saeed AI, Fleischmann RD, Peterson SN, Pieper R: The APEX Quantitative Proteomics Tool: generating protein quantitation estimates from LC-MS/MS proteomics results. *BMC Bioinformatics*. **9:529**, 2008

Bricker TM, Frankel LK: The structure and function of CP47 and CP43 in Photosystem II. *Photosynthesis Research* **72**: 131–146, 2002.

Bučinská L, Kiss É, Koník P, Knoppová J, Komenda J, Sobotka R: The Ribosome-Bound Protein Pam68 Promotes Insertion of Chlorophyll into the CP47 Subunit of Photosystem II. *Plant Physiology*, **176(4)**:2931–2942, 2018

Chapman J. R.: Mass Spectrometry of Proteins and Peptides. Humana Press Inc. Totowa, New Jersey, 2000

Chen Z, Fischer L, Tahir S, Bukowski-Wills JC, Barlow P, Rappsilber J: Quantitative cross-linking/mass spectrometry reveals subtle protein conformational changes. *Wellcome Open Res*. **1:5**, 2016

Chichili V. P. R, Kumar V, Sivaraman J.: A method to trap transient and weak interacting protein complexes for structural studies. *Intrinsically Disordered Proteins*, **1**:1:e25464, 2013

Chidgey JW, Linhartová M, Komenda J, Jackson PJ, Dickman MJ, Canniffe DP, Koník P, Pilný J, Hunter CN, Sobotka R: A Cyanobacterial Chlorophyll Synthase-HliD Complex Associates with the Ycf39 Protein and the YidC/Alb3 Insertase. *The Plant Cell*, **26**: 1267–1279, 2014

Chitnis VP, Chitnis PR: PsaL subunit is required for the formation of photosystem I trimers in the cyanobacterium *Synechocystis* sp. PCC 6803. *FEBS Letters*, **336(2)**: 330-334, 1993

Chiu YF, Chu HA: New Structural and Mechanistic Insights Into Functional Roles of Cytochrome b_{559} in Photosystem II. *Front Plant Sci* **13**:914922, 2022

Combe CW, Fischer L, Rappsilber J: xiNET: cross-link network maps with residue resolution. *Mol Cell Proteomics*. **14(4)**:1137-47, 2015

Cox J, Mann M: MaxQuant enables high peptide identification rates, individualized p.p.b.-range mass accuracies and proteome-wide protein quantification. *Nature Biotechnology* **26**:1367–1372, 2008

Cox J, Neuhauser N, Michalski A, Scheltema R, Olsen J, Mann M: Andromeda: A peptide search engine integrated into the MaxQuant environment. *Journal of Proteome Research* **10**:1794–1805, 2011

Delano WL: The PyMOL Molecular Graphics System, 2002

Demichev V, Messner CB, Vernardis SI, Lilley KS, Ralser M. DIA-NN: neural networks and interference correction enable deep proteome coverage in high throughput. *Nat Methods.* **17(1)**:41-44, 2020

Domínguez-Martín MA, Sauer PV, Kirst H, Sutter M, Bína D, Greber BJ, Nogales E, Polívka T, Kerfeld CA: Structures of a phycobilisome in light-harvesting and photoprotected states. *Nature* **609**: 835–845, 2022

Ducret, A, Oostveen, I.V, Eng, J.K, Yates, J.R, III and Aebersold, R.: High throughput protein characterization by automated reverse phase chromatography/ electrospray tandem mass spectrometry. *Protein Science*, **7**: 706-719, 1998

Dühring U, Irrgang KD, Lünser K, Kehr J, Wilde A. Analysis of photosynthetic complexes from a cyanobacterial ycf37 mutant. *Biochim Biophys Acta*. **1757(1)**:3-11, 2006

Dühring U, Ossenbühl F, Wilde A: Late Assembly Steps and Dynamics of the Cyanobacterial Photosystem I*. *JBC* **282(15)**: 10915-10921, 2007

Eisenhut M, Ruth W, Haimovich M, Bauwe H, Kaplan A, Hagemann M: The photorespiratory glycolate metabolism is essential for cyanobacteria and might have been conveyed endosymbiontically to plants. *PNAS* **105(44)**:17199-204, 2008

Ekman R, Silberring J, Westman-Brinkmalm A, Kraj A.: Mass spectrometry : instrumentation, interpretation, and applications. John Wiley & Sons, Inc, Hoboken, New Jersey, 2009

Feng Y, De Franceschi G, Kahraman A, Soste M, Melnik A, Boersema PJ, de Laureto PP, Nikolaev Y, Oliveira AP, Picotti P: Global analysis of protein structural changes in complex proteomes. *Nat Biotechnol.* **32(10)**:1036-44, 2014

Fresenborg LS, Graf J, Schätzle H, Schleiff E: Iron homeostasis of cyanobacteria: advancements in siderophores and metal transporters. In Advances in cyanobacterial biology. Academic Press, 2020

Fromme P, Jordan P, Krauß N: Structure of photosystem I. *Biochimica et Biophysica Acta – Bioenergetics*, **1507(1–3)**: 5-31, 2001

Funk Ch.: Functional analysis of the PsbX protein by deletion of the corresponding gene in *Synechocystis* sp. PCC 6803. *Plant Molecular Biology* **44**:815–827, 2000

Gao L, Wang J, Ge H, Fang L, Zhang Y, Huang X, Wang Y: Toward the complete proteome of *Synechocystis* sp. PCC 6803. *Photosynth Res*, **126**: 203-219, 2015

Ge H, Fang L, Huang X, Wang J, Chen W, Liu Y, Zhang Y, Wang X, Xu W, He Q, Wang Y: Translating Divergent Environmental Stresses into a Common Proteome Response through the Histidine Kinase 33 (Hik33) in a Model Cyanobacterium. *Mol Cell Proteomics*. **16(7)**:1258-1274, 2017

Gillet LC, Navarro P, Tate S, Röst H, Selevsek N, Reiter L, Bonner R, Aebersold R: Targeted data extraction of the MS/MS spectra generated by data-independent acquisition: a new concept for consistent and accurate proteome analysis. *Mol Cell Proteomics,* **11(6)**:O111.016717, 2012

Giles K, Pringle SD, Worthington KR, Little D, Wildgoose JL, Bateman RH: Applications of a travelling wave-based radio-frequency-only stacked ring ion guide. Rapid Commun. *Mass Spectrom,* **18**: 2401-2414, 2004

Gisriel CJ, Wang J, Liu J, Flesher DA, Reiss KM, Huang HL, Yang KR, Armstrong WH, Gunner MR, Batista VS, Debus RJ, Brudvig GW: High-resolution cryo-electron microscopy structure of photosystem II from the mesophilic cyanobacterium, *Synechocystis* sp. PCC 6803. *PNAS* **119(1)**:e2116765118, 2022

Götze M, Pettelkau J, Schaks S, Bosse K, Ihling CH, Krauth F, Fritzsche R, Kühn U, Sinz A: StavroX -a software for analyzing crosslinked products in protein interaction studies. *J Am Soc Mass Spectrom.* **23(1)**:76-87, 2012

Guan S, Taylor PP, Han Z, Moran MF, Ma B. Data Dependent-Independent Acquisition (DDIA) Proteomics. *J Proteome Res,* **19(8)**:3230-3237, 2020

Jayachandran B, Parvin TN, Alam MM, Chanda K, Mm B: Insights on Chemical Crosslinking Strategies for Proteins. *Molecules* **27(23)**:8124, 2022

He Q, Dolganov N, Bjorkman O, Grossman AR: The high light-inducible polypeptides in *Synechocystis* PCC6803. Expression and function in high light. *J Biol Chem*. **276(1)**:306-14, 2001

Henzel W. J, Watanabe C, Stults J.T.: Protein Identification: The Origins of Peptide Mass Fingerprinting. *J Am Soc Mass Spectrom* **14**: 931–942, 2003

Hu A, Noble WS and Wolf-Yadlin A. Technical advances in proteomics: new developments in data-independent acquisition [version 1; peer review: 3 approved]. *F1000Research* **5**(F1000 Faculty Rev):419, 2016

Huang G, Xiao Y, Pi X, Zhao L, Zhu Q, Wang W, Kuang T, Han G, Sui SF, Shen JR: Structural insights into a dimeric Psb27-photosystem II complex from a cyanobacterium *Thermosynechococcus vulcanus*. *PNAS* **118(5)**: e2018053118, 2021

Ido K, Kakiuchi S, Uno Ch, Nishimura T, Fukao Y, Noguchi T, Sato F, Ifuku K: The Conserved His-144 in the PsbP Protein Is Important for the Interaction between the PsbP N-terminus and the Cyt b 559 Subunit of Photosystem II. *JBC* **287(31)**: 26377–26387, 2012

Iwai M, Suzuki T, Kamiyama A, Sakurai I, Dohmae N, Inoue Y, Ikeuchi M: The PsbK Subunit is Required for the Stable Assembly and Stability of Other Small Subunits in the PSII complex in the Thermophilic Cyanobacterium *Thermosynechococcus elongatus* BP-1. *Plant Cell Physiol* **51(4)**: 554-560, 2010

Jackson PJ, Hitchcock A, Brindley AA, Dickman MJ, Hunter CN: Absolute quantification of cellular levels of photosynthesis-related proteins in *Synechocystis* sp. PCC 6803. *Photosynth Res*. **155(3)**:219-245, 2022

Kanehisa M, Furumichi M, Sato Y, Ishiguro-Watanabe M, Tanabe M: KEGG: integrating viruses and cellular organisms. *Nucleic Acids Res*. **49(D1)**:D545-D551, 2021

Katayama, M.: Chapter 2 - Fundamental physiological processes: Photosynthesis, light-harvesting complex, and carbon-concentrating mechanisms. Editors: Hakuto Kageyama, Rungaroon Waditee-Sirisattha, Academic Press, 2022

Kaneko T, Sato S, Kotani H, Tanaka A, Asamizu E, Nakamura Y, Miyajima N, Hirosawa M, Sugiura M, Sasamoto S, Kimura T, Hosouchi T, Matsuno A, Muraki A, Nakazaki N, Naruo K, Okumura S, Shimpo S, Takeuchi C, Wada T, Watanabe A, Yamada M, Yasuda M, Tabata S: Sequence Analysis of the Genome of the Unicellular Cyanobacterium *Synechocystis* sp. Strain PCC6803. II. Sequence Determination of the Entire Genome and Assignment of Potential Protein-coding Regions , *DNA Research*, **3**(3):109–136, 1996,

Katoh H, Hagino N, Grossman AR, Ogawa T. Genes essential to iron transport in the cyanobacterium *Synechocystis* sp. strain PCC 6803. *J Bacteriol* **183(9)**:2779-84, 2001

Kawakami K, Umena Y, Iwai M, Kawabata Y, Ikeuchi M, Kamiya N, Shen J.R.: Roles of PsbI and PsbM in photosystem II dimer formation and stability studied by deletion mutagenesis and X-ray crystallography. *BBA - Bioenergetics* **1807(3)**: 319-325, 2011

Keren N, Berg A, van Kan PJM, Levanon H, Ohad I.: Mechanism of photosystem II photoinactivation and D1 protein degradation at low light: The role of back electron flow. *PNAS* **94(4)**: 1579–1584, 1997

Kiss É, Knoppová J, Aznar GP, Pilný J, Yu J, Halada P, Nixon PJ, Sobotka R, Komenda J. A Photosynthesis-Specific Rubredoxin-Like Protein Is Required for Efficient Association of the D1 and D2 Proteins during the Initial Steps of Photosystem

II Assembly. *Plant Cell.* **31(9)**:2241-2258, 2019

Kiss É, Talbot J, Adams NBP, Opekar S, Moos M, Pilný J, Kvasov T, Schneider E, Koník P, Šimek P, Sobotka R. Chlorophyll biosynthesis under the control of arginine metabolism. *Cell Rep*. **42(11)**:113265, 2023

Kłodawska K, Kovács L, Várkonyi Z, Kis M, Sozer Ö, Laczkó-Dobos H, Kóbori O, Domonkos I, Strzałka K, Gombos Z, Malec P.: Elevated growth temperature can enhance photosystem I trimer formation and affects xanthophyll biosynthesis in Cyanobacterium *Synechocystis* sp. PCC6803 cells. *Plant Cell Physiol.* **56(3)**:558-71, 2015

Knoppová J, Sobotka R, Tichý M, Yu J, Koník P, Halada P, Nixon P. J, Komenda J.: Discovery of a Chlorophyll Binding Protein Complex Involved in the Early Steps of Photosystem II Assembly in Synechocystis. *The Plant Cell*, **26**: 1200–1212, 2014

Knoppová J, Yu J, Koník P, Nixon PJ, Komenda J: CyanoP is Involved in the Early Steps of Photosystem II Assembly in the Cyanobacterium Synechocystis sp. PCC 6803. *Plant and Cell Physiology*, **57(9)**:1921–1931, 2016

Knoppová J, Sobotka R, Yu J, Bečková M, Pilný J, Trinugroho JP, Csefalvay L, Bína D, Nixon PJ, Komenda J. Assembly of D1/D2 complexes of photosystem II: Binding of pigments and a network of auxiliary proteins. *Plant Physiol.* **189(2)**:790-804, 2022–

Komenda J, Knoppová J, Kopečná J, Sobotka R, Halada P, Yu J, Nickelsen J, Boehm M, Nixon P. J.: The Psb27 Assembly Factor Binds to the CP43 Complex of Photosystem II in the Cyanobacterium *Synechocystis* sp. PCC 6803. *Plant Physiol* **158(1)**: 476–486, 2012b

Komenda J, Nickelsen J, Tichý M, Prášil O, Eichacker LA, Nixon PJ: The Cyanobacterial Homologue of HCF136/YCF48 Is a Component of an Early Photosystem II Assembly Complex and Is Important for Both the Efficient Assembly and Repair of Photosystem II in *Synechocystis* sp. PCC 6803. *JBC* **283**: 22390-22399, 2008

Komenda J, Sobotka R. Cyanobacterial high-light-inducible proteins--Protectors of chlorophyll-protein synthesis and assembly. *Biochim Biophys Acta.* **1857(3)**:288-95, 2016

Komenda J, Sobotka R: Chlorophyll-binding subunits of photosystem I and II: Biosynthesis, chlorophyll incorporation and assembly. *Advances in Botanical Research,* 2019

Komenda J, Sobotka R, Nixon PJ.: Assembling and maintaining the Photosystem II complex in chloroplasts and cyanobacteria. *Current Opinion in Plant Biology* **15**: 245–251, 2012

Komenda J, Tichý M, Eichacker LA.: The PsbH protein is associated with the inner antenna CP47 and facilitates D1 processing and incorporation into PSII in the cyanobacterium *Synechocystis* PCC 6803. *Plant Cell Physiol.* **46(9)**: 1477–1483, 2005

Konert, MM, Wysocka, A, Koník, P. Sobotka, R: High-light-inducible proteins HliA and HliB: pigment binding and protein–protein interactions. *Photosynth Res* **152**, 317–332, 2022

Koník P, Skotnicová P, Gupta S, Tichý M, Sharma S, Komenda J, Sobotka R, Krynická V: The cyanobacterial FtsH4 protease controls accumulation of protein factors involved in the biogenesis of photosystem I. *Biochim Biophys Acta Bioenerg*. **1865(1)**:149017, 2024

Kopečná J, Komenda J, Bučinská L, Sobotka R: Long-term acclimation of the cyanobacterium *Synechocystis* sp. PCC 6803 to high light is accompanied by an enhanced production of chlorophyll that is preferentially channeled to trimeric photosystem I. *Plant Physiol*. **160(4)**:2239-50, 2012

Kopečná J, Sobotka R, Komenda J.: Inhibition of chlorophyll biosynthesis at the protochlorophyllide reduction step results in the parallel depletion of Photosystem I and Photosystem II in the cyanobacterium *Synechocystis* PCC 6803. *Planta* **237:**497-508, 2013

Koksharova OA, Wolk CP: Genetic tools for cyanobacteria. *Appl Microbiol Biotechnol*. **58(2)**:123-37, 2002

Krynická V, Skotnicová P, Jackson PJ, Barnett S, Yu J, Wysocka A, Kaňa R, Dickman MJ, Nixon PJ, Hunter CN, Komenda J. FtsH4 protease controls biogenesis of the PSII complex by dual regulation of high light-inducible proteins. *Plant Commun.* **9;4(1)**:100502, 2023

Lapthorn C, Pullen F, Chowdhry BZ: Ion mobility spectrometry-mass spectrometry (IMS-MS) of small molecules: separating and assigning structures to ions. *Mass Spectrom Rev*. **32(1)**:43-71, 2013

Leitner A, Walzthoeni T, Kahraman A, Herzog F, Rinner O, Beck M, Aebersold R.: Probing Native Protein Structures by Chemical Cross-linking, Mass Spectrometry, and Bioinformatics. *Mol Cell Proteomics*. **9(8)**: 1634–1649, 2010

Li M, Calteau A, Semchonok DA, Witt TA, Nguyen JT, Sassoon N, Boekema EJ, Whitelegge J, Gugger M, Bruce BD: Physiological and evolutionary implications of tetrameric photosystem I in cyanobacteria. *Nat Plants*. **5(12)**:1309-1319, 2019

Liu H, Huang RY, Chen J, Gross ML, Pakrasi HB. Psb27, a transiently associated protein, binds to the chlorophyll binding protein CP43 in photosystem II

assembly intermediates. *PNAS* **108(45)**:18536-41, 2011

Liu H, Zhang H, Weisz DA, Vidavsky I, Gross ML, Pakrasi HB: MS-based cross-linking analysis reveals the location of the PsbQ protein in cyanobacterial photosystem II. *PNAS* **111(12)**: 4638–4643, 2014

Liu L, Chen X, Zhang Y, Zhou B: Characterization, structure and function of linker polypeptides in phycobilisomes of cyanobacteria and red algae: An overview. *Biochimica et Biophysica Acta (BBA) – Bioenergetics*, **1708(2)**:133-142, 2005

Liu S, Li Z, Yu B, Wang S, Shen Y, Cong H: Recent advances on protein separation and purification methods. *Adv Colloid Interface Sci,* **284**:102254, 2020

Liu X, Sirotkin Y, Shen Y, Anderson G, Tsai YS, Ting YS, Goodlett DG, Smith RD, Bafna V, Pevzner PA.: Protein Identification Using Top-Down Spectra. *Molecular & Cellular Proteomics*, **11**: M111.008524, 2012

Mann M, Hendrickson RC, Pandey A: Analysis of Proteins and Proteomes by Mass Spectrometry. *Annual Review of Biochemistry*, **70(1)**: 437–473, 2001

Masojídek J, Torzillo G. Koblížek M: Photosynthesis in Microalgae. In Handbook of Microalgal Culture (eds A. Richmond and Q. Hu). 2013

Meetam M, Keren N, Ohad I, Pakrasi H. B.: The PsbY Protein Is Not Essential for Oxygenic Photosynthesis in the Cyanobacterium Synechocystis sp. PCC 6803. *Plant Physiol*. **121(4)**: 1267–1272, 1999

Mistry J, Chuguransky S, Williams L, Qureshi M, Salazar GA, Sonnhammer ELL, Tosatto SCE, Paladin L, Raj S, Richardson LJ, Finn RD, Bateman A: Pfam: The protein families database in 2021 *Nucleic Acids Research, **49(D1)**:*D412–D419, 2020

Murakami R, Ifuku K, Takabayashi A, Shikanai T, Endo T, Sato F: Characterization of an *Arabidopsis thaliana* mutant with impaired psbO, one of two genes encoding extrinsic 33-kDa proteins in photosystem II. *FEBS Letters* **532**: 138-142, 2002

Nellaepalli S, Ozawa SI, Kuroda H, Takahashi Y: The photosystem I assembly apparatus consisting of Ycf3-Y3IP1 and Ycf4 modules. *Nat Commun.* **9(1)**:2439, 2018

Nowaczyk MM, Krause K, Mieseler M, Sczibilanski A, Ikeuchi M, Rögner M: Deletion of psbJ leads to accumulation of Psb27–Psb28 photosystem II complexes in *Thermosynechococcus elongatus*. *BBA – Bioenergetics* **1817(8)**: 1339-1345, 2012

Nixon PJ, Barker M, Boehm M, de Vries R, Komenda J. FtsH-mediated repair of the photosystem II complex in response to light stress. J Exp Bot. 2005 Jan;56(411):357-63

Nixon PJ, Michoux F, Yu J, Boehm M, Komenda J: Recent advances in understanding the assembly and repair of photosystem II. *Annals of Botany* **106**: 1–16, 2010

Ong SE, Blagoev B, Kratchmarova I, Kristensen DB, Steen H, Pandey A, Mann M: Stable isotope labeling by amino acids in cell culture, SILAC, as a simple and accurate approach to expression proteomics. *Mol Cell Proteomics*. **1(5)**:376-86, 2002

Opatíková M, Semchonok DA, Kopečný D, Ilík P, Pospíšil P, Ilíková I, Roudnický P, Zeljković SĆ, Tarkowski P, Kyrilis FL, Hamdi F, Kastritis PL, Kouřil R: Cryo-EM structure of a plant photosystem II supercomplex with light-harvesting protein Lhcb8 and α-tocopherol. *Nat Plants* **9(8)**:1359-1369, 2023

Pappireddi N, Martin L, Wühr M: A Review on Quantitative Multiplexed Proteomics. *Chembiochem*. **20(10)**:1210-1224, 2019

Rappsilber J, Mann M & Ishihama Y.: Protocol for micro-purification, enrichment, pre-fractionation and storage of peptides for proteomics using StageTips. *Nat Protoc* **2**, 1896–1906, 2007

Rappsilber J: The beginning of a beautiful friendship: Cross-linking/mass spectrometry and modelling of proteins and multi-protein complexes. *Journal of Structural Biology* **173**: 530–540, 2011

Rinner O, Seebacher J, Walzthoeni T, Mueller L, Beck M, Schmidt A, Mueller M, Aebersold R: Identification of cross-linked peptides from large sequence databases. *Nature Methods* **5(4)**: 315-318, 2008

Rosenfeld, J, Capdevielle, J, Guillemot, J. C, Ferrara, P.: In-gel digestion of proteins for internal sequence analysis after one- or two-dimensional gel electrophoresis. *Analytical Biochemistry*, **203(1)**: 173-179, 1992

Rozanova S, Barkovits K, Nikolov M, Schmidt C, Urlaub H, Marcus K: Quantitative Mass Spectrometry-Based Proteomics: An Overview. In: Marcus, K, Eisenacher, M, Sitek, B. (eds) Quantitative Methods in Proteomics. *Methods in Molecular Biology*, **2228**. Humana, New York, NY, 2021

Santoni V, Molloy M, Rabilloud T.: Membrane proteins and proteomics: Un amour impossible?. *Electrophoresis*, 21: 1054-1070, 2000

Sánchez-Baracaldo P, Cardona T: On the origin of oxygenic photosynthesis and Cyanobacteria. *New Phytol*, **225**: 1440-1446, 2020

Sazuka T, Ohara O: Towards a proteome project of cyanobacterium *Synechocystis* sp. strain PCC6803: Linking 130 protein spots with their respective genes. *Electrophoresis*, **18(8)**: 1252–1258, 1997

Shevchenko A, Wilm M, Vorm O, Mann M. Mass spectrometric sequencing of

proteins silver-stained polyacrylamide gels. *Anal Chem*. **1;68(5)**:850-858, 1996

Shevchenko, A, Tomas, H, Havli, J. *et al.* In-gel digestion for mass spectrometric characterization of proteins and proteomes. *Nat Protoc* **1**, 2856–2860, 2006

Shi LX, Kim SJ, Marchant A, Robinson C, Schröder WP: Characterisation of the PsbX protein from Photosystem II and light regulation of its gene expression in higher plants. *Plant Mol Biol*. **40(4)**:737-44, 1999

Schopf WJ: The paleobiological record of photosynthesis. *Photosynth Res*. **107(1)**:87-101, 2011

Schopper S, Kahraman A, Leuenberger P, Feng Y, Piazza I, Müller O, Boersema P, Picotti P: Measuring protein structural changes on a proteome-wide scale using limited proteolysis-coupled mass spectrometry. *Nature Protocols*. **12**: 2391-2410, 2017

Schroeder M, Meyer SW, Heyman HM, Barsch A, Sumner LW.: Generation of a Collision Cross Section Library for Multi-Dimensional Plant Metabolomics Using UHPLC-Trapped Ion Mobility-MS/MS. *Metabolites*. **10(1)**:13, 2020

Schmidt, T., Skerra, A: The *Strep*-tag system for one-step purification and high-affinity detection or capturing of proteins. *Nat Protoc* **2**, 1528–1535, 2007

Shvartsburg AA, Smith RD. Fundamentals of traveling wave ion mobility spectrometry. *Anal Chem*. **80(24)**:9689-99, 2008

Simpson RJ: Proteins and Proteomics. A laboratory Manual. Cold Spring Harbor Laboratory Press, Cold Spring Harbor, New York, 2003

Spriestersbach A, Kubicek J, Schaefer F, Block H, Maertens, B.: Chapter One - Purification of His-Tagged Proteins. *Methods in Enzymology,* Academic Press, **559**: 1-15, 2015

Swiatek M, Kuras R, Sokolenko A, Higgs D, Olive J, Cinque G, Müller B, Eichacker LA, Stern DB, Bassi R, Herrmann RG, Wollman FA.: The Chloroplast Gene ycf9 Encodes a Photosystem II (PSII) Core Subunit, PsbZ, That Participates in PSII Supramolecular Architecture. *The Plant Cell* **13(6)**: 1347-1368, 2001

Tang XS, Fushimi K, Satoh K: Dl-D2 complex of the photosystem II reaction center from spinach Isolation and partial characterization. *FEBS Letters* **273**: 257-260, 1990

Terentyev VV: Macromolecular conformational changes in photosystem II: interaction between structure and function. *Biophys Rev*. **14(4)**:871-886 2022

Terpe K: Overview of tag protein fusions: from molecular and biochemical

fundamentals to commercial systems. *Appl Microbiol Biotechnol* **60**:523–533, 2003

Torabi S, Umate P, Manavski N, Plöchinger M, Kleinknecht L, Bogireddi H, Herrmann R. G, Wanner G, Schröder W. P.: PsbN Is Required for Assembly of the Photosystem II Reaction Center in *Nicotiana tabacum.The Plant Cell* **26(3)**: 1183-1199, 2014

Tyanova S, Temu T, Cox J: The MaxQuant computational platform for mass spectrometry-based shotgun proteomics. *Nature Protocols* **11**:2301–2319, 2016a

Tyanova S, Temu T, Sinitcyn P, Carlson A, Hein MY, Geiger T, Mann M, Cox J: The Perseus computational platform for comprehensive analysis of (prote)omics data. *Nature Methods* **13**:731–740, 2016b

Uetrecht C, Rose RJ, van Duijn E, Lorenzen K, Heck AJ: Ion mobility mass spectrometry of proteins and protein assemblies. *Chem Soc Rev*. **39(5)**:1633-55, 2010

Umena Y, Kawakami K, Shen JR, Kamiya N: Crystal structure of oxygen-evolving photosystem II at a resolution of 1.9 Å. *Nature* **473**: 55-61, 2011

Urban PL: Quantitative mass spectrometry: an overview. *Philos Trans A Math Phys Eng Sci*. **374(2079)**:20150382, 2016

Weisz DA, Liu H, Zhang H, Thangapandian S, Tajkhorshid E, Gross ML, Pakrasi HB: Mass spectrometry-based cross-linking study shows that the Psb28 protein binds to cytochrome b_{559} in Photosystem II. *PNAS* **114(9)**:2224-2229, 2017

Wiese S, Reidegeld KA, Meyer HE, Warscheid B. Protein labeling by iTRAQ: a new tool for quantitative mass spectrometry in proteome research. *Proteomics*. **7(3)**:340-50, 2007

Wiśniewski J, Zougman A, Nagaraj N, Mann M: Universal sample preparation method for proteome analysis. *Nat Methods* **6**: 359–362, 2009

Yılmaz Ş, Shiferaw GA, Rayo J, Economou A, Martens L, Vandermarliere E: Cross-linked peptide identification: A computational forest of algorithms. *Mass Spec Rev*. **37**: 738– 749, 2018

Yılmaz Ş, Busch F, Nagaraj N, Cox J: Accurate and Automated High-Coverage Identification of Chemically Cross-Linked Peptides with MaxLynx. *Anal Chem*. **25;94(3)**:1608-1617, 2022

Zabret J, Bohn S, Schuller SK, Arnolds O, Möller M, Meier-Credo J, Liauw P, Chan A, Tajkhorshid E, Langer JD, Stoll R, Krieger-Liszkay A, Engel BD, Rudack T, Schuller JM, Nowaczyk MM: Structural insights into photosystem II assembly.

Nat Plants **7(4)**:524-538, 2021

Zhao Z, Vercellino I, Knoppová J, Sobotka R, Murray JW, Nixon PJ, Sazanov LA, Komenda J: The Ycf48 accessory factor occupies the site of the oxygen-evolving manganese cluster during photosystem II biogenesis. *Nat Commun* **14**:4681, 2023

8. Appendix (published results)

PCP
PLANT & CELL PHYSIOLOGY

CyanoP is Involved in the Early Steps of Photosystem II Assembly in the Cyanobacterium *Synechocystis* sp. PCC 6803

Jana Knoppová[1,2], Jianfeng Yu[3], Peter Konik[1,2], Peter J. Nixon[3] and Josef Komenda[1,*]

[1]Institute of Microbiology, Center Algatech, Opatovický mlýn, 37981 Třeboň, Czech Republic
[2]Faculty of Science, University of South Bohemia, Branišovská 1760, 370 05 České Budějovice, Czech Republic
[3]Department of Life Sciences, Sir Ernst Chain Building-Wolfson Laboratories, Imperial College London, South Kensington Campus, London SW7 2AZ, UK
*Corresponding author: E-mail, komenda@alga.cz; Tel, +420 384340415.
(Received March 23, 2016; Accepted June 8, 2016)

Regular Paper

Although the PSII complex is highly conserved in cyanobacteria and chloroplasts, the PsbU and PsbV subunits stabilizing the oxygen-evolving Mn_4CaO_5 cluster in cyanobacteria are absent in chloroplasts and have been replaced by the PsbP and PsbQ subunits. There is, however, a distant cyanobacterial homolog of PsbP, termed CyanoP, of unknown function. Here we show that CyanoP plays a role in the early stages of PSII biogenesis in *Synechocystis* sp. PCC 6803. CyanoP is present in the PSII reaction center assembly complex (RCII) lacking both the CP47 and CP43 modules and binds to the smaller D2 module. A small amount of larger PSII core complexes co-purifying with FLAG-tagged CyanoP indicates that CyanoP can accompany PSII on most of its assembly pathway. A role in biogenesis is supported by the accumulation of unassembled D1 precursor and impaired formation of RCII in a mutant lacking CyanoP. Interestingly, the pull-down preparations of CyanoP-FLAG from a strain lacking CP47 also contained PsbO, indicating engagement of this protein with PSII at a much earlier stage in assembly than previously assumed.

Keywords: Cyanobacteria • CyanoP • Photosynthesis • Photosystem II • PsbP • *Synechocystis*.

Abbreviations: BN, Blue Native; CN, Clear Native; Hlip, high-light inducible protein; MS, mass spectrometry; OD, optical density; RCII, PSII reaction center assembly complex; RCC(2) and RCC(1), dimeric and monomeric PSII core complexes; WT, wild type.

Introduction

PSII is the multisubunit enzyme complex responsible for the highly energetically demanding water-splitting reaction of oxygenic photosynthesis. Isolated PSII complexes comprise four large membrane-intrinsic protein subunits involved in pigment and cofactor binding, 13 small polypeptides and three extrinsic subunits bound to the lumenal side of the complex. PSII biogenesis, as demonstrated in the cyanobacterium *Synechocystis* sp. PCC 6803 (hereafter *Synechocystis*), occurs in a step-wise process from smaller pre-complexes or modules (Nixon et al. 2010, Komenda et al. 2012a). Each module consists of one large subunit (D1, D2, CP47 and CP43), one or more low molecular mass subunits, pigments and other cofactors, and assembly factors. PSII assembly is initiated through interaction of the D1 and D2 modules to form the reaction center assembly complex, RCII (Komenda et al. 2008, Knoppová et al. 2014). The CP47 module is then attached to form the RC47 complex (Boehm et al. 2011, Boehm et al. 2012), followed by the CP43 module (Boehm et al. 2011) to give the monomeric non-oxygen-evolving reaction center core complex, RCC(1). The light-driven assembly of the oxygen-evolving oxo-metal cluster, attachment of the lumenal extrinsic subunits and PSII dimerization, give rise to the fully active complex (Komenda et al. 2008, Nixon et al. 2010).

The composition of the lumenal subunits surrounding the oxygen-evolving cluster differs between oxygenic autotrophs. In cyanobacteria, it consists of PsbO, PsbU and PsbV proteins, while in plants and green algae PsbU and PsbV have been replaced by structurally different proteins, PsbQ and PsbP. Cyanobacteria do possess homologs of PsbP and PsbQ, called CyanoP and CyanoQ (Kashino et al. 2002, De Las Rivas et al. 2004, Thornton et al. 2004). However, neither of them has been found in crystallographic studies of cyanobacterial PSII (Guskov et al. 2009, Umena et al. 2011), and their locations and roles are apparently different from those of their eukaryotic relatives (Fagerlund and Eaton-Rye 2011, Cormann et al. 2014, Liu et al. 2014, Ifuku 2015). Moreover, both CyanoP and CyanoQ are modified by lipidation, a feature absent in PsbP and PsbQ (Thornton et al. 2004, Fagerlund and Eaton-Rye 2011).

While CyanoQ is considered a constitutive component of highly active PSII (Kashino et al. 2002, Roose et al. 2007) and possibly contributes to PSII dimer stability (Liu et al. 2014), the location and role of CyanoP remain unclear. The results of physiological studies on *Synechocystis* mutants lacking CyanoP are rather inconsistent and do not reveal a clear phenotype that would indicate a function for the protein (Thornton et al. 2004, Ishikawa et al. 2005, Summerfield et al. 2005, Aoi et al. 2014). However, competitive growth experiments between different CyanoP mutant strains and the wild type (WT) showed a selective advantage for the presence of CyanoP even under mild laboratory growth conditions, confirming its functional significance (Sveshnikov et al. 2007). The same authors demonstrated an altered PSII charge recombination pattern in the mutants suggesting that the absence of CyanoP affects the donor side of PSII. The examination of a

Plant Cell Physiol. 57(9): 1921–1931 (2016) doi:10.1093/pcp/pcw115, Advance Access publication on 7 July 2016, available online at www.pcp.oxfordjournals.org

double mutant lacking both CyanoP and the PSII assembly factor Ycf48 showed just a minor additive affect of CyanoP deletion on the severe phenotype displayed by the *ycf48* mutant, with only small changes in the levels of PSII assembly complexes observed (Jackson and Eaton-Rye 2015). A possible role for CyanoP of *Thermosynechococcus elongatus* in PSII biogenesis has been recently indicated by in vitro protein interaction analysis employing surface plasmon resonance spectroscopy (Cormann et al. 2014). The authors localized the CyanoP-binding site in the center of PSII, at a position occupied by the PsbO subunit in the mature complex. In addition, in vitro reconstitution experiments showed selective binding of CyanoP to the inactive PSII monomer lacking PsbO, PsbV and PsbU. These findings indicate that CyanoP functions rather in the PSII life cycle than in the mature complex itself. However, the overall evidence linking CyanoP to the biogenesis or function of PSII is still not compelling.

In the present study, we show that the *Synechocystis* CyanoP is involved in the early steps of PSII assembly. We provide evidence for its association with the RCII assembly complex. Our results indicate that it probably binds to the D2 assembly module and assists in its interaction with the D1 module to optimize formation of the RCII assembly complex. Nevertheless, our experiments also show that the protein accompanies PSII further on its assembly pathway.

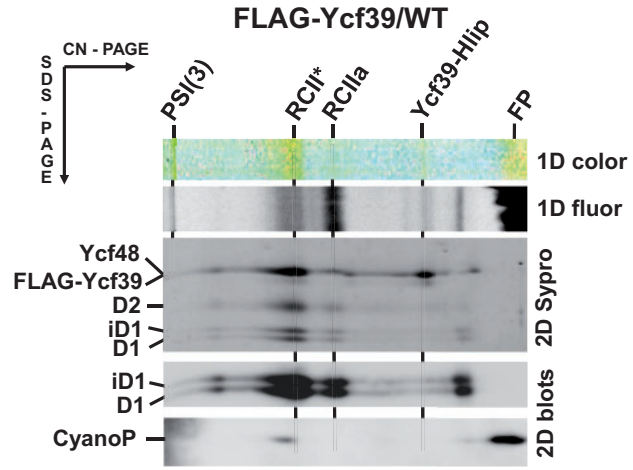

Fig. 1 CyanoP is present in the RCII* complex isolated from the strain expressing FLAG-Ycf39. The preparation isolated using anti-FLAG affinity gel was analyzed by 2D CN/SDS–PAGE. The native gel was photographed (1D color) and scanned for fluorescence (1D fluor). The 2D gel was stained by Sypro Orange (2D Sypro), electroblotted to a PVDF, [poly(vinylidene fluoride)] membrane and probed with antibodies specific for D1 and CyanoP (2D blots). The identity of other designated proteins was confirmed previously in Knoppová et al. (2014). Complexes are designated as follows: PSI(3), trimeric Photosystem I; RCII* and RCIIa, PSII reaction center assembly intermediates lacking CP47 and CP43; Yf39–Hlip, a complex of FLAG-Ycf39, HliC and HliD; FP, free pigments.

Results

Identification of CyanoP as a component of the PSII reaction center assembly complex

Previous work has shown that a *Synechocystis* mutant unable to synthesize the inner antenna CP47 cannot form the PSII core complex (RCC) and instead accumulates two forms of the PSII reaction center assembly complex, designated RCII* and RCIIa (Komenda et al. 2004, Dobáková et al. 2007, Komenda et al. 2008) (**Supplementary Fig. S1**). These assembly intermediates are present in low quantities in the WT and differ in size due to the presence of additional protein components (Knoppová et al. 2014). Our recent studies have revealed that the larger RCII* complex binds the accessory Ycf39–Hlip complex implicated in photoprotection and in Chl delivery to newly synthesized D1 (Knoppová et al. 2014, Staleva et al. 2015). Using a FLAG-tagged derivative of Ycf39, we were able to purify the RCII* complex from both the WT and a CP47-less strain (Knoppová et al. 2014). Protein analysis of the obtained RCII preparations using 2D Clear Native (CN)/SDS–PAGE followed by immunoblotting surprisingly revealed the presence of the CyanoP protein (**Fig. 1**; **Supplementary Fig. S2**), implying its involvement at an early step of PSII biogenesis. The position of the Cyano-P band under the RCII* complex is slightly shifted to a higher mass in comparison with the center of the RCII*, but this could be explained by an increase in the size of RCII* due to the bound CyanoP.

In order to confirm the association of CyanoP with RCII*, we constructed a CP47-less strain expressing FLAG-tagged CyanoP instead of the native protein (CyanoP-FLAG/ΔCP47). Given that CyanoP in *Synechocystis* is thought to be lipidated at the N-terminus (Thornton et al. 2004), the FLAG-tag was fused to the C-terminus. Purification of FLAG-tagged CyanoP under native conditions resulted in co-isolation of both forms of RCII as shown using 2D CN/SDS–PAGE (**Fig. 2**). The presence of the key RCII components including the accessory factors Ycf48 and Ycf39 was confirmed by mass spectrometry (MS) (**Fig. 2**; **Supplementary Table S1**). Moreover, both monomeric and trimeric forms of PSI were also found in the preparation. Remarkably, the PsbO extrinsic PSII subunit, which stabilizes the oxygen-evolving cluster, was also detected by MS sequencing. It is apparent from **Fig. 2** that most of the CyanoP-FLAG migrates as a free protein. This indicates both that the protein is present in an unassembled form and that its binding to the membrane complexes is rather weak so that it detaches during manipulations with the isolated preparation and/or during the native PAGE. A noteworthy feature of unassembled CyanoP as well as CyanoP-FLAG (**Figs. 1** and **2**, respectively) is their very fast migration in the native gel at the position of free pigments, unusual in comparison with other unassembled PSII-related proteins. This phenomenon is hard to explain; we can only speculate that the protein may attain an unusual conformation or may specifically bind charged detergents, which give it the characteristically high rate of migration.

As CyanoP has previously been assumed to associate with the fully assembled oxygen-evolving PSII complex and not with assembly complexes (Thornton et al. 2004, Ishikawa et al. 2005),

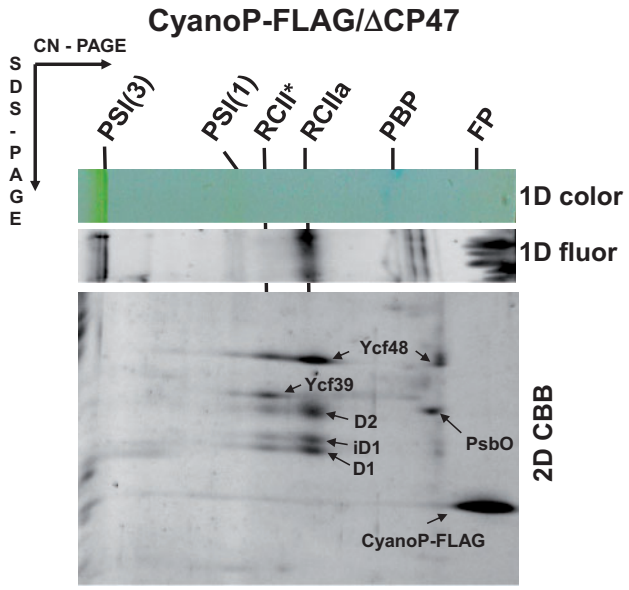

Fig. 2 RCII complexes co-purify with CyanoP-FLAG isolated from the strain expressing FLAG-tagged CyanoP and lacking CP47. The preparation isolated using anti-FLAG affinity resin was analyzed by 2D CN/SDS–PAGE. The native gel was photographed (1D color) and scanned for fluorescence (1D fluor). The 2D gel was stained by Coomassie Brilliant Blue (2D CBB) and designated proteins were identified by mass spectrometry. Complexes are designated as follows: PSI(3) and PSI(1), trimeric and monomeric PSI; RCII* and RCIIa, two PSII reaction center assembly intermediates lacking CP47 and CP43; PBP, fragment of phycobilisomes; FP, free pigments.

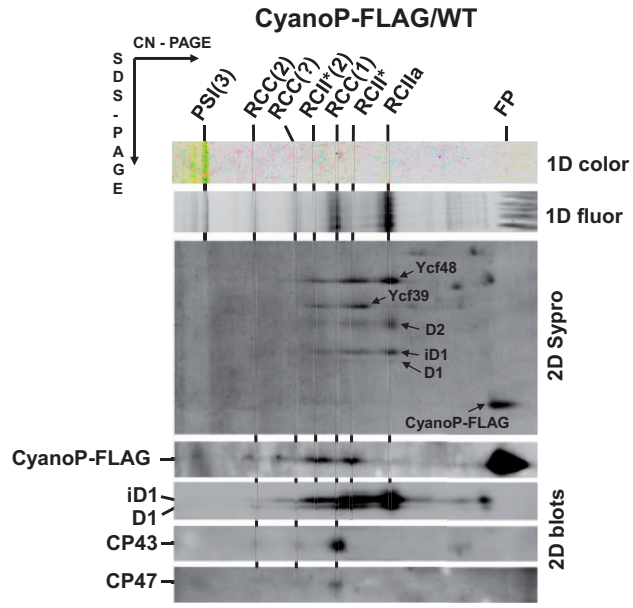

Fig. 3 RCII complexes and a small amount of PSII core co-purify with FLAG-tagged CyanoP expressed in the WT. The preparation isolated using anti-FLAG affinity resin was analyzed by 2D CN/SDS–PAGE. The CN gel was photographed (1D color) and scanned for fluorescence (1D fluor). The 2D gel was stained by Sypro Orange (2D Sypro) and immunoblotted (2D blots). Alternatively, the 2D gel was stained by Coomassie Brilliant Blue (not shown) and proteins designated here by arrows were identified by MS. Complexes are designated as in **Fig. 1**. RCC(2) and RCC(1) are dimeric and monomeric PSII core complexes; RCC(?) is an unusual RCC complex having mobility between that of the dimeric and monomeric form; RCII*(2) is a putative dimer of RCII*.

we also purified CyanoP-FLAG from the WT background (strain CyanoP-FLAG/WT). As shown in **Fig. 3**, CyanoP-FLAG again co-purified mainly with RCII complexes, although there was now also a small amount of highly fluorescing monomeric and dimeric PSII core complexes [RCC(1) and RCC(2), respectively] in the preparation as judged from CP47 and CP43 immunoblots. The relatively strong fluorescence signal of the RCCs on the native gel cannot be considered a measure of the abundance of this complex compared with RCII*, as the fluorescence of the latter is very low due to its quenching related to the attached Ycf39–Hlip complex (Knoppová et al. 2014, Staleva et al. 2015). Again the preparation contained small amounts of PSI and most CyanoP-FLAG migrated as an unassembled protein. Importantly, a FLAG-specific antibody showed an enhanced signal of CyanoP-FLAG in the region of the larger RCII complexes, confirming a more stable interaction of the protein with these complexes in agreement with **Fig. 1**. These results again support the view that CyanoP is mainly involved in biogenesis rather than as a component of the final fully active PSII complex.

The main evidence linking CyanoP to PSII comes from previous work reporting the loss of CyanoP accumulation in a PSII mutant (*psbDIC*/*psbDII* deletion strain) lacking both the D2 and CP43 subunits (Ishikawa et al. 2005). We therefore screened various PSII defective mutants using one-dimensional SDS–PAGE followed by CyanoP immunodetection (**Supplementary Fig. S3**). CyanoP was unambiguously detected in all the tested strains, including the *psbDIC*/*psbDII* deletion strain, designated here as ΔD2/ΔCP43. Indeed, CyanoP was present at higher levels in most of the PSII-less mutants (namely in the strains lacking D1 or CP47) in comparison with the WT, which again supports its role in the assembly of PSII rather than in the functioning of the mature complex.

CyanoP-FLAG interacts with the D2 assembly module and with CP43

In order to determine more precisely the potential binding partner(s) of CyanoP among the proteins involved in early PSII biogenesis, the CyanoP-FLAG construct was transformed into ΔD1 and ΔD2/ΔCP43 strains incapable of forming the reaction center assembly complex due to the lack of one of the key subunits. The resulting strains were designated as CyanoP-FLAG/ΔD1 and CyanoP-FLAG/ΔD2/ΔCP43, respectively. As shown in **Fig. 4**, FLAG-tagged CyanoP isolated from the strain lacking D1 co-purified with D2 and PsbE, which indicates that CyanoP could enter the RCII assembly complex as a component of the D2 assembly module. Surprisingly, the preparation also contained small amounts of CP43. Similar to the preparation

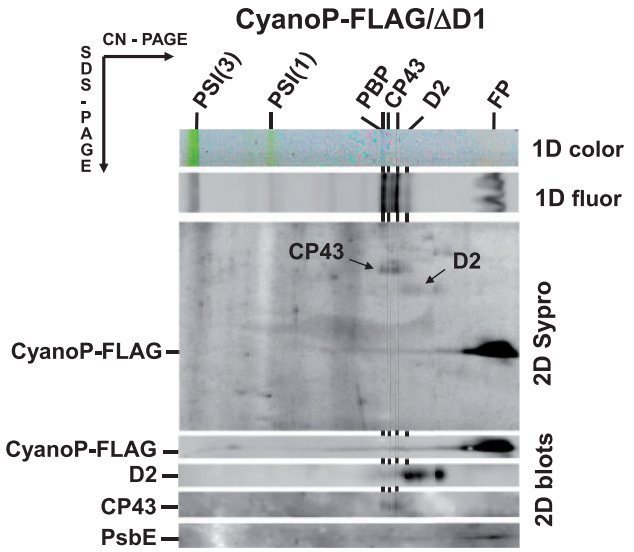

Fig. 4 CyanoP-FLAG isolated from the strain lacking D1 protein co-purifies with D2, CP43 and PsbE. The preparation isolated using anti-FLAG affinity resin was analyzed as in **Fig. 1** and **2**; the designated proteins were detected by specific antibodies. Complexes are designated as in **Fig. 2**. Three different forms of CP43 are indicated.

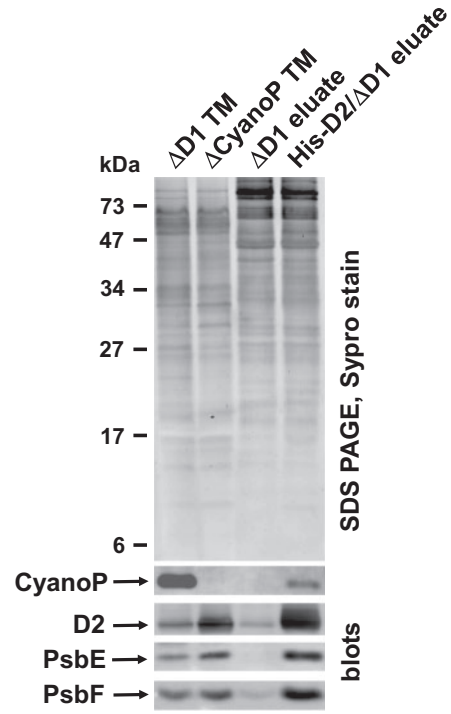

Fig. 5 Co-purification of CyanoP with His-tag D2 protein expressed in the strain lacking D1 (His-D2/ΔD1). The preparations from the His-D2/ΔD1 and the ΔD1 background strain as a control isolated using Ni-affinity resin were analyzed by 1D SDS–PAGE. Purification specificity is documented by specific occurrence of CyanoP, D2, PsbE and PsbF in the His-D2 preparation. The isolated membranes of ΔD1 and ΔCyanoP strains (ΔD1 TM and ΔCyanoP TM, respectively) containing 2 μg of Chl are used as a positive and negative control of the CyanoP content.

obtained from the CyanoP-FLAG/ΔCP47 strain, monomeric and trimeric PSI complexes were also present. To confirm binding of CyanoP to the D2 module, we constructed a strain expressing N-terminally His-tagged D2 protein and lacking D1 (His-D2/ΔD1). The pull-down preparation obtained by nickel affinity chromatography contained a large number of contaminating proteins, but, when compared with the control pull-down from the D1-less strain, it specifically contained D2, the Cyt b_{559} subunits PsbE and PsbF, and also CyanoP, again supporting the interaction of this protein with the D2 assembly module (**Fig. 5**).

In the strain expressing CyanoP-FLAG and lacking the D2 and CP43 subunits (CyanoP-FLAG/ΔD2/ΔCP43), FLAG-tagged CyanoP co-purified with the PSII assembly factor Ycf48 which could be detected even by staining (**Fig. 6**). Similar to previous findings, PSI was also found in this preparation. On the other hand, we were not able to detect CyanoP in the FLAG-Ycf39–D1 complex also containing Ycf48, isolated from the ΔD2/ΔCP43 strain (**Supplementary Fig. S4**), although the interaction of the two accessory factors was also expected in this case. However, there might be only a very low amount of CyanoP bound to Ycf48 in the purified complexes and this could be washed out during the purification procedure.

The absence of CyanoP leads to increased accumulation of unassembled D1 precursor in vivo

In order to check the effect of deleting CyanoP on the biosynthesis of PSII, we constructed a CyanoP deletion mutant (ΔCyanoP). The mutant and WT cells grown under standard growth conditions were radiolabeled at high irradiance and their solubilized membranes were subjected to 2D CN/SDS–

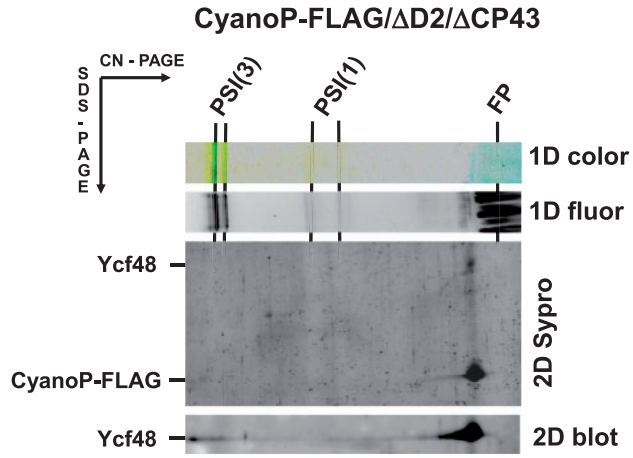

Fig. 6 CyanoP-FLAG isolated from the D2-less strain co-purifies with Ycf48. The preparation isolated using anti-FLAG affinity resin was analyzed as in **Fig. 1**, and the designated proteins were detected by specific antibodies. Complexes are designated as in **Fig. 2**.

PAGE analysis (**Fig. 7**). The autoradiogram showed a significant accumulation of the radiolabel in the unassembled precursor (pD1 and iD1) and mature forms of D1 protein (Nixon et al. 1992) in the mutant compared with its WT control (**Fig. 7**). The

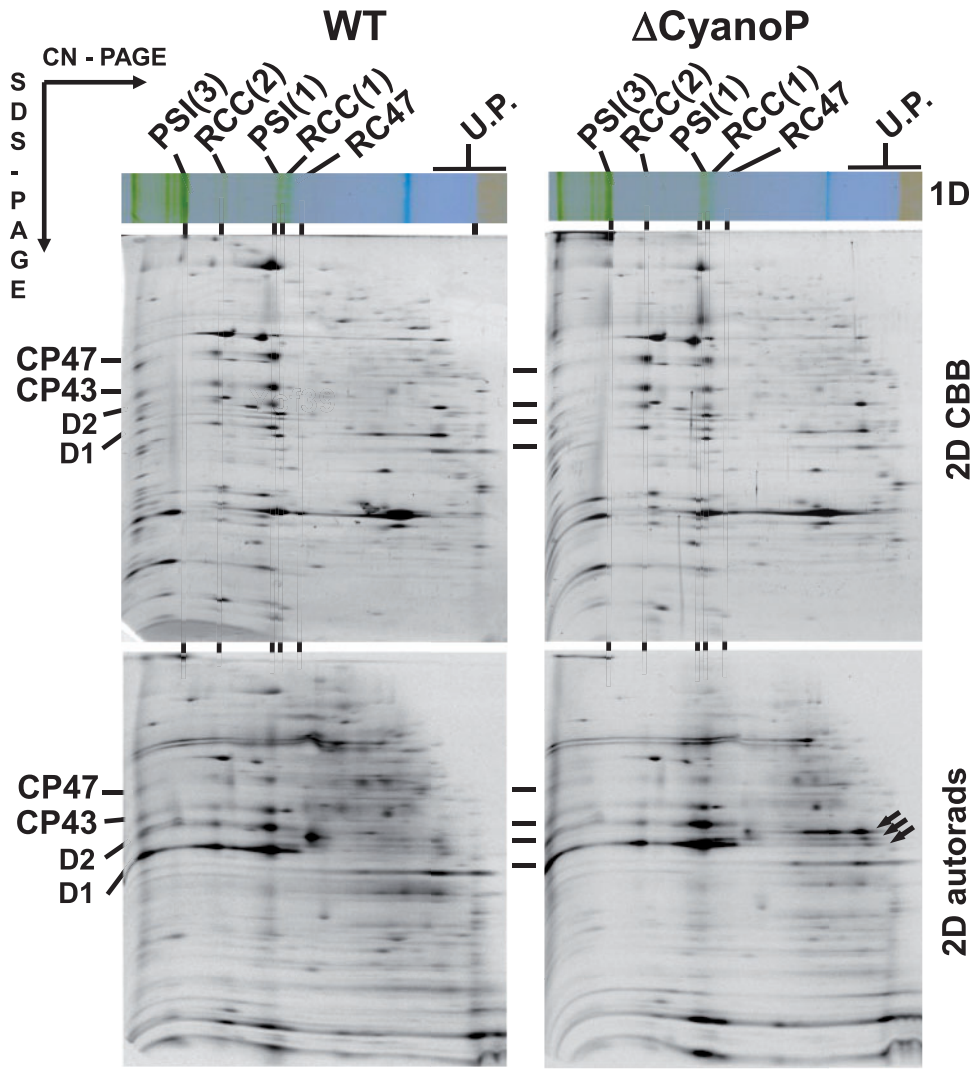

Fig. 7 A CyanoP deletion mutant (ΔCyanoP) shows significant accumulation of the radiolabel into the unassembled D1 protein compared with the WT. Membranes isolated from cells radioactively labeled under high irradiance were subjected to 2D CN/SDS–PAGE. The 2D gels were stained by Coomassie Blue (2D CBB) and exposed to a Phosphorimager plate (2D autorads). Complexes are designated as in Figs. 1 and 2, RC47, the reaction center core lacking CP43; U.P., unassembled proteins. Arrows indicate unassembled forms of unprocessed, partially processed and processed D1 protein (their identity was confirmed by immunodetection). Each loaded sample contained 5 μg of Chl.

same result was obtained when CyanoP was deleted from the strain lacking CP47 (**Supplementary Fig. S5**). Moreover, the analysis of non-labeled cells using 2D Blue Native (BN)/SDS–PAGE and subsequent immunodetection confirmed reduced accumulation of RCII in the ΔCyanoP/ΔCP47 mutant (**Fig. 8**). These results indicate that the incorporation of D1 into PSII complexes was impaired in vivo in the absence of CyanoP, consistent with a functional role for CyanoP at an early stage of PSII assembly.

CyanoP stabilizes machinery for synthesis of Chl proteins

Analysis by 2D electrophoresis and immunoblotting of the membrane proteins isolated from the ΔCyanoP/ΔCP47 strain and its ΔCP47 control revealed a noticeable fragmentation of some intrinsic membrane proteins in the absence of CyanoP, namely the PsbE subunit of PSII, the terminal enzyme of Chl biosynthesis, Chl synthase (ChlG), and the homolog of bacterial YidC insertase (SynYidC, Slr1471), which is proposed to facilitate the insertion of Chl-binding proteins into the thylakoid membrane (**Fig. 8**). The destabilization of PsbE, which binds to the D2 protein, is again consistent with the presence of CyanoP in the D2 assembly module. The fragmentation of ChlG and SynYidC in the absence of CyanoP suggests that CyanoP might be present close to where Chl-binding proteins are synthesized and integrated into the membrane, and that its presence may protect some components of the enzymatic machinery involved in these processes from proteolysis.

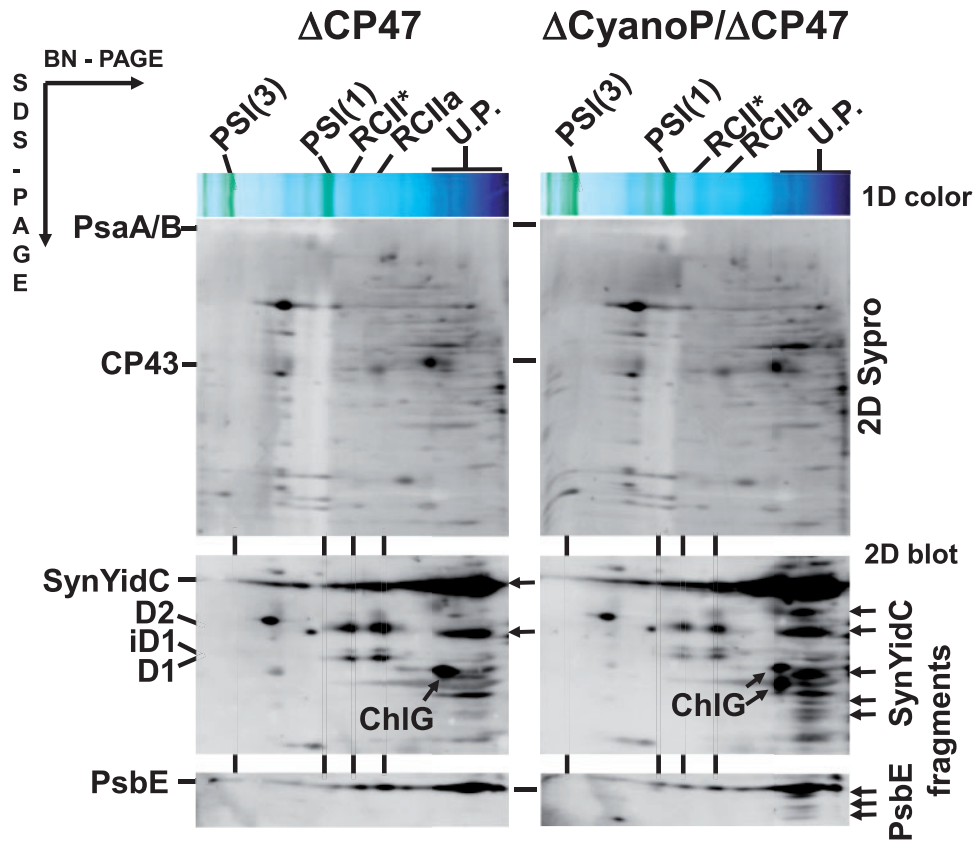

Fig. 8 CP47-less strain lacking CyanoP shows fragmented Chl synthase, SynYidC protein insertase and PsbE. Membranes isolated from ΔCP47 and ΔCyanoP/ΔCP47 strains were analyzed by 2D BN/SDS–PAGE. The native gel was photographed (1D color) and the 2D gel was stained by Sypro Orange (2D Sypro), electroblotted to a PVDF membrane and probed with antibodies specific for D1 and D2, Chl synthase (ChlG), homolog of bacterial membrane protein insertase YidC (SynYidC) and PsbE. Oblique arrows indicate ChlG-related bands and horizontal arrows indicate SynYidC- and PsbE-related fragments. Complexes are designated as in **Figs. 1** and **7**. Each loaded sample contained 5 μg of Chl.

Discussion

We show here that CyanoP is a component of the PSII reaction center assembly complex (**Figs. 1**, **2**) and is able to bind to PSII far earlier in biogenesis than previously thought. Smaller amounts of larger PSII core complexes were also detected in the CyanoP-FLAG preparation isolated from the WT background strain (**Fig. 3**), implying that the protein is also able to bind to the PSII complexes containing both the CP47 and CP43 inner antennae, but these latter subunits are clearly not needed for CyanoP binding. A functional role for CyanoP in optimizing the formation of the reaction center assembly complex is supported by the accumulation of newly synthesized unassembled D1 precursor in the absence of CyanoP in both the WT and ΔCP47 backgrounds (**Fig. 7** and **Supplementaty Fig. S5**, respectively) and decreased accumulation of RCII in the ΔCyanoP/ΔCP47 strain (**Fig. 8**).

Binding of CyanoP to low-abundance early assembly complexes helps explain the substoichiometric levels of CyanoP within the *Synechocystis* thylakoid membrane compared with other PSII subunits (Thornton et al. 2004, Aoi et al. 2014), as well as its depletion in isolated oxygen-evolving PSII complexes from *T. elongatus* (Michoux et al., 2014). The retardation of photoautotrophic growth and oxygen evolution previously seen in CyanoP null mutants under $CaCl_2$-depleted conditions (Thornton et al. 2004, Aoi et al. 2014) might therefore reflect perturbations in PSII assembly rather than a direct effect of CyanoP in the holoenzyme, although weak binding of CyanoP to the holoenzyme cannot be excluded.

Our pull-down experiments employing strains lacking either D1 or D2 subunits (**Figs. 4–6**) imply that CyanoP binds to the D2 protein and/or components associated with the D2 assembly module consisting of at least D2 and the PsbE and PsbF subunits of Cyt b_{559} (Müller and Eichacker 1999, Komenda et al. 2008). In contrast, binding of CyanoP to D1 is either absent or much weaker (**Fig. 6**; **Supplementary Fig. S4**). A model of the early assembly steps of PSII based on these results is depicted in **Fig. 9**. We hypothesize that the interaction between the D1 assembly factor Ycf48 and CyanoP indicated in **Fig. 6** might facilitate the association of the D1 and D2 assembly modules and formation of the PSII reaction center assembly complex. In the context of this model and the results of a recent study on the CyanoP function in PSII biogenesis (Jackson and Eaton-Rye, 2015) it appears that Ycf48 plays a more important role than CyanoP in the formation of the RCII assembly complex.

Binding of CyanoP to the lumenal surface of the PSII reaction center complex, before attachment of the extrinsic proteins, is

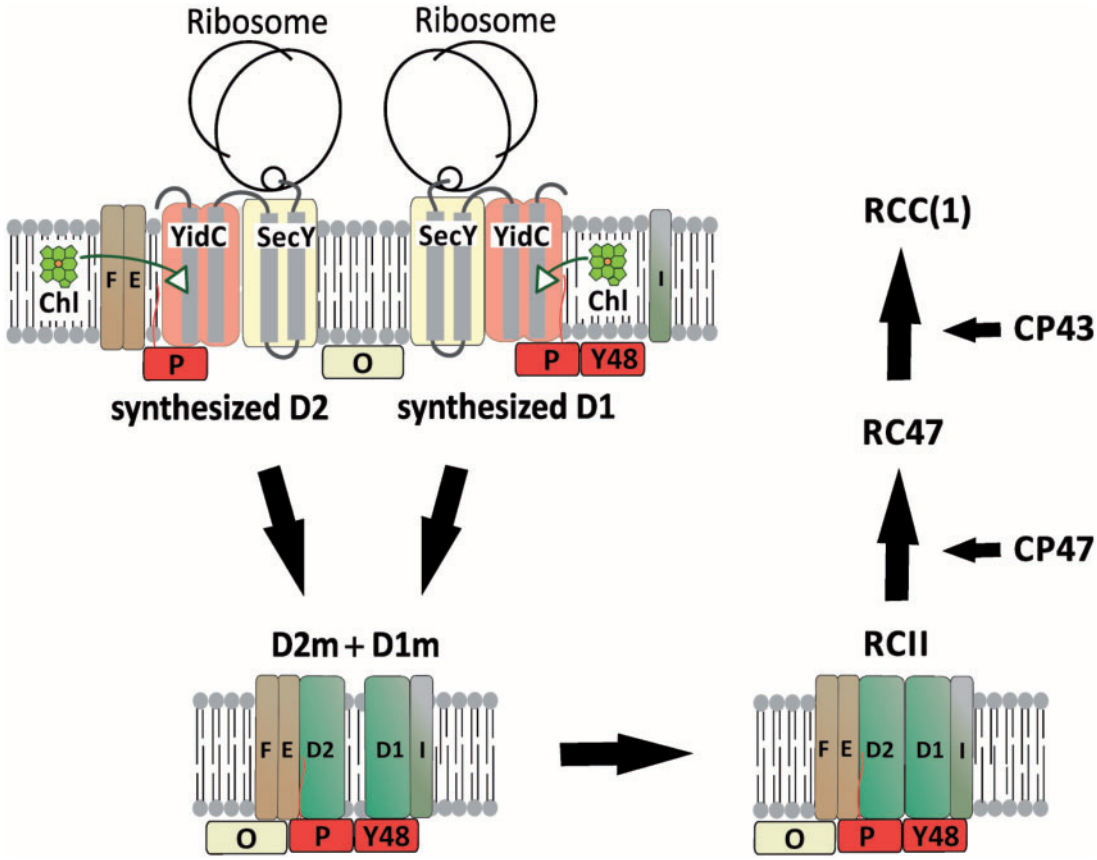

Fig. 9 Hypothetical model of the early steps of PSII biogenesis including the lumenal proteins CyanoP, Ycf48 and PsbO. The D1 and D2 modules (D1m and D2m) are formed after synthesis of D1 and D2 apoproteins and insertion of Chl with the assistance of ribosomes, the SecY translocon, YidC insertase and small PSII subunits (PsbE and PsbF for D2m and PsbI for D1m). Lumenal proteins CyanoP and Ycf48 facilitate interaction of D1m and D2m to form the RCII complex and possibly interact with other lumenal proteins such as PsbO. Other auxiliary factors involved in the initial phases of PSII assembly (Ycf39, HliC and HliD) are omitted to simplify the model. The red line attached to the box of 'P' indicates the lipid bound to the N-terminus of CyanoP.

compatible with recent results obtained by surface plasmon resonance spectroscopy indicating possible interactions between CyanoP and the C-terminal tail of D2 as well as the lumenal loop linking the first two transmembrane helices of D1 (Cormann et al. 2014). These regions are located in the center of the complex and are normally occupied by the PsbO subunit in the holoenzyme (Umena et al. 2011). In contrast earlier in silico docking models made between the crystal structures of the PSII dimer and CyanoP had positioned the protein on the lumenal face of the D2 subunit away from the other extrinsic proteins (Fagerlund and Eaton-Rye 2011, Bricker et al. 2012).

Sequence similarities between CyanoP and PsbP were originally interpreted in terms of a common function in binding to fully assembled PSII (Thornton et al. 2004). However, it is now known that CyanoP is just one member of a large PsbP superfamily which includes not only the extrinsic PsbP subunit of PSII but also PsbP-like (PPL) and PsbP-domain (PPD) proteins of largely unknown function. Some members have clear roles outside PSII, including PPL2 which is a subunit of the chloroplast NADH dehydrogenase-like complex (Ishihara et al. 2007, Ifuku et al. 2011) and PD1 which is required for assembly of PSI in plants (Liu et al. 2012). Despite their relatively low sequence similarities, the structural fold of the PsbP superfamily is thought to be conserved, with CyanoP representing the basal form of the PsbP superfamily (Michoux et al. 2010, Sato 2010, Bricker et al. 2013). The diversity in function of members of the PsbP superfamily presumably reflects the ability of the fold to accommodate changes in primary structure including enlargement/contraction of loop regions, extension of the N-terminal tail and alteration of surface residues (Michoux et al. 2010, Sato 2010, Bricker et al. 2013). Thus it seems plausible that PsbP evolved from CyanoP to bind more tightly to the PSII holoenzyme and at the same time to form new interactions with plant-specific components of PSII such as the CP26 light-harvesting complex and PsbR subunit recently detected in protein cross-linking experiments (Ido et al. 2014). In contrast, the cyanobacterial PsbU and PsbV proteins might have been less capable of evolving to form these new interactions and were therefore replaced in chloroplasts.

Phylogenetic studies suggest that the member of the PsbP superfamily in plants most closely related to CyanoP is actually

the PsbP-like protein PPL1 (Sato 2010, Bricker et al. 2013). The *ppl1* null mutant of Arabidopsis is able to assemble functional PSII but shows a defect in the recovery of PSII activity from photoinhibition (Ishihara et al. 2007) when damaged PSII complexes are replaced by either PSII repair or de novo assembly from newly synthesized PSII modules such as the RCII assembly complex (Knoppová et al. 2014). The retarded incorporation of newly synthesized D1 into the RCII assembly complex in the CyanoP null mutant (**Figs. 7**, **8**; **Supplementary Fig. S5**) thereby reducing the rate of synthesis of PSII is therefore consistent with an equivalent role for PPL1 in the assembly of PSII in chloroplasts.

Most Chl-binding proteins in chloroplasts of plants and algae seem to be integrated into the thylakoid membrane with the assistance of a homolog of the bacterial protein insertase YidC (Pasch et al. 2005, Göhre et al. 2006). In *Synechocystis*, it was demonstrated that the analogous protein, SynYidC (Slr1471), interacts directly with the D1 subunit precursor, and that it is involved in proper integration and assembly of the D1 into the thylakoid membrane and the RCII assembly complex (Ossenbühl et al. 2006). Importantly, the recent study of Chidgey et al. (2014) has shown that the machinery involved in assembly of Chl proteins in *Synechocystis* is located in a membrane-associated supercomplex linking the translation and translocation (insertion) processes with terminal steps of the Chl biosynthetic pathway, as demonstrated by co-isolation of FLAG-tagged Chl synthase (ChlG), the terminal enzyme of Chl biosynthesis, with ribosomal subunits, the SecY subunit of the Sec translocon, and SynYidC.

The destabilization of SynYidC and ChlG in a CP47-less mutant lacking CyanoP, demonstrated by an unusual fragmentation of these proteins (**Fig. 8**), implies a role for CyanoP as a lumenal factor stabilizing and protecting some components of the biogenesis machinery from proteolytic attacks. This is most probably a specific feature of the CP47-less mutant related to the generally disturbed PSII assembly process in this strain as this was found specifically in ΔCP47/ΔCyanoP and not in ΔCyanoP constructed in the WT background.

Given the previously demonstrated high specificity of FLAG-based purifications (Chidgey et al. 2014, Knoppová et al. 2014), the selective pull-down of the RCII assembly complexes having very low cellular abundance provides strong evidence for their association with CyanoP. We never identified any NADH dehydrogenase-related proteins, contradicting a possibility that CyanoP interacts with these complexes in analogy with the chloroplast ortholog PPL2 (Ishihara et al. 2007, Ifuku et al. 2011). On the other hand, the CyanoP-FLAG pull-downs isolated from various strains also contained a significant amount of PSI, mostly in the trimeric form, as observed previously for isolated FLAG-Ycf39, FLAG-ChlG and YidC-FLAG (Chidgey et al. 2014, Knoppová et al. 2014). Since the control pull-down performed using WT membranes contained only a negligible amount of PSI (Chidgey et al. 2014), and PSI subunits were not detected in pull-downs isolated from cells expressing FLAG-tagged versions of photosystem-unrelated proteins Sll1214 and Sll1874 (Chl cyclase enzymes) and their stabilization factor Ycf54 (Hollingshead et al. 2012), it seems probable that CyanoP-FLAG also interacts with PSI, either directly or indirectly. Indeed, we have suggested that Chl proteins of PSII are synthesized to a large extent using Chls released from trimeric PSI which appears to be a primary acceptor of a newly synthesized Chl (Kopečná et al. 2012). These results further support the involvement of PSI in the early steps of PSII biogenesis, as proposed originally from the detection of newly synthesized PSII subunits and PSII assembly factors in large PSI–PSII supercomplexes (Komenda et al. 2012b). In this respect, the presence of unassembled CP43 in some CyanoP-FLAG pull-downs could be a subpopulation of CP43 associated with PSI as observed previously (Komenda et al. 2012b).

Interestingly, the pull-down of CyanoP-FLAG expressed in a mutant deficient in CP47 also revealed its interaction with the PsbO oxygen-evolving enhancer protein (**Fig. 2**; **Supplementary Table S1**). This raises the possibility that this lumenal extrinsic protein participates in the PSII assembly process much earlier than previously assumed. The protein was abundant in the pull-down from the strain lacking CP47 while it was absent in the preparation isolated from CyanoP-FLAG/WT. Assuming that CP47 is the main binding partner of PsbO in the PSII holoenzyme (Umena et al. 2011), the weaker interaction with the RCII assembly complex is maintained during the pull-down procedure only in the absence of CP47. The putative engagement of PsbO in the RCII assembly is also included in the model in **Fig. 9**.

Materials and Methods

Construction and cultivation of cyanobacterial strains

The following, previously described strains of the glucose-tolerant *Synechocystis* sp. PCC 6803 strain (Williams 1988) were used: (i) the CP47 deletion strain (ΔCP47), in which the *psbB* gene is replaced by a spectinomycin resistance cassette (Eaton-Rye and Vermaas 1991); (ii) the *psbA* triple deletion strain (ΔD1) with cassette-less deletions in *psbA1* and *psbA3* genes and the *psbA2* gene replaced by a chloramphenicol resistance cassette (Nagarajan et al. 2011); and (iii) the *psbDIC/psbDII* deletion strain (ΔD2) with the *psbDIC* and *psbDII* genes encoding the D2 protein replaced by a chloramphenicol and a spectinomycin resistance cassette, respectively (Vermaas et al. 1990).

The transformation vector used to disrupt the CyanoP gene *sll1418* was constructed in two steps. First, an intermediate vector, namely pGEMT-sll1418, was constructed via overlap extension PCR with the following primer sets. Primers Sll1418-1F and Sll1418-2R were used to amplify 445 bp upstream flanking sequence of the CyanoP open reading frame (ORF), and primer set Sll1418-3F and Sll1418-4R were used to obtain the 555 bp downstream fragments (for primer sequences, see **Supplementary Table S2**). Both upstream and downstream fragments were then mixed as the DNA template for overlap extension reaction with primer set Sll1418-1F and Sll1418-4R. The resulting fragments, which carry an *Eco*RV restriction site instead of *sll1418*, were then cloned into the multiple cloning region of the pGEM-T Easy vector. Further modifications on pGEMT-sll1418 were then carried out by inserting a chloramphenicol resistance cassette into the *Eco*RV site via restriction digestion and ligation to create the final transformation vector termed psll1418-CamA (**Supplementary Fig. S6**). Sequencing confirmed that the orientation of the resistance cassette was the same as the orientation of the *sll1418* gene. The pSll1418-CamA plasmid was then used to transform the WT cells to obtain the ΔCyanoP strain. Transformants were selected for chloramphenicol resistance, and PCR was used to show integration of the selectable marker and elimination of the WT *sll1418* gene copy. Genomic DNA isolated from the ΔCyanoP strain was then used for transformation of the ΔCP47 strain lacking the CP47 antenna to obtain the ΔCyanoP/ΔCP47 double mutant.

The strains expressing N-terminal FLAG-tag Ycf39 (FLAG-Ycf39/WT and FLAG-Ycf39/ΔCP47) were constructed as described in Knoppová et al. (2014).

The C-terminal FLAG-tag CyanoP strains (CyanoP-FLAG/WT, ΔCP47, ΔD1 and ΔD2, respectively) were prepared by replacing the *sll1418* gene using the synthetic DNA construct (Genscript) containing the upstream region (292 bp), the *sll1418* plus 3×FLAG sequence (Sigma), a zeocin resistance cassette and the downstream region (269 bp) as depicted in **Supplementary Fig. S7**. Transformants were selected for zeocin resistance, and PCR was used to confirm full segregation of the mutants. The correct sequence of the construct was confirmed by DNA sequencing in all the transformants.

The His-D2/ΔD1 strain was constructed according to the following procedure. The background strain ΔPsbDIC/ΔD1, in which the *psbDI* and *psbC* genes were deleted and replaced by a Kan^R/SacB cassette (Lea-Smith et al. 2013), was generated by transforming the ΔD1 (ΔPsbA) strain (Nagarajan et al. 2011) with plasmid ppsbDCks and selecting on kanamycin. Plasmid ppsbDCks was generated by inserting a Kan^R/SacB marker into the unique *Eco*RV site of pGEMT-psbDC. Plasmid pGEMT-psbDC was generated by fusing 445 bp of DNA upstream of *psbDI* to 555 bp of DNA downstream of *psbC* by overlap extension PCR (Higuchi et al. 1988) using primer sets PsbDC-1F and PsbDC-2R for the upstream region, and PsbDC-3F and PsbDC-4R for the downstream region (for primers, see **Supplementary Table S2**), then cloning into the pGEM-T Easy vector via TA cloning according to the manufacturer's protocol. The N-terminal His-tag D2 construct was generated by overlap extension PCR in a similar fashion. First, primer set PsbDC-1F and PsbD-His-2R and primer set PsbD-His-3F and PsbDC-4R were used to amplify the respective sequences from WT genomic DNA. The resulting upstream and downstream fragments were then fused via overlap extension PCR using primer set PsbDC-1F and PsbDC-4R. The full-length PCR fragments were then ligated into pGEM-T Easy vector, yielding plasmid pGEMT-his-psbD. To obtain strain His-PsbD/ΔD1, the ΔPsbDIC/ΔD1 mutant was transformed with pGEMT-his-psbD followed by selection on BG11 plates supplemented with 5 mM glucose, 10 μM DCMU and 5% (w/v) sucrose. The second copy of the D2 gene, *psbDII*, was then deleted according to the following steps. First, the flanking sequences of the *psbDII* ORF were PCR amplified from WT genomic DNA using primer set PsbDII-1F and PsbDII-2R for the upstream region, and PsbDII-3F and PsbDII-4R for the downstream region. The resulting PCR fragments were then subjected to overlap extension PCR using primer set PsbDII-1F and PsbDII-4R, and the fused PCR fragment was cloned into pGEM-T Easy to yield plasmid pGEMT-psbDII. An erythromycin resistance cassette was inserted into pGEMT-psbDII via the engineered *Eco*RV site located at the junction of the upstream and downstream sequences. The new vector, namely pGEMT-psbDII-EryA, was then used to transform the His-PsbD/ΔD1 mutant to create, after the full selection, the His-D2/ΔD1 strain expressing exclusively the His-tagged version of D2.

The strains were grown in a rotary shaker under moderate light conditions (40 μmol photons m^{-2} s^{-1}) at 30°C in liquid BG11 medium. Non-autotrophically cultured mutants were supplemented with 5 mM glucose. For protein purification, 2 or 4 liters of cells were grown photomixotrophically in 10 liter flasks under approximately 100 μmol photons m^{-2} s^{-1} in BG11 medium supplemented with 5 mM glucose. The cell culture was agitated with a magnetic stirrer and bubbled with air. The FLAG-tag Ycf39 strains were cultivated in BG-11 medium lacking Cu^{2+} to induce expression of the FLAG-Ycf39 protein (Knoppová et al. 2014). The CyanoP-FLAG/WT was grown in 1 liter conical flasks in a rotary shaker under light increasing from approximately 100 to 400 μmol photons m^{-2} s^{-1} during the growth, and the culture was supplemented with 1 mM glucose.

Chl content

The Chl concentration was measured in 100% methanol extracts according to Wellburn (1994).

Radioactive labeling

Radioactive pulse labeling of the cells was performed at 500 μmol photons m^{-2} s^{-1} and 30°C using a mixture of [^{35}S]methionine and [^{35}S]cysteine (Trans-label, MP Biochemicals) as described previously (Dobáková et al. 2009).

Preparation of membrane fraction

Small-scale membrane fractions were prepared by breaking the cells with zirkonia/silica beads using a Mini-Beadbeater (BioSpec) according to the procedure described in Komenda and Barber (1995). For native electrophoresis, the cells were broken and resuspended in buffer B (25 mM MES/NaOH, pH 6.5, 10 mM $CaCl_2$, 10 mM $MgCl_2$, 25% glycerol), and for one-dimensional SDS–PAGE they were broken in TA buffer (25 mM Tris–HCl, pH 7.5, 1 mM aminocaproic acid) and resuspended in TA plus 1 M sucrose.

Large-scale membrane preparations for purification were isolated in buffer B containing EDTA-free protease inhibitor cocktail (Roche or Sigma-Aldrich) as described in Chidgey et al. (2014).

FLAG- and His-tag protein purification

The membranes were solubilized with 1.5 % (w/v) *n*-dodecyl-β-D-maltoside (β-DDM) for 60 min under mild mixing at 10°C. The solubilized fraction was separated by centrifugation (43,000 rcf/20 min, 4°C). The purification was performed on a chromatography column using 0.3–0.4 ml of ANTI-FLAG M2 affinity gel (Sigma-Aldrich) for the FLAG-tagged proteins, or 0.8 ml of Protino Ni-NTA agarose (Macherey-Nagel) for His-tagging. All the purification steps were run at 10°C. The solubilized material was loaded onto the column and the flow-through was collected and loaded repeatedly 4–5 times. In the case of the FLAG-tag purification, the gel was washed 5–6 times with 1 ml of buffer B containing 0.04% β-DDM (washing buffer, WB). Thereafter, the gel was resuspended in 200–300 μl of WB and transferred into a Costar Spin-X centrifuge tube filter (Corning). After 30 min incubation with 3×FLAG peptide (Sigma-Aldrich) of final concentration 150 mg ml^{-1}, the specifically bound protein complexes were eluted by centrifugation (400 rcf/2 min, 4°C). For the His-tag purification, the gel was first washed three times with two gel volumes of WB (3× 2GV), then successively with WB containing an increasing concentration range of imidazole (IM) according to the following scheme: 3× 2GV 10 mM IM, 5× 1GV 20 mM IM and 3× 0.5GV 30 mM IM, and then again with 1× 3GV of WB. After the washing steps, the gel was incubated for 5 min with 0.5GV of elution buffer (WB plus 200 mM IM), transferred into a centrifuge tube filter and spun down (400 rcf/2 min, 4°C) to obtain the eluate.

In the case of FLAG-tag purifications, the concentration of Chl in solubilized material loaded onto the column was 350–400 μg ml^{-1}, with the exception of the CyanoP-FLAG/ΔCP47 where it was 560 μg ml^{-1}. The total Chl amount varied between 3 and 6 mg, corresponding to the volume of the solubilized fraction (7–10 ml). In the His-D2/ΔD1 and the ΔD1 used as a control, the Chl concentration was 305 and 330 μg ml^{-1}, respectively, which gave 2.9 and 3.1 mg of Chl in the total volume of 9.5 ml. The control was used in this case due to the generally lower specificity of the His purification in order to exclude non-specific interactions, and the purification procedures were performed simultaneously.

Analysis of proteins and their complexes

The composition of membrane protein complexes was analyzed as described in Komenda et al. (2012b) by CN or BN electrophoresis in a 4–14% gradient polyacrylamide gel in combination with SDS–PAGE in a denaturing 12–20% gradient gel (acrylamide to bis-acrylamide ratio 38) containing 7 M urea. One-dimensional SDS–PAGE was carried out either in the same 12–20% denaturing gel (as in **Fig. 9** and **Supplementary S3**) or in its modified version of a 16–20% gradient where the original acrylamide to bis-acrylamide ratio of 38 was changed to 60 (**Fig. 5**). The concentration of membrane samples loaded onto the gel is indicated in the figure legends. A 60 μl aliquot of the pull-down preparations was loaded for each analysis.

The first-dimensional native gels were photographed (1D color) and scanned for fluorescence (1D fluo). The proteins separated using the denaturing SDS gels were visualized by staining with either Coomassie Brilliant Blue (CBB) or Sypro Orange (Sypro) and detected by MS or immunoblotting. The primary antibodies against D1, D2, CP47, CP43 and Cyt b_{559} subunits PsbE and PsbF used in this study were previously described by Komenda et al. (2004) and Dobáková et al. (2007). The antibody against *Synechocystis* YidC (SynYidC) was kindly provided by Professor Jörg Nickelsen (Ludwig-Maximilians University, Munich, Germany). Further we employed a commercial anti-FLAG (Abgent) and the antibody against the *Synechocystis* PsbP homolog CyanoP (Agrisera).

We also used our own antibodies raised against *Escherichia coli*-expressed Ycf48, peptide 311–322 of Ycf39, and peptide 89–104 of ChlG.

Protein identification by mass spectrometry

The MS analyses of protein bands excised from the gel or the liquid pull-down preparations of the tagged proteins were done on a NanoAcquity UPLC (Waters) online-coupled to an ESI Q-ToF Premier mass spectrometer (Waters) as described in Janouškovec et al. (2013).

Supplementary data

Supplementary data are available at PCP online.

Funding

This study was supported by the Grant Agency of the Czech Republic [P501-12-G055 to J. Kno, P.K. and J.K.]; the Czech Academy of Sciences [RVO61388971 to J. Kno, P.K. and J.K.]; the Czech Ministry of Education [projects LM2015055 and LO1416 to J. Kno, P.K. and J.K.]; the Biotechnology and Biological Sciences Research Council (BBSRC) [grants BB/I00937X/1 and BB/L003260/1 to J.Y. and P.J.N.]

Disclosures

The authors have no conflicts of interest to declare.

References

Aoi, M., Kashino, Y. and Ifuku, K. (2014) Function and association of CyanoP in photosystem II of *Synechocystis* sp. PCC 6803. *Res. Chem. Intermed.* 40: 3209–3217.

Boehm, M., Romero, E., Reisinger, V., Yu, J.F., Komenda, J., Eichacker, L.A., et al. (2011) Investigating the early stages of photosystem II assembly in *Synechocystis* sp. PCC 6803. Isolation of CP47 and CP43 complexes. *J. Biol. Chem.* 286: 14812–14819.

Boehm, M., Yu, J., Reisinger, V., Bečková, M., Eichacker, L.A., Schlodder, E., et al. (2012) Subunit composition of CP43-less photosystem II complexes of *Synechocystis* sp. PCC 6803: implications for the assembly and repair of photosystem II. *Philos. Trans. R. Soc. B: Biol. Chem.* 367: 3444–3454.

Bricker, T.M., Roose, J.L., Fagerlund, R.D., Frankel, L.K. and Eaton-Rye, J.J. (2012) The extrinsic proteins of photosystem II. *Biochim. Biophys. Acta* 1817: 121–142.

Bricker, T.M., Roose, J.L., Zhang, P. and Frankel, L.K. (2013) The PsbP family of proteins. *Photosynth. Res.* 116: 235–250.

Chidgey, J.W., Linhartová, M., Komenda, J., Jackson, P.J., Dickman, M.J., Canniffe, D.P., et al. (2014) A cyanobacterial chlorophyll synthase–HliD complex associates with the Ycf39 protein and the YidC/Alb3 insertase. *Plant Cell* 26: 1267–1279.

Cormann, K.U., Bartsch, M., Rogner, M. and Nowaczyk, M.M. (2014) Localization of the CyanoP binding site on photosystem II by surface plasmon resonance spectroscopy. *Front. Plant Sci.* 5: 595.

De Las Rivas, J., Balsera, M. and Barber, J. (2004) Evolution of oxygenic photosynthesis: genome-wide analysis of the OEC extrinsic proteins. *Trends Plant Sci.* 9: 18–25.

Dobáková, M., Sobotka, R., Tichý, M. and Komenda, J. (2009) Psb28 protein is involved in the biogenesis of the photosystem II inner antenna CP47 (PsbB) in the cyanobacterium *Synechocystis* sp PCC 6803. *Plant Physiol.* 149: 1076–1086.

Dobáková, M., Tichý, M. and Komenda, J. (2007) Role of the PsbI protein in photosystem II assembly and repair in the cyanobacterium Synechocystis sp PCC 6803. *Plant Physiol.* 145: 1681–1691.

Eaton-Rye, J.J. and Vermaas, W.F.J. (1991) Oligonucleotide-directed mutagenesis of *psbB*, the gene encoding CP47, employing a deletion mutant strain of the cyanobacterium *Synechocystis* sp. PCC 6803. *Plant Mol. Biol.* 17: 1165–1177.

Fagerlund, R.D. and Eaton-Rye, J.J. (2011) The lipoproteins of cyanobacterial photosystem II. *J. Photochem. Photobiol. B* 104: 191–203.

Gohre, V., Ossenbuhl, F., Crevecoeur, M., Eichacker, L.A. and Rochaix, J.D. (2006) One of two Alb3 proteins is essential for the assembly of the photosystems and for cell survival in *Chlamydomonas*. *Plant Cell* 18: 1454–1466.

Guskov, A., Kern, J., Gabdulkhakov, A., Broser, M., Zouni, A. and Saenger, W. (2009) Cyanobacterial photosystem II at 2.9-angstrom resolution and the role of quinones, lipids, channels and chloride. *Nat. Struct. Mol. Biol.* 16: 334–342.

Higuchi, R., Krummel, B. and Saiki, R.K. (1988) A general method of in vitro preparation and specific mutagenesis of DNA fragments: study of protein and DNA interactions. *Nucleic Acids Res.* 16: 7351–7367.

Hollingshead, S., Kopečná, J., Jackson, P.J., Canniffe, D.P., Davison, P.A., Dickman, M.J., et al. (2012) Conserved chloroplast open-reading frame ycf54 is required for activity of the magnesium protoporphyrin monomethylester oxidative cyclase in *Synechocystis* PCC 6803. *J. Biol. Chem.* 287: 27823–27833.

Ido, K., Nield, J., Fukao, Y., Nishimura, T., Sato, F. and Ifuku, K. (2014) Cross-linking evidence for multiple interactions of the PsbP and PsbQ proteins in a higher plant photosystem II supercomplex. *J. Biol. Chem.* 289: 20150–20157.

Ifuku, K. (2015) Localization and functional characterization of the extrinsic subunits of photosystem II: an update. *Biosci. Biotechnol. Biochem.* 79: 1223–1231.

Ifuku, K., Endo, T., Shikanai, T. and Aro, E.M. (2011) Structure of the chloroplast NADH dehydrogenase-like complex: nomenclature for nuclear-encoded subunits. *Plant Cell Physiol.* 52: 1560–1568.

Ishihara, S., Takabayashi, A., Ido, K., Endo, T., Ifuku, K. and Sato, F. (2007) Distinct functions for the two PsbP-like proteins PPL1 and PPL2 in the chloroplast thylakoid lumen of *Arabidopsis*. *Plant Physiol.* 145: 668–679.

Ishikawa, Y., Schroder, W.P. and Funk, C. (2005) Functional analysis of the PsbP-like protein (sll1418) in *Synechocystis* sp PCC 6803. *Photosynth. Res.* 84: 257–262.

Jackson, S.A. and Eaton-Rye, J.J. (2015) Characterization of a *Synechocystis* sp. PCC 6803 double mutant lacking the CyanoP and Ycf48 proteins of photosystem II. *Photosynth. Res.* 124: 217–229.

Janouškovec, J., Sobotka, R., Lai, D.H., Flegontov, P., Koník, P., Komenda, J., et al. (2013) Split photosystem protein, linear-mapping topology, and growth of structural complexity in the plastid genome of *Chromera velia*. *Mol. Biol. Evol.* 30: 2447–2462.

Kashino, Y., Lauber, W.M., Carroll, J.A., Wang, Q.J., Whitmarsh, J., Satoh, K., et al. (2002) Proteomic analysis of a highly active photosystem II preparation from the cyanobacterium *Synechocystis* sp. PCC 6803 reveals the presence of novel polypeptides. *Biochemistry* 41: 8004–8012.

Knoppová, J., Sobotka, R., Tichý, M., Yu, J., Konik, P., Halada, et al. (2014) Discovery of a chlorophyll binding protein complex involved in the early steps of photosystem II assembly in *Synechocystis*. *Plant Cell* 26: 1200–1212.

Komenda, J. and Barber, J. (1995) Comparison of *psbO* and *psbH* deletion mutants of *Synechocystis* PCC 6803 indicates that degradation of D1 protein is regulated by the Q_B site and dependent on protein-synthesis. *Biochemistry* 34: 9625–9631.

Komenda, J., Knoppová, J., Kopečná, J., Sobotka, R., Halada, P., Yu, J.F., et al. (2012b) The Psb27 assembly factor binds to the CP43 complex of

photosystem II in the cyanobacterium *Synechocystis* sp. PCC 6803. *Plant Physiol.* 158: 476–486.

Komenda, J., Nickelsen, J., Tichý, M., Prášil, O., Eichacker, L.A. and Nixon, P.J. (2008) The cyanobacterial homologue of HCF136/YCF48 is a component of an early photosystem II assembly complex and is important for both the efficient assembly and repair of photosystem II in *Synechocystis* sp. PCC 6803. *J. Biol. Chem.* 283: 22390–22399.

Komenda, J., Reisinger, V., Muller, B.C., Dobáková, M., Granvogl, B. and Eichacker, L.A. (2004) Accumulation of the D2 protein is a key regulatory step for assembly of the photosystem II reaction center complex in *Synechocystis* PCC 6803. *J. Biol. Chem.* 279: 48620–48629.

Komenda, J., Sobotka, R. and Nixon, P.J. (2012a) Assembling and maintaining the photosystem II complex in chloroplasts and cyanobacteria. *Curr. Opin. Plant Biol.* 15: 245–251.

Kopečná, J., Komenda, J., Bučinská, L. and Sobotka, R. (2012) Long-term acclimation of the cyanobacterium *Synechocystis* sp. PCC 6803 to high light is accompanied by an enhanced production of chlorophyll that is preferentially channeled to trimeric photosystem I. *Plant Physiol.* 160: 2239–2250.

Lea-Smith, D.J., Ross, N., Zori, M., Bendall, D.S., Dennis, J.S., Scott, S.A., et al. (2013) Thylakoid terminal oxidases are essential for the cyanobacterium *Synechocystis* sp. PCC 6803 to survive rapidly changing light intensities. *Plant Physiol.* 162: 484–495.

Liu, H., Zhang, H., Weisz, D.A., Vidavsky, I., Gross, M.L. and Pakrasi, H.B. (2014) MS-based cross-linking analysis reveals the location of the PsbQ protein in cyanobacterial photosystem II. *Proc. Natl Acad. Sci. USA* 111: 4638–4643.

Liu, J., Yang, H.X., Lu, Q.T., Wen, X.G., Chen, F., Peng, L.W., et al. (2012) PSBP-DOMAIN PROTEIN1, a nuclear-encoded thylakoid lumenal protein, is essential for photosystem I assembly in Arabidopsis. *Plant Cell* 24: 4992–5006.

Michoux, F., Takasaka, K., Boehm, M., Nixon, P.J. and Murray, J.W. (2010) Structure of CyanoP at 2.8 angstrom: implications for the evolution and function of the PsbP subunit of photosystem II. *Biochemistry* 49: 7411–7413.

Müller, B. and Eichacker, L.A. (1999) Assembly of the D1 precursor in monomeric photosystem II reaction center precomplexes precedes chlorophyll a-triggered accumulation of reaction center II in barley etioplasts. *Plant Cell* 11: 2365–2377.

Nagarajan, A., Winter, R., Eaton-Rye, J. and Burnap, R. (2011) A synthetic DNA and fusion PCR approach to the ectopic expression of high levels of the D1 protein of photosystem II in *Synechocystis* sp. PCC 6803. *J. Photochem. Photobiol. B* 104: 212–219.

Nixon, P.J., Michoux, F., Yu, J.F., Boehm, M. and Komenda, J. (2010) Recent advances in understanding the assembly and repair of photosystem II. *Ann. Bot.* 106: 1–16.

Nixon, P.J., Trost, J.T. and Diner, B.A. (1992) Role of the carboxy terminus of polypeptide-D1 in the assembly of a functional water-oxidizing manganese cluster in photosystem-II of the cyanobacterium *Synechocystis* sp. PCC 6803—assembly requires a free carboxyl group at C-terminal position 344. *Biochemistry* 31: 10859–10871.

Ossenbuhl, F., Inaba-Sulpice, M., Meurer, J., Soll, J. and Eichacker, L.A. (2006) The *Synechocystis* sp. PCC 6803 oxa1 homolog is essential for membrane integration of reaction center precursor protein pD1. *Plant Cell* 18: 2236–2246.

Pasch, J.C., Nickelsen, J. and Schünemann, D. (2005) The yeast split-ubiquitin system to study chloroplast membrane protein interactions. *Appl. Microbiol. Biot.* 69: 440–447.

Roose, J.L., Kashino, Y. and Pakrasi, H.B. (2007) The PsbQ protein defines cyanobacterial photosystem II complexes with highest activity and stability. *Proc. Natl Acad. Sci. USA* 104: 2548–2553.

Sato, N. (2010) Phylogenomic and structural modeling analyses of the PsbP superfamily reveal multiple small segment additions in the evolution of photosystem II-associated PsbP protein in green plants. *Mol. Phylogenet. Evol.* 56: 176–186.

Staleva, H., Komenda, J., Shukla, M.K., Šlouf, V., Kaňa, R., Polívka, T., et al. (2015) Mechanism of photoprotection in the cyanobacterial ancestor of plant antenna proteins. *Nat. Chem. Biol.* 11: 287–291.

Summerfield, T.C., Winter, R.T. and Eaton-Rye, J.J. (2005) Investigation of a requirement for the PsbP-like protein in *Synechocystis* sp PCC 6803. *Photosynth. Res.* 84: 263–268.

Sveshnikov, D., Funk, C. and Schroder, W.P. (2007) The PsbP-like protein (sll1418) of *Synechocystis* sp. PCC 6803 stabilises the donor side of photosystem II. *Photosynth. Res.* 93: 101–109.

Thornton, L.E., Ohkawa, H., Roose, J.L., Kashino, Y., Keren, N. and Pakrasi, H.B. (2004) Homologs of plant PsbP and PsbQ proteins are necessary for regulation of photosystem II activity in the cyanobacterium *Synechocystis* 6803. *Plant Cell* 16: 2164–2175.

Umena, Y., Kawakami, K., Shen, J.R. and Kamiya, N. (2011) Crystal structure of oxygen-evolving photosystem II at a resolution of 1.9 A. *Nature* 473: 55–60.

Vermaas, W., Charite, J. and Eggers, B. (1990) System for site-directed mutagenesis in the psbDI/C operon of *Synechocystis* sp. PCC 6803. *In* Current Research in Photosynthesis. Edited by Baltscheffsky, M. pp. 231–238. Springer, Berlin.

Wellburn, A.R. (1994) The spectral determination of chlorophyll-a and chlorophyll-b, as well as total carotenoids, using various solvents with spectrophotometers of different resolution. *J. Plant Physiol.* 144: 307–313.

Williams, J.G.K. (1988) Construction of specific mutations in photosystem II photosynthetic reaction center by genetic-engineering methods in *Synechocystis* 6803. *Methods Enzymol.* 167: 766–778.

CellPress
PARTNER JOURNAL

Molecular Plant
Research Article

Association of Psb28 and Psb27 Proteins with PSII-PSI Supercomplexes upon Exposure of *Synechocystis* sp. PCC 6803 to High Light

Martina Bečková[1,2], Zdenko Gardian[2,3], Jianfeng Yu[4], Peter Konik[1,2], Peter J. Nixon[4] and Josef Komenda[1,2,*]

[1]Institute of Microbiology, Center Algatech, Opatovický mlýn, 37981 Třeboň, Czech Republic

[2]Faculty of Science, University of South Bohemia, Branišovská 1760, 37005 České Budějovice, Czech Republic

[3]Institute of Plant Molecular Biology, Biology Centre Academy of Sciences, Branišovská 31, 37005 České Budějovice, Czech Republic

[4]Sir Ernst Chain Building-Wolfson Laboratories, Department of Life Sciences, Imperial College London, South Kensington Campus, London SW7 2AZ, UK

***Correspondence: Josef Komenda (komenda@alga.cz)**

http://dx.doi.org/10.1016/j.molp.2016.08.001

ABSTRACT

Formation of the multi-subunit oxygen-evolving photosystem II (PSII) complex involves a number of auxiliary protein factors. In this study we compared the localization and possible function of two homologous PSII assembly factors, Psb28-1 and Psb28-2, from the cyanobacterium *Synechocystis* sp. PCC 6803. We demonstrate that FLAG-tagged Psb28-2 is present in both the monomeric PSII core complex and a PSII core complex lacking the inner antenna CP43 (RC47), whereas Psb28-1 preferentially binds to RC47. When cells are exposed to increased irradiance, both tagged Psb28 proteins additionally associate with oligomeric forms of PSII and with PSII-PSI supercomplexes composed of trimeric photosystem I (PSI) and two PSII monomers as deduced from electron microscopy. The presence of the Psb27 accessory protein in these complexes suggests the involvement of PSI in PSII biogenesis, possibly by photoprotecting PSII through energy spillover. Under standard culture conditions, the distribution of PSII complexes is similar in the wild type and in each of the single *psb28* null mutants except for loss of RC47 in the absence of Psb28-1. In comparison with the wild type, growth of mutants lacking Psb28-1 and Psb27, but not Psb28-2, was retarded under high-light conditions and, especially, intermittent high-light/dark conditions, emphasizing the physiological importance of PSII assembly factors for light acclimation.

Key words: Psb28 proteins, photosystem I and II, *Synechocystis*

Bečková M., Gardian Z., Yu J., Konik P., Nixon P.J., and Komenda J. (2017). Association of Psb28 and Psb27 Proteins with PSII-PSI Supercomplexes upon Exposure of *Synechocystis* sp. PCC 6803 to High Light. Mol. Plant. **10**, 62–72.

INTRODUCTION

The photosystem II (PSII) complex is the light-driven water-plastoquinone oxidoreductase of oxygenic photosynthesis, responsible for splitting water into molecular oxygen and releasing protons and electrons for the generation of the ATP and NADPH needed for the fixation of carbon dioxide in cyanobacteria, algae, and plants. The most active form of PSII is a dimer whose structure from thermophilic cyanobacteria is now known to a resolution of 1.9 Å (Umena et al., 2011). The PSII monomer features 17 transmembrane protein subunits, three peripheral proteins and about 80 cofactors (Guskov et al., 2009). The transmembrane reaction center (RCII) subunits D1 and D2 are essential for the binding of cofactors involved in primary charge separation and subsequent electron transfer (Diner et al., 2001). The chlorophyll-containing CP47 and CP43 inner antenna complexes that deliver energy from the outer antennae to the reaction center are located on either side of the D1-D2 heterodimer. CP43 also has a role with D1 in binding the Mn_4CaO_5 cluster involved in water splitting (Ferreira et al., 2004).

Assembly of PSII is thought to be a stepwise process (Komenda et al., 2004) proceeding through several intermediate complexes. Initially, the large pigment proteins form pre-complexes (or modules) with small transmembrane polypeptides, pigments, and possibly other cofactors (Komenda et al., 2012b). First the D1

Published by the Molecular Plant Shanghai Editorial Office in association with Cell Press, an imprint of Elsevier Inc., on behalf of CSPB and IPPE, SIBS, CAS.

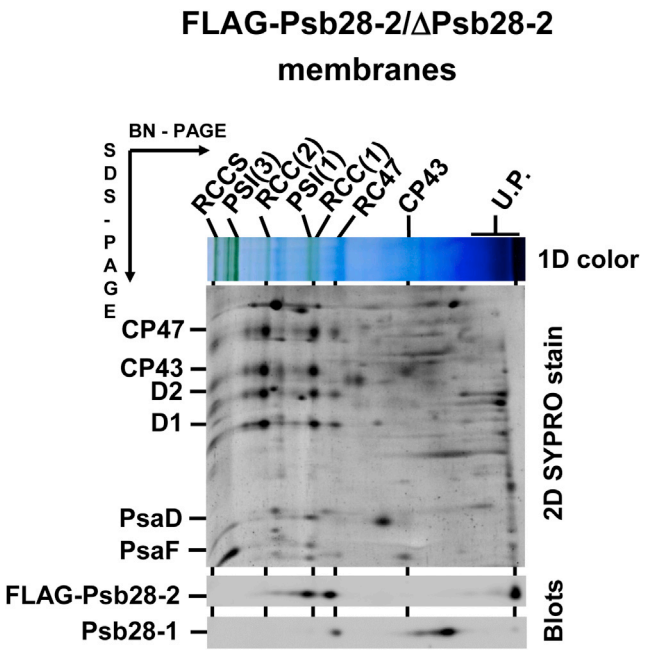

Figure 1. Two-Dimensional Protein Analysis of a *Synechocystis* 6803 Strain FLAG-Psb28-2/ΔPsb28-2 Expressing the FLAG-Psb28-2 Protein Instead of Psb28-2.

Solubilized membranes isolated from the strain corresponding to 4 μg of Chl*a* were analyzed by blue-native PAGE in the first dimension (1D color) and by SDS–PAGE in the second dimension. The gel was stained with SYPRO orange (2D SYPRO stain); proteins were blotted onto PVDF membrane and subsequently probed with specific antibodies (Blots). The designation of complexes: RCCS, supercomplex of PSI trimer and PSII dimer; PSI(3) and PSI(1), trimeric and monomeric photosystem I; RCC(2) and RCC(1), dimeric and monomeric PSII core complexes; RC47, the monomeric PSII core complex lacking CP43; U.P., unassembled proteins.

and D2 modules form a reaction center intermediate complex (RCII) to which the CP47 module is attached to form a core complex lacking CP43 (termed RC47). Subsequent attachment of the CP43 module leads to the formation of a PSII monomeric core complex (RCC(1)) with assembly completed by dimerization to form RCC(2) (reviewed in Nixon et al., 2010). Light-driven assembly of the Mn_4CaO_5 cluster and attachment of the lumenal extrinsic subunits is thought to occur after formation of RCC(1) (Nixon et al., 2010). Correct and efficient assembly of PSII is controlled by a number of auxiliary protein factors that are absent from the final functional PSII complex. Some of these, such as the Psb28 proteins (Pfam: PF03912), are highly conserved and are found both in cyanobacteria and chloroplasts.

The genome of the cyanobacterium *Synechocystis* sp. PCC 6803 (hereafter *Synechocystis* 6803) codes for two Psb28 homologs: Psb28-1 (encoded by gene *sll1398*) and Psb28-2 (encoded by gene *slr1739*) (Boehm et al., 2012). Psb28-1 (also named Psb13 and Ycf79) was first identified as a component of a His-tagged PSII preparation isolated from *Synechocystis* 6803 (Kashino et al., 2002) and, subsequently, shown to be a hydrophilic protein peripherally attached to the membrane (Dobáková et al., 2009). The absence of transmembrane structural motifs was later confirmed by the determination of the solution structure of His-tagged Psb28-1 by NMR (PDB: 2KVO; Yang et al., 2011). Psb28-1 in *Synechocystis* 6803 most probably exists as a dimer (Bialek et al., 2013) and has been detected in the RC47 complex (Dobáková et al., 2009; Boehm et al., 2012; Sakata et al., 2013) in the vicinity of the PsbH subunit (Dobáková et al., 2009).

The phenotype of *psb28-1* null mutants of *Synechocystis* 6803 is controversial. The knockout mutant constructed by Dobáková et al. (2009) exhibited slower autotrophic growth, accelerated turnover of the D1 subunit, decreased synthesis of the CP47 inner antenna, and a lower cellular level of chlorophyll (Chl) in comparison with wild type (WT). In contrast, the phenotype of the null mutant described by Sakata et al. (2013) was much milder, showing just growth retardation under increased temperature, especially when combined with inactivation of the *dgdA* gene causing a defect in the biosynthesis of digalactosyldiacylglycerol.

The genomes of *Synechocystis* 6803 and some other cyanobacteria contain another *psb28* gene designated *psb28-2*. A knockout mutant of *Synechocystis* 6803 lacking Psb28-2 behaves like WT, and deletion of the *psb28-2* gene in the Psb28-1-less strain does not show an additional effect, indicating that Psb28-2 is not able to substitute for Psb28-1 (Sakata et al., 2013). The structure of Psb28-2 is thought to be similar to that of Psb28-1 (Mabbitt et al., 2014) except that it likely exists as a monomer (Bialek et al., 2013), due to the lack of several amino acid residues putatively involved in dimerization of Psb28 (Mabbitt et al., 2014). Psb28-2 like Psb28-1 has been detected in RC47 complexes (Boehm et al., 2012).

The physiological importance of Psb28 proteins in PSII assembly and function in *Synechocystis* 6803 remains unknown. Here we show that, under increased irradiance, both proteins together with Psb27, a lumenal accessory protein associated with non-oxygen-evolving PSII core complexes (Nowaczyk et al., 2006), become components of PSII-PSI supercomplexes, the formation of which may be an important step in PSII biogenesis especially under high irradiance. Consistent with this, we show that growth of both the *Psb27* and *Psb28-1* mutants is affected under conditions of continuous and especially intermittent high light.

RESULTS

Differences in the Association of Psb28 Proteins with PSII

Previous work has shown that both Psb28-1 and Psb28-2 are able to bind to the RC47 complex (Dobáková et al., 2009; Boehm et al., 2012; Bialek et al., 2013). However, the weak Psb28-2 signal detected by immunoblotting in this earlier work prevented a complete analysis of the binding of Psb28-2 to other types of PSII complexes. To address this problem, we used commercial FLAG-tag specific antibodies to detect expression of a Psb28-2 derivative containing a 3xFLAG tag fused to the N terminus (FLAG-Psb28-2) (Boehm et al., 2012). Two-dimensional (2D) gel electrophoresis of solubilized thylakoids isolated from this strain confirmed the presence of the protein not only in RC47 but also at similar levels in the monomeric PSII core complex (RCC(1)) (Figure 1). Additional probing of the same blot with an antibody against Psb28-1 detected Psb28-1 just in RC47, in agreement with earlier work (Dobáková et al., 2009). The

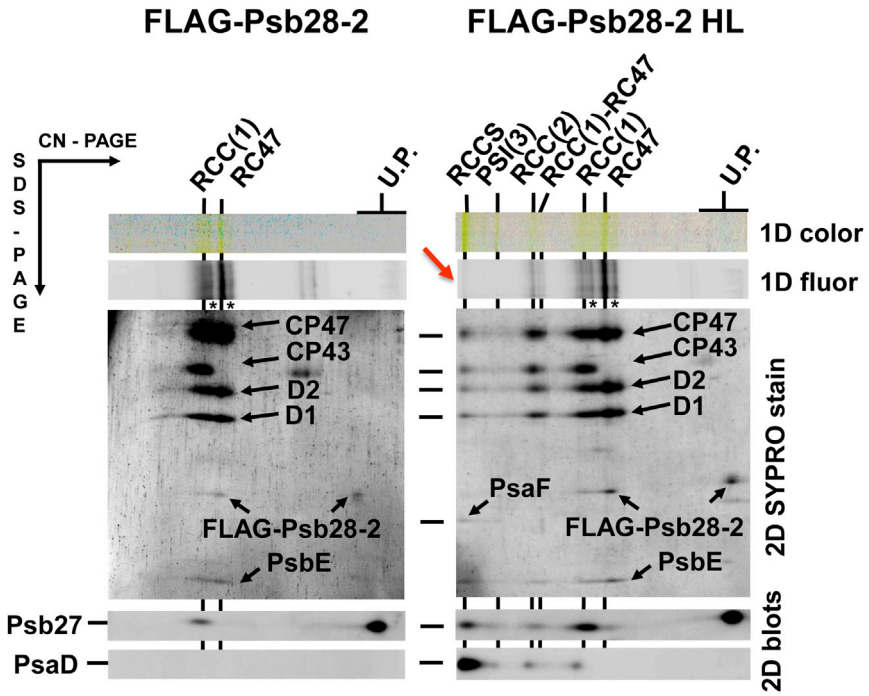

Figure 2. Two-Dimensional Protein Analysis of N-Terminally FLAG-tagged Psb28-2 Preparation (FLAG-Psb28-2) Isolated by Affinity Chromatography from Cells of FLAG-Psb28-2/ΔPsb28-2 Strain Grown Under Low (Left) or High (HL, Right) Irradiance.

Preparations were analyzed by CN PAGE in the first dimension, and the native gel was photographed (1D color) and scanned with an LAS-4000 camera for Chl fluorescence (1D fluor); after SDS–PAGE in the second dimension, the gel was stained with SYPRO orange (2D SYPRO stain), electroblotted to PVDF membrane, and probed with the antibody specific for Psb27 and PsaD (2D blots). The designation of complexes as in Figure 1, RCC(1)-RC47 is a PSII dimeric core complex lacking one of the CP43 inner antenna. The red arrow points to the fluorescence quenching in RCCS. Asterisks indicate PSII complexes lacking FLAG-Psb28-2.

apparent masses of the RC47 complexes containing Psb28-1 and FLAG-Psb28-2 in RC47 were slightly different, suggesting that the two Psb28 proteins might not bind to the same complex. The position of unassembled Psb28-1 in the native gel was also in agreement with its postulated dimeric structure, whereas unassembled FLAG-Psb28-2 migrated as a monomer.

FLAG-Psb28-2-containing complexes immunopurified under mild solubilization conditions were also examined by 2D gel electrophoresis. In the first dimension, we used clear-native (CN) PAGE, which enables sensitive identification of PSII complexes directly in the gel due to the emission of Chl fluorescence. This analysis confirmed the association of FLAG-Psb28-2 with RC47 but, unlike a previous study (Boehm et al., 2012) (see also Supplemental Figure 1), we observed a monomeric PSII core complex RCC(1) in the pull-down experiment (Figure 2, left panel), possibly because the use of a milder MES buffer containing Mg^{2+} and Ca^{2+} ions stabilized binding of CP43 within the isolated RCC(1) complex during purification. Immunoblotting showed that RCC(1) complexes isolated using FLAG-Psb28-2 contained another PSII assembly factor, Psb27 (Figure 2). Both the RC47 and RCC(1) complexes were present in two versions: a larger one containing FLAG-Psb28-2 and a smaller one lacking FLAG-Psb28-2 as judged from the relative migration of the FLAG-tagged protein band (Figure 2, complexes with asterisks). This suggests that a sub-population of FLAG-tagged Psb28-2 is released from PSII complexes during native PAGE and migrates in the region of unassembled proteins. This is even better documented in Supplemental Figure 1 when the 2D gel analysis was performed using FLAG-tagged Psb28-2 isolated by the previously described method (Boehm et al., 2012).

Although the amount of SYPRO-stained FLAG-Psb28-2 in Figure 2 seemed to be sub-stoichiometric in comparison with the pulled down larger PSII proteins, comparison of the staining obtained with SYPRO orange, used in this study due to its compatibility with immunoblotting, and with Coomassie blue (CBB) (Supplemental Figure 1) showed that the reason is the lower stainability of the tagged Psb28-2 and other smaller proteins (e.g., PsbE) by SYPRO stain. Indeed, comparison of the approximate intensity ratio of the FLAG-Psb28-2 and CP47 in the SYPRO-stained and CBB-stained gels showed much higher value with CBB staining (Supplemental Figure 1).

To exclude the effect of the position of the FLAG tag on the binding specificity of the Psb28 proteins, we analyzed membranes of two other strains expressing either N-terminally tagged Psb28-1 or C-terminally tagged Psb28-2 (FLAG-Psb28-1 and Psb28-2-FLAG, respectively) from their native promoters (Supplemental Figure 2). Membrane protein analysis confirmed that the position of the tag did not affect the binding specificity of each of the Psb28 proteins to PSII since FLAG-Psb28-1 was found in RC47 and Psb28-2-FLAG in both RC47 and RCC(1) (Supplemental Figure 2). In addition, RC47 and RCC(1) were both pulled down by Psb28-2-FLAG (Supplemental Figure 3).

Both FLAG-Tagged Psb28 Proteins Associate with Large PSII-PSI Supercomplexes under Increased Irradiance

We found that exposure of cells to increased irradiance led to an altered composition of the resulting pull-down preparations. FLAG-Psb28-2 isolated from more illuminated cultures contained a higher proportion of dimeric PSII core complexes and, in addition, a non-fluorescent large Chl-protein complex visible at the edge of the CN gel (Figure 2, right panel). The 2D gel showed that the latter complex contained all four large PSII Chl-binding proteins, but its pigmentation was clearly higher than that of PSII core complexes. The absorption spectrum of the band showing a maximum at about 677 nm and a main 77 K fluorescence band peaking at 722 nm pointed to the presence of the photosystem I (PSI) complex (Figure 3, right panel). This was

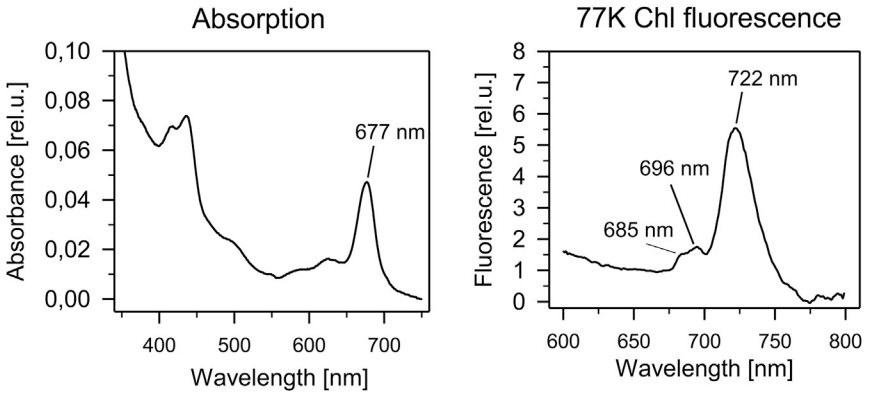

Figure 3. The Room Temperature Absorption (Left) and 77K Chl Fluorescence (Right) Spectra of the RCCS Band Cut from the CN Gel Shown in Figure 2 (Right).
The absorption spectrum was measured using a Shimadzu UV-3000 spectrometer; the fluorescence spectrum was measured using an Aminco Bowman Series 2 luminescence spectrometer.

further confirmed by mass spectrometry analysis, which showed the presence of the PsaA, PsaF, and PsaL subunits of PSI (Table 1). The presence of PSI in the complex was also confirmed by immunodetection of the PsaD protein; the weaker signals detected in smaller complexes most probably reflect the presence of PSI trimeric, dimeric, and monomeric complexes (Figure 2 and Supplemental Figure 2D blots). Therefore, we ascribe the large complex to a supercomplex of PSII and PSI (RCCS, Figure 2, right panel). In agreement with previously published data, the supercomplex also contained Psb27 (Komenda et al., 2012a), a lumenal accessory protein associated with non-oxygen-evolving PSII core complexes (Nowaczyk et al., 2006), which suggests a role for the supercomplex in PSII assembly/repair. A similar pattern of PSII complexes was also obtained when we affinity purified C-terminally tagged Psb28-2 (Psb28-2-FLAG) from cells grown under standard and high irradiance (Supplemental Figure 3). The complexes again contained Psb27.

We further tested whether FLAG-tagged Psb28-1 also co-isolated with RCCS under increased irradiance. Psb28-1-FLAG co-purified with RC47, a very small amount of RCC(1) and RCC(1)-RC47 complex, when isolation was performed from cells grown under standard conditions (Figure 4, left panel). Here again the seemingly low level of the pulled down Psb28-1-FLAG was related to the weaker staining of the protein by SYPRO orange (Supplemental Figure 4). When isolated from cells exposed to high irradiance, the preparation additionally contained a significant amount of the PSII-PSI supercomplex (Figure 4, right panel). The presence of PSI was again confirmed by identification of both PsaD in the complex by immunoblotting (Figure 4 and 2D blots) and PsaE in the pull-down by mass spectrometry (Supplemental Table 1). We never identified Psb28-2 in Psb28-1-FLAG pull-down, confirming their independent binding (not shown).

To further characterize the PSII-PSI supercomplex, we subjected the Psb28-1-FLAG preparation to single-particle analysis. Due to the low amount of supercomplexes in the preparation (Figure 5A), the resolution of the obtained images was rather limited; nevertheless it was sufficient for the unequivocal identification of PSI trimers in the particles. The shape and size of the additional structures attached to the PSI trimer corresponded well to two monomeric PSII complexes (Figure 5B). Results from single-particle analysis also supported the presence of RCC(1)-RC47 complexes (Figure 5C), which were detected by 2D gel electrophoresis on the basis of a relative decrease in intensity of the CP43 band in the complex compared with RCC(1) complexes (Figure 4).

The PSII-PSI supercomplexes were present in WT cells even under standard light conditions, and their quantity only slightly increased after exposure of the cells to high light (Supplemental Figure 5). These data indicate that these complexes are constitutively present in cells, but after high-light treatment there is an increase in the amount of a specific fraction that binds the Psb28 and Psb27 proteins.

We also tested unspecific binding of RCCS and other PSII complexes to FLAG-affinity resin using solubilized membranes from the control WT strain subjected to high irradiance. No apparent Chl-containing complexes present in the eluate excluded an artifactual binding of RCCS to the affinity resin (Supplemental Figure 5).

Differences in the Profile of PSII Complexes in psb28 Null Mutants

Previous results have suggested that the strain lacking Psb28-1 shows impaired synthesis of CP47 and PSI and accumulates lower levels of Chl in the cell (Dobáková et al., 2009). However, this phenotype was not observed in a second independently constructed *psb28-1* mutant (Sakata et al., 2013). Since this disagreement could be caused by differences in the genetic backgrounds of the two WT strains used to make the mutants, we constructed two new Psb28-1- and Psb28-2-less mutants using a different WT strain. In our original study (Dobáková et al., 2009), we used a WT strain very similar to the glucose-tolerant GT-O2 strain (Morris et al., 2014), which was subsequently shown to exhibit partial Chl depletion upon autotrophic growth conditions (GT-W; Tichý et al., 2016). The new set of mutants was instead constructed in the GT-P strain similar to the GT-Kazusa strain (Supplemental Figure 6), which contains a similar content of Chl as the standard motile PCC 6803 strain (Tichý et al., 2016). The resulting *psb28* mutants were found to have a similar cellular Chl content as the control and contained very similar levels of PSI and both monomeric and dimeric PSII core complexes as revealed by CN gel electrophoresis (Figure 6) in agreement with Sakata et al. (2013). This result indicates that the decreased level of Chl in the Psb28-1-less strain seen by Dobáková et al. (2009) was most probably related to the Chl-deficient phenotype of the WT strain originally used for mutant construction.

Nevertheless, when we performed radioactive labeling of proteins in the new strains, the Psb28-1-less mutant still showed lower labeling of CP47 and PSI in comparison with the other

Protein, UniProtKB no.	Size (Da), length (no. of amino acids)	Coverage (%)	Detected/theoretical no. of peptides	PLGS score
CP47, P05429	55 903, 507	5	1/27	208
D1, P14660	39 695, 360	3	1/14	130
PsaA, P29254	82 950, 751	5	3/34	338
PsaF, P29256	18 249, 165	19	2/11	95
PsaL, P37277	16 624, 157	25	2/6	160

Table 1. List of Proteins Identified by Mass Spectrometry in the CN-PAGE-Separated PSII-PSI Supercomplex RCCS of the Psb28-2-FLAG Pull-Down (Figure 2) Isolated from High-Light-Treated Cells of the *Synechocystis* Strain Expressing Psb28-2-FLAG.
The PLGS score is a statistical measure of peptide assignment accuracy; it is calculated with Protein Lynx Global Server (PLGS 2.2.3) software (Waters).

two strains (Supplemental Figure 7). Another common feature of the new ΔPsb28-1 strain shared with the one constructed by Dobáková et al. (2009) was the lack of detectable RC47 complex and a lower level of free unassembled CP47, while in the strain lacking Psb28-2, the RC47 complex was clearly visible and was even more abundant than in WT (Figure 6, right panel and quantification table). All three strains show the presence of PSI-PSII supercomplexes under both standard and high-light conditions indicating that the accumulation of PSII supercomplexes is not dependent on the presence of Psb28 proteins.

Loss of Psb28-1 but Not Psb28-2 Impairs Growth in Continuous High Light and Especially Intermittent Light

Under standard illumination conditions, growth of the *psb28-1* and *psb28-2* null mutants on agar plates was indistinguishable to WT (Figure 7, left panels). Under high irradiance, the strain lacking Psb28-1 grew slightly slower than the WT and Psb28-2-less strains but its sensitivity to high light was exacerbated when we used intermittent (5 min dark and 5 min 400 μmol photons m^{-2} s^{-1}) instead of continuous (400 μmol photons m^{-2} s^{-1}) high light (Figure 7, upper right panel). When the *psb28-2* gene was additionally inactivated in the Psb28-1 mutant, the growth of the resulting double mutant was identical to that of the psb28-1 mutant under all tested conditions (not shown). A *psb27* null mutant also grew more slowly under intermittent light in comparison with WT (Figure 7, lower right panel). Finally, we constructed the Psb27/Psb28-1 double mutant, which showed the slowest growth of all the tested strains in high continuous light and did not grow at all in intermittent light.

As the Psb28-1-less strain showed a light-sensitive phenotype, we checked whether it is a light-inducible stress protein like members of the family of high-light-inducible proteins (Hlips, He et al., 2001). While the level of Psb28-1 remained the same after 2 h exposure of WT cells to 500 μmol photons m^{-2} s^{-1}, the content of HliA/B in these cells sharply increased, meaning that pool of Psb28-1 in the cell is stable and the protein is not high-light inducible.

DISCUSSION

Many cyanobacteria, like *Synechocystis* 6803, encode two different Psb28 proteins. Here we confirm that under standard cultivation conditions both Psb28-1 and Psb28-2 associate with the RC47 complex. One difference between the two forms of Psb28 is that Psb28-2 is found at higher levels in the monomeric RCC(1) complex (Figures 1, 2, and 4). When the Psb28 proteins were purified from cells exposed to increased irradiance, oligomeric PSII complexes, small amounts of PSI, and especially PSII-PSI supercomplexes now appeared in the affinity-purified preparations. Interestingly, the Psb27 assembly factor was also present in these complexes in accordance with previous results indicating a close relationship between Psb27 and Psb28 proteins (Kashino et al., 2002; Liu et al., 2011a, 2011b; Nowaczyk et al., 2012). Association of Psb27 with large PSI-PSII complexes has also been demonstrated in previous studies (Liu et al., 2011b; Komenda et al., 2012a). Given that Psb27 is associated with PSII complexes lacking a functional oxygen-evolving complex (Nowaczyk et al., 2006), the complexes containing both Psb27 and Psb28 are therefore likely to be involved in de novo assembly and/or repair of PSII.

Single-particle analysis of preparations isolated using FLAG-tagged Psb28 proteins from high-light exposed cells showed the presence of large particles containing PSI trimer together with two additional densities corresponding in size and shape to two PSII monomers; however, the organization of the two monomers is clearly different from their arrangement in the known dimeric crystal structures, which would suggest binding to trimeric PSI as monomers rather than a dimer (Figure 5). The close association of PSI trimeric complexes with PSII complexes containing the Psb28 and Psb27 assembly factors supports our previous hypothesis that PSI might play a protective role during PSII biogenesis (Komenda et al., 2012a). Indeed this association between PSII and PSI in the supercomplexes resulted in the loss of Chl fluorescence of otherwise highly fluorescent PSII complexes, indicating efficient energy spillover to PSI (Figures 2 and 4). Thus, the formation of PSI-PSII supercomplexes might reflect a light-induced response of the PSII assembly machinery to protect PSII assembly complexes via efficient PSI-mediated quenching of harmful excitation energy absorbed by these intermediates. Moreover, as we have recently identified trimeric PSI as the main sink for newly synthesized Chl (Kopečná et al., 2012), association of PSII assembly complexes with PSI trimeric complexes may also allow production of PSII assembly modules using Chl released from trimeric PSI.

The crystal structure of Psb28 from *Thermosynechococcus elongatus* suggests that the proximity of the C termini of the two monomers in the dimer does not allow tagging of the molecule without destabilization of the dimer, and this was supported by

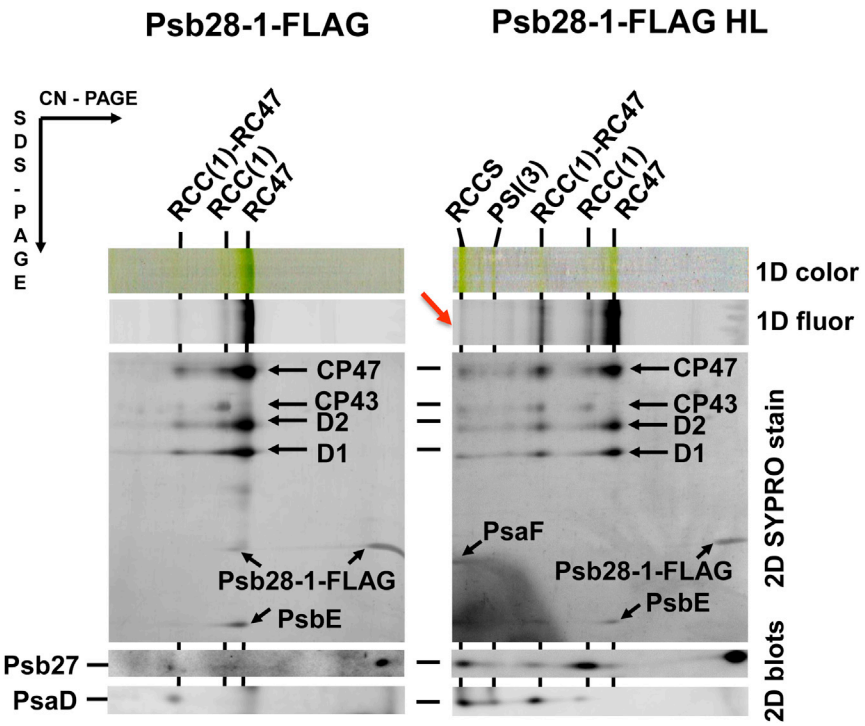

Figure 4. Two-Dimensional Protein Analysis of FLAG-tagged Psb28-1 Preparation Isolated by Affinity Chromatography from Cells of Psb28-1-FLAG/ΔPsb28-1 Strain Grown Under Low (Left) or high (HL, Right) Irradiance.

Preparations were analyzed by CN PAGE in the first dimension, and the native gel was photographed (1D color) and scanned by an LAS-4000 camera for Chl fluorescence (1D fluor); after SDS–PAGE in the second dimension, the gel was stained with SYPRO orange (2D SYPRO stain), electroblotted to PVDF membrane, and probed with the specific antibodies against Psb27 and PsaD (2D blots). The designation of complexes as in Figure 1, RCC(1)-RC47 is a PSII dimeric core complex lacking one of the CP43 inner antenna. The red arrow points to the fluorescence quenching in RCCS.

analysis of the strain expressing Psb28-1 with an FLAG tag on the C terminus. Nevertheless, the FLAG-tagged protein was still able to bind to RC47 in cells (Supplemental Figure 2, left) and PSII co-purified with the isolated tagged protein, suggesting that the dimeric structure of the Psb28-1 protein is not needed for binding to PSII (Figure 4).

Binding of Psb28 proteins to PSII is dependent on the presence of PsbH (Dobáková et al., 2009; Bialek et al., 2013); this fact, together with the inhibitory effect of deleting *psb28-1* on synthesis of CP47, led to speculation that Psb28-1 is bound to CP47. However, taking into account the oligomeric structure of native Psb28-1 together with the presence of a long N-terminal helix of PsbH stretching over CP47, it is also possible that Psb28 binds more in the center of PSII than previously envisaged and so prevents binding of CP43 to RC47 thereby allowing accumulation of RC47 in the membrane.

PsbH is also essential for the binding to PSII of HliB (also termed ScpD), a member of the family of high-light-inducible proteins (Hlips) (He et al., 2001) or small chlorophyll-a/b-binding-like proteins (Scps) (Funk and Vermaas, 1999). We show that expression of Hlips is quickly induced upon increase of irradiance, while the Psb28-1 protein is present constitutively in cells and its content does not respond to high light (Figure 8). Although we cannot exclude that all Psb28-1 proteins weakly interact with PSII in the membrane and this interaction is disrupted during native PAGE, there is nevertheless a fraction of Psb28-1 that binds to RC47 more stably and which is identified in the native gels as the component of the complex (Figure 1; Dobáková et al., 2009). Thus, it seems that the Psb28-1 protein is available for binding to PSII before the production of Hlips and that its prompt binding may be important for Psb28-1 function during high/intermittent light stress.

WT-like sensitivity to continuous high light (Figure 7) and the presence of RC47 in the Psb28-2-less strain (Figure 6) on the one hand and similarity between the Psb28-1-less strain and the *psb28-1/psb28-2* double mutant on the other hand (Sakata et al., 2013) suggest that Psb28-2 is not a redundant Psb28-1 copy with the same function. Instead, we speculate that Psb28-2 may act as an antagonist that prevents formation of RC47 by excluding Psb28-1 from its binding site. That the two Psb28 proteins might play different roles is in line with the upregulation of the *psb28-1* transcript level but downregulation of *psb28-2* in a *Synechocystis* 6803 mutant lacking the PsbO protein (Schriek et al., 2008), which is highly sensitive to photoinhibition and exhibits very fast D1 turnover (Komenda and Barber, 1995). Similarly, the expression profiles of the *psb28-1* and *psb28-2* genes were found to be quite different under a variety of environmental conditions in a very recent transcriptomic study (Hernández-Prieto et al., 2016), again supporting a distinct functional role for each protein.

In the absence of Psb28-1, the RC47 complex is undetectable in cells grown under standard conditions, while in WT cells this complex is detectable. This difference has previously been related to an effect on CP47 synthesis as the *psb28-1*-null mutant contains an increased level of RCII, the assembly complex that immediately precedes RC47 in the PSII assembly pathway (Dobáková et al., 2009). For the newly constructed *psb28-1* mutant described here, there was also reduced synthesis of CP47 (autoradiogram in Supplemental Figure 7). Interestingly, unlike the *Synechocystis* 6803 CP43-less mutant, the CP47-less mutant shows a Chl-deficient phenotype reflecting reduced PSI accumulation (Supplemental Figure 8), and the decreased synthesis of PSI detected in the *psb28*-null mutant could similarly be related to the lower synthesis of CP47 (autoradiogram in Supplemental Figure 7). A specific effect on the synthesis of PSI and CP47 has also been seen in the *Δpor* (Kopečná et al., 2013) and *Δgun4* (Sobotka et al., 2008) mutants disrupted in the PChlide reduction and Mg-chelatase steps, respectively, and in the *ycf54* mutant affected

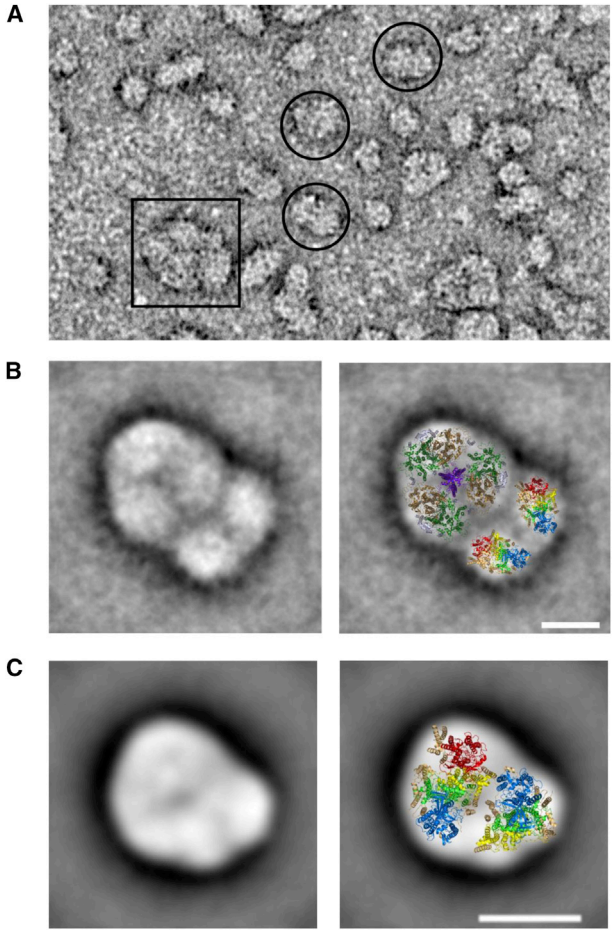

Figure 5. Electron Microscopic Analysis of Complexes Co-isolated with Psb28-1-FLAG from High-Light Exposed Culture.
(A) Electron micrographs of negatively stained complexes. The labeled RCCS and RCC(1)-RC47 particles are in square and circles, respectively.
(B) The top view projection map of the RCCS supercomplex containing trimeric PSI complex and two PSII monomers. The negatively stained particle (left) was obtained by classification of 95 particles. Right: the projection was overlaid with a cyanobacterial X-ray models of the PSI trimer and two PSII core complexes.
(C) The negatively stained particles of RCC(1)-RC47 (left) was obtained by classification of 5600 particles. The projection was overlaid with a cyanobacterial X-ray model of the PSII monomer and PSII monomer lacking CP43 and associated proteins (PsbK, PsbZ, and Psb30).
Color designation of proteins: PsaA, brown; PsaB, dark green; PsaL, violet; other small PSI subunits, gray; D1, yellow; D2, light green; CP47, blue; CP43, red; small PSII subunits, ochre. The coordinates are taken from the PDB (http://www.rcsb.org/pdb): PSI code, PDB: 1JB0 (Jordan et al., 2001); PSII code, PDB: 2AXT (Loll et al., 2005). The scale bars represent 10 nm.

in the function of aerobic cyclase involved in the synthesis of the fifth Chl ring (Hollingshead et al., 2016). Given that newly synthesized Chl in *Synechocystis* 6803 is preferentially incorporated into the PSI trimer (Kopečná et al., 2012) and that this complex is particularly deficient in the CP47-less, *Δpor* and *Δgun4* mutants, Psb28-1 could regulate this main pathway for Chl incorporation. A link between Psb28-1 and the synthesis of Chl-binding proteins is also suggested from analysis of gene transcription during the diurnal cycle of the nitrogen-fixing cyanobacterium *Cyanothece* sp. ATCC 51142. Unlike transcripts for other PSII-associated genes, *psb28* transcripts preferentially accumulate during the dark period when Chl biosynthesis is activated and PSI proteins in particular are synthesized, probably in readiness for the start of the light period (Stöckel et al., 2011).

Previous studies on *psb28* mutants constructed in *Synechocystis* 6803 have led to conflicting results regarding the importance of Psb28-1 for accumulation and assembly of both photosystems. By constructing new deletion mutants in a WT strain of *Synechocystis* 6803 that is known not to be affected in chlorophyll biosynthesis, we have confirmed that Psb28-1 has very little impact on growth under standard continuous illumination (40 μmol photons m^{-2} s^{-1}). Importantly, we have been able to show here that Psb28-1 and Psb27 are needed for optimal growth especially under intermittent high-light/dark conditions (Figure 7). This phenotype has not been reported before for cyanobacteria. In the case of higher plants, Psb28 is already known to be required for normal growth and pigmentation of rice plants (Jung et al., 2008). The mechanism of Psb28-1 action remains unclear, but it apparently differs from that of Psb27, since the intermittent high-light/dark condition affected the growth of the Psb27/Psb28-1 double mutant more severely than each of the single mutants (Figure 7).

METHODS

Construction of Mutant Strains

The non-motile, glucose-tolerant strain of *Synechocystis* sp. PCC 6803 GT-P (Tichý et al., 2016) was used in this study as a WT strain and as a background for the generated deletion mutant strains (ΔPsb28-1, ΔPsb28-2, ΔPsb28-1/ΔPsb28-2, and ΔPsb27/ΔPsb28-1) and FLAG-tagged mutants (Psb28-1-FLAG, FLAG-Psb28-1, Psb28-2-FLAG, and FLAG-Psb28-2).

Deletion Mutant Strains

The psb28-1 knockout vector was constructed in two steps. First, the upstream region of *sll1398* was PCR amplified from WT genomic DNA of *Synechocystis* PCC 6803 with the primer set Sll1398-1F and Sll1398-2R, and the downstream region was amplified with Sll1398-3F and Sll1398-4R. The resulting PCR fragments were then mixed together to serve as the DNA template to perform overlap extension PCR with primer set Sll1398-1F and Sll1398-4R. The joint PCR fragment, which has the entire sll1398 ORF replaced with an EcoRV restriction site, was cloned into pGEM-T Easy vector (Promega). The resulting plasmid, namely pGEMSll1398, was then used as an intermediate vector for insertion of either kanamycin or chloramphenicol cassette via an EcoRV restriction site to create the final transformation vectors termed pSll1398Cam and pSll1398Kan (Supplemental Figure 6). The sequencing confirmed that the orientation of the resistance cassette was the same as the orientation of the gene of interest. The plasmid pSll1398Cam was used for transformation of the WT and ΔPsb27 strain to create deletion mutants ΔPsb28-1 and ΔPsb27/ΔPsb28-1, respectively. The segregation was checked by PCR. Transformants were selected for Cam^R antibiotic resistance and PCR was used to show integration of the selectable marker and elimination of the WT gene copy.

The psb27 and psb28-2 knockout vector was constructed using an identical approach. The resulting plasmids pGEMSlr1645 and pGEMSlr1739 were then used as intermediate vectors for insertion of gentamicin, kanamycin, or chloramphenicol cassette via EcoRV restriction site to create the final transformation vectors termed pSlr1645Gent, pSlr1739Kan, and pSlr1739Cam. The pSlr1739Cam, which has a chloramphenicol

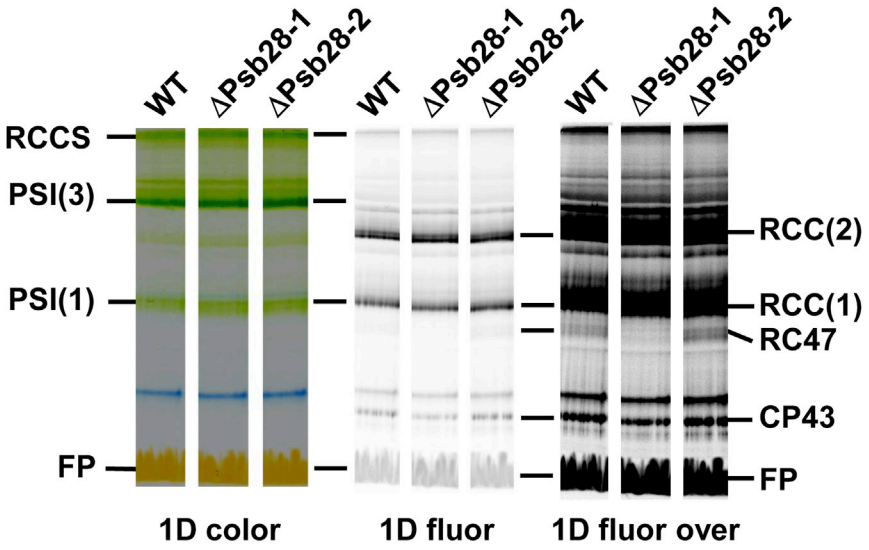

Strain	RC47 band (% of WT)	CP43 band (% of WT)
WT	100	100
ΔPsb28-1	25±6	69±4
ΔPsb28-2	177±17	121±7

Figure 6. Pigment-Protein Analysis of Membranes Isolated from WT, ΔPsb28-1, and ΔPsb28-2 *Synechocystis* 6803 Strains by CN PAGE.

Strains were grown at irradiance of 40 μmol photons m^{-2} s^{-1}. Each sample contained 4 μg of Chl*a* corresponding to the same $OD_{750\ nm}$. The native gel was photographed (1D color) and scanned with an LAS-4000 camera for Chl fluorescence before (1D fluor) and after enhancement of the signal (1D fluor over). Signals of RC47 and CP43 in 1D fluor were quantified with ImageQuant software and expressed as % of the WT band intensity. The values represent means of three independent measurements ± SD.

resistance cassette, was used for transformation of WT to create a deletion mutant ΔPsb28-2 and the pSlr1739Kan for transformation of the ΔPsb28-1 strain with Cam^R to create a double mutant ΔPsb28-1/ΔPsb28-2. The pSlr1645Gent was used for transformation of WT to create a deletion mutant ΔPsb27. Segregations were again checked by PCR. The transcription orientation of antibiotic cassettes was again along the genes of interest.

FLAG-Tagged Mutant Strains

The constructs Sll1398C′FLAG and Slr1739C′FLAG, designed to place the C-terminally FLAG-tagged *sll1398* and *slr1739* genes under the native promoters, consist of an upstream region, a gene with three repetitions of an eight amino acid FLAG sequence (3 × AspTyrLysAspAspAspAspLys; Sigma-Aldrich) on the C terminus, a zeocine cassette in reversed orientation, and downstream region of the corresponding gene (Supplemental Figure 9, right). The constructs were commercially synthesized and cloned to the pUC57 plasmid by EcoRV (Gene Synthesis Service, GenScript; Supplemental Figure 9, left). The obtained plasmids pUC57Sll1398C′FLAG and pUC57Slr1739C′FLAG were then used to transform the WT cells to yield strains expressing C-terminally FLAG-tagged Psb28-1 and Psb28-2. The complete segregation was checked by PCR (data not shown).

To create N-terminally FLAG-tagged Psb28-1, the pUC57Sll1398C′FLAG plasmid was used to generate pUC57Sll1398N′FLAG vector by replacing sll1398-FLAG with the FLAG-sll1398 sequence using NdeI and AvrII restriction sites. The N-terminally FLAG-tagged Psb28-2 was placed under the petJ promoter in a ΔPsb28-2 background (Boehm et al., 2012).

Cultivation Conditions of Cyanobacterial Strains

The cells used in this study were grown in 100 mL of liquid BG11 medium using 250 mL flasks on an orbital shaker at 29°C under continuous light of 40 μmol photons m^{-2} s^{-1} (normal light). For (photo)heterotrophic growth conditions, the medium was supplemented with 5 mM glucose.

The cells used for protein purification were grown in 4 L of BG11 medium containing 1 mM glucose using 10 L flasks. The culture was air bubbled, stirred, and incubated at 29°C under continuous surface illumination of 120 μmol photons m^{-2} s^{-1} from a light source placed on one side of the flask (creating low-light conditions, due to the big volume of the culture). For high-light cultivation, the cells were grown in 400 mL of liquid BG11 medium using 1 L flasks containing 1 mM glucose and cultivated on an orbital shaker under gradually increasing surface illumination of 20–120 μmol photons m^{-2} s^{-1}. WT cells were always grown under the same conditions as the mutant strains.

Growth Assay on Agar Plates

Cells of *Synechocystis* 6803 strains used for growth assay were cultivated autotrophically in 70 mL of liquid BG11 medium using 250 mL flasks on an orbital shaker at 29°C under continuous light of 40 μmol photons m^{-2} s^{-1} (normal light). After reaching the exponential phase, the cells were diluted to $OD_{750\ nm}$ 0.1, 0.05, and 0.025 and spotted on autotrophic BG11 agar plates containing 10 mM TES/NaOH, pH 8.2. One plate was always incubated at 40 μmol photons m^{-2} s^{-1} for 4 days, and identical plate was incubated under intermittent light conditions (5 min dark and 5 min 400 μmol photons m^{-2} s^{-1}) or continuous high light (400 μmol photons m^{-2} s^{-1}) for 4 days.

Radioactive Labeling

Radioactive pulse labeling of the cells was performed at 500 μmol of photons m^{-2} s^{-1} and 30°C using a mixture of [^{35}S]Met and [^{35}S]Cys (Trans-label, MP Biochemicals) as described previously (Dobáková et al., 2009).

Protein Analysis

The Chl*a* content of the samples was determined by extraction into methanol and absorption measurements at 666 and 720 nm (Wellburn, 1994).

Membranes were prepared by breaking the cells with zirconia/silica beads in A buffer (25 mM MES/NaOH [pH 6.5], 10 mM $CaCl_2$, 10 mM $MgCl_2$, and 20% glycerol). The broken cells were centrifuged at 20,000 *g* for 20 min and the pelleted thylakoid membranes were then resuspended in half volume of the supernatant, which represents the soluble fraction, in buffer A. The Chl concentration of 1% (w/v) *n*-dodecyl-β-D-maltoside solubilized membranes was measured by extraction into methanol and absorption measurements at 666 and 720 nm.

Thylakoid membranes corresponding to 4 μg of Chl*a* were solubilized with 1% (w/v) *n*-dodecyl-β-D-maltoside and separated on a 4%–14% (w/v)

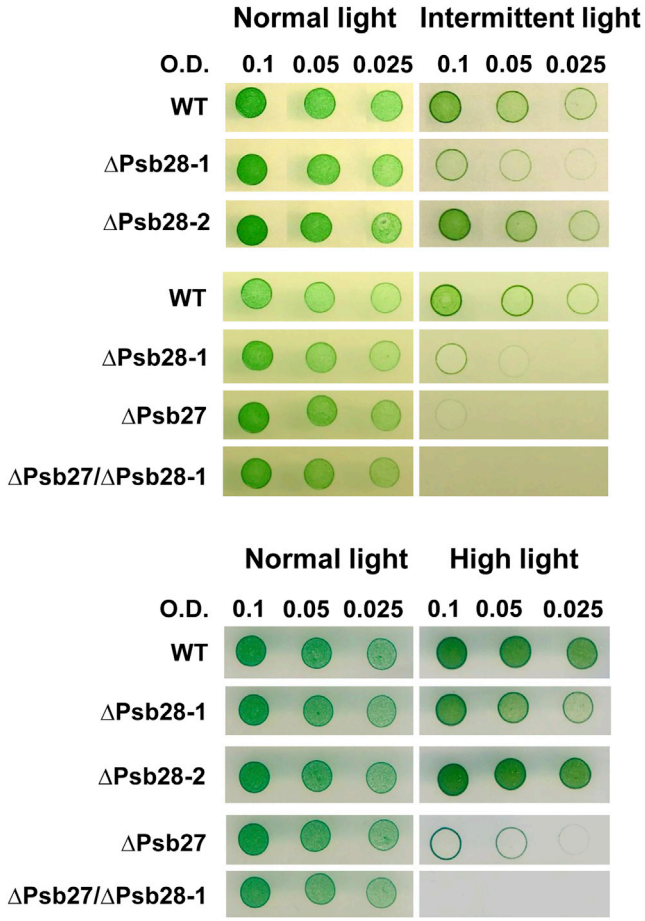

Figure 7. Growth Assay on Agar Plates of WT, ΔPsb28-1, ΔPsb28-2, ΔPsb27, and ΔPsb27/ΔPsb28-1.

Each strain was cultivated autotrophically in liquid BG11 medium at 40 μmol photons m^{2-} s^{-1}. After reaching the exponential phase, the cells were diluted to $OD_{750\ nm}$ 0.1, 0.05, and 0.025 and spotted on autotrophic agar plates. Identical plates were incubated for 4 days either at 40 μmol photons m^{2-} s^{-1} (left) or under intermittent light conditions (5 min dark and 5 min 400 μmol photons m^{2-} s^{-1}, upper right) or at constant high light (400 μmol photons m^{2-} s^{-1}, lower right).

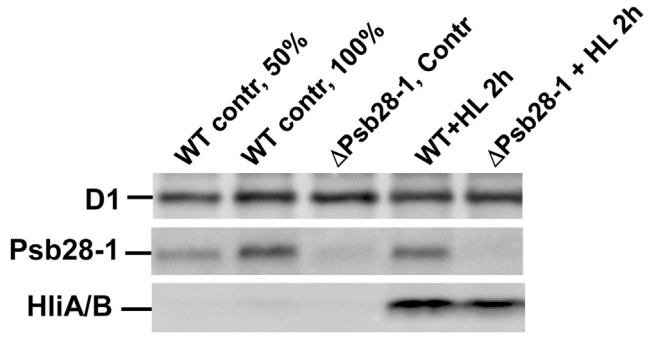

Figure 8. Protein Analysis of WT and ΔPsb28 Cells Grown under Standard (contr) and High (500 μmol photons m^{-2} s^{-1}) Irradiance for 2 h (HL 2h).

Membranes isolated from the cells corresponding to 4 μg of Chl*a* (only lane designated WT contr, 50% contained 2 μg of Chl*a*) were separated by SDS–PAGE, and proteins were blotted onto PVDF membrane and subsequently probed with antibody specific to the D1 protein (loading control), Psb28-1, and HliA/B.

polyacrylamide CN PAGE linear gradient gel (Wittig et al., 2007) or a 4%–14% (w/v) polyacrylamide blue-native PAGE linear gradient gel (Komenda et al., 2012a). Chl fluorescence of separated PSII complexes was recorded using an LAS-4000 camera (Fujifilm, Japan). Gel stripes from the first dimension were incubated in 25 mM Tris/HCl buffer (pH 7.5) containing 1% DTT (w/v) and 1% SDS (v/v) at room temperature for 30 min and then separated on 12%–20% (w/v) polyacrylamide SDS–PAGE gel containing 7 M urea, the second dimension. The gels were stained either with CBB or, for immunoblotting, with fluorescence dye SYPRO orange (Sigma-Aldrich), blotted onto PVDF membrane, and subsequently used for immunodetection. Membranes were incubated with specific primary antibodies raised against Psb27 and PsaD (Komenda et al., 2012a), Psb28 (Dobáková et al., 2009), FLAG (Abgent), and HliA/B (Agrisera), and then with secondary antibody horseradish peroxidase conjugate (Sigma-Aldrich). After incubation with chemiluminescent substrate, Luminata Crescendo (Merck) blots were scanned with an LAS-4000 camera.

Isolation of FLAG-Tagged Proteins

For isolation of FLAG-tagged proteins, membranes were prepared by breaking the cells with zirconia/silica beads in buffer A (25 mM MES/NaOH [pH 6.5], 10 mM $CaCl_2$, 10 mM $MgCl_2$, and 25% glycerol) with protease inhibitor (SIGMAFAST Protease Inhibitor Cocktail Tablets, EDTA-Free, Sigma-Aldrich), separated from the soluble fraction by centrifugation at 60,000 *g* for 20 min; pelleted membranes were resuspended in buffer A and solubilized in 1.5% (w/v) *n*-dodecyl-β-D-maltoside. The supernatant was then loaded onto a column containing 300 μL of anti-FLAG M2 affinity gel (Sigma-Aldrich) pre-equilibrated with buffer A containing 0.04% *n*-dodecyl-β-D-maltoside (A-DDM buffer). To remove any loosely bound contaminants, the column was first washed with 5 mL of buffer A-DDM and then the FLAG-tagged protein was eluted by a 30 min incubation of resin in 200 μL of A-DDM buffer containing 20% glycerol and 150 μL of 3xFLAG peptide (Sigma-Aldrich). Resin was removed by centrifugation at 500 *g* for 5 min. The preparations obtained were separated by 2D gel electrophoresis with subsequent western blotting or Coomassie staining.

Spectroscopy Analysis

Chl fluorescence emission spectra a 77 K were measured using an Aminco Bowman Series 2 luminescence spectrometer (Spectronic Unicam) and fluorescence spectra were recorded in the range 600–800 nm.

Absorption spectra of whole cells and FLAG preparations were recorded in the range 350–750 nm using a Shimadzu UV-3000 spectrophotometer.

Transmission Electron Microscopy

Freshly prepared complexes were used for electron microscopy. The specimens were placed on glow-discharged carbon-coated copper grids and negatively stained with 2% uranyl acetate, visualized by a JEOL JEM-2100F transmission electron microscope (JEOL Japan, using 200 kV at 20,000× magnification) and processed by image analysis. Transmission electron microscopy images were recorded with a bottom-mount Gatan CCD Orius SC1000 camera, corresponding to a pixel size of 3.4 Å. Image analyses were carried out using the Spider and Web software package (Frank et al., 1996). The selected projections were rotationally and translationally aligned, and treated by multivariate statistical analysis in combination with a classification procedure (Van Heel and Frank, 1981; Harauz et al., 1988). Classes from each of the subsets were used for refinement of alignments and subsequent classifications. For the final sum, the best of the class members were summed using a cross-correlation coefficient of the alignment procedure as a quality parameter. The projection was overlaid with cyanobacterial X-ray models of PSI (PDB: 1JB0, Jordan et al., 2001) and monomer of PSII core complexes (PDB: 2AXT, Loll et al., 2005).

Protein Identification by Mass Spectrometry

The MS analyses of protein bands excised from the gel or the liquid pull-down preparations of the tagged proteins were done on a NanoAcquity UPLC (Waters) coupled online to an ESI Q-ToF Premier mass spectrometer (Waters) as described in Janouškovec et al. (2013).

SUPPLEMENTAL INFORMATION

Supplemental Information is available at *Molecular Plant Online*.

FUNDING

We gratefully acknowledge support from the Grant Agency of the Czech Republic (project P501/12/G055), the Czech Academy of Sciences (RVO 60077344 and RVO61388971), the Czech Ministry of Education (projects LO1416 and CZ 1.05/2.1.00/19.0392) and BBSRC (projects BB/L003260/1 and BB/I00937X/1).

AUTHOR CONTRIBUTIONS

M.B. constructed the strains expressing FLAG-tagged Psb28 proteins, performed most of the biochemical experiments, and participated in writing; Z.G. carried out the electron microscopy study; J.Y. constructed the Psb28 deletion mutants; P.K. performed the mass spectrometric analyses; P.J.N. planned the research, evaluated data, and drafted the manuscript; J.K. planned the research, participated in the experimental design and in experiments, evaluated data, and drafted the manuscript.

ACKNOWLEDGMENTS

We thank Eva Prachová and Jiří Šetlík for excellent technical assistance. No conflict of interest declared.

Received: March 20, 2016
Revised: June 29, 2016
Accepted: August 4, 2016
Published: August 12, 2016

REFERENCES

Bialek, W., Wen, S., Michoux, F., Bečková, M., Komenda, J., Murray, J.W., and Nixon, P.J. (2013). Crystal structure of the Psb28 accessory factor of *Thermosynechococcus elongatus* photosystem II at 2.3 A. Photosynth. Res. **117**:375–383.

Boehm, M., Yu, J., Reisinger, V., Bečková, M., Eichacker, L.A., Schlodder, E., Komenda, J., and Nixon, P.J. (2012). Subunit composition of CP43-less photosystem II complexes of *Synechocystis* sp. PCC 6803: implications for the assembly and repair of photosystem II. Philos. Trans. R. Soc. B Biol. Sci. **367**:3444–3454.

Diner, B.A., Schlodder, E., Nixon, P.J., Coleman, W.J., Rappaport, F., Lavergne, J., Vermaas, W.F.J., and Chisholm, D.A. (2001). Site-directed mutations at D1-His198 and D2-His197 of photosystem II in *Synechocystis* PCC 6803: sites of primary charge separation and cation and triplet stabilization. Biochemistry **40**:9265–9281.

Dobáková, M., Sobotka, R., Tichý, M., and Komenda, J. (2009). Psb28 protein is involved in the biogenesis of the Photosystem II inner antenna CP47 (PsbB) in the cyanobacterium *Synechocystis* sp. PCC 6803. Plant Physiol. **149**:1076–1086.

Ferreira, K.N., Iverson, T.M., Maghlaoui, K., Barber, J., and Iwata, S. (2004). Architecture of the photosynthetic oxygen-evolving center. Science **303**:1831–1838.

Frank, J., Radermacher, M., Penczek, P., Zhu, J., Li, Y., Ladjadj, M., and Leith, A. (1996). SPIDER and WEB: processing and visualization of images in 3D electron microscopy and related fields. J. Struct. Biol. **116**:190–199.

Funk, C., and Vermaas, W. (1999). A cyanobacterial gene family coding for single-helix proteins resembling part of the light-harvesting proteins from higher plants. Biochemistry **38**:9397–9404.

Guskov, A., Kern, J., Gabdulkhakov, A., Broser, M., Zouni, A., and Saenger, W. (2009). Cyanobacterial photosystem II at 2.9-A resolution and the role of quinones, lipids, channels and chloride. Nat. Struct. Mol. Biol. **16**:334–342.

Harauz, G., Boekema, E., and van Heel, M. (1988). Statistical image analysis of electron micrographs of ribosomal subunits. Methods Enzymol. **164**:35–49.

He, Q., Dolganov, N., Bjorkman, O., and Grossman, A.R. (2001). The high light-inducible polypeptides in *Synechocystis* PCC6803. Expression and function in high light. J. Biol. Chem. **276**:306–314.

Hernández-Prieto, M.A., Semeniuk, T.A., Giner-Lamia, J., and Futschik, M.E. (2016). The transcriptional landscape of the photosynthetic model cyanobacterium *Synechocystis* sp. PCC6803. Sci. Rep. **6**:22168.

Hollingshead, S., Kopečná, J., Armstrong, D.R., Bučinská, L., Jackson, P.J., Chen, G.E., Dickman, M.J., Williamson, M.P., Sobotka, R., and Hunter, C.N. (2016). Synthesis of chlorophyll-binding proteins in a fully-segregated Δycf54 strain of the cyanobacterium *Synechocystis* PCC 6803. Front. Plant Sci. **7**:292.

Janouškovec, J., Sobotka, R., Lai, D.H., Flegontov, P., Koník, P., Komenda, J., Ali, S., Prášil, O., Pain, A., Oborník, M., et al. (2013). Split photosystem protein, linear-mapping topology, and growth of structural complexity in the plastid genome of chromera velia. Mol. Biol. Evol. **30**:2447–2462.

Jordan, P., Fromme, P., Witt, H.T., Klukas, O., Saenger, W., and Krauss, N. (2001). Three-dimensional structure of cyanobacterial photosystem I at 2.5 A resolution. Nature **411**:909–917.

Jung, K.-H., Lee, J., Dardick, C., Seo, Y.-S., Cao, P., Canlas, P., Phetsom, J., Xu, X., Ouyang, S., An, K., et al. (2008). Identification and functional analysis of light-responsive unique genes and gene family members in rice. PLoS Genet. **4**:e1000164.

Kashino, Y., Lauber, W.M., Carroll, J.A., Wang, Q.J., Whitmarsh, J., Satoh, K., and Pakrasi, H.B. (2002). Proteomic analysis of a highly active photosystem II preparation from the cyanobacterium *Synechocystis* sp. PCC 6803 reveals the presence of novel polypeptides. Biochemistry **41**:8004–8012.

Komenda, J., and Barber, J. (1995). Comparison of PsbO and PsbH deletion mutants of *Synechocystis* PCC-6803 indicates that degradation of D1 protein is regulated by the Q(b) site and dependent on protein-synthesis. Biochemistry **34**:9625–9631.

Komenda, J., Reisinger, V., Muller, B.C., Dobáková, M., Granvogl, B., and Eichacker, L.A. (2004). Accumulation of the D2 protein is a key regulatory step for assembly of the photosystem II reaction center complex in *Synechocystis* PCC 6803. J. Biol. Chem. **279**:48620–48629.

Komenda, J., Knoppová, J., Kopečná, J., Sobotka, R., Halada, P., Yu, J.F., Nickelsen, J., Boehm, M., and Nixon, P.J. (2012a). The Psb27 assembly factor binds to the CP43 complex of photosystem II in the cyanobacterium *Synechocystis* sp. PCC 6803. Plant Physiol. **158**:476–486.

Komenda, J., Sobotka, R., and Nixon, P.J. (2012b). Assembling and maintaining the Photosystem II complex in chloroplasts and cyanobacteria. Curr. Opin. Plant Biol. **15**:245–251.

Kopečná, J., Komenda, J., Bučinská, L., and Sobotka, R. (2012). Long-term acclimation of the cyanobacterium *Synechocystis* sp. PCC 6803 to high light is accompanied by an enhanced production of chlorophyll that is preferentially channeled to trimeric Photosystem I. Plant Physiol. **160**:2239–2250.

Kopečná, J., Sobotka, R., and Komenda, J. (2013). Inhibition of chlorophyll biosynthesis at the protochlorophyllide reduction step results in the parallel depletion of Photosystem I and Photosystem II in the cyanobacterium *Synechocystis* PCC 6803. Planta **237**:497–508.

Liu, H.J., Huang, R.Y.C., Chen, J.W., Gross, M.L., and Pakrasi, H.B. (2011a). Psb27, a transiently associated protein, binds to the chlorophyll binding protein CP43 in photosystem II assembly intermediates. Proc. Natl. Acad. Sci. USA **108**:18536–18541.

Liu, H.J., Roose, J.L., Cameron, J.C., and Pakrasi, H.B. (2011b). A genetically tagged Psb27 protein allows purification of two consecutive photosystem II (PSII) assembly intermediates in *Synechocystis* 6803, a cyanobacterium. J. Biol. Chem. **286**:24865–24871.

Loll, B., Kern, J., Saenger, W., Zouni, A., and Biesiadka, J. (2005). Towards complete cofactor arrangement in the 3.0 angstrom resolution structure of photosystem II. Nature **438**:1040–1044.

Mabbitt, P.D., Wilbanks, S.M., and Eaton-Rye, J.J. (2014). Structure and function of the hydrophilic photosystem II assembly proteins: psb27, Psb28 and Ycf48. Plant Physiol. Biochem. (Paris) **81**:96–107.

Morris, J.N., Crawford, T.S., Jeffs, A., Stockwell, P.A., Eaton-Rye, J.J., and Summerfield, T.C. (2014). Whole genome re-sequencing of two 'wild-type' strains of the model cyanobacterium *Synechocystis* sp. PCC 6803. N. Z. J. Bot. **52**:36–47.

Nixon, P.J., Michoux, F., Yu, J.F., Boehm, M., and Komenda, J. (2010). Recent advances in understanding the assembly and repair of photosystem II. Ann. Bot. (Lond.) **106**:1–16.

Nowaczyk, M.M., Hebeler, R., Schlodder, E., Meyer, H.E., Warscheid, B., and Rogner, M. (2006). Psb27, a cyanobacterial lipoprotein, is involved in the repair cycle of photosystem II. Plant Cell **18**:3121–3131.

Nowaczyk, M.M., Krause, K., Mieseler, M., Sczibilanski, A., Ikeuchi, M., and Rogner, M. (2012). Deletion of psbJ leads to accumulation of Psb27-Psb28 photosystem II complexes in *Thermosynechococcus elongatus*. Biochim. Biophys. Acta **1817**:1339–1345.

Sakata, S., Mizusawa, N., Kubota-Kawai, H., Sakurai, I., and Wada, H. (2013). Psb28 is involved in recovery of photosystem II at high temperature in *Synechocystis* sp. PCC 6803. Biochim. Biophys. Acta **1827**:50–59.

Schriek, S., Aguirre-von-Wobeser, E., Nodop, A., Becker, A., Ibelings, B.W., Bok, J., Staiger, D., Matthijs, H.C.P., Pistorius, E.K., and Michel, K.P. (2008). Transcript profiling indicates that the absence of PsbO affects the coordination of C and N metabolism in *Synechocystis* sp. PCC 6803. Physiol. Plant **133**:525–543.

Sobotka, R., Duerhring, U., Komenda, J., Peter, E., Gardian, Z., Tichý, M., Grimm, B., and Wilde, A. (2008). Importance of the cyanobacterial GUN4 protein for chlorophyll metabolism and assembly of photosynthetic complexes. J. Biol. Chem. **283**:25794–25802.

Stöckel, J., Jacobs, J.M., Elvitigala, T.R., Liberton, M., Welsh, E.A., Polpitiya, A.D., Gritsenko, M.A., Nicora, C.D., Koppenaal, D.W., Smith, R.D., et al. (2011). Diurnal rhythms result in significant changes in the cellular protein complement in the cyanobacterium *Cyanothece* 51142. PLoS One **6**:e16680.

Tichý, M., Bečková, M., Kopečná, J., Noda, J., Sobotka, R., and Komenda, J. (2016). Strain of *Synechocystis* PCC 6803 with aberrant assembly of Photosystem II contains tandem duplication of a large chromosomal region. Front. Plant Sci. **7**:648.

Umena, Y., Kawakami, K., Shen, J.R., and Kamiya, N. (2011). Crystal structure of oxygen-evolving photosystem II at a resolution of 1.9 A. Nature **473**:55–60.

Van Heel, M., and Frank, J. (1981). Use of multivariate statistics in analyzing the images of biological macromolecules. Ultramicroscopy **6**:187–194.

Wellburn, A.R. (1994). The spectral determination of chlorophyll-a and chlorophyll-b, as well as total carotenoids, using various solvents with spectrophotometers of different resolution. J. Plant Physiol. **144**:307–313.

Wittig, I., Karas, M., and Schagger, H. (2007). High resolution clear native electrophoresis for in-gel functional assays and fluorescence studies of membrane protein complexes. Mol. Cell. Proteomics **6**:1215–1225.

Yang, Y., Ramelot, T.A., Cort, J.R., Wang, D., Ciccosanti, C., Hamilton, K., Nair, R., Rost, B., Acton, T.B., Xiao, R., et al. (2011). Solution NMR structure of photosystem II reaction center protein Psb28 from *Synechocystis* sp. strain PCC 6803. Proteins Struct. Funct. Bioinf. **79**:340–344.

PHILOSOPHICAL TRANSACTIONS B

rstb.royalsocietypublishing.org

Research

Cite this article: Bečková M, Yu J, Krynická V, Kozlo A, Shao S, Koník P, Komenda J, Murray JW, Nixon PJ. 2017 Structure of Psb29/Thf1 and its association with the FtsH protease complex involved in photosystem II repair in cyanobacteria. *Phil. Trans. R. Soc. B* **372**: 20160394.
http://dx.doi.org/10.1098/rstb.2016.0394

Accepted: 1 February 2017

One contribution of 16 to a discussion meeting issue 'Enhancing photosynthesis in crop plants: targets for improvement'.

Subject Areas:
plant science

Keywords:
photoinhibition, thylakoid formation 1 gene, D1 subunit, *Synechocystis*, thylakoid membrane, hypersensitive response

Authors for correspondence:
Josef Komenda
e-mail: komenda@alga.cz
James W. Murray
e-mail: j.w.murray@imperial.ac.uk
Peter J. Nixon
e-mail: p.nixon@imperial.ac.uk

†These authors contributed equally to this work.

Electronic supplementary material is available online at https://dx.doi.org/10.6084/m9.figshare.c.3817852.

THE ROYAL SOCIETY PUBLISHING

Structure of Psb29/Thf1 and its association with the FtsH protease complex involved in photosystem II repair in cyanobacteria

Martina Bečková[1,2,†], Jianfeng Yu[3,†], Vendula Krynická[1], Amanda Kozlo[3], Shengxi Shao[3], Peter Koník[1,2], Josef Komenda[1,2], James W. Murray[3] and Peter J. Nixon[3]

[1]Institute of Microbiology, Center Algatech, Opatovický mlýn, 37981 Třeboň, Czech Republic
[2]Faculty of Science, University of South Bohemia, Branišovská 1760, 370 05 České Budějovice, Czech Republic
[3]Sir Ernst Chain Building-Wolfson Laboratories, Department of Life Sciences, Imperial College London, South Kensington Campus, London SW7 2AZ, UK

PJN, 0000-0003-1952-6937

One strategy for enhancing photosynthesis in crop plants is to improve their ability to repair photosystem II (PSII) in response to irreversible damage by light. Despite the pivotal role of thylakoid-embedded FtsH protease complexes in the selective degradation of PSII subunits during repair, little is known about the factors involved in regulating FtsH expression. Here we show using the cyanobacterium *Synechocystis* sp. PCC 6803 that the Psb29 subunit, originally identified as a minor component of His-tagged PSII preparations, physically interacts with FtsH complexes *in vivo* and is required for normal accumulation of the FtsH2/FtsH3 hetero-oligomeric complex involved in PSII repair. We show using X-ray crystallography that Psb29 from *Thermosynechococcus elongatus* has a unique fold consisting of a helical bundle and an extended C-terminal helix and contains a highly conserved region that might be involved in binding to FtsH. A similar interaction is likely to occur in Arabidopsis chloroplasts between the Psb29 homologue, termed THF1, and the FTSH2/FTSH5 complex. The direct involvement of Psb29/THF1 in FtsH accumulation helps explain why THF1 is a target during the hypersensitive response in plants induced by pathogen infection. Downregulating FtsH function and the PSII repair cycle via THF1 would contribute to the production of reactive oxygen species, the loss of chloroplast function and cell death.

This article is part of the themed issue 'Enhancing photosynthesis in crop plants: targets for improvement'.

1. Introduction

Plants exposed to excessive light suffer from impaired photosynthetic activity termed chronic photoinhibition [1,2]. One of the main targets of damage is the oxygen-evolving photosystem II (PSII) complex embedded in the thylakoid membrane system, which uses light energy to extract electrons from water to feed into the photosynthetic electron transport chain to produce the ATP and NADPH required for CO_2 fixation [3]. Irreversible inactivation of PSII occurs at all light intensities [4,5], but activity can be restored through the operation of a repair cycle that replaces damaged protein subunits, mainly the D1 reaction centre subunit, with a newly synthesized copy [1,6]. Only when repair cannot match damage is there a net loss of PSII activity. Consequently, improving the efficiency of the repair cycle, which itself is susceptible to oxidative

damage [7], is a potential route to enhance photosynthesis in crop plants exposed to light stress.

Repair of PSII occurs in all organisms that carry out oxygenic photosynthesis [8,9]. Although there are some differences in the structures of PSII in cyanobacteria and chloroplasts [10], many of the accessory factors and proteases involved in PSII assembly and repair are conserved [11,12], making cyanobacteria extremely useful models to study the molecular details of PSII biogenesis [13].

The main pathway for degrading damaged D1 during repair involves proteolysis by specific members of the FtsH family of ATP-dependent metalloproteases in both cyanobacteria [14,15] and chloroplasts [16–18]. In the case of the cyanobacterium *Synechocystis* sp. PCC 6803 (hereafter *Synechocystis* 6803), electron microscopy has revealed the isolated FtsH complex to be hexameric and composed of alternating FtsH2 and FtsH3 subunits [19], which, based on phylogenetic analyses, have been classified as type B and type A FtsH isoforms, respectively [20,21]. Although structural confirmation is currently lacking, similar hexameric hetero-complexes consisting of type A and type B subunits are likely to be involved in PSII repair in chloroplasts [18,21], with the dominant complex in Arabidopsis composed of FTSH2 (a type B subunit orthologous to FtsH2) and FTSH5 (a type A subunit orthologous to FtsH3) [21]. The Arabidopsis FTSH2 and FTSH5 subunits are also called VAR2 and VAR1, respectively, due to the yellow variegated phenotype of the *var2* and *var1* null mutants [21]. As the chloroplast FtsH proteases are nuclear-encoded in Arabidopsis, the gene products are written in uppercase and the mutants in lower case and in italics.

How expression of FtsH complexes is regulated in response to light stress is unclear. Recent studies of the variegated *thf1* (*thylakoid formation 1*) mutant of Arabidopsis [22] have indicated that the THF1 protein is required for normal accumulation of FTSH2/VAR2 and FTSH5/VAR1 and that this effect is post-transcriptional [23,24]. The THF1 homologue in cyanobacteria, designated Psb29 or Thf1, was originally identified as a sub-stoichiometric component of isolated His-tagged PSII preparations of *Synechocystis* 6803 [25] and a role in the maintenance of PSII was suggested on the basis of the enhanced sensitivity of PSII activity to light stress in a *Synechocystis* 6803 *psb29* null mutant, but specific effects on FtsH were not examined [26]. A reduction in the level of FtsH was recently reported in a *psb29* null mutant of the cyanobacterium *Synechococcus* sp. PCC 7942, but changes to the expression of individual FtsH subunits were not investigated [27]. In addition it has been proposed that Psb29/Thf1 interacts with photosystem I [27].

Here we show that Psb29 in *Synechocystis* 6803, like THF1 in Arabidopsis, is important for normal accumulation of the FtsH heterocomplex involved in PSII repair. Furthermore, affinity purification data suggest that Psb29 physically interacts with FtsH complexes *in vivo*. To gain further insights into Psb29, we have determined the crystal structure of Psb29 encoded by *Thermosynechococcus elongatus*, a thermophilic cyanobacterium widely used to study structural aspects of PSII assembly and repair [28,29]. Psb29 contains a highly conserved surface on one face of the molecule that might be important for specific protein/protein interactions such as with FtsH. A striking feature of Psb29 is the presence of a long alpha helix at the C-terminus extending from the globular protein domain.

2. Material and methods

(a) Cyanobacterial strains and growth conditions

All mutants were constructed in the glucose-tolerant WT-P strain of *Synechocystis* sp. PCC 6803 [30] and grown using BG11 medium as described in [31]. For mixotrophic cultivation, glucose was normally added to 5 mM. For protein and RNA analyses, 50–100 ml liquid cultures of *Synechocystis* 6803 were grown on an orbital shaker in BG11 medium in 250 ml conical flasks at 29°C under moderate light conditions (40 µmol photons m^{-2} s^{-1}). For purification of protein complexes, the FtsH2-FLAG strain was grown as described above in 500 ml of medium using 2 l conical flasks. For purification of Psb29-FLAG protein complexes, 4 l of Psb29-FLAG strain were grown in a 10 l flask in BG11 medium supplemented with 1 mM glucose, agitated with magnetic stirrer and bubbled with air. In both cases, surface irradiance was increased to 100 µmol photons m^{-2} s^{-1} of light to compensate for the longer path length of the flasks. For spot growth tests, 2.5 µl of mixotrophic culture and 10^2, 10^3 and 10^4 serial dilutions were spotted onto BG11 agar plates and grown for 7 days.

(b) Construction of cyanobacterial mutants

The transformation vector for disruption of *psb29* gene in *Synechocystis* 6803 (Cyanobase designation *sll1414*) was constructed in two steps. First, the flanking sequencing of *sll1414*, 445 bp upstream and 555 bp downstream, was PCR amplified with primer set sll1414-1F (AGTTTCTCGTTCTGCCGCCTCAG CTCTT) and sll1414-2R (AATGGGGCCTCATAGTGGGGCAT GGATTGAAGATATCAGGGCCGATTACAAAGGGGGGGATA GT), and sll1414-3F (ACTATCCCCCCCTTTGTAATCGGCCC TGATATCTTCAATCCATGCCCCACTATGAGGCCCCATT) and sll1414-4R (ATTAACTCCCCATCCACTTCCACTTCGATGAT). The resulting PCR products were then mixed as DNA template for overlap extension PCR with primer set sll1414-1F and sll1414-4R. The fused PCR fragment containing an EcoRV restriction site instead of *sll1414* ORF was then cloned into pGEM-T Easy vector. In the second step, a DNA cassette that confers chloramphenicol resistance was inserted into the EcoRV site. Two transformation vectors were selected due to the nature of blunt-end ligation: pSll1414camA has the chloramphenicol marker integrated in the same direction as *sll1414*, whereas, pSll1414camB has the marker in the opposite direction. Both plasmids were used to transform the glucose-tolerant WT-P strain of *Synechocystis* 6803, yielding strains ΔPsb29camA and ΔPsb29camB.

The transformation vectors for expressing C-terminal 3xFLAG-tagged derivatives of Psb29 and FtsH2 at the *psbA2* locus were generated by cloning PCR fragments into the NdeI and NheI sites of pPD-CFLAG [32]. The coding sequence of *psb29* (*sll1414*) was amplified with primer pair CF-Psb29-F (TTTTTTCATATGA CTAAAATTCGCACTGTTTCTGACGCCAA) and CF-Psb29-R (TTTTTTGCTAGCGCTTTCGGAACTCTCCGCTGTGGTT) and the coding sequence of *ftsH2* (*slr0228*) was amplified with primer set CF-FtsH2-F (TTTTTTCATATGAAATTTTCCTGG.AGAACT GCCCTACTT) and CF-FtsH2-R (TTTTTTGCTAGCTAGTTGGG GAATTAACTGTTCCTTGACGGGA). The *Synechocystis* 6803 mutant ΔPsb29camA was used as background strain to generate Psb29-FLAG/ΔPsb29 and insertion mutant *slr0228::cm*^{R} [15] was transformed to generate FtsH2-FLAG/ΔFtsH2.

(c) Preparation of membranes, FLAG-tag immunoaffinity purification and protein analysis

Preparation of membranes by breaking cells using a Mini-Beadbeater-16 (BioSpec) and anti-FLAG pull downs were performed as described in [33]. The chlorophyll concentration of cells and various preparations was measured by extracting into methanol and measuring the absorbances at 666 and 720 nm [34]. Analysis of protein complexes was performed

Table 1. Data collection and refinement statistics for the Psb29 structures. Values in brackets refer to the high resolution shell. DLS, Diamond Light Source.

crystal form	P6322	A-P21	B-P21	I222
PDB	5MLF	5MJO	5MJR	5MJW
structure	Psb29 full-length	Psb29 truncated	Psb29 truncated	Psb29 truncated
crystallization condition	16% w/v PEG 6 K, 80 mM sodium citrate pH 5	0.1 M Bicine pH 9.0, 20% w/v PEG 6 K	0.1 M sodium citrate pH 5, 20% w/v PEG 6 K	0.2 M sodium malonate pH 7, 20% w/v PEG 3350
beamline	DLS I03	DLS I04-1	DLS I04-1	DLS I03
wavelength (Å)	0.9537	0.91730	0.91730	0.97630
space group	$P6_322$	$P2_1$	$P2_1$	I222
unit cell a,b,c (Å) α, β, γ (°)	138.91,138.91,205.91, 90,90,120	31.240, 56.730, 47.730, 90, 104.720,90	39.640, 56.040, 44.530 90, 105.760, 90	62.850, 86.610, 116.020, 90, 90, 90
resolution	56–3.64 (3.73–3.64)	46–1.55 (1.59–1.55)	42.9–1.38 (1.42–1.38)	55.3–2.47 (2.53–2.47)
total no. reflections	278837 (21276)	392216 (28397)	259805 (18416)	73967 (5401)
no. unique reflections	20447 (1466)	23219 (1702)	38130 (2813)	11662 (838)
completeness (%)	99.92 (100.0)	99.0 (99.2)	98.7 (98.3)	99.6 (98.8)
multiplicity	13.6 (14.5)	16.9 (16.7)	6.8 (6.5)	6.3
<I/sigmaI>	7.4 (4.5)	18.4 (3.4)	16.0 (2.8)	16.5 (3.4)
Rmerge	0.394 (0.764)	0.114 (1.098)	0.071 (0.796)	0.062 (0.827)
Wilson B ($Å^2$)	17.2	15.9	13.1	73.2
refinement				
program	phenix.refine	refmac	refmac	refmac
% test set	5.13	5.1	5.0	4.8
R_{cryst}	0.3110	0.13321	0.11356	0.21760
R_{free}	0.3575	0.19243	0.15544	0.24978
RMS				
bonds (Å)	0.002	0.024	0.026	0.008
angles (°)	0.471	2.070	2.181	1.191
Ramachandran plot (molprobity)				
most favoured (%)	96.52	98.91	98.37	96.37
outliers (%)	0	0	0	0.52

using two dimensional clear-native/SDS polyacrylamide gel electrophoresis (2D-CN/SDS PAGE) on a 4 to 14% native and 12 to 20% SDS gel containing 7 M urea, respectively [33]. The gels were stained either with Coomassie Blue and the visualized bands subjected to mass spectrometric (MS) analysis or with the fluorescence dye SYPRO Orange, then blotted onto PVDF membrane for immunodetection. Proteins were detected using antibodies specific for FtsH1, FtsH2, FtsH3 and global FtsH (FtsHg) [19], Phb1 and Phb3 [35] and Psb29 using an antiserum raised against a peptide corresponding to residues 155–172 of *Synechocystis* Psb29 conjugated to keyhole limpet haemocyanin (Clonestar, Brno, Czech Republic).

(d) Mass spectrometric identification of proteins

The MS analyses of protein bands excised from gels were done on a NanoAcquity UPLC (Waters) on-line coupled to an ESI Q-ToF Premier mass spectrometer (Waters), as described in [36].

(e) Determination of *ftsH2* and *ftsH3* transcript levels

Determination of the *ftsH2* and *ftsH3* transcript levels by quantitative PCR was performed as described in [31] using specific primers for *ftsH2* and *ftsH3* and Transcriptor Reverse Transcriptase (Roche). The *rnpB* gene encoding the B subunit of ribonuclease P was used as a reference and the analysis was performed in triplicate using three independent cultures.

(f) Expression of Psb29 and structure solution

The coding sequence of Psb29 from *T. elongatus* (Cyanobase designation: Tlr1134) was cloned into the BamHI and XhoI sites of the modified pRSETA expression vector [28] following amplification of *psb29* using primer set Tlr1134-F (GGATCCGTGCAA AATCCTCGAACTGTCTCTGATACCAAACG) and Tlr1134-R (CTCGAGTCAAGCGGGTGCATCGGAGCTGGCAT). The resulting vector pRSETAPsb29 encodes a recombinant protein consisting of a 6xHis tag at the N-terminus followed by a thrombin cleavage site then Psb29. The *E. coli* strain KRX was used for recombinant Psb29 expression. Psb29 expression in transformed cells was induced at an OD_{730} of 0.8 with 1 g l^{-1} rhamnose and cells were then grown at 18°C overnight. Cells were lysed by sonication in lysis buffer (50 mM Tris-HCl pH 7.9, 500 mM NaCl, 1 mM $MgCl_2$). In some preparations, the lysis buffer was supplemented with a Complete Protease Inhibitor Cocktail Tablet – EDTA (Roche, UK). The supernatant was mixed with a Ni-IDA resin (Generon, UK). Non-specifically bound proteins were removed

by washing three times with wash buffer (20 mM Tris-HCl pH 7.9, 500 mM NaCl, 60 mM imidazole) and Psb29 was eluted with elution buffer (20 mM Tris-HCl pH 7.9, 500 mM NaCl, 1M imidazole). The protein was concentrated to around 10 mg ml^{-1} in 20 mM Tris-HCl pH 7.9, 500 mM NaCl and used for crystallization trials. Concentrated samples were placed in sitting drop vapour diffusion crystallization screens using a Mosquito® robot (TTP LabTech, UK).

For preparations in the presence of protease inhibitor, the only crystals obtained were of needle morphology in $P6_322$, which diffracted very weakly. If protease inhibitor was omitted, crystals were readily obtained in three crystal forms. Two of these were in $P2_1$ (designated A-$P2_1$ and B-$P2_1$) and the third in I222. The structure was solved by single-wavelength anomalous dispersion (SAD) with the A-$P2_1$ crystal form, soaked overnight with 1 mM dipotassium tetraiodomercurate (Jena Bioscience). The $P6_322$ form was soaked overnight in 1 mM 4-(Chloromercuri)benzensulfonic acid sodium salt (Jena Bioscience), but this was not used for phase determination. Crystals were cryoprotected in the mother liquor with 30% glycerol added, and flash-cooled in a loop into liquid nitrogen. Diffraction data were collected at Diamond Light Source and processed using xia2 [37] with XDS [38]. See table 1 for data collection and refinement information. Heavy atom sites for A-$P2_1$ were found and the structure phased using the autoSHARP [39] pipeline. The initial model was built with Buccaneer [40] and refined with REFMAC [41]. The B-$P2_1$,I222 and $P6_322$ crystal forms were solved by molecular replacement with Phaser [42] using the A-$P2_1$ structure as a model. These structures were refined with REFMAC or phenix.refine [43]. Structures were validated using MolProbity [44].

(g) Bioinformatics

211 Psb29 sequences were retrieved by blasting Psb29 from *Synechocystis* 6803 (*sll1414* gene product) against UniProt KnowledgeBase Reference proteomes (http://www.uniprot.org). The cut-off threshold was empirically set to 1×10^{-4} after manually examining the resulting hits. 103 records were from cyanobacteria, 84 from plant, 11 from green algae, 12 from red algae and one from a virus that infects the green alga *Chlorella* sp. strain NC64A. 211 sequences were then aligned using MAFFT version 7 programme with the 'G-INS-I' setting applied [45]. Gaps within the alignment were trimmed by trimAl using the 'gappyout' method [46] and then the alignment was subjected to maximum-likelihood based phylogenetic inference, PhyML. ETE3 toolkit [47] was used to automate the above process; the PhyML setting was '+G+I+F, 4 classes and aLRT branch supports, default models JTT/GTR' [48]. The final unrooted tree was organized and beautified with iTOL [49]. Subsets of 103 cyanobacterial and 84 plant Psb29 sequences were clustered according to their phylogeny. The trimmed alignments used in the conservation analysis were subjected to identity and similarity calculations using MatGAT [50]. The evolutionary conservation was analysed using ConSurf 2016 server [51]. The above MAFFT alignment was trimmed of columns containing gaps of over 90%; columns corresponding to the chloroplast transit peptide domain of *Arabidopsis thaliana* THF1, predicted by ChloroP 1.1 Server [52], were also removed.

3. Results

(a) Psb29 is required for normal expression of FtsH2 and FtsH3 in *Synechocystis* 6803

To test whether Psb29 plays a role in the expression of FtsH in *Synechocystis* 6803, we performed an immunoblotting analysis of membranes isolated from a *psb29* null mutant, ΔPsb29camA,

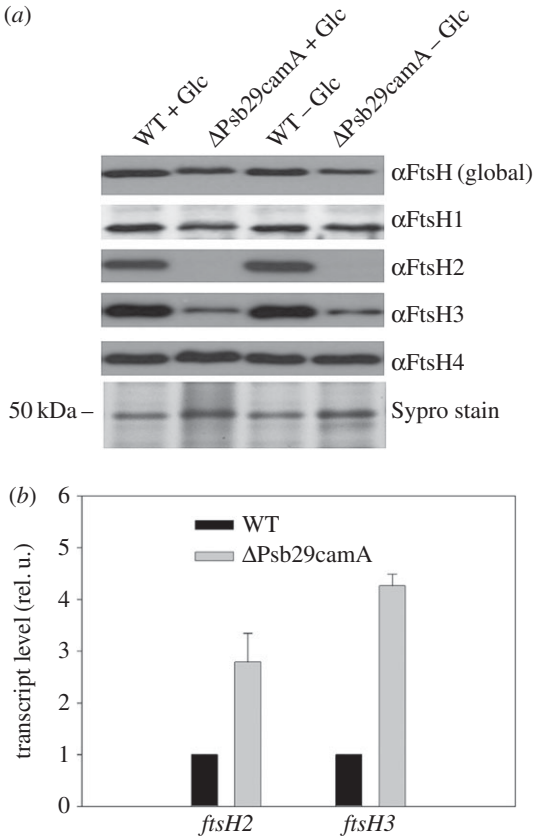

Figure 1. (*a*) Immunochemical analysis of FtsH subunits in WT and ΔPsb29camA grown either in the presence (+Glc) or absence (−Glc) of glucose until an OD_{730} of 0.6–0.8. Protein loading assessed by protein staining (Sypro stain). (*b*) Relative transcript levels of *ftsH2* and *ftsH3* in WT and ΔPsb29camA determined by RT-PCR.

in which the *psb29* gene was replaced by a chloramphenicol-resistance cassette (electronic supplementary material, figure S1*a*,*b*). Cultures grown to late-exponential phase under either photoautotrophic or mixotrophic conditions were analysed. Antibodies specific for each of the four FtsH proteins encoded by *Synechocystis* 6803 revealed that levels of FtsH2 and FtsH3 were decreased substantially in the mutant compared to the WT control, consistent with a specific effect on the accumulation of the FtsH2/FtsH3 hetero-complex, whereas there was less of an impact on FtsH1 and FtsH4 (figure 1*a*). Similar results were also obtained with a *psb29* null mutant, ΔPsb29camB, containing the chloramphenicol-resistance cassette inserted in the opposite orientation (electronic supplementary material, figure S1*a*–*c*). Reverse-transcription PCR confirmed that *ftsh2* and *ftsH3* were still transcribed in ΔPsb29camA so the effect of Psb29 on the expression of FtsH2 and FtsH3 occurred after transcription (figure 1*b*). The 2–5-fold increase in *ftsH2* and *ftsH3* transcripts in ΔPsb29camA might reflect a compensatory mechanism to increase expression. Importantly, immunoblotting experiments showed that FtsH2 and FtsH3 expression was reduced but not blocked totally in the absence of Psb29 (electronic supplementary material, figure S1*c*).

(b) Psb29 interacts with FtsH complexes

To test whether Psb29 interacts with FtsH we generated two strains of *Synechocystis* 6803 expressing either Psb29 or FtsH2 tagged at the C-terminus by addition of a 3XFLAG tag. Expression of the tagged proteins under the control of the *psbA2* promoter in the relevant *ftsH2* or *psb29* null mutant

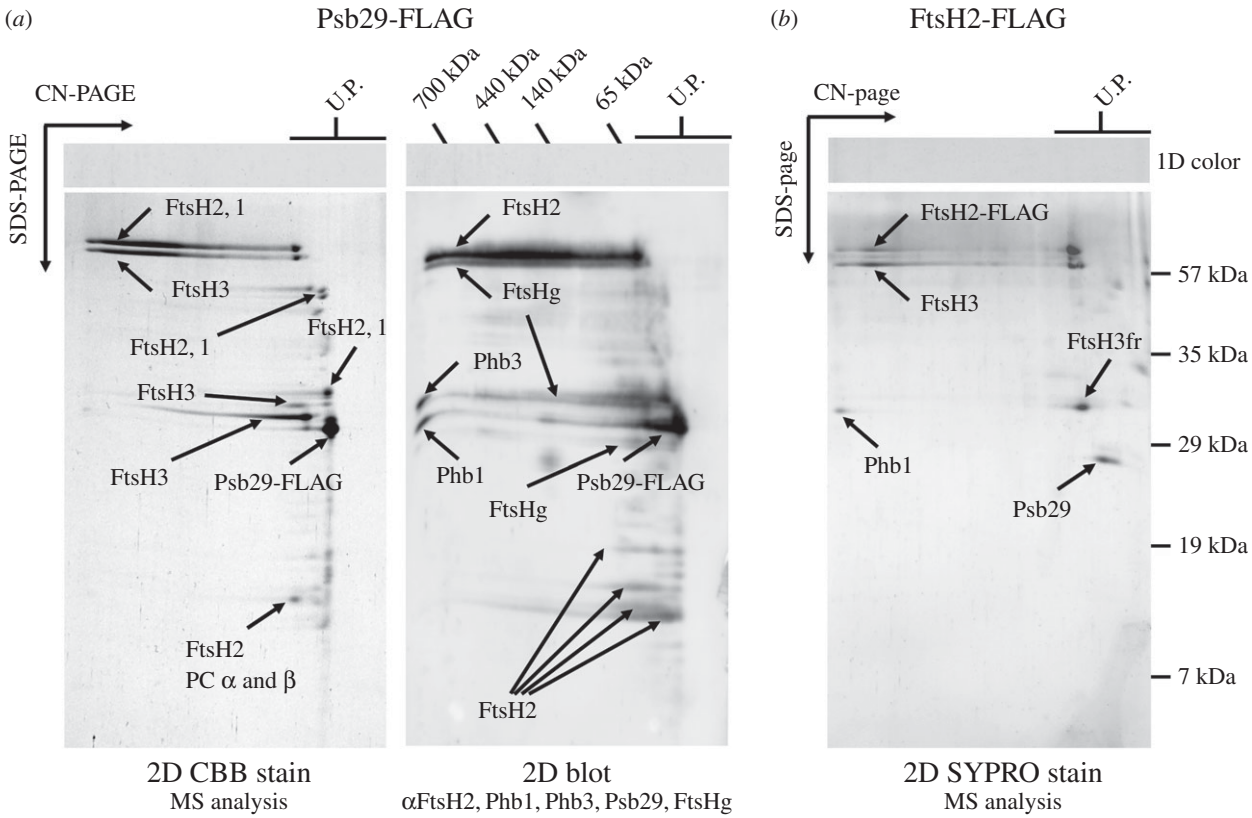

Figure 2. (*a*) Isolation of FLAG-tagged Psb29 and identification of co-purifying proteins by 2D gel electrophoresis followed by Coomassie Brilliant Blue (CBB) staining and mass spectrometry (left panel) or by sequential immunochemical detection with antibodies in the order shown starting with FtsH2 (right panel). The global FtsH antibody recognizes all FtsH isoforms (FtsHg) whereas the other FtsH antibodies are specific for each subunit. (*b*) Isolation of FLAG-tagged FtsH2 and detection of proteins by mass spectrometry after staining gel with Sypro orange (SYPRO stain).

restored photoautotrophic growth at high irradiances, indicating that the tagged proteins were still functional (electronic supplementary material, figure S2). Immunoaffinity purification of Psb29-FLAG from detergent-solubilised membranes using anti-FLAG antibodies, followed by 2D gel electrophoresis (clear-native in the first dimension and denaturing in the second) and detection of proteins by protein staining, immunoblotting and mass spectrometry revealed the presence of large complexes containing FtsH2, FtsH3 and FtsH1 (figure 2*a*), which we assign to FtsH2/FtsH3 and FtsH1/FtsH3 heterocomplexes based on previous studies [19]. Also detected were minor amounts of fragments derived from FtsH1, FtsH2 and FtsH3 that migrated as unassembled proteins, and two members of the Band 7 superfamily: prohibitin (Phb1) previously detected in FtsH2/FtsH3 preparations [19] and Phb3 [35]. Psb29-FLAG did not co-migrate with FtsH in the native gel, suggesting detachment during electrophoresis. The reciprocal immunoaffinity purification using the FtsH2-FLAG strain confirmed the co-purification of Psb29 with FtsH2 and FtsH3 (figure 2*b*). Overall these data support the direct interaction of Psb29 with FtsH2/FtsH3 complexes.

(c) Crystal structure of Psb29 from *T. elongatus*

To gain structural information on Psb29, we over-expressed Psb29 encoded by the cyanobacterium *T. elongatus* as an N-terminal His-tagged protein in *E. coli* and isolated the protein by Ni-affinity chromatography. Four crystal forms were obtained by hanging drop vapour diffusion; X-ray diffraction data were collected at resolutions from 3.6 Å to 1.4 Å and the structure of Psb29 determined by heavy atom SAD (table 1). The most complete structure consisting of residues 4 to 206 of the predicted 222 residues of Psb29 was obtained from $P6_322$ needle-shaped crystals containing seven copies of Psb29 in the asymmetric unit, which form a continuous cylindrical shell of protein in the crystal, with the C-terminus of the protein forming a helix extending from the compact protein fold into the middle of the cylindrical protein shell (electronic supplementary material, figure S3*a*). Each Psb29 subunit consists of 9 alpha helices (figure 3). A search using PDBeFOLD [53] found no known structures with greater than 70% similarity, indicating that the specific fold is novel.

Psb29 in the other crystal forms was proteolytically cleaved at the C-terminus. In the B-$P2_1$ crystal form, the new carboxy terminus at residue Ala189 is clearly visible in the electron density (electronic supplementary material, figure S3*b*). It is likely that proteolytic cleavage of the C-terminal helix allows more compact higher resolution crystal lattices to form, as there is insufficient space in these lattices to accommodate the C-terminal helix observed in the $P6_322$ crystal form. The I222 crystal form shows a domain-swapping of the N-terminal helix from the N-terminus to residue Ile22, creating a domain-swapped dimer (electronic supplementary material, figure S3*c*). Given that the domain-swap is not observed in the other crystal forms, this is probably a crystallization artefact.

(d) Comparison of Psb29/THF1 sequences

Bioinformatic analyses revealed that Psb29 and its eukaryotic homologue THF1 are found solely in oxygenic photosynthetic organisms (electronic supplementary material, figure S4). One exception is a virus infecting the green alga *Chlorella* sp. strain

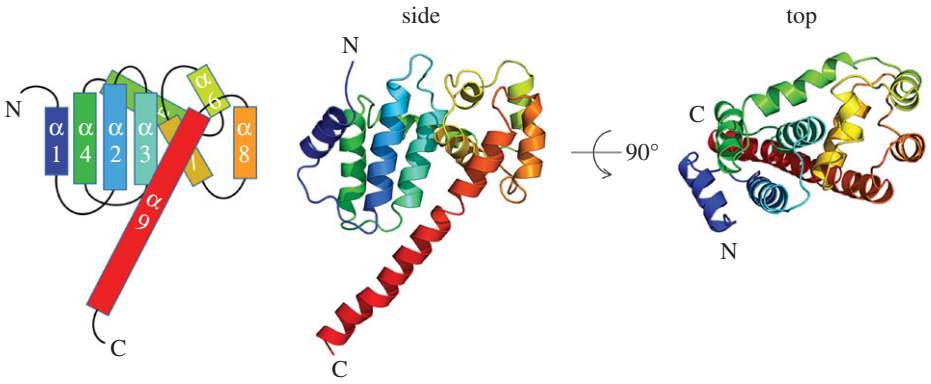

Figure 3. Structure of Psb29 (PDB: 5MLF) encoded by *T. elongatus* showing side and top views and cartoon representation of the 9 alpha helices.

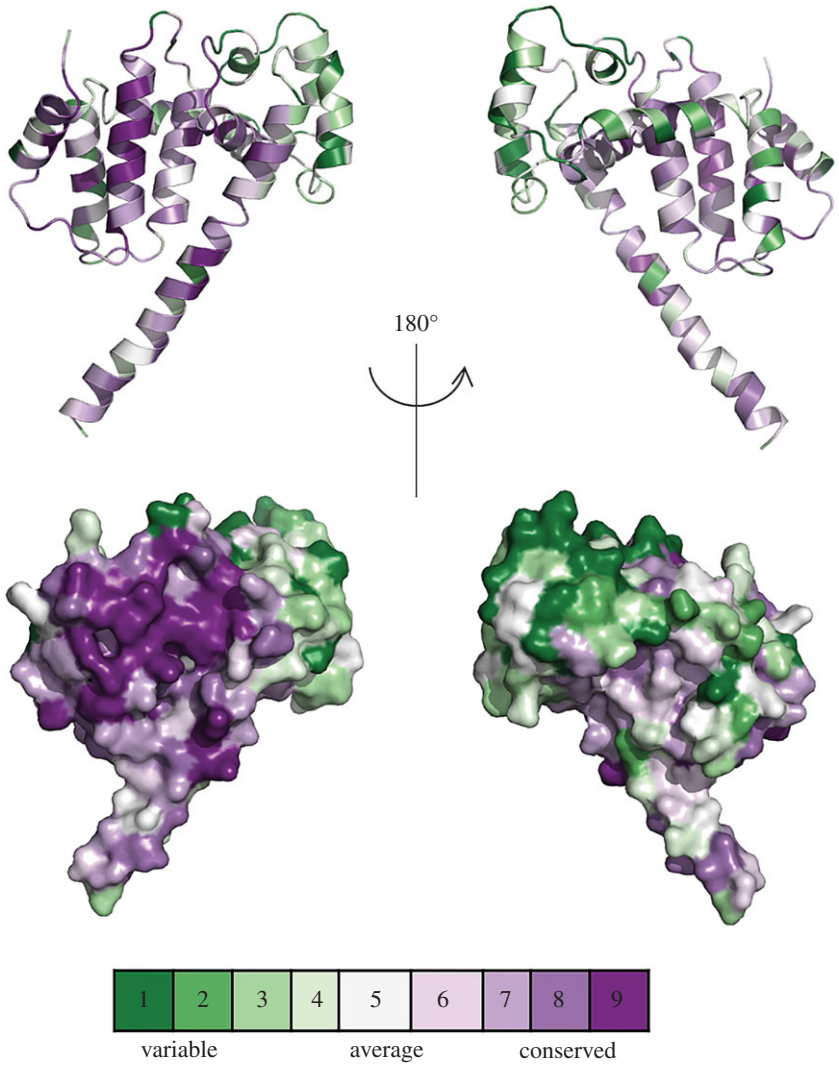

Figure 4. Highly conserved residues in *T. elongatus* Psb29. A ConSurf analysis was performed based on the alignment of 211 Psb29/THF1 sequences from oxygenic phototrophs. The front and back views highlight the conserved and variable regions of Psb29 using the following colouring scheme: purple, 9 = maximal conservation; white, 5 = average conservation; green, 1 = maximal variability.

NC64A that possesses a Psb29-encoding gene closely related to green algal Psb29 sequences (electronic supplementary material, figure S4). In the proteome database interrogated on 11th November 2016, 103 out of 106 cyanobacteria were found to encode Psb29 homologues. The genome sequences of the three remaining cyanobacteria, *Limnoraphis robusta* CS-951, *Leptolyngbya valderiana* BDU 20041, and *Cyanobium* sp. PCC 7001 (*Synechococcus* sp. PCC 7001) are still incomplete and so still yet might encode Psb29.

Overall Psb29 from *T. elongatus* shows a mean sequence similarity of 59.2% with the 102 cyanobacterial Psb29 sequences examined and 53.7% with the 84 plant THF1 sequences. Six residues are totally conserved in cyanobacterial and plant Psb29/THF1 sequences (electronic supplementary material, figure S5): based on the structure described here, F14, V35, L39, G55 and G138 (*T. elongatus* numbering) appear important for the packing of alpha helices and R133 at the beginning of helix 7 is within H-bonding distance of E36 in

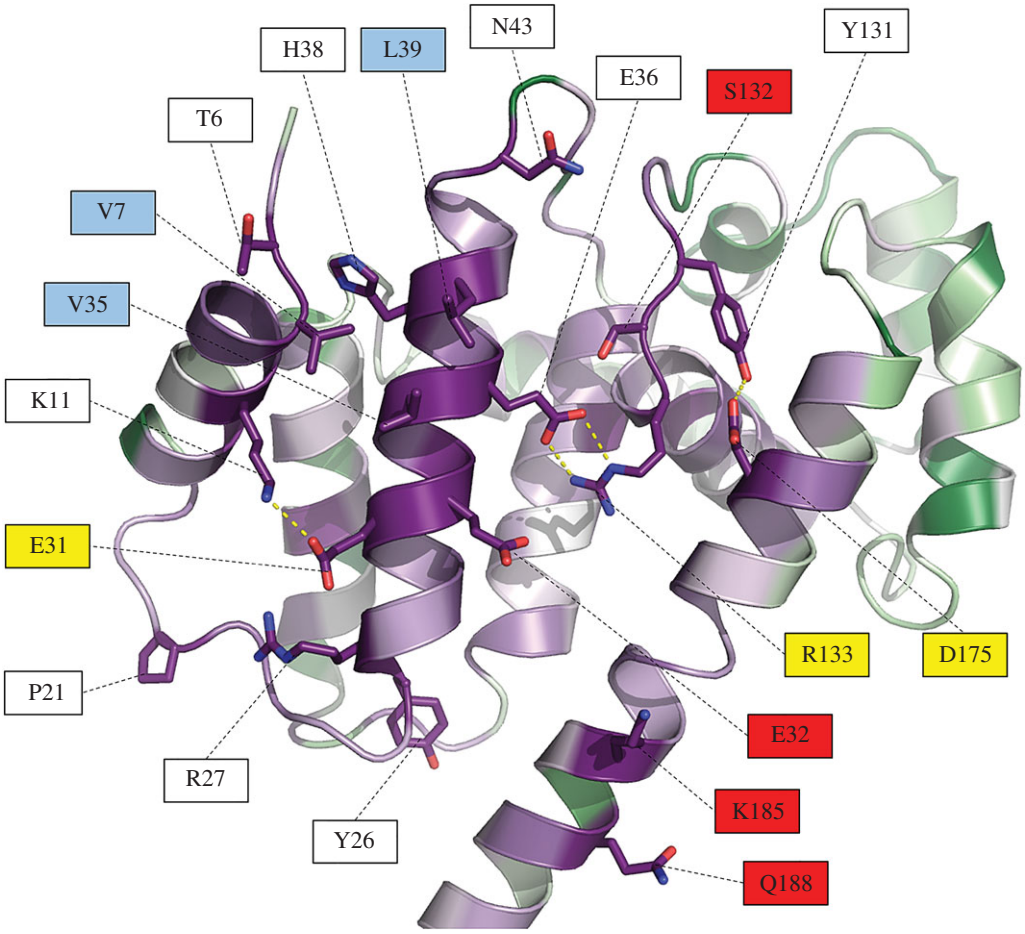

Figure 5. Close-up view of the conserved residues of Psb29/THF1 identified by ConSurf analysis. The most conserved residues that are not buried within the Psb29 structure are shown in stick form, with red indicating oxygen atoms and blue nitrogen atoms. Intra-protein side-chain polar contacts are shown as yellow dashed lines. Some residues are colour-coded to indicate possible type of interaction. Red labels indicate potential hydrogen bonding/charged residues that might stabilize protein/protein interactions; yellow labels indicate residues possibly involved in both stabilizing the structure and interacting with proteins; light blue labels indicate potential hydrophobic contact sites.

the middle of helix 2 (electronic supplementary material, figure S4). These sequence identities would suggest a high degree of conservation of tertiary structure between Psb29 and THF1 in this region of the molecule. A ConSurf analysis in which all Psb29/THF1 sequences were fitted into the *T. elongatus* structure revealed high sequence conservation on one face of the molecule, which would indicate an important role for this region in protein function (figure 4). There are several conserved residues in this region that might play a role in binding interacting partners such as FtsH (figure 5).

The alignment of Psb29/THF1 sequences revealed a variety of small insertions and deletions. In the case of plant THF1, these insertion/deletion events correspond to *T. elongatus* residues 121–122 and 151–154, which lie in loop regions connecting alpha helices 6–7 and 7–8, respectively (electronic supplementary material, figure S5), in the more divergent region of Psb29. The C-terminal end of the protein is also poorly conserved (electronic supplementary material, figures S5 and S6).

4. Discussion

Previous work in Arabidopsis has shown that the absence of THF1 leads to a 40–80% decrease in the amount of the type A and type B FTSH subunits involved in PSII repair as judged by immunoblotting [23]. We show here that loss of Psb29 has a similar effect in cyanobacteria, as levels of the FtsH2 and FtsH3 subunits that form the FtsH heterocomplex involved in PSII repair in *Synechocystis* 6803 are likewise reduced in *psb29* null mutants (figure 1; electronic supplementary material, figure S1*c*). These data suggest a conserved role for Psb29/THF1 in fine-tuning the expression of thylakoid FtsH heterocomplexes.

Importantly, we have provided evidence that Psb29 interacts directly with FtsH2/FtsH3 complexes (figure 2). Thus we suggest that Psb29/THF1 plays a direct role in the accumulation of FtsH heterocomplexes. Based on the co-purification of FtsH1 with Psb29-FLAG (figure 2*a*), it is possible that Psb29 is also involved in the accumulation of FtsH1/FtsH3 heterocomplexes [19]. However, levels of FtsH1 were much less affected than FtsH2 and FtsH3 in the *psb29* null mutant under the conditions examined (figure 1).

Recent work, based on the analysis of cross-linked membrane protein complexes by sucrose density gradient centrifugation, has concluded that Psb29 in the cyanobacterium *Synechococcus* sp. PCC 7942 binds to PSI complexes [27]. However, pull-down experiments were not done to confirm cross-linking between Psb29 and PSI. In light of our data, we suggest that further work is needed to exclude the possibility that Psb29 is actually cross-linked to FtsH complexes, which then co-sediment with PSI. Reduced expression of PSI was

also reported in a *psb29* null mutant [27] but this might be related to effects on expression of FtsH2 rather than a direct effect of Psb29 [54].

We have also presented the first structural information on Psb29. The first 3 and last 16 residues could not be identified in the most complete crystal structure, possibly because of structural flexibility or because of some proteolytic degradation. The fitting of cyanobacterial and plant Psb29/THF1 proteins into the *T. elongatus* crystal structure using ConSurf has allowed us to identify a highly conserved surface on Psb29 that might be involved in protein/protein interactions, such as with FtsH (figures 4 and 5). Recent work has indicated that residues 223–295 of THF1 of *Nicotiana benthamiana*, encompassing part of helix 8, all of helix 9 and most of the C-terminal tail, is a target for a sub-group of nucleotide-binding leucine-rich-repeat (NB-LRR) proteins involved in plant immunity [55]. Thus some of the observed sequence variation between Psb29 and THF1 might reflect changes in THF1 function since the divergence of plants and cyanobacteria.

PSII repair is one of several photoprotective mechanisms used by plants [2]. Despite its physiological importance, little work has been directed at enhancing PSII repair in crop plants, either in terms of robustness or speed of response. In the case of plants, damaged PSII complexes must migrate from the appressed membranes in the grana to the margins to be repaired [56]. This means that prompt degradation of damaged D1 might become a bottleneck in the repair process and that enhancing the expression of FTSH proteases, or DEG proteases that act as a second-line of defence [17], might delay or prevent chronic photoinhibition. Our work now identifies Psb29/THF1 as an additional target for manipulation.

Work in cyanobacteria has highlighted D1 synthesis as a weak link in PSII repair due to reactive oxygen species (ROS)-mediated oxidation of elongation factor EF-G required for protein translation [57]. Attempts to improve protein synthesis by mutating the two Cys residues of EF-G sensitive to oxidative damage has had limited success [58]. Instead a more promising approach is the over-expression of enzymes to detoxify ROS [59]. Prompt replacement of D1 during repair might also be helped by increasing the pool of unassembled D1 in the membrane that could be tapped into to replace damaged D1. One approach might be to over-express the higher plant homologues of Ycf48 and the Ycf39/Hlip complex, which have been shown to stabilize unassembled D1 in cyanobacteria [60,61].

Although upregulating FtsH activity and the PSII repair cycle would seem beneficial for plant growth, there appear to be situations where plants deliberately downregulate chloroplast FtsH activity, which is known to lead to the enhanced production of ROS even under non-photoinhibitory conditions [62]. The source of ROS is not clear but they could be produced by defective PSII complexes that have not been promptly repaired. One dramatic example is the hypersensitive response (HR), which is induced to kill plant cells infected by pathogens so as to limit the zone of infection [63]. Although chloroplast FtsH had previously been implicated in HR [64], the mechanism has been unclear. Recent evidence has suggested a role for THF1 in the signal transduction pathway [55,65]. Our data would suggest that loss of THF1 in the chloroplast plays a direct role in the decrease of FtsH activity, either by destabilizing FtsH complexes, as observed in the Arabidopsis *thf1* null mutant [23] and/or by impairing assembly. Evidence from both cyanobacteria [66] and *Chlamydomonas reinhardtii* [67] suggests that upregulating synthesis of FtsH is important for acclimation to higher light intensities as well as possibly replacing damaged FtsH.

Data accessibility. This article has no additional data.

Authors' contributions. M.B., J.Y., V.K., S.S., J.K., A.K. and J.W.M. contributed to the acquisition of data. All authors were involved in the design, analysis and interpretation of the data and the drafting of the article.

Competing interests. We have no competing interests.

Funding. P.J.N. and J.W.M. gratefully acknowledge the BBSRC for financial support (grant BB/I00937X/1 and BB/L003260/1). M.B., V.K., P.K. and J.K. were supported by the Grant Agency of the Czech Republic (P501-12-G055) and Czech Ministry of Education (projects CZ.1.05/2.1.00/19.0392 and LO1416). S.S. is a recipient of an Imperial College/China Scholarship Council PhD scholarship.

Acknowledgements. We thank Diamond Light Source for access to the macromolecular crystallography beamlines I03 and I04-1 (via proposal mx7299) that contributed to the results presented here.

References

1. Adir N, Zer H, Shochat S, Ohad I. 2003 Photoinhibition—a historical perspective. *Photosynth. Res.* **76**, 343–370. (doi:10.1023/A:1024969518145)
2. Takahashi S, Badger MR. 2011 Photoprotection in plants: a new light on photosystem II damage. *Trends Plant Sci.* **16**, 53–60. (doi:10.1016/j.tplants.2010.10.001)
3. Barber J *et al.* 2016 Photosystem II: the water splitting enzyme of photosynthesis and the origin of oxygen in our atmosphere. *Q. Rev. Biophys.* **49**, e14. (doi:10.1017/S0033583516000093)
4. Tyystjärvi E, Aro EM. 1996 The rate constant of photoinhibition, measured in lincomycin-treated leaves, is directly proportional to light intensity. *Proc. Natl Acad. Sci. USA* **93**, 2213–2218. (doi:10.1073/pnas.93.5.2213)
5. Park Y, Anderson JM, Chow WS. 1996 Photoinactivation of functional photosystem II and DI-protein synthesis *in vivo* are independent of the modulation of the photosynthetic apparatus by growth irradiance. *Planta* **61**, 300–309. (doi:10.1007/BF00206257)
6. Komenda J, Sobotka R, Nixon PJ. 2012 Assembling and maintaining the Photosystem II complex in chloroplasts and cyanobacteria. *Curr. Opin. Plant Biol.* **15**, 245–251. (doi:10.1016/j.pbi.2012.01.017)
7. Nishiyama Y, Allakhverdiev SI, Murata N. 2011 Protein synthesis is the primary target of reactive oxygen species in the photoinhibition of photosystem II. *Physiol. Plant.* **142**, 35–46. (doi:10.1111/j.1399-3054.2011.01457.x)
8. Hoffman-Falk H, Mattoo AK, Marder JB, Edelman M, Ellis RJ. 1982 General occurrence and structural similarity of the rapidly synthesized, 32,000-dalton protein of the chloroplast membrane. *J. Biol. Chem.* **257**, 4583–4587.
9. Ohad I, Kyle DJ, Arntzen CJ. 1984 Membrane protein damage and repair: removal and replacement of inactivated 32 kilodalton polypeptides in chloroplast membranes. *J. Cell Biol.* **99**, 481–485. (doi:10.1083/jcb.99.2.481)
10. Nelson N, Junge W. 2015 Structure and energy transfer in photosystems of oxygenic photosynthesis. *Annu. Rev. Biochem.* **84**, 659–683. (doi:10.1146/annurev-biochem-092914-041942)
11. Nickelsen J, Rengstl B. 2013 Photosystem II assembly: from cyanobacteria to plants. *Annu. Rev. Plant Biol.* **64**, 609–635. (doi:10.1146/annurev-arplant-050312-120124)
12. Lu Y. 2016 Identification and roles of Photosystem II assembly, stability, and repair factors in Arabidopsis.

Front. Plant Sci. **7**, 168. (doi:10.3389/fpls.2016.00168)

13. Nixon PJ, Michoux F, Yu J, Boehm M, Komenda J. 2010 Recent advances in understanding the assembly and repair of photosystem II. *Ann. Bot.* **106**, 1–16. (doi:10.1093/aob/mcq059)
14. Silva P, Thompson E, Bailey S, Kruse O, Mullineaux CW, Robinson C, Mann NH, Nixon PJ. 2003 FtsH is involved in the early stages of repair of photosystem II in *Synechocystis* sp PCC 6803. *Plant Cell* **15**, 2152–2164. (doi:10.1105/tpc.012609)
15. Komenda J, Barker M, Kuviková, S., De Vries R, Mullineaux CW, Tichý, M, Nixon PJ. 2006 The FtsH protease slr0228 is important for quality control of photosystem II in the thylakoid membrane of *Synechocystis* sp. PCC 6803. *J. Biol. Chem.* **281**, 1145–1151. (doi:10.1074/jbc.M503852200)
16. Bailey S, Thompson E, Nixon PJ, Horton P, Mullineaux CW, Robinson C, Mann NH. 2002 A critical role for the Var2 FtsH homologue of *Arabidopsis thaliana* in the photosystem II repair cycle *in vivo*. *J. Biol. Chem.* **277**, 2006–2011. (doi:10.1074/jbc.M105878200)
17. Kato Y, Sun X, Zhang L, Sakamoto W. 2012 Cooperative D1 degradation in the photosystem II repair mediated by chloroplastic proteases in Arabidopsis. *Plant Physiol.* **159**, 1428–1429. (doi:10.1104/pp.112.199042)
18. Malnoe A, Wang F, Girard-Bascou J, Wollman F.-A, de Vitry C. 2014 Thylakoid FtsH protease contributes to photosystem II and cytochrome b6f remodeling in *Chlamydomonas reinhardtii* under stress conditions. *Plant Cell* **26**, 373–390. (doi:10.1105/tpc.113.120113)
19. Boehm M, Yu J, Krynicka V, Barker M, Tichy M, Komenda J, Nixon PJ, Nield J. 2012 Subunit organization of a *Synechocystis* hetero-oligomeric thylakoid FtsH complex involved in photosystem II repair. *Plant Cell* **24**, 3669–3683. (doi:10.1105/tpc.112.100891)
20. Yu F, Park S, Rodermel SR. 2004 The *Arabidopsis* FtsH metalloprotease gene family: interchangeability of subunits in chloroplast oligomeric complexes. *Plant J.* **37**, 864–876. (doi:10.1111/j.1365-313X.2003.02014.x)
21. Sakamoto W, Zaltsman A, Adam Z, Takahashi Y. 2003 Coordinated regulation and complex formation of yellow variegated1 and yellow variegated2, chloroplastic FtsH metalloproteases involved in the repair cycle of photosystem II in Arabidopsis thylakoid membranes. *Plant Cell* **15**, 2843–2855. (doi:10.1105/tpc.017319)
22. Wang Q, Sullivan RW, Kight A, Henry RL, Huang J, Jones AM, Korth KL. 2004 Deletion of the chloroplast-localized thylakoid formation1 gene product in Arabidopsis leads to deficient thylakoid formation and variegated leaves 1. *Plant Physiol.* **136**, 3594–3604. (doi:10.1104/pp.104.049841)
23. Zhang L *et al.* 2009 Activation of the heterotrimeric G protein α-subunit GPA1 suppresses the ftsh-mediated inhibition of chloroplast development in Arabidopsis. *Plant J.* **58**, 1041–1053. (doi:10.1111/j.1365-313X.2009.03843.x)
24. Wu W *et al.* 2013 Proteomic evidence for genetic epistasis: ClpR4 mutations switch leaf variegation to virescence in Arabidopsis. *Plant J* **76**, 943–956. (doi:10.1111/tpj.12344)
25. Kashino Y, Lauber WM, Carroll JA, Wang Q, Whitmarsh J, Satoh K, Pakrasi HB. 2002 Proteomic analysis of a highly active Photosystem II preparation from the cyanobacterium *Synechocystis* sp. PCC 6803 reveals the presence of novel polypeptides. *Biochemistry* **41**, 8004–8012. (doi:10.1021/bi026012+)
26. Keren N, Ohkawa H, Welsh EA, Liberton M, Pakrasi HB. 2005 Psb29, a conserved 22-kD protein, functions in the biogenesis of Photosystem II complexes in *Synechocystis* and *Arabidopsis*. *Plant Cell* **17**, 2768–2781. (doi:10.1105/tpc.105.035048)
27. Zhan J, Zhu X, Zhou W, Chen H, He C, Wang Q. 2016 Thf1 interacts with PS I and stabilizes the PS I complex in *Synechococcus* sp. PCC7942. *Mol. Microbiol.* **102**, 738–751. (doi:10.1111/mmi.13488)
28. Michoux F, Takasaka K, Boehm M, Nixon PJ, Murray JW. 2010 Structure of CyanoP at 2.8 Å: implications for the evolution and function of the PsbP subunit of Photosystem II. *Biochemistry* **49**, 7411–7413. (doi:10.1021/bi1011145)
29. Michoux F, Takasaka K, Boehm M, Komenda J, Nixon PJ, Murray JW. 2012 Crystal structure of the Psb27 assembly factor at 1.6 Å: implications for binding to Photosystem II. *Photosynth. Res.* **110**, 169–175. (doi:10.1007/s11120-011-9712-7)
30. Tichý M, Bečková M, Kopečná J, Noda J, Sobotka R, Komenda J. 2016 Strain of *Synechocystis* PCC 6803 with aberrant assembly of Photosystem II contains tandem duplication of a large chromosomal region. *Front. Plant Sci.* **7**, 1–10. (doi:10.3389/fpls.2016.00648)
31. Krynická V, Tichý M, Krafl J, Yu J, Kaňa R, Boehm M, Nixon PJ, Komenda J. 2014 Two essential FtsH proteases control the level of the Fur repressor during iron deficiency in the cyanobacterium *Synechocystis* sp. PCC 6803. *Mol. Microbiol.* **94**, 609–624. (doi:10.1111/mmi.12782)
32. Hollingshead S, Kopecna J, Jackson PJ, Canniffe DP, Davison PA, Dickman MJ, Sobotka R, Hunter CN. 2012 Conserved chloroplast open-reading frame *ycf54* is required for activity of the magnesium protoporphyrin monomethylester oxidative cyclase in *Synechocystis* PCC 6803. *J. Biol. Chem.* **287**, 27 823–27 833. (doi:10.1074/jbc.M112.352526)
33. Chidgey JW *et al.* 2014 A cyanobacterial chlorophyll synthase-HliD complex associates with the Ycf39 protein and the YidC/Alb3 insertase. *Plant Cell* **26**, 1267–1279. (doi:10.1105/tpc.114.124495)
34. Wellburn AR. 1994 The spectral determination of chlorophylls a and b, as well as total carotenoids, using various solvents with spectrophotometers of different resolution. *J. Plant Physiol.* **144**, 307–313. (doi:10.1016/S0176-1617(11)81192-2)
35. Boehm M, Nield J, Zhang P, Aro E-M, Komenda J, Nixon PJ. 2009 Structural and mutational analysis of band 7 proteins in the cyanobacterium *Synechocystis* sp. strain PCC 6803. *J. Bacteriol.* **191**, 6425–6435. (doi:10.1128/JB.00644–09)
36. Janouškovec J *et al.* 2013 Split photosystem protein, linear-mapping topology, and growth of structural complexity in the plastid genome of *Chromera velia*. *Mol. Biol. Evol.* **30**, 2447–2462. (doi:10.1093/molbev/mst144)
37. Winter G. 2010 Xia2: an expert system for macromolecular crystallography data reduction. *J. Appl. Crystallogr.* **43**, 186–190. (doi:10.1107/S0021889809045701)
38. Kabsch W. 2010 XDS. *Acta Crystallogr. D Biol. Crystallogr.* **66**, 125–132. (doi:10.1107/S0907444909047337)
39. Vonrhein C, Blanc E, Roversi P, Bricogne G. 2007 Automated structure solution with autoSHARP. *Methods Mol. Biol.* **364**, 215–230. (doi:10.1385/1-59745-266-1:215)
40. Cowtan K. 2006 The Buccaneer software for automated model building. 1. Tracing protein chains. *Acta Crystallogr. D Biol. Crystallogr.* **62**, 1002–1011. (doi:10.1107/S0907444906022116)
41. Murshudov GN, Vagin AA, Dodson EJ. 1997 Refinement of macromolecular structures by the maximum-likelihood method. *Acta Crystallogr. D Biol. Crystallogr.* **53**, 240–255. (doi:10.1107/S0907444996012255)
42. McCoy AJ, Grosse-Kunstleve RW, Adams PD, Winn MD, Storoni LC, Read RJ. 2007 Phaser crystallographic software. *J. Appl. Crystallogr.* **40**, 658–674. (doi:10.1107/S0021889807021206)
43. Afonine PV *et al.* 2012 Towards automated crystallographic structure refinement with *phenix.refine*. *Acta Crystallogr. D Biol. Crystallogr.* **68**, 352–367. (doi:10.1107/S0907444912001308)
44. Chen VB, Arendall WB, Headd JJ, Keedy DA, Immormino RM, Kapral GJ, Murray LW, Richardson JS, Richardson DC. 2010 *MolProbity*: all-atom structure validation for macromolecular crystallography. *Acta Crystallogr. D Biol. Crystallogr.* **66**, 12–21. (doi:10.1107/S0907444909042073)
45. Katoh K, Standley DM. 2013 MAFFT multiple sequence alignment software version 7: Improvements in performance and usability. *Mol. Biol. Evol.* **30**, 772–780. (doi:10.1093/molbev/mst010)
46. Capella-Gutiérrez S, Silla-Martínez JM, Gabaldón T. 2009 trimAl: a tool for automated alignment trimming in large-scale phylogenetic analyses. *Bioinformatics* **25**, 1972–1973. (doi:10.1093/bioinformatics/btp348)
47. Huerta-Cepas J, Serra F, Bork P. 2016 ETE 3: reconstruction, analysis, and visualization of phylogenomic data. *Mol. Biol. Evol.* **33**, 1635–1638. (doi:10.1093/molbev/msw046)
48. Guindon S, Dufayard JF, Lefort V, Anisimova M, Hordijk W, Gascuel O. 2010 New algorithms and methods to estimate maximum-likelihood phylogenies: assessing the performance of PhyML 3.0. *Syst. Biol.* **59**, 307–321. (doi:10.1093/sysbio/syq010)
49. Letunic I, Bork P. 2016 Interactive tree of life (iTOL) v3: an online tool for the display and annotation of phylogenetic and other trees. *Nucleic Acids Res.* **44**, W242–W245. (doi:10.1093/nar/gkw290)

50. Campanella JJ, Bitincka L, Smalley J. 2003 MatGAT: an application that generates similarity/identity matrices using protein or DNA sequences. *BMC Bioinformatics* **4**, 29. (doi:10.1186/1471-2105-4-29)
51. Ashkenazy H, Abadi S, Martz E, Chay O, Mayrose I, Pupko T, Ben-Tal N. 2016 ConSurf 2016: an improved methodology to estimate and visualize evolutionary conservation in macromolecules. *Nucleic Acids Res.* **44**, 1–7. (doi:10.1093/nar/gkw408)
52. Emanuelsson O, Nielsen H, von Heijne G. 1999 ChloroP, a neural network-based method for predicting chloroplast transit peptides and their cleavage sites. *Protein Sci.* **8**, 978–984. (doi:10.1110/ps.8.5.978)
53. Krissinel E, Henrick K. 2004 Secondary-structure matching (SSM), a new tool for fast protein structure alignment in three dimensions. *Acta Crystallogr. D Biol. Crystallogr.* **60**, 2256–2268. (doi:10.1107/S0907444904026460)
54. Mann NH, Novac N, Mullineaux CW, Newman J, Bailey S, Robinson C. 2000 Involvement of an FtsH homologue in the assembly of functional photosystem I in the cyanobacterium *Synechocystis* sp. PCC 6803. *FEBS Lett.* **479**, 72–77. (doi:10.1016/S0014-5793(00)01871-8)
55. Hamel L-P, Sekine K-T, Wallon T, Sugiwaka Y, Kobayashi K, Moffett P. 2016 The chloroplastic protein THF1 interacts with the coiled-coil domain of the disease resistance protein N′ and regulates light-dependent cell death. *Plant Physiol.* **171**, 658–674. (doi:10.1104/pp.16.00234)
56. Pribil M, Labs M, Leister D. 2014 Structure and dynamics of thylakoids in land plants. *J. Exp. Bot.* **65**, 1955–1972. (doi:10.1093/jxb/eru090)
57. Kojima K, Oshita M, Nanjo Y, Kasai K, Tozawa Y, Hayashi H, Nishiyama Y. 2007 Oxidation of elongation factor G inhibits the synthesis of the D1 protein of photosystem II. *Mol. Microbiol.* **65**, 936–947. (doi:10.1111/j.1365-2958.2007.05836.x)
58. Ejima K, Kawaharada T, Inoue S, Kojima K, Nishiyama Y. 2012 A change in the sensitivity of elongation factor G to oxidation protects photosystem II from photoinhibition in *Synechocystis* sp. PCC 6803. *FEBS Lett.* **586**, 778–783. (doi:10.1016/j.febslet.2012.01.042)
59. Sae-Tang P, Hihara Y, Yumoto I, Orikasa Y, Okuyama H, Nishiyama Y. 2016 Overexpressed superoxide dismutase and catalase act synergistically to protect the repair of PSII during photoinhibition in *Synechococcus elongatus* PCC 7942. *Plant Cell Physiol.* **57**, 1899–1907. (doi:10.1093/pcp/pcw110)
60. Komenda J, Nickelsen J, Tichý, M, Prášil O, Eichacker LA, Nixon PJ. 2008 The cyanobacterial homologue of HCF136/YCF48 is a component of an early photosystem II assembly complex and is important for both the efficient assembly and repair of photosystem II in *Synechocystis* sp. PCC 6803. *J. Biol. Chem.* **283**, 22 390–22 399. (doi:10.1074/jbc.M801917200)
61. Knoppová J, Sobotka R, Tichy M, Yu J, Konik P, Halada P, Nixon PJ, Komenda J. 2014 Discovery of a chlorophyll binding protein complex involved in the early steps of photosystem II assembly in *Synechocystis*. *Plant Cell* **26**, 1–14. (doi:10.1105/tpc.114.123919)
62. Kato Y, Miura E, Ido K, Ifuku K, Sakamoto W. 2009 The variegated mutants lacking chloroplastic FtsHs are defective in D1 degradation and accumulate reactive oxygen species. *Plant Physiol.* **151**, 1790–1801. (doi:10.1104/pp.109.146589)
63. Mur LAJ, Kenton P, Lloyd AJ, Ougham H, Prats E. 2008 The hypersensitive response; the centenary is upon us but how much do we know? *J. Exp. Bot.* **59**, 501–520. (doi:10.1093/jxb/erm239)
64. Seo S, Okamoto M, Iwai T, Iwano M, Fukui K, Isogai A, Nakajima N, Ohashi Y. 2000 Reduced levels of chloroplast FtsH protein in tobacco mosaic virus–infected tobacco leaves accelerate the hypersensitive reaction. *Plant Cell* **12**, 917–932. (doi:10.1105/tpc.12.6.917)
65. Wangdi T, Uppalapati SR, Nagaraj S, Ryu C-M, Bender CL, Mysore KS. 2010 A virus-induced gene silencing screen identifies a role for *Thylakoid Formation1* in *Pseudomonas syringae* pv *tomato* symptom development in tomato and Arabidopsis. *Plant Physiol.* **152**, 281–292. (doi:10.1104/pp.109.148106)
66. Barker MRGR. 2006 The role of the DegP/HtrA and FtsH proteases in protection of *Synechocystis* sp. PCC 6803 from abiotic stress. PhD thesis, University of London.
67. Wang F, Qi Y, Malnoë A, Choquet Y, Wollman F-A, de Vitry C. 2016 The high light response and redox control of thylakoid FtsH protease in *Chlamydomonas reinhardtii*. *Mol. Plant* **43**, 18–27. (doi:10.1016/j.molp.2016.09.012)

The Ribosome-Bound Protein Pam68 Promotes Insertion of Chlorophyll into the CP47 Subunit of Photosystem II[1][OPEN]

Lenka Bučinská,[a,b] Éva Kiss,[a] Peter Koník,[a,b] Jana Knoppová,[a] Josef Komenda,[a] and Roman Sobotka[a,b,2]

[a]Laboratory of Photosynthesis, Centre Algatech, Institute of Microbiology, Academy of Sciences, 37981 Třeboň, Czech Republic

[b]Faculty of Science, University of South Bohemia, 37005 České Budějovice, Czech Republic

ORCID IDs: 0000-0001-8652-5323 (P.K.); 0000-0003-4588-0328 (J.K.); 0000-0002-6359-7604 (J.Kno.); 0000-0001-5909-3879 (R.S.).

Photosystem II (PSII) is a large enzyme complex embedded in the thylakoid membrane of oxygenic phototrophs. The biogenesis of PSII requires the assembly of more than 30 subunits, with the assistance of a number of auxiliary proteins. In plants and cyanobacteria, the photosynthesis-affected mutant 68 (Pam68) is important for PSII assembly. However, its mechanisms of action remain unknown. Using a *Synechocystis* PCC 6803 strain expressing Flag-tagged Pam68, we purified a large protein complex containing ribosomes, SecY translocase, and the chlorophyll-binding PSII inner antenna CP47. Using 2D gel electrophoresis, we identified a pigmented Pam68-CP47 subcomplex and found Pam68 bound to ribosomes. Our results show that Pam68 binds to ribosomes even in the absence of CP47 translation. Furthermore, Pam68 associates with CP47 at an early phase of its biogenesis and promotes the synthesis of this chlorophyll-binding polypeptide until the attachment of the small PSII subunit PsbH. Deletion of both Pam68 and PsbH nearly abolishes the synthesis of CP47, which can be restored by enhancing chlorophyll biosynthesis. These results strongly suggest that ribosome-bound Pam68 stabilizes membrane segments of CP47 and facilitates the insertion of chlorophyll molecules into the translated CP47 polypeptide chain.

Photosystem II (PSII) is a large protein-cofactor complex embedded in the thylakoid membranes of oxygenic phototrophs. The key large structural components of PSII are the chlorophyll (Chl)-binding proteins D1, D2, CP43, and CP47, subjoined with other small and extrinsic subunits (Umena et al., 2011). According to this model, PSII is assembled in a stepwise manner from four preassembled smaller subcomplexes called modules (Komenda et al., 2012). Each module consists of one large Chl-binding subunit (D1, D2, CP43, or CP47) and several low molecular mass membrane polypeptides. PSII assembly is initiated through the association of D1 and D2 modules to form an assembly intermediate, termed the Reaction Center II (RCII) complex. The CP47 assembly module (CP47m) is then attached to RCII (Boehm et al., 2011), which results in a CP43-less core complex called "RC47" (Boehm et al., 2012). The active, oxygen-evolving PSII is completed by the addition of the CP43 module (Boehm et al., 2011) and attachment of the lumenal extrinsic proteins (Nixon et al., 2010). Biogenesis of PSII is a highly complex process requiring many auxiliary proteins that are not present in the fully assembled complex. A number of these assembly factors have been described (Komenda et al., 2012; Heinz et al., 2016). However, their precise functions remain mostly unknown, and only a few of them have been connected with a specific assembly step (Knoppová et al., 2014; Bečková et al., 2017).

The fully assembled PSII contains 35 Chl molecules, most of them bound to the inner PSII antennas CP47 (16) and CP43 (14). According to this model, Chl molecules are integrated directly into synthesized CP47 and CP43, and the insertion of Chl appears to be a prerequisite for the correct folding and stability of these polypeptides (for review, see Sobotka, 2014). However, little is known about how Chl proteins are produced. PSII Chl-binding subunits are integral membrane proteins most likely cotranslationally inserted into the thylakoid membrane with the assistance of the protein translocation apparatus. This process usually includes the SecYEG translocon, which forms a protein-conducting channel, and an associated insertase/foldase YidC (Sachelaru et al., 2013). Chl synthase is the last enzyme of Chl biosynthesis, and it was recently shown to physically interact with YidC insertase (Chidgey et al., 2014). This interaction suggests that Chl molecules are

[1] This work was supported by project 17-08755S of the Grant Agency of the Czech Republic and by the Czech Ministry of Education (projects CZ 1.05/2.1.00/19.0392 and LO1416).

[2] Address correspondence to sobotka@alga.cz.

The author responsible for distribution of materials integral to the findings presented in this article in accordance with the policy described in the Instructions for Authors (www.plantphysiol.org) is: Roman Sobotka (sobotka@alga.cz).

L.B. constructed the strains and employed most of the biochemical methods under the supervision of R.S.; P.K. performed protein identification by LC-MS/MS; J.K. and J.Kno were responsible for ^{35}S radiolabeling; E.K. performed various mutant characterizations; R.S., L.B., E.K., and J.K. designed the study and wrote the paper; R.S. supervised the whole study; and all authors discussed the results and commented on the manuscript.

[OPEN] Articles can be viewed without a subscription.

www.plantphysiol.org/cgi/doi/10.1104/pp.18.00061

passed directly from Chl synthase to the nascent apoprotein chain in the vicinity of the translocon.

The small PSII subunit PsbH and two assembly factors, hypothetical chloroplast open reading frame 48 (Ycf48) and photosynthesis-affected mutant 68 (Pam68), were found to be important for the accumulation of CP47m (Komenda, 2005; Rengstl et al., 2013). Here, we identified the cyanobacterial Pam68 protein as a ribosomal factor that is in contact with the nascent CP47 in the vicinity of the SecY translocase. Our data suggest that Pam68 stabilizes membrane segments of CP47 during Chl insertion.

RESULTS

Pam68 Associates with the CP47 Protein at an Early Stage of PSII Biogenesis

To identify proteins interacting with Pam68, we constructed a *Synechocystis* sp. PCC 6803 strain (hereafter *Synechocystis*) expressing a Flag-tagged Pam68 derivative (Pam68.f protein). This protein was purified from solubilized membranes using an anti-Flag gel, and the obtained elution was analyzed by SDS-PAGE. The identities of prominent protein bands were determined by mass spectrometry (MS; Supplemental Fig. S1A). We identified CP47 and ribosomal subunits, which were missing in the control pull-down, as putative interactors (Supplemental Fig. S1A). Consistent with our previous reports, Photosystem I (PSI) subunits were the only substantial contaminants (Knoppová et al., 2014; Bečková et al., 2017). Furthermore, our control purification of the Flag-tagged ferrochelatase enzyme (FeCh) showed that the 3×Flag-tag does not bind ribosome subunits nonspecifically (Supplemental Fig. S1B).

Because membrane-bound ribosomes were present in the Pam68.f elution, we checked for the presence of SecY translocase and YidC insertase. Indeed, both these proteins coeluted with Pam68.f (Supplemental Fig. S1C). Additionally, our data support the interaction of the lumenal Ycf48 protein with Pam68, as previously suggested (Rengstl et al., 2013). Moreover, CP47 was the only PSII subunit detected in the Pam68.f elution. Remarkably, the PsbH subunit was hardly detectable even by specific antibodies, despite a high level of CP47 protein in the elution. PsbH is a component of CP47m (Boehm et al., 2011); hence, the absence of PsbH in the Pam68.f pull-down indicates that the association of CP47 with Pam68 is an early event that occurs before the attachment of PsbH to CP47.

To elucidate whether Pam68.f physically interacts with unassembled CP47 in the absence of PsbH, we purified Pam68.f from the PsbH-less strain, and both elutions (Pam68.f and Pam68.f/ΔPsbH) were analyzed by 2D Clear-Native/SDS-PAGE (CN/SDS-PAGE). On the stained gels, we identified large (50S) and small (30S) ribosome subunits and two fractions of Pam68.f comigrating with 50S and with CP47, respectively. The Pam68.f-CP47 complex exhibited Chl fluorescence, and its green pigmentation was visible on the CN gel (Fig. 1A).

In addition to the ribosome subunits, FtsH proteases, and a smeary band of SecY, the Pam68.f elutions also contained two unknown proteins (Sll1830 and Ssr0332). Whereas Sll1830 migrated as a free protein, the small Ssr0332 protein comigrated with the 50S ribosomal subunit. Another identified protein was light-repressed protein A (LrtA, Sll0947), which showed sequence similarity to the bacterial pY factor associated with stalled ribosomes (Galmozzi et al., 2016). A similar pattern of ribosomal proteins, but with higher levels of LrtA, was also obtained in the Pam68.f pull-down isolated from the Δ*psbB* (ΔCP47) mutant background (Supplemental Fig. S2). This result implies that Pam68 remains associated with a pool of membrane-bound ribosomes even when no CP47 translation occurs in the cell. Notably, the electrophoretic mobility of Pam68.f proteins purified from the Δ*psbH* and wild-type backgrounds were slightly different, indicating a posttranslational modification of Pam68.f upon the *psbH* deletion (Fig. 1A). This shift allowed us to distinguish that the spot of Pam68.f comigrating with 50S in the Pam68.f/ΔPsbH pulldown (just above the Rpl6 protein) consists of only Pam68.f, with no other (ribosomal) proteins. There is no spot in this position in the Pam68.f elution (Fig. 1A).

To better visualize the pattern of proteins on the 2D gel, the separation of Pam68.f/ΔPsbH and the control ΔPsbH pull-downs on 2D CN/SDS-PAGE was followed by immunoblotting. The immunodetection determined a fraction of YidC, Ycf48, and SecY comigrating with 50S, as expected for the isolated ribosome-translocon apparatus (Fig. 1B). However, the barely visible (SecY) or invisible (YidC, Ycf48) staining of these proteins on the gel indicates that they are substantially less abundant than Pam68. Hence, it is unlikely that they connect Pam68.f with ribosomes. CP47 was found in a spot that had the same mobility as the dissociated Pam68.f, suggesting a mutual complex.

We used an independent approach to verify the interaction between the unassembled CP47 and Pam68 proteins. We isolated CP47m and a nascent CP47m lacking PsbH (CP47m/ΔPsbH) via His-tagged CP47 from *Synechocystis* strains accumulating these complexes due to the absence of the D1 or D1/PsbH PSII subunits, respectively (Boehm et al., 2011; D'Haene et al., 2015). The Pam68 protein was copurified with CP47m/ΔPsbH but was not detected in the CP47m elution (Fig. 1C). Therefore, either the binding of PsbH to the CP47-Pam68 complex is considerably weaker than to CP47, or Pam68 and PsbH share a similar binding side.

N-Terminal Segment of Pam68 Is Required for the Interaction with Ribosomes

To verify that the interaction of Pam68 with ribosomes is not an artifact of the pull-down assay, solubilized membrane complexes from the *pam68.f* strain were separated by 2D CN/SDS-PAGE, stained by SYPRO Orange, and blotted onto a polyvinylidene fluoride (PVDF) membrane. Pam68.f comigrated with the 50S and, unexpectedly, also with the 30S subunit (Fig. 2A). On the other hand, Pam68.f spots in the

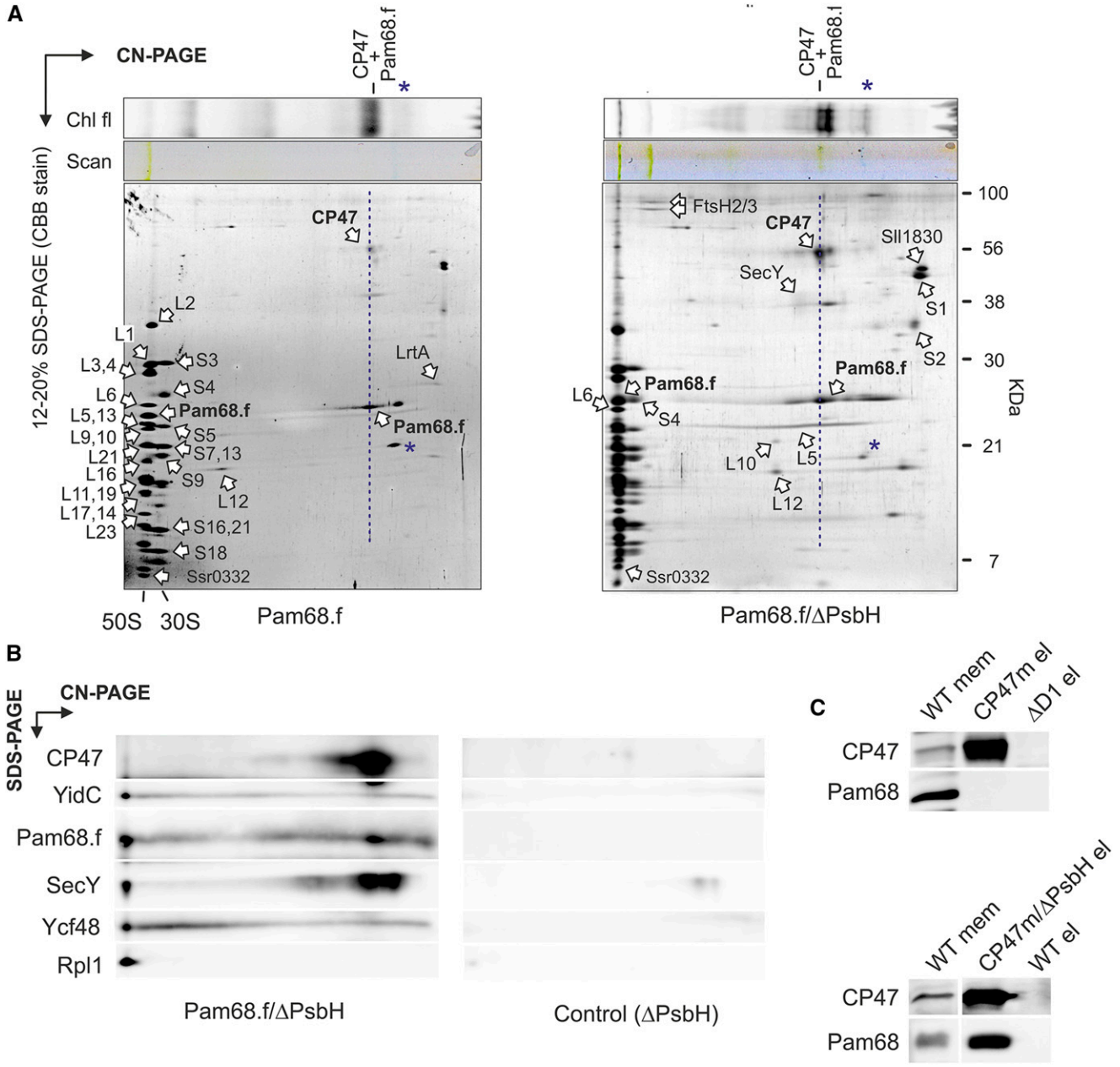

Figure 1. Identification of Pam68 as a component of the CP47 assembly module. A, The Pam68.f pull-down (left-hand gel) and the Pam68.f/ΔPsbH pull-down (right-hand gel) were separated by CN-PAGE, whereas SDS-electrophoresis was used for the second dimension. Individual protein spots were cut and identified by MS (Supplemental Dataset). The dashed blue line highlights the comigration of Pam68.f with CP47; note that CP47 exhibits Chl fluorescence demonstrating the presence of Chl molecules. Asterisks mark phycobiliproteins contaminating the elutions. B, The Pam68.f/ΔPsbH pull-down prepared from a different cell culture was separated together with the control ΔPsbH elution by 2D electrophoresis and blotted. The indicated proteins were sequentially detected by specific antibodies and the separate segments of the 2D blot with the individual antibody signals are shown. C, The CP47 assembly modules containing PsbH (CP47m) and lacking PsbH (CP47m/ΔPsbH) were purified on a nickel column. The eluted proteins were separated by SDS-PAGE together with the control pull-downs of wild type and ΔD1. The separated proteins were blotted, and the blot was sequentially probed with the indicated antibodies; the separate segments of the blot with individual antibody signals are shown. Chl fl, Chl fluorescence.

region of smaller complexes did not align with either of the CP47m forms (both are known to contain PsbH; Komenda, 2005). These results suggest that complexes between Pam68.f and the CP47m forms are not detectable in the 2D gel of the *pam68.f* membranes (Fig. 2A). This observation is consistent with the proposed transient interaction between Pam68 and the newly synthesized CP47; the transient complex pool is

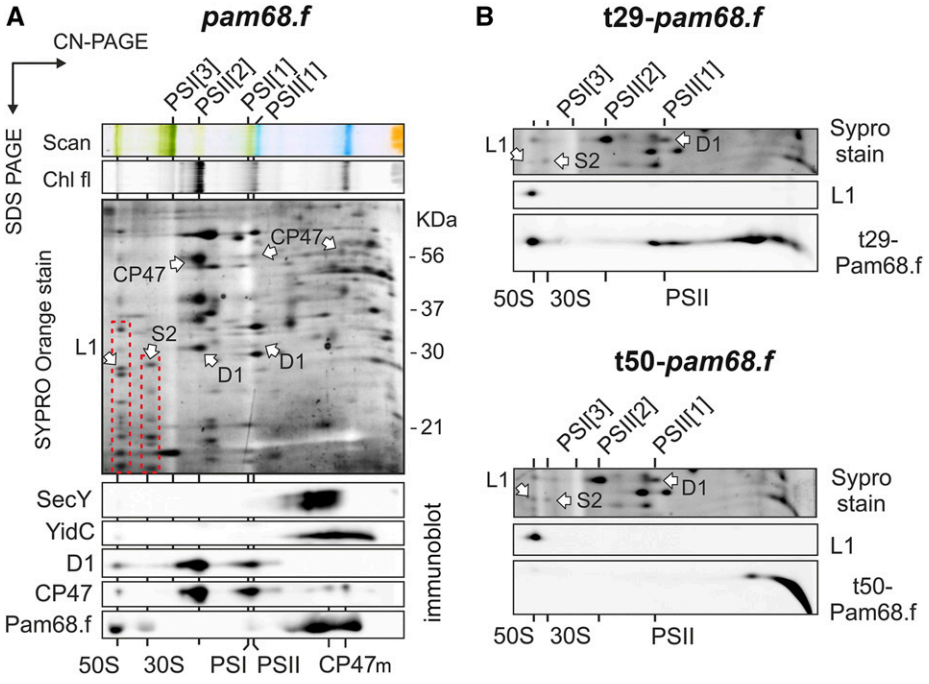

Figure 2. 2D CN/SDS-PAGE and immunodetection of membrane protein complexes from strains expressing full-length or truncated Pam68.f. A, Solubilized membrane proteins from the *pam68.f* strain were separated by 2D CN/SDS-PAGE. The 2D gel was stained with SYPRO Orange, blotted, and the 2D blot was sequentially probed by the indicated antibodies. Separate segments of the 2D blot with individual antibody signals are shown. The large and small ribosomal subunits are highlighted on the stained gel by red dashed boxes; protein spots belonging to Rpl1 and Rps2 were identified previously (Chidgey et al., 2014). Chl fluorescence was detected after excitation by blue light. CP47m marks two forms of the CP47 assembly module detected in the *Synechocystis* membrane fraction (Komenda, 2005). B, The same analysis was performed on membranes isolated from strains expressing the truncated variants t29-Pam68.f (top panel) and t50-Pam68 (bottom panel). Only a region of the SYPRO Orange stained gel around the Rpl1 protein (SYPRO stain) and separate segments of the 2D blot with signals of anti-Rpl1 and anti-Flag antibodies are shown. Complexes are designated as in (B). Chl fl, Chl fluorescence; L1, Rpl1; PSI[3], trimer of PSI; PSII[1], monomer of PSII; PSII[2], dimer of PSII; S2, Rps2.

apparently below the detection limit of the immunoblot analysis.

According to this model, ribosomes can be docked to bacterial membranes via interaction with the large subunit and the SecYEG translocon, or alternatively, with YidC insertase (Prinz et al., 2000; Seitl et al., 2014). However, the interaction between the membrane-bound ribosomes and SecY or YidC in isolated thylakoids was not preserved in our 2D gel system (Fig. 2A). Therefore, it is unlikely that SecY/YidC facilitates the observed association of Pam68.f with ribosomes.

It is likely that Pam68 interacts directly with ribosomal proteins from both the 50S and 30S subunits. The 30S subunit of the membrane-docked ribosome is close to the membrane surface (approximately 10 nm; Frauenfeld et al., 2011). Theoretically, the strongly positively charged N terminus of Pam68.f is long enough (65 amino acids, approximately 20 nm; Supplemental Fig. S3) to reach the 30S subunit. To test this possibility, we constructed strains expressing variants of Pam68.f truncated either up to the V29 (t29-*pam68.f* strain) or the S50 amino acid residues (t50-*pam68.f*). The t29-Pam68.f protein still comigrated with ribosomes on the 2D gel (Fig. 2B), but the more truncated t50-Pam68.f protein was not detectable in any larger complexes, which supports the role of the Pam68 N-terminal segment in the interaction with ribosomes.

A close relationship between the cyanobacterial Pam68 and ribosomes can also be inferred from the existence of an operon of the *pam68* and the *rps15* genes, which is highly conserved among the cyanobacterial genomes. According to the STRING database (http://string-db.org/), there are only a few examples of sequenced cyanobacterial genomes (e.g. *Gloeobacter violaceus*) where these two genes are not organized in tandem. In the *Synechocystis* genome, the *pam68* gene is transcribed from the *rps15* promoter as a single mRNA with *rps15* (Mitschke et al., 2011). Interestingly, the *rps15-pam68* mRNA belongs to a small group of ribosomal transcripts that are significantly up-regulated under stress conditions with the strongest expression under low temperature (Kopf et al., 2014; Supplemental Fig. S4). Indeed, we found the Pam68 protein level to be high during high light or chilling stress (Supplemental Fig. S5).

Enhanced Chl Biosynthesis Rescues the Abolished CP47 Synthesis in the ΔpsbH/Δpam68 Strain

The results described above imply that Pam68 functions during the synthesis and/or folding of CP47 before it associates with PsbH, which also facilitates CP47 synthesis (Komenda, 2005). To test whether PsbH can compensate for the absence of Pam68, we characterized the *Synechocystis* Δ*pam68* and Δ*psbH* mutants and the Δ*psbH*/Δ*pam68* double mutant. Under moderate light intensities (40 μmol photons m^{-2} s^{-1}), Δ*pam68* grew similarly as the wild-type strain and had a similar Chl content (Supplemental Fig. S6, A and B). The Δ*psbH* mutation affected both the growth rate and Chl content; nevertheless, this mutant grew fairly well photoautotrophically (Supplemental Fig. S6, A and B). However, even the single Δ*pam68* mutant stopped proliferating on plates under more severe conditions, such as dark-/high-light fluctuation or low temperature (Fig. 3A). Moreover, the level of PsbH was merely affected in the Δ*pam68* strain and, vice versa, the level of Pam68 in the Δ*psbH* strain remained comparable to wild type (Fig. 3B).

Unlike the strains containing single mutations, the double mutant showed extremely slow autotrophic growth (double time approximately 20 d), accumulated only traces of Chl and died immediately after exposure to mild stress conditions (Fig. 3A; Supplemental Fig. S6). However, photoautotrophy of the Δ*psbH*/Δ*pam68* strain can be restored by the expression of Pam68.f (Fig. 3C), which provides evidence that the poor phenotype of the double mutant is not caused by a position effect, e.g. lower levels of Rps15. To obtain enough cells of the poor-growing Δ*psbH*/Δ*pam68* mutant, we first grew all strains with Glc supplementation. Then, we characterized the phenotype 2 d after removing Glc from the media. As revealed by the CN-PAGE separation of membrane complexes (Fig. 3D), the levels of PSI and PSII were virtually unchanged in the Δ*pam68* strain, but the Δ*psbH* strain contained much less dimeric PSII. In the double mutant, very little PSI and only traces of the PSII complexes were detectable. Thus, both PsbH and Pam68 play distinct roles in the accumulation of PSII; the parallel elimination of both of these proteins is nearly fatal for cell viability.

For a closer look at the role of PsbH and Pam68 in the synthesis of PSII wild type, Δ*pam68*, Δ*psbH*, and Δ*psbH*/Δ*pam68* cells were pulse-labeled and the isolated membrane complexes analyzed by 2D CN/SDS-PAGE (Fig. 4). Consistent with the previously published analysis of Δ*pam68* (Rengstl et al., 2013), this strain showed less labeled CP47 and CP43 in total, and lacked the labeled unassembled CP47. In addition, we observed severe accumulation of RCIIa and RCII* assembly intermediates, which is a typical feature of cells deficient in the formation of CP47m (Knoppová et al., 2014). The obtained pattern for Δ*psbH* differed from the Δ*pam68* strain by having only weakly labeled dimeric PSII and also less synthesized D1. A detectable pool of unassembled CP47 was also absent and both RCII complexes accumulated, which implies that the rate of CP47m formation limits the process of PSII assembly. In the Δ*psbH*/Δ*pam68* strain, the capacity to synthesize PSII was extremely weak, almost certainly caused by the lack of CP47m because the intensively labeled RCII complexes resembled the canonical pattern of the ΔCP47 strain (Fig. 4; Komenda et al., 2004).

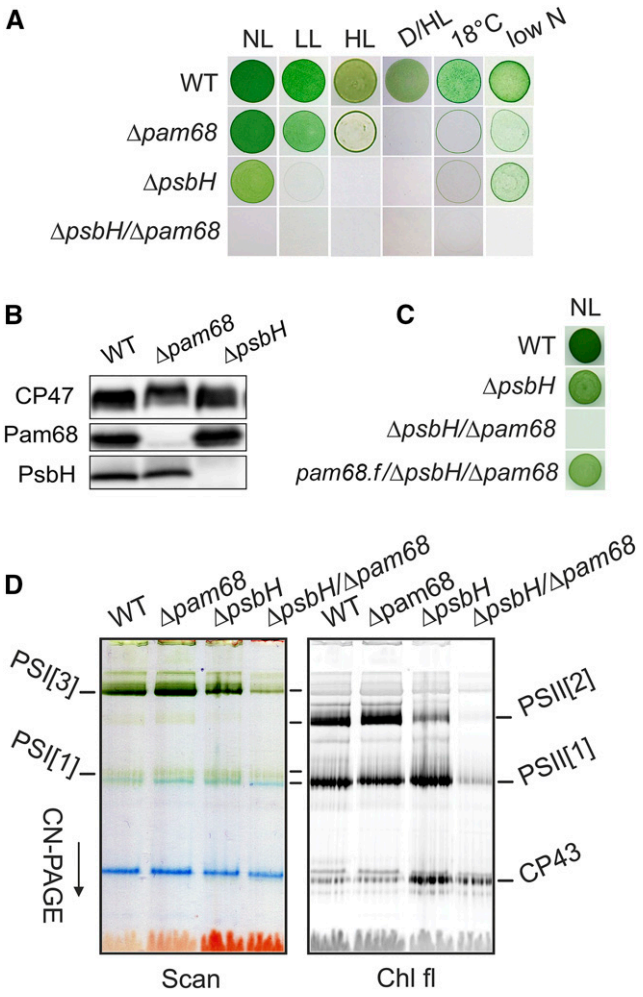

Figure 3. Characterization of the *Synechocystis* strains lacking Pam68, PsbH, or both of these proteins. A, Autotrophic growth of the wild-type and mutant strains on agar plates under various conditions. Growth for 5 d under normal light (40 μmol photons m^{-2} s^{-1}), low light (10 μmol photons m^{-2} s^{-1}), high light (400 μmol photons m^{-2} s^{-1}), fluctuating dark/high light conditions (5 min dark, 5 min 400 μmol photons m^{-2} s^{-1}), 18°C at 40 μmol photons m^{-2} s^{-1}, and low nitrogen (0.1 mM $NaNO_3$). B, Levels of PsbH and Pam68 in the Δ*pam68* and Δ*psbH* strains under normal light conditions. A comparable amount of Chl was loaded for each strain. C, Autotrophic growth of the *pam68.f*/Δ*pam68*/Δ*psbH* strain expressing the Pam68.f protein under the regulation of the *psbAII* promoter. D, Membranes, isolated from the wild-type and mutant strains grown as described in (A), were solubilized and separated by CN-PAGE. D/HL, dark/high light; HL, high light; LL, low light; NL, normal light; PSI[3], trimer of PSI; PSII[1], monomer of PSII; PSII[2], dimer of PSII.

Based on the available PSII structure (Umena et al., 2011), the N-terminal segment of PsbH creates a network of hydrogen bonds with the stromal loops connecting the first four helixes of CP47 (Supplemental Fig. S7). Therefore, the PsbH protein could fix the nascent CP47 in

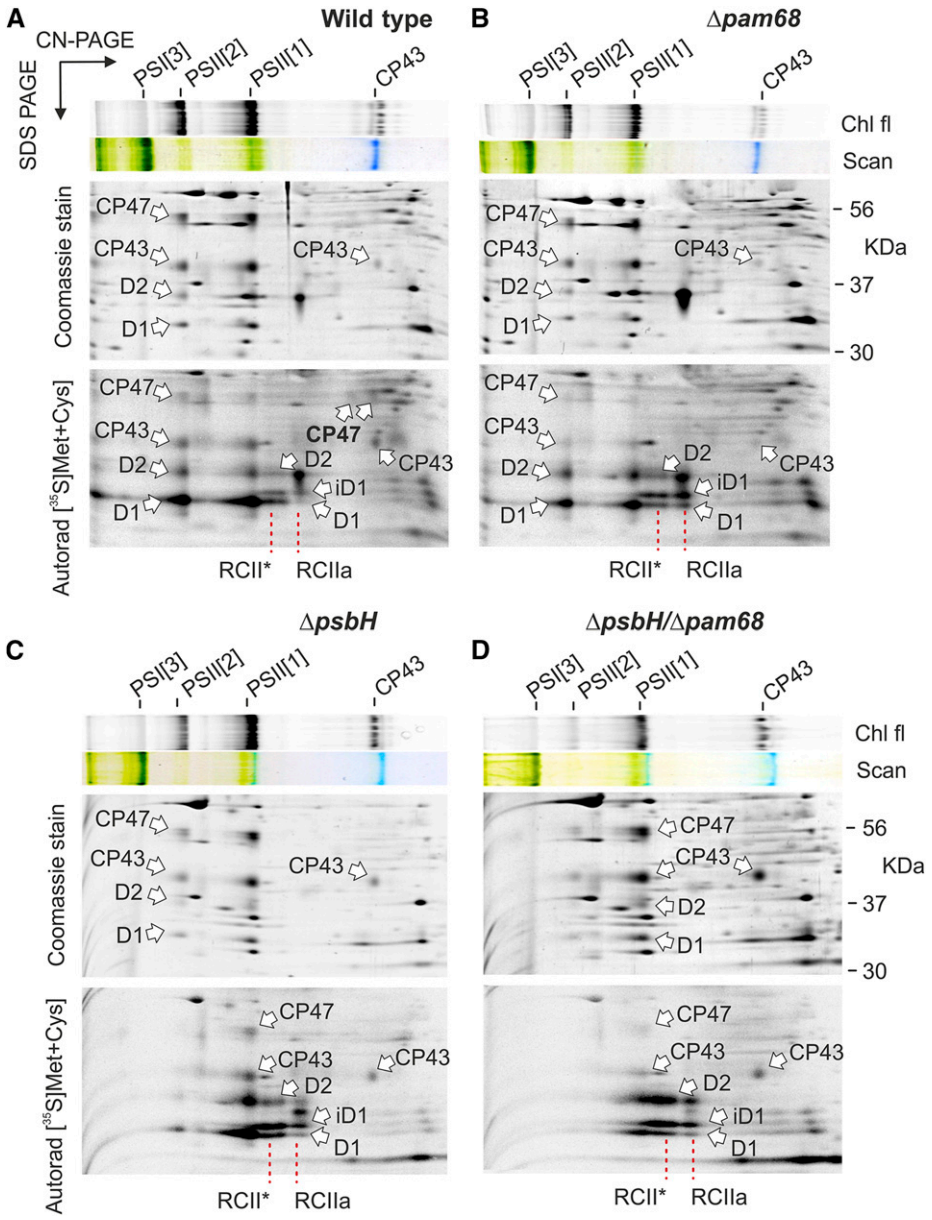

Figure 4. Synthesis of PSII subunits in the Δ*pam68*, Δ*psbH*, and Δ*psbH*/Δ*pam68* mutant strains. Wild-type (A) and the mutant Δ*pam68* (B), Δ*psbH* (C), and Δ*psbH*/Δ*pam68* (D) cells grown for 2 d without Glc were radiolabeled with a mixture of [^{35}S]Met/Cys using a 30-min pulse. Isolated membrane proteins were separated by CN-PAGE on a 4% to 14% linear gradient gel, whereas 12% to 20% SDS-electrophoresis was used for the second dimension. The same amounts of Chl were loaded for each strain. Note that the Δ*psbH*/Δ*pam68* strain contains three-times less Chl per cell than Δ*psbH*, meaning that the membrane proteins from the double mutant were overloaded on a per-cell basis to obtain a detectable radioactivity signal of the assembled PSII. The 2D gels were stained with Coomassie Blue, and the labeled proteins were detected by a phosphoimager (Autorad). Chl fluorescence emitted by Chl was detected by LAS 4000 (Fuji) after excitation by blue light. Chl fl, Chl fluorescence; iD1, incompletely processed form of the D1 precursor; PSI[3], trimer of PSI; PSII[1], monomer of PSII; PSII[2], dimer of PSII; RCII*, assembly intermediate (reaction center complex) lacking CP47m (Knoppová et al., 2014); RCIIa, PSII assembly intermediate (reaction center complex) lacking CP43m (Knoppová et al., 2014).

a position that facilitates prompt insertion of Chl molecules. Moreover, the C-terminal region of Pam68 may play a similar role. To test the importance of both proteins for Chl insertion into CP47, we removed Glc from the Δ*psbH*/Δ*pam68* liquid culture, while supplementing it with 200 nM N-methyl mesoporphyrin IX. This compound is a specific inhibitor of the FeCh enzyme and a partial inhibition of FeCh strongly enhances Chl biosynthesis (Sobotka et al., 2005). Remarkably, the Δ*psbH*/Δ*pam68* cells treated with the FeCh inhibitor started to grow much faster than the control cells without the inhibitor (Fig. 5A). The control culture had very low Chl content on a per-cell basis, whereas the treated cells progressively built up new Chl-complexes, and in 4 d reached approximately 85% of the Chl level when compared to wild type (Fig. 5B).

Precursors of the Chl biosynthetic pathway differed dramatically between treated and untreated cells. Whereas monovinyl-chlorophyllide was the only detectable Chl precursor in the untreated cells, the inhibitor-treated cells contained a spectrum of Chl precursors typical for wild type (Pilný et al., 2015; Supplemental Fig. S8). Because the earlier precursors upstream of chlorophyllide were below the detection level in the untreated double mutant, this chlorophyllide pool originated almost certainly from Chl recycling and not from de novo synthesis (Vavilin et al., 2005; Kopečná et al., 2015). We repeated the protein radiolabeling experiment described above using Δ*psbH*/Δ*pam68* cells treated with the FeCh inhibitor. The assembly of PSII was restored (Fig. 5C), suggesting that boosting of the ceased Chl

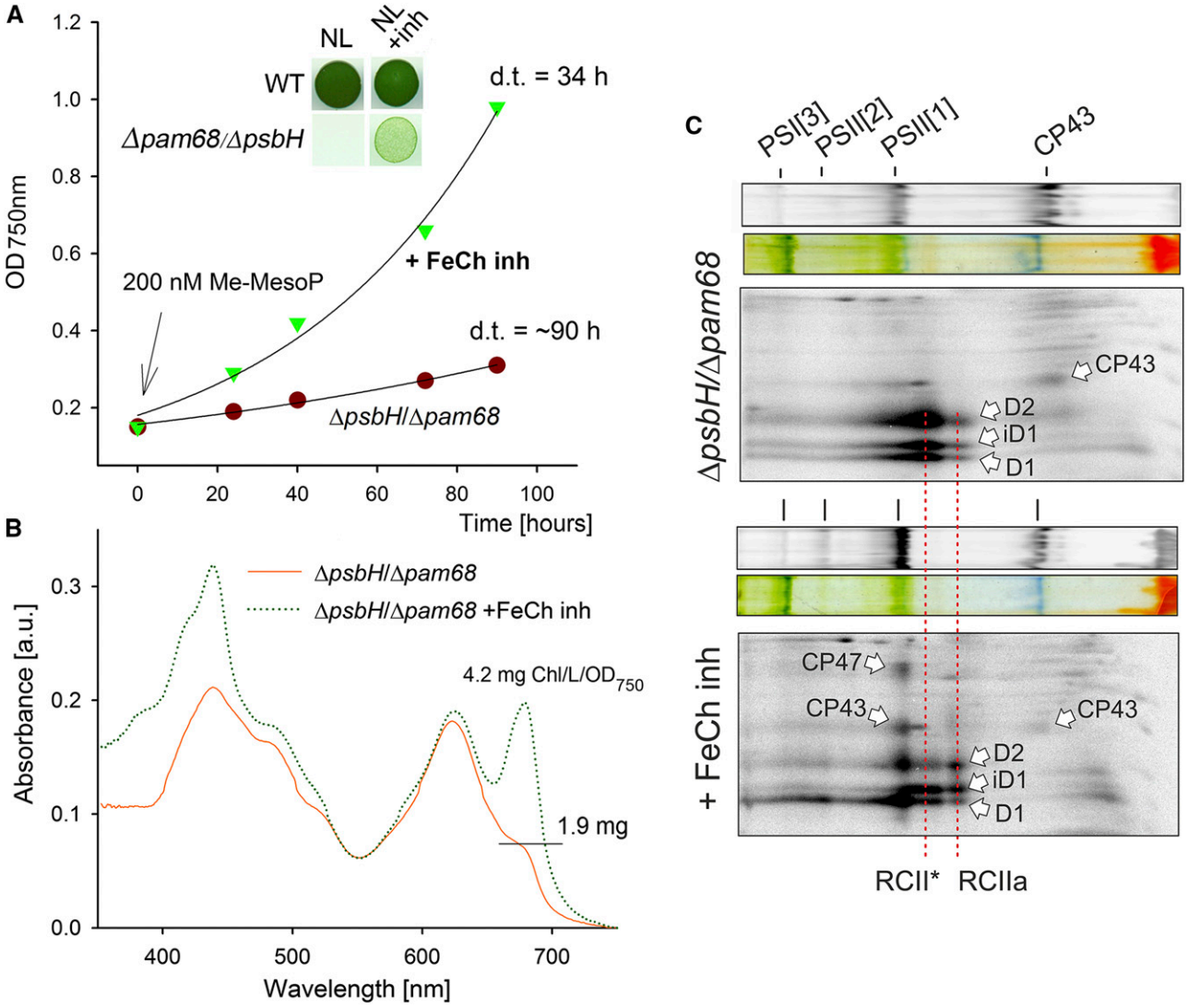

Figure 5. Abolished synthesis of CP47 in the Δ*psbH*/Δ*pam68* mutant is rescued by enhanced Chl biosynthesis. A, The Δ*psbH*/Δ*pam68* cells grown mixotrophically were harvested and resuspended in a growth medium without Glc. The obtained culture was divided into two flasks, with one of them supplemented with N-methyl-mesoporphyrin IX (Me-MesoP, FeCh inhibitor). The photoautotrophic growth was then monitored. The inset shows the same growth experiment but with 200 nM Me-MesoP added into the plate. B, Absorbance spectra of mutant cells growing for 4 d in the presence or absence of FeCh inhibitor. Spectra were normalized to light scattering at 750 nm. Also shown is the Chl content determined spectroscopically in methanol extract and normalized per $OD_{750\ nm}$. C, Δ*psbH*/Δ*pam68* cells grown for 2 d photoautotrophically in the presence of 200 nM FeCh inhibitor were radiolabeled with a mixture of [^{35}S]Met/Cys; incorporation of radioactivity into core PSII subunits was detected after 2D CN/SDS-PAGE. The same amounts of Chl were loaded of each sample. a.u., absorbance units; d.t., doubling time; iD1, incompletely processed form of the D1 precursor; PSI[3], trimer of PSI; PSII[1], monomer of PSII; PSII[2], dimer of PSII; RCII*, assembly intermediate (reaction center complex) lacking CP47m (Knoppová et al., 2014); RCIIa, PSII assembly intermediate (reaction center complex) lacking CP43m (Knoppová et al., 2014).

biosynthesis restores the formation of CP47m in the mutant lacking both Pam68 and PsbH.

DISCUSSION

The Pam68 protein was first described in the Arabidopsis (*Arabidopsis thaliana*) *pam68*-null mutant, which accumulated only approximately 10% of PSII (Armbruster et al., 2010). The function of Pam68 was originally linked to the synthesis or maturation of the D1 subunit of PSII (Armbruster et al., 2010); however, a strong relationship between Pam68 and CP47 was also suggested, based on the low level of Pam68 detected in the *Synechocystis* CP47-less strain (Rengstl et al., 2011). Our results agree with a recent study, which demonstrated that the lack of Pam68 in *Synechocystis* limits the synthesis of CP47 and CP43 (Rengstl et al., 2013). Given that the mechanism of PSII biogenesis is highly conserved, it is likely that the eukaryotic Pam68 is involved

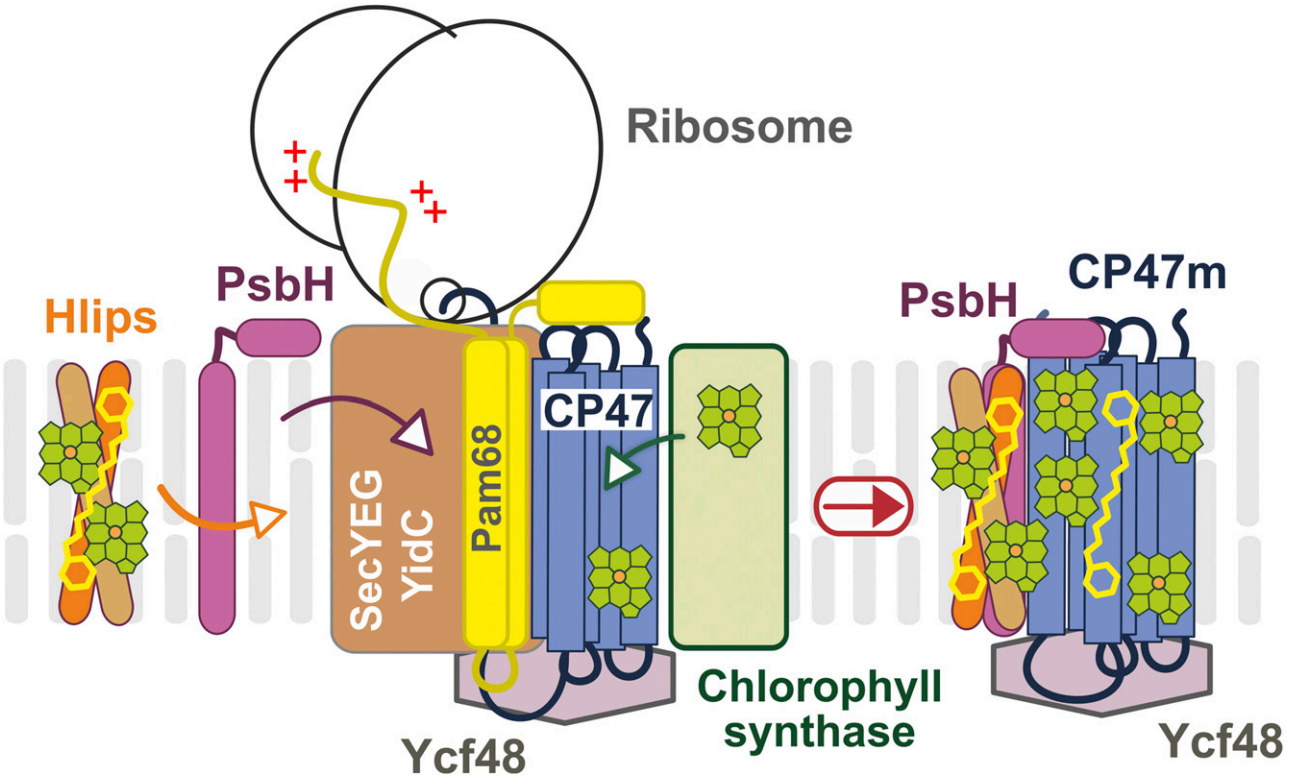

Figure 6. A working model of CP47m synthesis with Pam68 as a ribosome-interacting factor. The CP47 protein is translated by membrane-bound ribosomes and inserted into the membrane by the SecYEG translocon together with YidC insertase. Chl is loaded into the nascent polypeptide cotranslationally from Chl-synthase when the transmembrane segments are released from the translocase channel to YidC (Chidgey et al., 2014). The N-terminal region of the Pam68 protein is associated with the translating ribosome, whereas the C terminus segment interacts with stromal loops of the nascent CP47 chain after it emerges from the translocon. This interaction fixes the CP47 transmembrane segments in a position that facilitates the insertion of Chl molecules. A similar role can be played by the Ycf48 protein at the lumenal site of CP47 (Crawford et al., 2016). Subsequently, PsbH replaces Pam68 and recruits the photoprotective high-light-inducible proteins that associate with CP47 in the vicinity of PsbH (Promnares et al., 2006). Hlips, high-light-inducible proteins.

in the synthesis of CP47. Indeed, using a standard methodology (^{35}S radiolabeling combined with 2D gel-electrophoresis), the synthesis of CP47 in the Arabidopsis *pam68*-null mutant was hardly detectable (Armbruster et al., 2010).

In contrast to Arabidopsis, the inactivation of *pam68* in *Synechocystis* had no obvious effect on the PSII level under standard growth conditions, although the synthesis of CP47 and CP43 was visibly affected in both organisms (Rengstl et al., 2013; Fig. 4). However, after 3 h of high light treatment (2000 μmol photons m^{-2} s^{-1}), the levels of functional PSII in the Δ*pam68* strain decreased by approximately 50% (Rengstl et al., 2013). In addition, we demonstrated the importance of Pam68 under fluctuating light conditions, low temperature, and nitrogen limitation (Fig. 3). These observations imply that Pam68 is essential once the synthesis of CP47 becomes difficult and limits PSII biogenesis.

The PsbH protein is required for sufficient CP47 synthesis in plants as well as in cyanobacteria (Komenda, 2005; Levey et al., 2014); the *Synechocystis* Δ*psbH* mutant shows a noticeable growth defect even under nonstress conditions (Supplemental Fig. S6, A and B). However, the phenotype of this strain is probably quite complex, because PsbH also stabilizes electron transfer processes between Q_A and Q_B in the PSII complex (Komenda et al., 2002). It is further essential for the association of photoprotective high-light-inducible proteins to CP47 (Promnares et al., 2006; Fig. 6), and creates an environment for binding of a red Chl molecule in CP47, which is also supposed to have a protective function (D'Haene et al., 2015). However, we expect that the impaired CP47 synthesis/stability is the major reason for the slow growth of the Δ*psbH* mutant (Supplemental Fig. S6A). This conclusion is supported by the fact that the growth rate of this strain can also be improved by the inhibition of FeCh (Supplemental Fig. S6C), and is consistent with the very poor phenotype of the Δ*psbH*/Δ*pam68* double mutant. Therefore, PsbH appears to be more crucial for the biogenesis than for the functioning of fully assembled PSII complexes. Similarly, the PsbI subunit was found to be more important for attachment of CP43m to RCII, rather than for PSII activity (Dobáková et al., 2007). Other small PSII subunits may also play roles in assembly.

We present a working model of CP47m synthesis (Fig. 6). Pam68 is firmly bound to the translating ribosome via the N-terminal segment, whereas its C-terminal end interacts with the stromal loops of the nascent CP47 chain emerging from the translocon. We speculate that the coordination of Pam68 (stromal side), YidC (lateral site; Hennon et al., 2015), and Ycf48 (lumenal site; Crawford et al., 2016) fixes the CP47 helix pairs in a position that is amenable to Chl binding. The Pam68 C terminus contains highly conserved charged residues (Supplemental Fig. S3) that can form a network of hydrogen bounds resembling the interaction of the N terminus of PsbH with CP47 (see Supplemental Fig. S7). The synthesis of CP47 is impaired in the Δ*pam68* strain even under nonstressful conditions (Fig. 4), suggesting that Pam68 permanently assists during CP47 synthesis. Because Pam68 is particularly critical for the mutant lacking PsbH, it is probable that both proteins can work similarly as chaperones facilitating the folding of CP47 and/or the loading of Chl into the newly synthesized apopolypeptide chain.

Based on previous data and the results of our radiolabeling experiment (Rengstl et al., 2013; Fig. 4), Pam68 appears to also facilitate the synthesis of the CP43 protein and PSI. However, the interaction of Pam68 with these proteins is either too weak to detect, or the lower levels of CP43 and PSI in the absence of Pam68 is a secondary phenotype caused by the feeble CP47 synthesis. The second possibility is more probable, as the mutant lacking CP47 has been shown to contain considerably lower cellular level of Chl in comparison with wild type, implying that the level of CP43 and PSI is lower in the absence of CP47 (Bečková et al., 2017). Although this approach is frequently used, we are aware that arresting particular PSII assembly steps to accumulate specific assembly intermediates may affect other cellular processes, including the synthesis of Chl-binding proteins. The Flag-tag technology used here has the advantage of allowing the purification of PSII assembly intermediates that only exist temporarily in the cell (such as the Pam68.f-CP47m complex) directly from the wild-type background.

The synthesis of CP47 is very sensitive to Chl availability (Hollingshead et al., 2016), which may explain why the lack of Pam68 is not tolerated under stress conditions. The Chl pathway can be temporarily switched-off after a shift to stressful conditions (Kopecná et al., 2012) and when the de novo Chl amount decreases, a fine structural stabilization of the nascent CP47 is likely to be particularly important for the smooth loading of Chls. After addition of the FeCh inhibitor, the pool of available Chl increased, and the impaired CP47 synthesis was rescued (Fig. 5). Thus, a high concentration of Chl molecules around the translated CP47 increases the chance that all Chls are inserted in time even if the orientation of CP47 is not perfect. A similar effect of FeCh inhibition was reported earlier in the *Synechocystis* strain harboring a mutated CP47 protein (Sobotka et al., 2005).

The observed tight binding of Pam68 to the ribosome is intriguing. A high level of LrtA protein, which associates with the 30S ribosomal subunit (Galmozzi et al., 2016), was present in the Pam68.f pull-downs prepared from strains lacking CP47 (Supplemental Fig. S2). As the potential function of LrtA is to stabilize stalled ribosomal 70S particles (Di Pietro et al., 2013), its appearance in the elution indicates that Pam68 interacts with both the SecY-bound idle ribosomes as well as with the actively translating ribosomes. In *Synechocystis*, Pam68 is not an abundant membrane protein (it is not detectable in the stained SDS PAGE gel with separated cellular membrane proteins), and there is only a limited pool of membrane-bound ribosomes associated with Pam68. It is possible that these ribosomes differ structurally from other ribosomes in the cell. The heterogenic nature of ribosomes is demonstrated by the variable stoichiometry among core ribosomal subunits or between the monosome/polysome arrangement of ribosomes according to environmental conditions (Xue and Barna, 2012; Slavov et al., 2015). Similarly, the plastid-encoded Rps15 is not an essential ribosomal subunit in plants, but under chilling stress, the tobacco (*Tobacco nicotiana*) Δ*rps15* knockdown showed a drastic reduction in the number of plastid ribosomes (Fleischmann et al., 2011). In *Synechocystis*, the *rps15-pam68* operon as well as the *rps18*, *rps20*, and *rps25* genes are up-regulated under cold stress, whereas many ribosomal genes are simultaneously down-regulated (Supplemental Fig. S4). This result supports the existence of a pool of modified, stress-induced type of ribosomes in cyanobacteria. It is possible that Pam68 has a higher affinity for the stress-induced type of ribosomes. Once bound to SecY, the ribosome might serve as an anchor to localize Pam68 in the vicinity of the translocon machinery. Under severe conditions with limited Chl availability and/or lowered membrane fluidity (chilling stress), Pam68 can promptly assist during the synthesis of CP47.

MATERIALS AND METHODS

Synechocystis Strains and Growth Conditions

All the *Synechocystis* strains used are summarized in Supplemental Table S1. The Δ*pam68* strain was kindly provided by Jörg Nickelsen (Ludwig-Maximilians University), and is described in Armbruster et al. (2010). The Δ*psbH*/Δ*pam68* double mutant was prepared by transformation of the Δ*psbH* strain (D'Haene et al., 2015) by genomic DNA isolated from the Δ*pam68* strain. The *Synechocystis* strain expressing the Pam68 protein fused with 3×Flag at the C terminus (the *pam68.f* strain) was constructed using pPD-CFLAG plasmid as described in Hollingshead et al. (2012). The *pam68.f* construct was further transformed into the Δ*psbH* and Δ*psbB* cells (Eaton-Rye and Vermaas, 1991) to express the Pam68.f protein in these genetic backgrounds. Derivatives of Pam68.f truncated at the amino acid 29 (the t29-*pam68.f* strain) or 50 (the t50-*pam68.f* strain) were constructed by PCR amplification of the *Synechocystis pam68* gene lacking the 3′ part (primers are listed in Supplemental Table S2). The obtained PCR products were cloned into a pPD-CFLAG plasmid and transformed into wild type. To be able to express Pam68.f in the Δ*pam68*/Δ*psbH* mutant (already resistant to kanamycin), we replaced the kanamycin-resistance cassette in the pPD-CFLAG plasmid with an erythromycin-resistance cassette, cloned the *pam68* gene into this modified construct. and fully segregated the *pam68.f*/Δ*pam68*/Δ*psbH* strain.

Unless stated otherwise, strains were grown photoautotrophically in liquid BG-11 medium on a rotary shaker under moderate (normal) light intensities (40 μE m^{-2} s^{-1}) at 28°C. For purification of the Pam68.f protein under native conditions, 4 L of *pam68.f* and *pam68.f*/Δ*psbH* cells were grown in a 10 L flask in BG-11 medium supplemented by 5 mM Glc under normal light conditions and bubbled with air. Strains lacking PSII (Δ*psbB*) were supplemented with 5 mM Glc and grown under lower light intensities (10 μE m^{-2} s^{-1}).

Absorption Spectra and Determination of Chl Content

Absorption spectra of the whole cells were measured at room temperature with a UV-3000 spectrophotometer (Shimadzu). Chl was extracted from cell pellets (2 mL, OD_{750} = approximately 0.3) with 100% (v/v) methanol, and its concentration was measured spectrophotometrically according to Porra et al. (1989).

Preparation of Cellular Membranes

Cell cultures were harvested at optical densities of 750 nm = approximately 0.5 to 0.7. Cells were pelleted, washed, and resuspended with buffer A (25 mM MES/NaOH, pH 6.5, 10 mM CaCl2, 10 mM MgCl2, 25% [v/v] glycerol) for the preparation of membranes for 2D electrophoresis and purification of Pam68.f. For nickel-affinity chromatography, the membrane fraction was prepared in 25 mM Na-P buffer, pH 7.5, 50 mM NaCl, 10% (v/v) glycerol (buffer B). Cells were broken using glass beads (0.1 mm diameter), and the membrane fraction was separated from soluble proteins by centrifugation at high speed (65,000 × *g*, 20 min).

Isolation of Protein Complexes by Affinity Chromatography

Cellular membranes containing approximately 1 mg/mL Chl were solubilized for 1 h with 1% (w/v) β-dodecyl-maltoside at 10°C and centrifuged for 20 min at 65,000*g* to remove cell debris. The Pam68.f complexes were purified using an anti-Flag-M2 agarose column (Sigma-Aldrich). To remove contaminants, the anti-Flag-resin was washed with 20 resin volumes of buffer A containing 0.04% β-dodecyl-maltoside. The Pam68.f complex was eluted with 2.5 resin volumes of buffer A containing 150 μg/mL 3×Flag peptide (Sigma-Aldrich) and 0.04% β-dodecyl-maltoside. For purification of the His-tagged proteins, solubilized membrane complexes were loaded onto a nickel-affinity chromatography column (Protino Ni–NTA-agarose; Macherey-Nagel). Proteins bound to the column were washed with buffer B containing 0.04% β-dodecyl-maltoside and increasing concentrations of imidazole (5, 10, 20, and 30 mM); His-tagged proteins were finally eluted with 150 mM imidazole.

Electrophoresis and Immunoblotting

The protein composition of the purified complexes was analyzed by electrophoresis in a denaturing 12% to 20% linear gradient polyacrylamide gel containing 7 M urea (Dobáková et al., 2009). Proteins were stained either by Coomassie Brilliant Blue or SYPRO Orange stain and subsequently transferred onto a PVDF membrane for immunodetection (see below). For native electrophoresis, solubilized membrane proteins or isolated complexes were separated on 4% to 12% CN-PAGE (Wittig et al., 2007). Individual components of protein complexes were resolved by incubating the gel strip from the first dimension in 2% (w/v) SDS and 1% (w/v) DTT for 30 min at room temperature, and proteins were separated along the second dimension by SDS-PAGE in a denaturing 12% to 20% polyacrylamide gel containing 7 M urea (Dobáková et al., 2009). Proteins were stained by Coomassie Brilliant Blue or by SYPRO Orange; in the latter case, they were subsequently transferred onto a PVDF membrane. Membranes were incubated with specific primary antibodies and then with a secondary antibody conjugated with horseradish peroxidase (Sigma-Aldrich). The following primary antibodies were used in the study: anti-SecY and anti-YidC (Linhartová et al., 2014), anti-CP47, anti-D1 and anti-PsbH (Komenda, 2005), anti-Pam68 (Armbruster et al., 2010), anti-Rpl1 (Agrisera), anti-Flag (Sigma-Aldrich), and anti-Ycf48 (which was raised in rabbit against recombinant *Synechocystis* Ycf48 and provided by Peter Nixon, Imperial College, London).

Protein Radiolabeling

For protein labeling, the cells were incubated with using a mixture of [^{35}S]Met and [^{35}S]Cys (Translabel; MP Biochemicals) as described in Dobáková et al. (2009). After separation of labeled proteins by CN-PAGE in the first dimension, the polyacrylamide gel was scanned for Chl fluorescence and then treated for second-dimension separation with 18% SDS-PAGE. The 2D gel was exposed to a Phosphorimager plate (GE Healthcare) overnight and stained by Coomassie Brilliant Blue and scanned by Storm (GE Healthcare).

Protein Identification by LC-MS/MS Analysis

Gel slices were placed in 200 μL of 40% acetonitrile, 200 mM ammonium bicarbonate and incubated at 37°C for 30 min, after which the solution was discarded. This procedure was performed twice, and the gel was subsequently dried in a vacuum centrifuge. Ten microliters of 40 mM ammonium bicarbonate in 9% acetonitrile containing 0.4 μg trypsin (proteomics grade; Sigma-Aldrich) were added to the gel slice and left to soak in the solution at 4°C for 45 min. To digest proteins, 20 μL of 9% (v/v) acetonitrile in 40 mM ammonium bicarbonate was added to the gel and incubated at 37°C overnight. Peptides were purified using ZipTip C18 pipette tips (Millipore). MS analysis was performed on a NanoAcquity UPLC (Waters) on-line coupled to the ESI Q-ToF Premier mass spectrometer (Waters). One microliter of the sample was diluted in 3% (v/v) acetonitrile/0.1% (v/v) formic acid, and tryptic peptides were desalted on a Symmetry C18 Trapping column (180 μm i.d., 20 mm length, particle size 5 μm, reverse phase; Waters) with a flow rate of 15 μL/min for 1 min. Trapping was followed by a reverse-phase UHPLC using the BEH300 C18 analytical column (75 μm i.d. 150 mm length, particle size 1.7 μm, reverse phase; Waters). The linear gradient elution ranged from 97% solvent A (0.1% formic acid) to 40% solvent B (0.1% formic acid in acetonitrile) at a flow rate of 0.4 μL/min. Eluted peptides flowed directly into the ESI source. Raw data were acquired in the data-independent MS^E identity mode (Waters). Precursor ion spectra were acquired with a collision energy of 5 V and fragment ion spectra with a collision energy of 20 V to 35 V ramp in alternating 1 s scans. Data-dependent analysis mode was used for the second analysis; peptide spectra were acquired with a collision energy of 5 V and peptides with charge states of + 2, +3, and + 4 were selected for MS/MS analysis. Fragment spectra were collected with a collision energy of 20 V to 40 V ramp. In both modes, the acquired spectra were submitted for database search using the PLGS2.3 software (Waters) against *Synechocystis* protein databases from the Cyanobase Web site (http://genome.microbedb.jp/cyanobase/). Acetyl N-terminal, deamidation N and Q, carbamidomethyl C, and oxidation M were set as variable modifications. Identification of three consecutive *y*-ions or *b*-ions was required for a positive peptide match.

Accession Numbers

Pam68, BAA16881.1; CP47, BAA10458.1; PsbH, BAA17629.1, SecY; BAA17331.1, YidC - BAA18244.1.

Supplemental Data

The following supplemental materials are available.

Supplemental Table S1. A list of *Synechocystis* strains used in this study.

Supplemental Table S2. A list of primers used to clone the *pam68.f* gene and its two truncated variants (*t29-pam68.f* and *t50-pam68.f*) into the pPD-CFLAG plasmid (adding of 3×Flag tag at the C terminus).

Supplemental Figure S1. Identification of proteins copurified with Pam68.f.

Supplemental Figure S2. 2D CN/SDS-PAGE of the Pam68.f complex purified from the *pam68.f*/Δ*psbB* strain (A) and the control ΔCP47 (B).

Supplemental Figure S3. Conservation profile and the prediction of secondary structure of the *Synechocystis* Pam68 protein.

Supplemental Figure S4. Coexpression of the cyanobacterial *pam68-rps15* operon with a subset of ribosomal genes.

Supplemental Figure S5. Accumulation of the Pam68 protein under stress conditions.

Supplemental Figure S6. Growth rate and whole cell spectra of the wild-type and mutant strains.

Supplemental Figure S7. Stromal view of the CP47–PsbH complex with indicated hydrogen bonds between the CP47 and the PsbH N terminus.

Supplemental Figure S8. Changes in the levels of Chl precursors in the Δ*psbH*/Δ*pam68* strain after treatment with FeCh inhibitor.

Supplemental Dataset. MS data—numbers of identified trypsin peptides for 2D gel protein spots.

Received January 17, 2018; accepted February 7, 2018; published February 20, 2018.

LITERATURE CITED

Armbruster U, Zühlke J, Rengstl B, Kreller R, Makarenko E, Rühle T, Schünemann D, Jahns P, Weisshaar B, Nickelsen J, Leister D (2010) The Arabidopsis thylakoid protein PAM68 is required for efficient D1 biogenesis and photosystem II assembly. Plant Cell **22:** 3439–3460

Bečková M, Gardian Z, Yu J, Koník P, Nixon PJ, Komenda J (2017) Association of Psb28 and Psb27 proteins with PSII-PSI supercomplexes upon exposure of *Synechocystis* sp. PCC 6803 to high light. Mol Plant **10:** 62–72

Boehm M, Romero E, Reisinger V, Yu J, Komenda J, Eichacker LA, Dekker JP, Nixon PJ (2011) Investigating the early stages of photosystem II assembly in *Synechocystis* sp. PCC 6803: isolation of CP47 and CP43 complexes. J Biol Chem **286:** 14812–14819

Boehm M, Yu J, Reisinger V, Bečková M, Eichacker LA, Schlodder E, Komenda J, Nixon PJ (2012) Subunit composition of CP43-less photosystem II complexes of *Synechocystis* sp. PCC 6803: implications for the assembly and repair of photosystem II. Philos Trans R Soc Lond B Biol Sci **367:** 3444–3454

Chidgey JW, Linhartová M, Komenda J, Jackson PJ, Dickman MJ, Canniffe DP, Koník P, Pilný J, Hunter CN, Sobotka R (2014) A cyanobacterial chlorophyll synthase-HliD complex associates with the Ycf39 protein and the YidC/Alb3 insertase. Plant Cell **26:** 1267–1279

Crawford TS, Eaton-Rye JJ, Summerfield TC (2016) Mutation of Gly195 of the ChlH subunit of Mg-chelatase reduces chlorophyll and further disrupts PS II assembly in a Ycf48-deficient strain of *Synechocystis* sp. PCC 6803. Front Plant Sci **7:** 1060

D'Haene SE, Sobotka R, Bučinská L, Dekker JP, Komenda J (2015) Interaction of the PsbH subunit with a chlorophyll bound to histidine 114 of CP47 is responsible for the red 77K fluorescence of Photosystem II. Biochim Biophys Acta **1847:** 1327–1334

Di Pietro F, Brandi A, Dzeladini N, Fabbretti A, Carzaniga T, Piersimoni L, Pon CL, Giuliodori AM (2013) Role of the ribosome-associated protein PY in the cold-shock response of *Escherichia coli*. MicrobiologyOpen **2:** 293–307

Dobáková M, Sobotka R, Tichý M, Komenda J (2009) Psb28 protein is involved in the biogenesis of the photosystem II inner antenna CP47 (PsbB) in the cyanobacterium *Synechocystis* sp. PCC 6803. Plant Physiol **149:** 1076–1086

Dobáková M, Tichý M, Komenda J (2007) Role of the PsbI protein in photosystem II assembly and repair in the cyanobacterium *Synechocystis* sp. PCC 6803. Plant Physiol **145:** 1681–1691

Eaton-Rye JJ, Vermaas WFJ (1991) Oligonucleotide-directed mutagenesis of psbB, the gene encoding CP47, employing a deletion mutant strain of the cyanobacterium *Synechocystis* sp. PCC 6803. Plant Mol Biol **17:** 1165–1177

Fleischmann TT, Scharff LB, Alkatib S, Hasdorf S, Schöttler MA, Bock R (2011) Nonessential plastid-encoded ribosomal proteins in tobacco: a developmental role for plastid translation and implications for reductive genome evolution. Plant Cell **23:** 3137–3155

Frauenfeld J, Gumbart J, Sluis EO, Funes S, Gartmann M, Beatrix B, Mielke T, Berninghausen O, Becker T, Schulten K, Beckmann R (2011) Cryo-EM structure of the ribosome-SecYE complex in the membrane environment. Nat Struct Mol Biol **18:** 614–621

Galmozzi CV, Florencio FJ, Muro-Pastor MI (2016) The cyanobacterial ribosomal-associated protein LrtA Is involved in post-stress survival in *Synechocystis* sp. PCC 6803. PLoS One **11:** e0159346

Heinz S, Liauw P, Nickelsen J, Nowaczyk M (2016) Analysis of photosystem II biogenesis in cyanobacteria. Biochim Biophys Acta **1857:** 274–287

Hennon SW, Soman R, Zhu L, Dalbey RE (2015) YidC/Alb3/Oxa1 family of insertases. J Biol Chem **290:** 14866–14874

Hollingshead S, Kopečná J, Armstrong DR, Bučinská L, Jackson PJ, Chen GE, Dickman MJ, Williamson MP, Sobotka R, Hunter CN (2016) Synthesis of chlorophyll-binding proteins in a fully segregated Δ*ycf54* strain of the cyanobacterium *Synechocystis* PCC 6803. Front Plant Sci **7:** 292

Hollingshead S, Kopecná J, Jackson PJ, Canniffe DP, Davison PA, Dickman MJ, Sobotka R, Hunter CN (2012) Conserved chloroplast open-reading frame *ycf54* is required for activity of the magnesium protoporphyrin monomethylester oxidative cyclase in *Synechocystis* PCC 6803. J Biol Chem **287:** 27823–27833

Knoppová J, Sobotka R, Tichý M, Yu J, Koník P, Halada P, Nixon PJ, Komenda J (2014) Discovery of a chlorophyll binding protein complex involved in the early steps of photosystem II assembly in *Synechocystis*. Plant Cell **26:** 1200–1212

Komenda J (2005) Autotrophic cells of the *Synechocystis psbH* deletion mutant are deficient in synthesis of CP47 and accumulate inactive PS II core complexes. Photosynth Res **85:** 161–167

Komenda J, Lupínková L, Kopecký J (2002) Absence of the *psbH* gene product destabilizes photosystem II complex and bicarbonate binding on its acceptor side in *Synechocystis* PCC 6803. Eur J Biochem **269:** 610–619

Komenda J, Reisinger V, Müller BC, Dobáková M, Granvogl B, Eichacker LA (2004) Accumulation of the D2 protein is a key regulatory step for assembly of the photosystem II reaction center complex in *Synechocystis* PCC 6803. J Biol Chem **279:** 48620–48629

Komenda J, Sobotka R, Nixon PJ (2012) Assembling and maintaining the Photosystem II complex in chloroplasts and cyanobacteria. Curr Opin Plant Biol **15:** 245–251

Kopecná J, Komenda J, Bucinská L, Sobotka R (2012) Long-term acclimation of the cyanobacterium *Synechocystis* sp. PCC 6803 to high light is accompanied by an enhanced production of chlorophyll that is preferentially channeled to trimeric photosystem I. Plant Physiol **160:** 2239–2250

Kopečná J, Pilný J, Krynická V, Tomčala A, Kis M, Gombos Z, Komenda J, Sobotka R (2015) Lack of phosphatidylglycerol inhibits chlorophyll biosynthesis at multiple sites and limits chlorophyllide reutilization in the cyanobacterium *Synechocystis* 6803. Plant Physiol **169:** 1307–1017

Kopf M, Klähn S, Scholz I, Matthiessen JK, Hess WR, Voß B (2014) Comparative analysis of the primary transcriptome of *Synechocystis* sp. PCC 6803. DNA Res **21:** 527–539

Levey T, Westhoff P, Meierhoff K (2014) Expression of a nuclear-encoded psbH gene complements the plastidic RNA processing defect in the PSII mutant hcf107 in *Arabidopsis thaliana*. Plant J **80:** 292–304

Linhartová M, Bučinská L, Halada P, Ječmen T, Setlík J, Komenda J, Sobotka R (2014) Accumulation of the Type IV prepilin triggers degradation of SecY and YidC and inhibits synthesis of Photosystem II proteins in the cyanobacterium *Synechocystis* PCC 6803. Mol Microbiol **93:** 1207–1223

Mitschke J, Georg J, Scholz I, Sharma CM, Dienst D, Bantscheff J, Voss B, Steglich C, Wilde A, Vogel J, Hess WR (2011) An experimentally anchored map of transcriptional start sites in the model cyanobacterium *Synechocystis* sp. PCC6803. Proc Natl Acad Sci USA **108:** 2124–2129

Nixon PJ, Michoux F, Yu J, Boehm M, Komenda J (2010) Recent advances in understanding the assembly and repair of photosystem II. Ann Bot **106:** 1–16

Pilný J, Kopečná J, Noda J, Sobotka R (2015) Detection and quantification of heme and chlorophyll precursors using a High Performance Liquid Chromatography (HPLC) system equipped with two fluorescence detectors. Bio Protoc **5:** e1390

Porra RJ, Thompson WA, Kriedmann PE (1989) Determination of accurate extinction coefficients and simultaneous equations for assaying chlorophylls a and b extracted with four different solvents: verification of the concentration of chlorophyll standards by atomic absorption spectroscopy. Biochim Biophys Acta **975:** 384–394

Prinz A, Behrens C, Rapoport TA, Hartmann E, Kalies KU (2000) Evolutionarily conserved binding of ribosomes to the translocation channel via the large ribosomal RNA. EMBO J **19:** 1900–1906

Promnares K, Komenda J, Bumba L, Nebesářová J, Vácha F, Tichý M (2006) Cyanobacterial small chlorophyll-binding protein ScpD (HliB) is located on the periphery of photosystem II in the vicinity of PsbH and CP47 subunits. J Biol Chem **281:** 32705–32713

Rengstl B, Knoppová J, Komenda J, Nickelsen J (2013) Characterization of a *Synechocystis* double mutant lacking the photosystem II assembly factors YCF48 and Sll0933. Planta **237:** 471–480

Rengstl B, Oster U, Stengel A, Nickelsen J (2011) An intermediate membrane subfraction in cyanobacteria is involved in an assembly network for Photosystem II biogenesis. J Biol Chem **286:** 21944–21951

Sachelaru I, Petriman NA, Kudva R, Kuhn P, Welte T, Knapp B, Drepper F, Warscheid B, Koch HG (2013) YidC occupies the lateral gate of the SecYEG translocon and is sequentially displaced by a nascent membrane protein. J Biol Chem **288:** 16295–16307

Seitl I, Wickles S, Beckmann R, Kuhn A, Kiefer D (2014) The C-terminal regions of YidC from *Rhodopirellula baltica* and *Oceanicaulis alexandrii* bind to ribosomes and partially substitute for SRP receptor function in *Escherichia coli*. Mol Microbiol **91:** 408–421

Slavov N, Semrau S, Airoldi E, Budnik B, van Oudenaarden A (2015) Differential stoichiometry among core ribosomal proteins. Cell Reports **13:** 865–873

Sobotka R (2014) Making proteins green; biosynthesis of chlorophyll-binding proteins in cyanobacteria. Photosynth Res **119:** 223–232

Sobotka R, Komenda J, Bumba L, Tichý M (2005) Photosystem II assembly in CP47 mutant of *Synechocystis* sp. PCC 6803 is dependent on the level of chlorophyll precursors regulated by ferrochelatase. J Biol Chem **280:** 31595–31602

Umena Y, Kawakami K, Shen JR, Kamiya N (2011) Crystal structure of oxygen-evolving photosystem II at a resolution of 1.9 Å. Nature **473:** 55–60

Vavilin D, Brune DC, Vermaas W (2005) ^{15}N-labeling to determine chlorophyll synthesis and degradation in *Synechocystis* sp. PCC 6803 strains lacking one or both photosystems. Biochim Biophys Acta **1708:** 91–101

Wittig I, Karas M, Schägger H (2007) High resolution clear native electrophoresis for in-gel functional assays and fluorescence studies of membrane protein complexes. Mol Cell Proteomics **6:** 1215–1225

Xue S, Barna M (2012) Specialized ribosomes: a new frontier in gene regulation and organismal biology. Nat Rev Mol Cell Biol **13:** 355–369

Photosynthesis Research (2022) 152:317–332
https://doi.org/10.1007/s11120-022-00904-z

ORIGINAL ARTICLE

High-light-inducible proteins HliA and HliB: pigment binding and protein–protein interactions

Minna M. Konert[1] · **Anna Wysocka**[1] · **Peter Koník**[2] · **Roman Sobotka**[1]

Received: 10 November 2021 / Accepted: 15 February 2022 / Published online: 26 February 2022

Abstract

High-light-inducible proteins (Hlips) are single-helix transmembrane proteins that are essential for the survival of cyanobacteria under stress conditions. The model cyanobacterium *Synechocystis* sp. PCC 6803 contains four Hlip isoforms (HliA-D) that associate with Photosystem II (PSII) during its assembly. HliC and HliD are known to form pigmented (hetero)dimers that associate with the newly synthesized PSII reaction center protein D1 in a configuration that allows thermal dissipation of excitation energy. Thus, it is expected that they photoprotect the early steps of PSII biogenesis. HliA and HliB, on the other hand, bind the PSII inner antenna protein CP47, but the mode of interaction and pigment binding have not been resolved. Here, we isolated His-tagged HliA and HliB from *Synechocystis* and show that these two very similar Hlips do not interact with each other as anticipated, rather they form HliAC and HliBC heterodimers. Both dimers bind Chl and β-carotene in a quenching conformation and associate with the CP47 assembly module as well as later PSII assembly intermediates containing CP47. In the absence of HliC, the cellular levels of HliA and HliB were reduced, and both bound atypically to HliD. We postulate a model in which HliAC-, HliBC-, and HliDC-dimers are the functional Hlip units in *Synechocystis*. The smallest Hlip, HliC, acts as a 'generalist' that prevents unspecific dimerization of PSII assembly intermediates, while the N-termini of 'specialists' (HliA, B or D) dictate interactions with proteins other than Hlips.

Keywords *Synechocystis* · High-light-inducible proteins · Photosystem II · CP47 · Chlorophyll

Introduction

The structure and function of photosynthetic reaction centers are highly conserved between all oxygenic phototrophs. Photosystem I (PSI) consists of two large pigment-binding reaction center proteins (PsaA and PsaB) and ten to fourteen smaller subunits depending on the species (Jordan et al. 2001; Ben-Shem et al. 2003; Mazor et al. 2017; Malavath et al. 2018). Photosystem II (PSII) reaction centers, on the other hand, contain four major pigment-binding proteins (D1, D2, CP43, CP47) in addition to sixteen smaller membrane spanning subunits and three extrinsic lumenal subunits of the oxygen-evolving complex (Umena et al. 2011; Wei et al. 2016). The PSII reaction center proteins D1 and D2 contain the chlorophylls (Chls) and pheophytins responsible for primary charge separation, while the two inner antenna proteins, CP43 and CP47, transfer captured light energy to the reaction center. Both photosystems utilize additional light-harvesting antenna systems to increase their light-harvesting capacity. Cyanobacteria contain the peripheral phycobilisome antennae, whereas in plants and different types of algae, the outer light-harvesting antennae of PSI and PSII are composed of membrane embedded light-harvesting complex proteins (LHCs). LHCs belong to the LHC superfamily, which is characterized by a highly conserved Chl-binding motif (ExxN/HxR; Engelken et al. 2010). LHCs contain this motif in two of their three transmembrane helices. The conserved Glu and Arg residues from one helix form salt bridges with the Arg and Glu residues of the other helix, respectively, locking the helices in a cross formation that is further stabilized by associated carotenoid (Car) and Chl molecules (Kühlbrandt et al. 1994; Bassi et al. 1999; Liu et al. 2004).

✉ Minna M. Konert
koskela@alga.cz

[1] Institute of Microbiology of the Czech Academy of Sciences, Novohradská 237 - Opatovický mlýn, 37901 Třeboň, Czech Republic

[2] Institute of Chemistry, Faculty of Science, University of South Bohemia, Branišovská 1760, 37005 České Budějovice, Czech Republic

LHC superfamily proteins are present in all oxygenic phototrophs, but they vary in the number of transmembrane helices and Chl-binding motifs, and not all of them function in light harvesting (Engelken et al. 2010). The most ancient LHC proteins are cyanobacterial high-light-inducible proteins (Hlips), which contain a single transmembrane helix with the ExxNxR motif. Homologues of Hlips called one-helix proteins (OHPs; an alternative name Ycf17 is used in some algae) also seem to be ubiquitous in oxygenic eukaryotes (Engelken et al. 2010). The model cyanobacterium *Synechocystis* sp. PCC 6803 (hereafter *Synechocystis*) contains four Hlip isoforms (HliA-D) and one Hlip-like domain fused to the ferrochelatase enzyme (Pazderník et al. 2019). Based on known LHC structures, it has been proposed that Hlips and OHPs form pigment-binding dimers (Staleva et al. 2015; Hey and Grimm 2018). Indeed, pigment binding has been demonstrated experimentally for purified *Synechocystis* HliC- and HliD-dimers (Staleva et al. 2015; Shukla et al. 2018) and in vitro refolded plant OHPs (Hey and Grimm 2020).

Expression of Hlip genes is highly induced by stress conditions (Dolganov et al. 1995; He et al. 2001) and, as shown by studies made on ΔHlip strains, Hlips are essential for cell survival already under moderately high light intensities (He et al. 2001; Havaux et al. 2003). The exact mechanism of how Hlips ensure cell survival under adverse conditions remains unclear, but all four *Synechocystis* Hlips have been indicated in one way or another in PSII assembly (Komenda and Sobotka 2016). PSII assembly is a complicated and highly regulated process that is initiated by the formation of four separate PSII assembly modules. Each module contains one major Chl-binding PSII subunit (D1, D2, CP43 or CP47) preloaded with pigments and subjoined by small PSII subunits. The modules then assemble in a stepwise manner forming several distinct PSII assembly intermediates (Komenda et al. 2012b). First, the D1 and D2 modules dimerize to form the PSII reaction center core (RCII). Next, the CP47 module (CP47m) attaches to RCII, yielding the RC47 assembly intermediate (Dobáková et al. 2009; Boehm et al. 2012). The addition of the CP43 module to RC47 results in the monomeric (non-oxygen-evolving) PSII reaction center core complex (RCCII). Finally, the lumenal oxygen-evolving complex is assembled and the resulting PSII-monomers dimerize to the fully active PSII-dimer (Becker et al. 2011).

In addition to de novo biosynthesis, PSII also undergoes rapid repair cycles in the cell due to its susceptibility to photo-oxidative damage (Vass 2012). It is likely that PSII assembly and repair utilize, at least partially, the same accessory proteins and involve similar intermediary complexes (Komenda et al. 2012b; Järvi et al. 2015). Both PSII assembly and repair rely on the assistance of various proteins (assembly factors) that are not part of the active PSII complex. These factors bind to the assembly or repair intermediates during different stages: for instance, the RCII complex is associated with lumenal proteins Ycf48 and CyanoP, whereas the later PSII intermediates contain Psb28 and Psb27 factors connected to CP47 and CP43 antenna subunits, respectively. *Synechocystis* HliC and HliD form a heterodimer that binds tightly to the PSII assembly factor Ycf39; the resulting HliCD-Ycf39 subcomplex interacts with RCII, giving rise to a complex called RCII* (Knoppová et al. 2014). The HliCD-dimer is capable of quenching light energy via energy transfer from Chl to *β*-carotene (*β*-Car) (Staleva et al. 2015), and thus very likely protects the newly forming reaction center against photo-oxidation. Moreover, it has been proposed that HliCD-Ycf39 aids in the delivery of Chl to the nascent D1 reaction center protein, as another protein partner of HliCD is the Chl synthase enzyme (ChlG) (Chidgey et al. 2014). In the course of PSII biosynthesis, the HliCD-Ycf39 subcomplex is detached prior to the formation of RC47 (Knoppová et al. 2014). Similar to HliC and HliD, plant OHPs bind the plant homologue of Ycf39 (HCF244) and associate with RCII (Myouga et al. 2018; Hey and Grimm 2018; Li et al. 2019).

In contrast to HliC and HliD, much less is known about the HliA and HliB proteins. In *Synechocystis*, HliA, HliB, and HliC associate with the CP47 antenna, but the stage(s) of PSII biogenesis at which this occurs remain to be clarified (Promnares et al. 2006; Yao et al. 2007; Pascual-Aznar et al. 2021). In addition, whether HliA and HliB bind pigments or interact with other Hlips is not known. In this study, we characterized HliA- and HliB-associated protein complexes purified from *Synechocystis*. We found that both HliA and HliB form heterodimers with HliC and that the resulting HliAC and HliBC pairs bind Chl and *β*-Car in a quenched configuration. Both dimers associate with the CP47m as well as later PSII assembly intermediates, RC47 and RCCII. Using a detailed mass spectrometry analysis of the isolated HliA/B complexes, we identified several previously uncharacterized proteins that potentially participate in PSII biogenesis. The results presented here make a complete picture of the *Synechocystis* Hlip 'interactome.'

Results

HliAC and HliBC heterodimers bind pigments in an energy-dissipating configuration

To study the biochemical properties of HliA and HliB, we expressed N-terminally His-tagged recombinant proteins (9.0 kDa and 8.7 kDa, respectively) in *Synechocystis* cells under the strong, high-light-inducible *psbA2* promoter and deleted the respective native genes to create the strains *his-hliA*/Δ*hliA* and *his-hliB*/Δ*hliB*. We tested the accumulation of recombinant proteins by shifting the cells from normal

light (40 µmol m^{-2} s^{-1}) to high light (500 µmol m^{-2} s^{-1}) for up to 5 h. Cellular levels of His-HliA and His-HliB proteins were comparable with their native counterparts in wild-type cells (WT) (Supplemental Fig. 1) confirming that the ectopically expressed His-HliA/B were present in membranes at physiologically relevant concentrations. For all of the following experiments, we used a membrane fraction isolated from cells treated by high light for 3 h.

In order to establish whether HliA and HliB bind pigments, we first purified the His-tagged Hlips from n-dodecyl *β*-D-maltoside (DDM)-solubilized membranes in phosphate buffer (pH 7.8) containing no Mg^{2+} and Ca^{2+} ions; these conditions, according to our previous results, destabilize the interaction between Hlips and PSII subunits allowing isolation of free Hlip-dimers (Shukla et al. 2018). His-HliA/B eluates showed a similar yellow-green color and, as revealed by 2D clear native (CN)/SDS-electrophoresis, they contained mostly free Hlip-dimers composed of the His-tagged bait proteins in complex with HliC (5.2 kDa; Fig. 1). Quantification of the proteins from the Coomassie-stained 2D gel yielded a ratio of 1:0.6 for His-HliA and HliC (Fig. 1a), and 1:0.7 for His-HliB and HliC (Fig. 1b). We did not detect the native HliA in His-HliB pull-down nor the native HliB in His-HliA pull-down. HliD was not present in either eluate. Based on these results, we concluded that HliC is the preferred Hlip interacting with HliA and HliB in vivo. The eluates also contained low amounts of the RCCII and RC47 assembly complexes, as revealed by Chl fluorescence imaging of the CN strips and the pattern of PSII reaction center proteins on the 2D gels. Importantly, free Hlips co-migrated with pigments but did not show any Chl fluorescence in the CN gel, indicating that they were present in a quenched conformation.

To characterize the (His-)HliAC and (His-)HliBC-dimers further, we cut the Hlip-bands from the CN gel strips as indicated (Fig. 1) and measured their in-gel absorption spectra (Fig. 2a). The spectra were almost identical with Chl absorption maxima at 437 nm and 677 nm and a Car peak around 488 nm with a shoulder at 520 nm (Fig. 2a). Next, we eluted the Hlips from the gel, extracted pigments into methanol

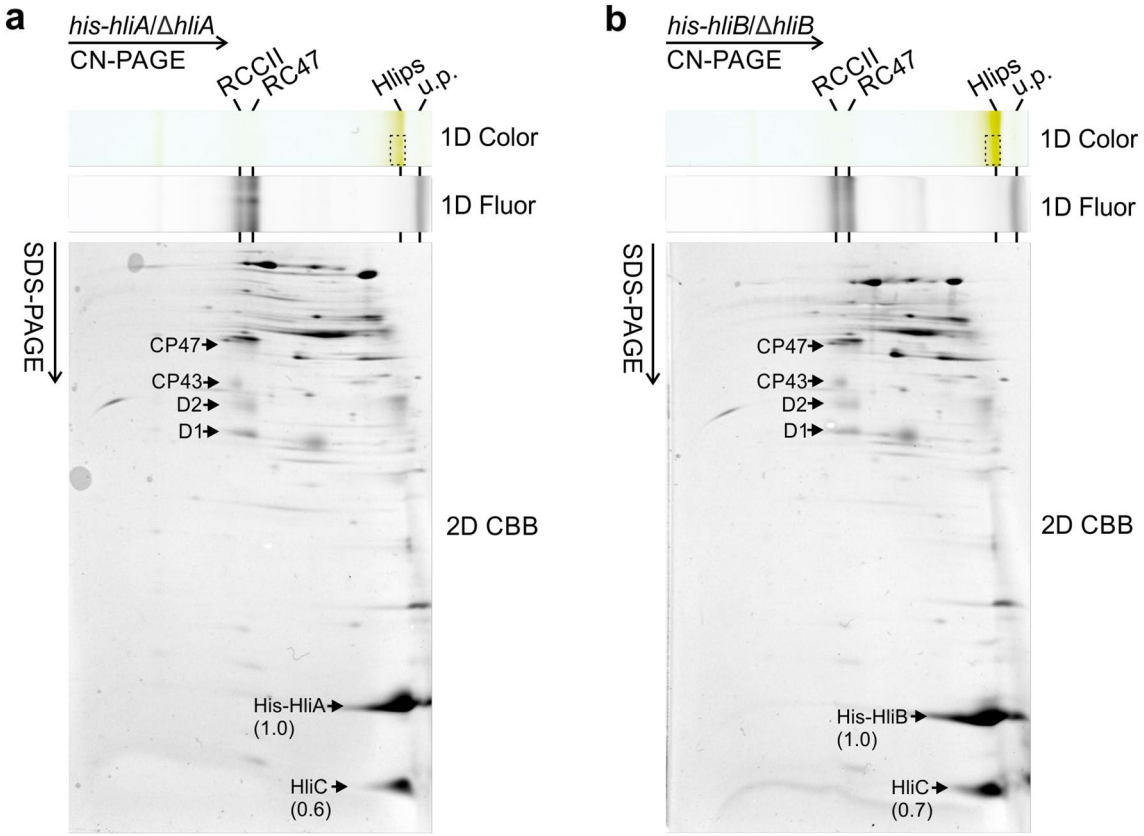

Fig. 1 Two-dimensional CN/SDS-PAGE separation of Ni-NTA pull-downs from *his-hliA*/Δ*hliA* (**a**) and *his-hliB*/Δ*hliB* (**b**) strains Hlip complexes were purified in phosphate buffer from the membrane fractions of high-light -treated cells and separated by 2D CN/SDS-PAGE. The pigment–protein bands containing (His-)HliAC and (His-)HliBC heterodimers that were cut for absorption spectrum and pigment measurements (Fig. 2; Table 1) are indicated by dashed-line boxes. His-HliA, His-HliB, and HliC abundances were quantified from the Coomassie-stained gels and the raw intensities were normalized to the molecular weights of the proteins. The molar ratios of the proteins are indicated in brackets. *CBB* coomassie stain, *Fluor* Chl fluorescence, *u.p.* unbound pigments

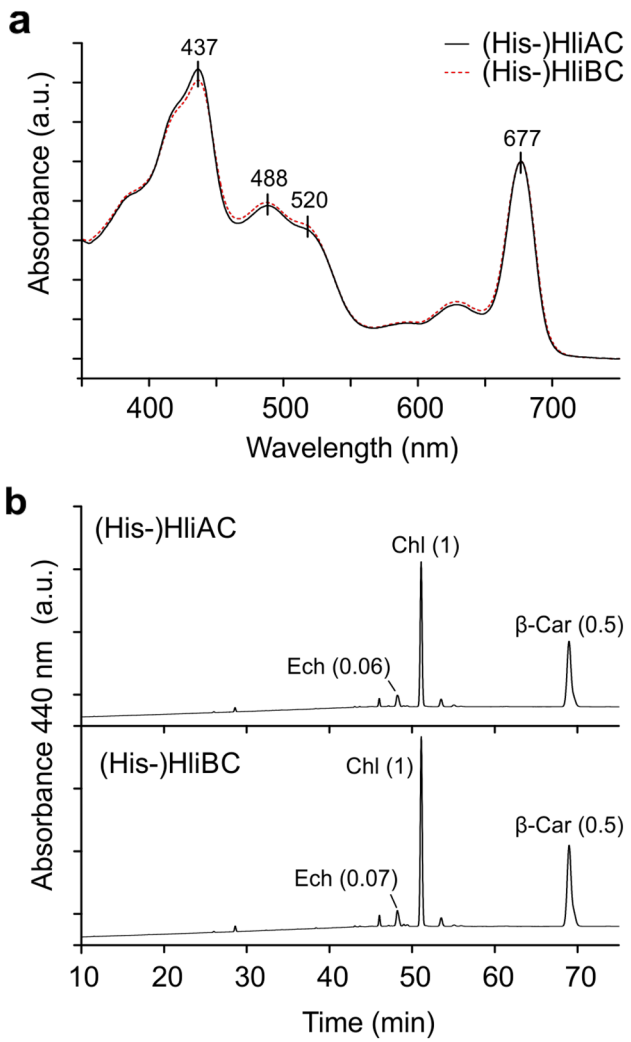

Fig. 2 Absorption spectra (**a**) and pigment analysis (**b**) of purified Hlips. **a** (His-)HliAC- and (His-)HliBC-dimers were cut from CN-PAGE (see Fig. 1) and in-gel absorption spectra recorded. Spectra were normalized to Chl Q_Y band (677 nm). Absorption maxima of Chl *a* (437 nm and 677 nm) and Cars (488 nm and 520 nm) are indicated above the spectra. Spectra represent an average from three independent purifications. **b** Pigments were eluted from the CN-PAGE separated Hlips (see Fig. 1) and analyzed with HPLC. The eluted pigments were quantified (see Table 1) and the relative amounts compared to Chl calculated (indicated in brackets). *Ech* echinenone, *a.u.* arbitrary units

and quantified individual pigment species by HPLC (Fig. 2b, Table 1). In addition to Chl and *β*-Car as the main pigments, both Hlip-dimers contained small amounts of echinenone and *β*-cryptoxanthin. The Chl to total Car ratio in (His-)HliAC- and (His-)HliBC-dimers was 1:0.6.

HliA and HliB are specifically associated with the assembling PSII complexes

To clarify the association of HliA and HliB with different PSII (sub)complexes, we separated solubilized cellular membranes by 2D CN/SDS-PAGE and immunodetected both Hlips and their expected interaction partner, CP47 (Supplemental Fig. 2). However, this time we used a mildly acidic MES buffer (pH 6.5) supplemented with Mg^{2+} and Ca^{2+} for membrane isolation and solubilized the thylakoids using a combination of DDM together with the very mild detergent glycodiosgenin (GDN) in order to stabilize protein–protein interactions (Chae et al. 2012). The majority of Hlips in WT co-migrated with the RCCII complex and CP47m (Supplemental Fig. 2a) in agreement with previous findings (Promnares et al. 2006). Notably, CP47m was observed as at least three distinct spots with Hlips present as a diffuse signal around the two higher molecular weight forms. According to published results (Boehm et al. 2011; Pascual-Aznar et al. 2021), the fastest migrating CP47m spot corresponds to a 'standard' CP47m complex containing CP47 subjoined with the small PSII subunits PsbH, PsbL, and PsbT. A fraction of CP47m further associates with the small Psb35 protein and the mass difference between the RC47m and RC47m-Psb35 complexes is clearly resolved by CN gel (Pascual-Aznar et al. 2021). Thus, it seems likely that the higher MW CP47m forms detected here represent CP47m + Hlips with and without Psb35. Minor HliA/B signals were also observed around the RC47 complex and in the high molecular weight region. Notably, almost no Hlips were detected as free dimers, indicating that our solubilization conditions preserved the native interactions of Hlips.

To differentiate between the highly similar HliA and HliB, which react with the same antibody, we also utilized the single-mutant strains Δ*hliA* and Δ*hliB* (Supplemental

Table 1 Pigment composition of the purified (His-)HliAC- and (His-)HliBC-dimers Purified proteins were separated on CN-PAGE and gel bands containing Hlip-dimers (see Fig. 1) were cut for pigment analysis by HPLC (Fig. 2b)

Protein complex	Pigment				
	Chlorophyll *a*	*β*-carotene	Echinenone	*β*-cryptoxanthin	Chl:Car ratio
His-HliAC	1.000	0.524 (±0.005)	0.061 (±0.000)	0.021 (±0.001)	1:0.6
His-HliBC	1.000	0.515 (±0.006)	0.070 (±0.004)	0.021 (±0.001)	1:0.6

Pigment stoichiometries were normalized to Chl = 1. The relative pigment quantifications are an average (± standard deviation) of three independent pull-downs

Car total carotenoids

Fig. 2b, c). Both Hlips had a very similar distribution in the gel, with the majority of the protein found in RCCII and CP47m. Both Hlips were also observed in the two higher molecular weight spots of CP47m as in WT. Interestingly, a significant amount of HliA was also observed in the high molecular weight region at the top of the gel, whereas HliB was more enriched around CP47m. Neither Hlip was present in high quantities in the dimeric PSII, suggesting a preferential binding to assembly and/or repair complexes. To study the effect of HliC on HliA/B localization, we created Δ*hliA*/Δ*hliC* and Δ*hliB*/Δ*hliC* strains and repeated the experiment (Supplemental Fig. 2d, e). The signal of immunodetected Hlips was very faint, indicating an important role of HliC for the stability of HliA/B (see later). The Hlips also dispersed to multiple (unidentified) protein complexes that seemed to be distinct from their native localization, suggesting that HliC is important not only for HliA/B accumulation, but also for their proper targeting in the cell.

To obtain more detailed insight on the HliA/B interactomes and their dependency on HliC, we isolated thylakoid membranes and performed pull-downs from high-light-treated WT, *his-hliA*/Δ*hliA*, *his-hliB*/Δ*hliB*, *his-hliA*/Δ*hliA*/Δ*hliC*, and *his-hliB*/Δ*hliB*/Δ*hliC* strains. In order to preserve a maximal amount of native interactions, we performed the pull-downs in similar mild conditions as was used for the 2D-analysis of thylakoids (solubilization with DDM/GDN in MES buffer). The membranes were first analyzed by 1D SDS-PAGE followed by immunodetection to compare the levels of (His-)HliA/B proteins in the strains (Fig. 3a). Notably, the presence of His-HliA and native HliA in the membranes lowered dramatically after deletion of the *hliC* gene. Amounts of His-HliB and native HliB were also significantly reduced in Δ*hliC*, but to a lesser extent than (His-)HliA. We then analyzed the Ni-NTA pull-downs by CN-PAGE (Fig. 3b). Four green bands co-eluted specifically with His-HliA and His-HliB proteins and an additional, fast migrating green-yellow band was visible in the His-HliB eluate. In accordance with the dramatic reduction in His-HliA/B levels upon deletion of *hliC*, the eluates from Δ*hliC* background contained significantly less pigment–protein complexes; while some complexes were still present in the *his-hliB*/Δ*hliB*/Δ*hliC* pull-down, no visible bands were detected in the CN-separated *his-hliA*/Δ*hliA*/Δ*hliC* eluate (Fig. 3b).

The eluates obtained from *his-hliA*/Δ*hliA* and *his-hliB*/Δ*hliB* were further separated by 2D CN/SDS-PAGE (Fig. 4). The green bands co-eluting with the Hlips were identified as RCCII, RC47, and CP47m assembly intermediates; the small green-yellow band in *his-hliB*/Δ*hliB* was identified as free Hlip-dimers. In both eluates, the CP47m was present as two distinct bands: with and without Hlips. This implied that a fraction of Hlips was stripped out from the CP47m during CN-PAGE; indeed free (His-)HliAC- and (His-)HliBC-dimers were detectable on the Coomassie-stained 2D gels

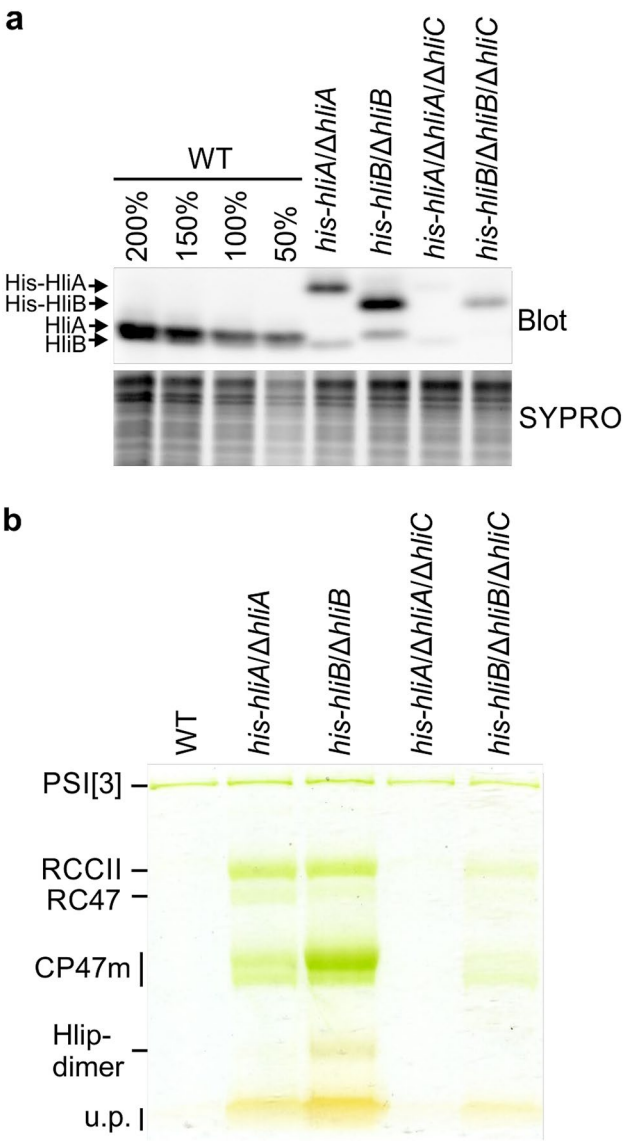

Fig. 3 Accumulation of Hlips in the thylakoid membranes (**a**) and CN-PAGE separation of Ni-NTA pull-downs (**b**) from WT, *his-hliA*/Δ*hliA*, *his-hliB*/Δ*hliB*, *his-hliA*/Δ*hliA*/Δ*hliC*, and *his-hliB*/Δ*hliB*/Δ*hliC* strains. **a** Membranes from high-light-treated cells were isolated in MES buffer, separated on SDS-PAGE and immunoblotted using an antibody against HliA/B. The different Hlip-forms are indicated with arrows. Total staining of the gel with SYPRO® Orange prior to blotting is shown as loading control. **b** Hlip complexes were purified in MES buffer using a combination of DDM and GDN detergents. The eluates were separated on CN-PAGE and the gel was scanned. Protein complexes were identified based on 2D-analysis of the gel strips (see Fig. 4). *PSI[3]* trimeric PSI, *u.p.* unbound pigments

(Fig. 4). Free (His-)HliBC was more abundant, and the pigments associated with the dimer were readily visible on the CN gel (Fig. 3b). In agreement with preferential binding of HliBC to CP47m (Supplemental Fig. 2), the CP47m to RCCII ratio in the His-HliB preparation was much higher than in the His-HliA pull-down (Fig. 4). Even though the

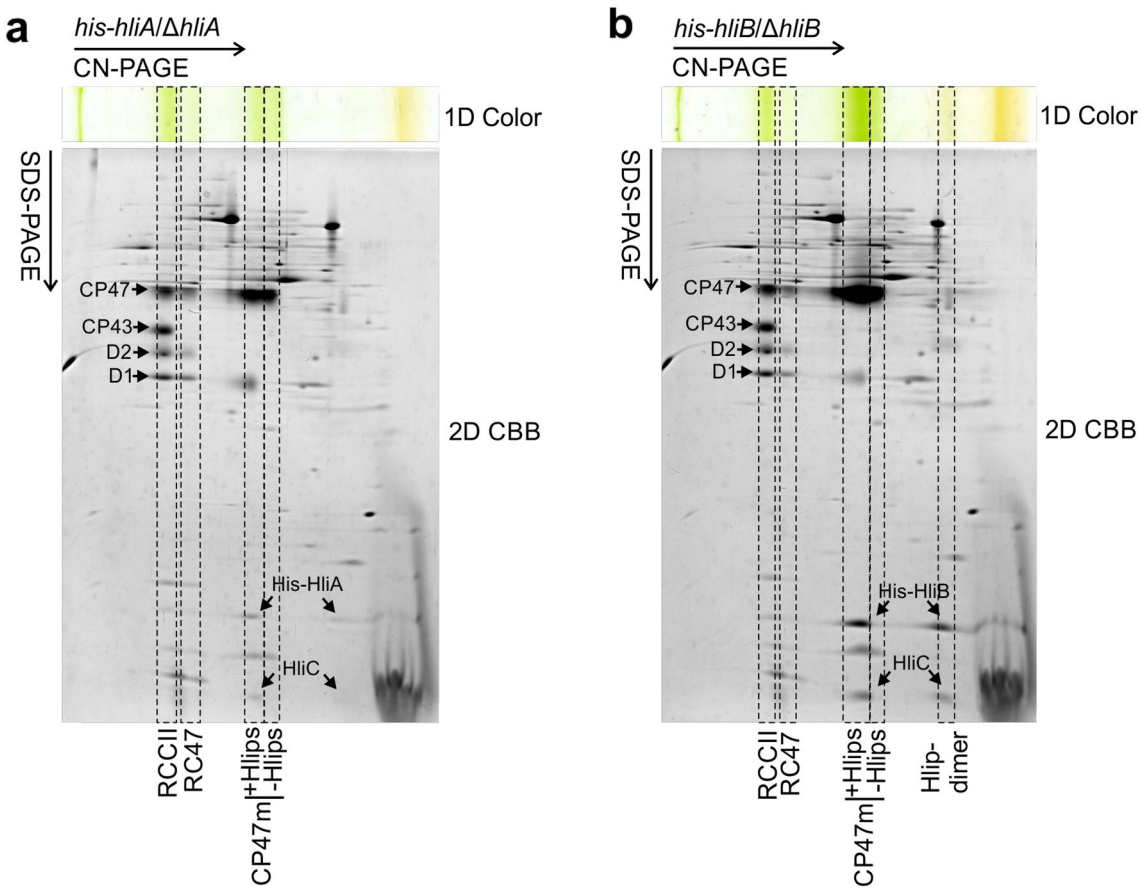

Fig. 4 Two-dimensional CN/SDS-PAGE separation of His-HliA and His-HliB pull-downs CN-PAGE strips from *his-hliA*/Δ*hliA* and *his-hliB*/Δ*hliB* pull-downs (see Fig. 3b) were separated in the second dimension with SDS-PAGE and the gels were stained with Coomassie blue (CBB). Protein complexes co-eluted with Hlips are marked by dashed line boxes. Chl-binding PSII subunits and Hlips are indicated with arrows

RC47 assembly intermediate was below/close to the detection limit in the 2D-blots from thylakoid membranes (Supplemental Fig. 2), it was clearly visible in the His-HliA/B pull-downs (Fig. 4) demonstrating the presence of Hlips in this complex as well.

To get a holistic view of all the HliA/B interactors, we repeated the pull-downs three times and analyzed the eluates with mass spectrometry (Fig. 5, Supplemental Data 2). PSII core subunits were clearly enriched in the pull-downs from *his-hliA*/Δ*hliA* and *his-hliB*/Δ*hliB* (Fig. 5a and b), while PSI was not significantly enriched, consistent with the CN-PAGE analysis where PSI[3] was a contamination present also in the WT control elution (Fig. 3b). In addition to the PSII subunits (D1, D2, CP43, CP47, cytochrome b_{559} α and β, and PsbH), the assembly factors Psb27, Psb28-1, Psb28-2, Psb35, Ycf48, and CyanoP were significantly enriched. Moreover, no oxygen-evolving complex proteins were detected, confirming that the eluates consisted only of PSII assembly intermediates or PSII repair complexes and not of fully assembled PSII. As was already observed in the phosphate buffer preparations (Fig. 1), native HliB was not present in the *his-hliA*/Δ*hliA* pull-down and vice versa. HliD was not detected in either eluate, whereas HliC was enriched in both, confirming that HliA and HliB dimerize preferentially with HliC in vivo. A set of previously unknown interactors were also detected. Most notably, the export proteins SecD and SecF, and the uncharacterized proteins Slr2105 and Sll1071 were enriched in both eluates. The *his-hliB*/Δ*hliB* eluates contained an additional set of eighteen high confidence interactors, most of which are uncharacterized proteins (Supplemental Data 2).

MS analysis of *his-hliA*/Δ*hliA*/Δ*hliC* and *his-hliB*/Δ*hliB*/Δ*hliC* pull-downs (Fig. 5c, d; Supplemental Data 2) was in line with the reduction of Hlips (Fig. 3a) and their aberrant localization in the thylakoid membranes (Supplemental Fig. 2d, e) upon deletion of *hliC*. Due to low accumulation of the bait proteins, we obtained significantly less interacting proteins compared to the preparations containing HliC. Intriguingly, both Hlips co-purified with a significant amount of HliD and HliD-specific partners,

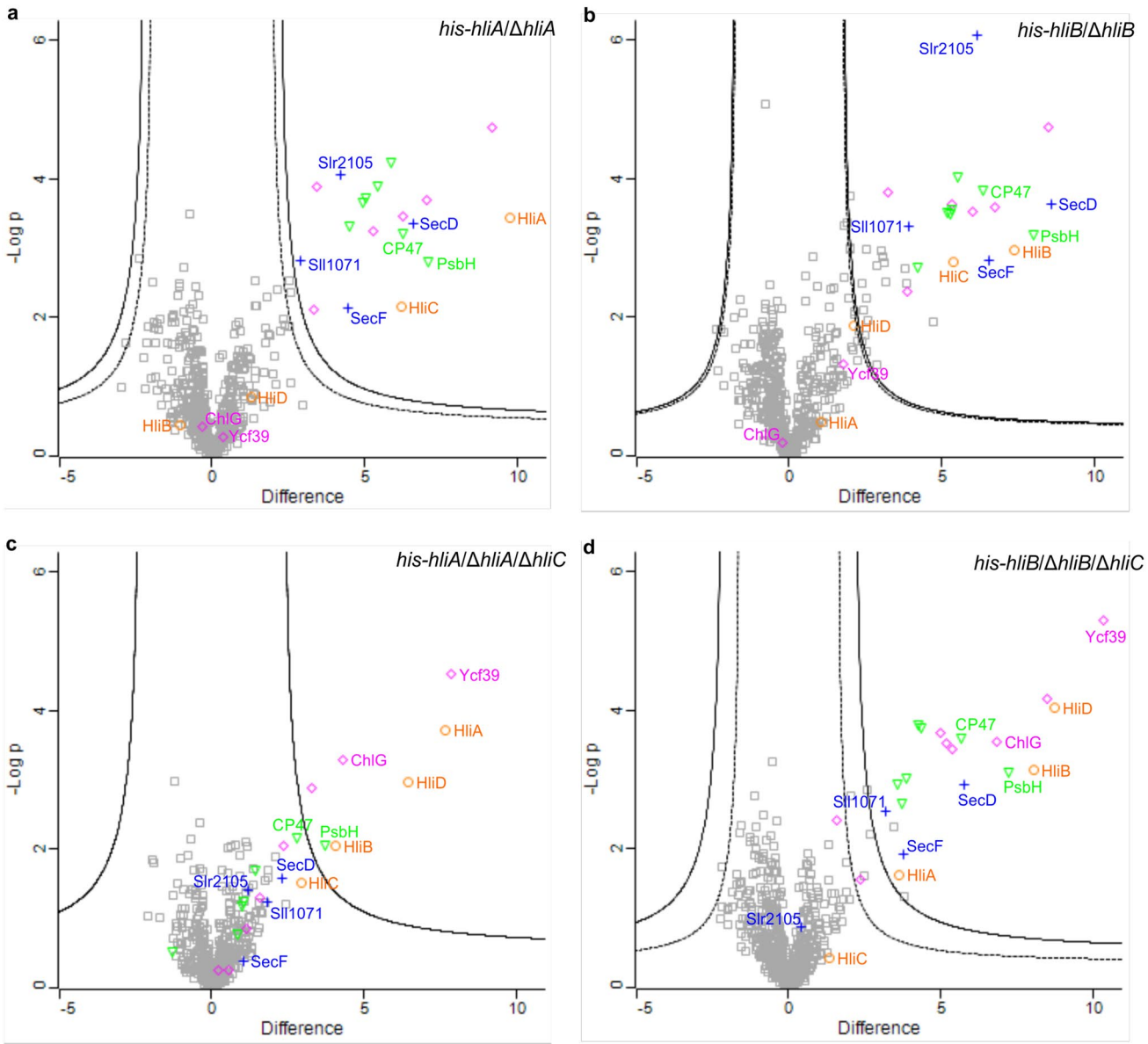

Fig. 5 Volcano plots of *his-hliA*/Δ*hliA* (**a**), *his-hliB*/Δ*hliB* (**b**), *his-hliA*/Δ*hliA*/Δ*hliC* (**c**), and *his-hliB*/Δ*hliB*/Δ*hliC* (**d**) pull-downs analyzed by MS Pull-downs from WT thylakoids were used as a negative control. The differences between the sample and control (log_2-transformed intensities) are plotted on the *x*-axis and the negative logarithms of p-values on the *y*-axis. All pull-downs were performed three times. Cut-offs for high confidence (FDR = 0.1%) and low-confidence (FDR = 1%) interactors are marked by solid and dashed lines, respectively (lines in panels b and c are overlapping). Individual proteins are indicated with gray squares. All proteins that were enriched in both *his-hliA*/Δ*hliA* and *his-hliB*/Δ*hliB*, all Hlips and the HliD-interactors Ycf39 and ChlG have been indicated with different colors and symbols in each plot: Hlips are indicated with orange circles, PSII subunits with green triangles, known PSII assembly factors with magenta diamonds, and novel HliA/B interactors with blue crosses. Hlips and their direct interactors (ChlG, CP47, PsbH, and Ycf39) as well as the novel co-eluted proteins (SecD, SecF, Sll1071, and Slr2105) are additionally marked with corresponding font colors

Ycf39 and ChlG. Deletion of HliC resulted in the presence of small amounts of native HliB in the His-HliA elution and, analogously, HliA was co-purified with His-HliB. Overall, the MS results confirmed our observations from the CN-PAGE analysis (Fig. 3b): the His-HliA eluate did not contain significant amounts of PSII core subunits nor the novel interactors (Fig. 5c), whereas some PSII assembly complexes were still enriched with His-HliB, even in the absence of HliC (Fig. 5d). Moreover, some interaction with SecD and SecF as well as Sll1071 was retained in *his-hliB*/Δ*hliB*/Δ*hliC*.

Lysine 35 destabilizes HliA in the absence of HliC

HliC and HliD proteins form a heterodimer, but homodimers of these Hlips can also accumulate in large quantities, particularly if one of the two is eliminated (Staleva et al. 2015; Shukla et al. 2018). The amino-acid sequences of HliA and HliB are very similar (87% amino-acid identity). However, in contrast to HliB, which is still rather stable in the absence of HliC, the accumulation of HliA depends strictly upon HliC (Fig. 3a). The most plausible explanation for this result is a fast degradation of monomeric, pigment-less HliA produced in the absence of HliC. As we discuss later, HliB is most likely able to form homodimers, whereas HliA seems to occur in the cell almost exclusively in heterodimers with HliC.

To clarify the mechanism of selective Hlip pairing, we created point-mutated His-HliA constructs at residues E22 and K35. These two sites are the most divergent between HliA and HliB and therefore might be important for determining the difference between these proteins (Fig. 6). The mutants His-HliA(E22P) and His-HliA(K35E) were created to mimic HliB and the mutant His-HliA(K35A) to mimic HliC (Fig. 6). All mutated His-HliA variants were expressed in the Δ*hliA*/Δ*hliC* background and membranes from high-light-treated cells were analyzed with 1D-SDS-PAGE (Fig. 7a). An immunoblot of the gel showed that the level of His-HliA(E22P) remained low in the membranes, while

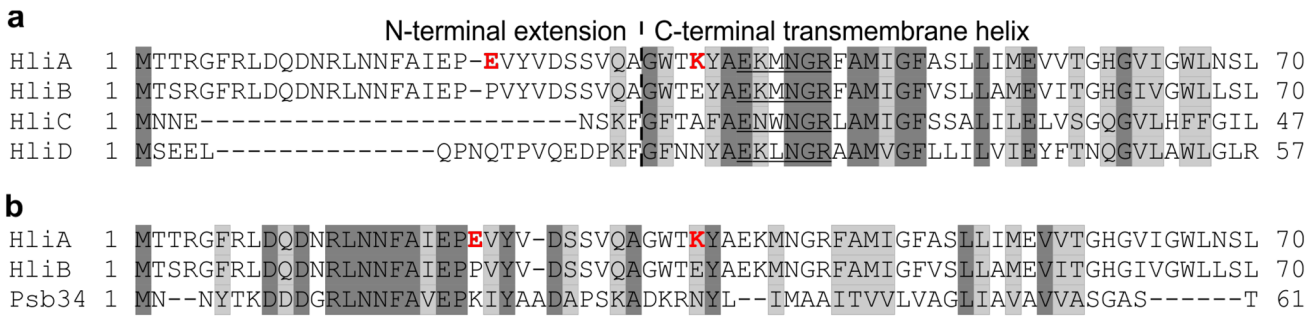

Fig. 6 Sequence comparisons of *Synechocystis* Hlips and Psb34. **a** Alignment of *Synechocystis* Hlips. The conserved LHC-motif is underlined. **b** Alignment of *Synechocystis* HliA, HliB, and Psb34 proteins. Identical amino-acid residues are highlighted with dark gray and highly similar residues with light gray. Amino-acid residues mutated in this work in His-HliA are indicated in bold and red

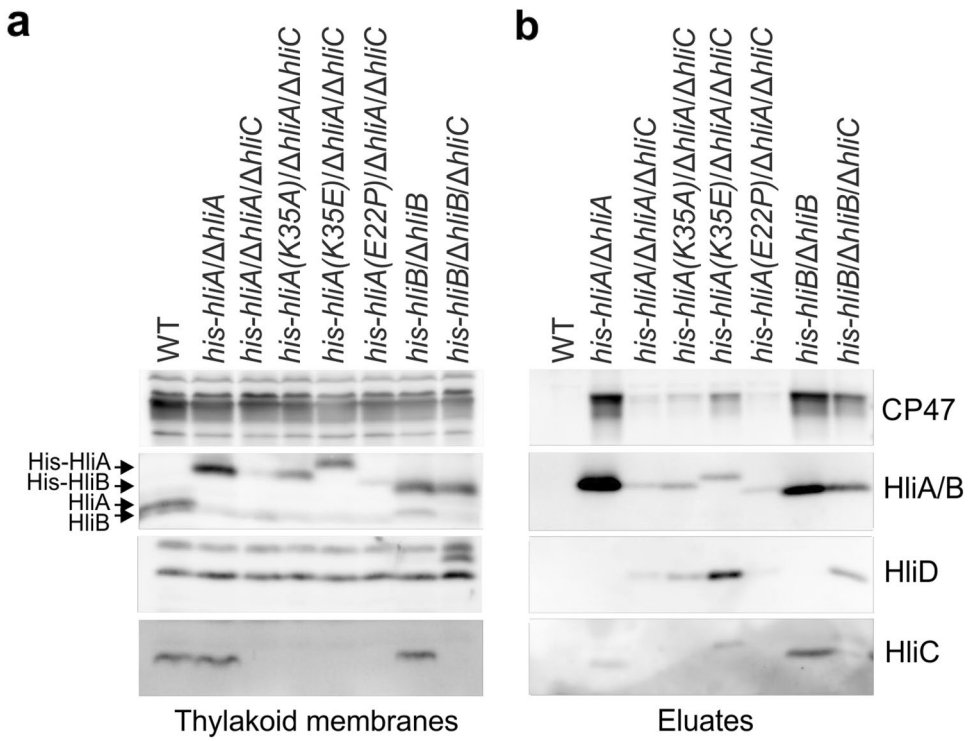

Fig. 7 Stability of His-tagged Hlips including their mutant variants and the level of co-eluted proteins Cells expressing His-HliA, His-HliB, or His-HliA variants were treated with 500 µmol m^{-2} s^{-1} light for 3 h prior to thylakoid isolation and affinity purification. **a** Thylakoid membranes were loaded based on Chl content (2–5 µg, depending on the antibody; 200% of WT thylakoids was loaded on the HliA/B blot to increase the visibility of the native proteins). **b** Pull-downs of His-tagged Hlips were performed with equal amounts of starting material and equal volumes of the final eluates were loaded on the gel. Proteins were separated on SDS-PAGE and blotted. Blots were probed with specific antibodies against the indicated proteins; HliA and HliB can be detected with the same antibody raised against HliA

both K35 variants were able to accumulate to a higher extent – up to a comparable amount with His-HliB expressed in the Δ*hliC* background. We also investigated the effect of the point mutations on protein–protein interactions by performing pull-downs in MES buffer (Fig. 7b). With the increased accumulation of His-HliA(K35A) and His-HliA(K35E) in the thylakoid membranes, the proteins also co-purified with more CP47. Interestingly, the amount of HliD was also increased in both eluates.

Discussion

The universal and specific features of pigment binding to Hlips

In this study, we isolated and characterized highly pure (His-)HliAC- and (His-)HliBC-dimers by a combination of nickel-affinity chromatography and CN-PAGE separation (Fig. 1). The dimers were pigmented with a Chl:Car ratio of 1:0.6, very close to the 1:0.57 reported previously for homo-oligomeric HliC isolated from the genetic background accumulating HliC as the only Hlip (Shukla et al. 2018). The pigment configuration of dimeric HliC, purified by a combination of nickel-affinity chromatography and anion-exchange chromatography in DDM, was accordingly suggested to correspond to 4 Chls and 2 Cars (Shukla et al. 2018). Here, we utilized A8-35 amphipol for separation of Hlip-dimers during CN-PAGE and analyzed the pigments from gel-extracted proteins. This method prevented the commonly observed (unspecific) oligomerization of Hlips during the gel run (see, e.g., Shukla et al. 2018, Fig. 1) and yielded extremely pure and probably very well-preserved native conformations of Hlips. The observed Chl:Car ratio of 1:0.6 suggests the alternative possibility that dimeric HliC as well as HliAC and HliBC bind 5 Chls and 3 Cars, with the third Car binding site being weaker. In contrast to other Hlip-dimers, HliCD contains 5–6 Chls per 2 Cars (ratio 1:0.36; Niedzwiedzki et al. 2016) but, as demonstrated recently, another (weak) xanthophyll-binding site in HliCD facilitates its interaction with Chl synthase (Proctor et al. 2020). Indeed, a small fraction of echinenone and β-cryptoxanthin (~15% of total Cars), found in both HliAC and HliBC, might partially replace β-Car in a less specific, more polar and peripheral binding site.

Similar to HliC (Hontani et al. 2018; Shukla et al. 2018) and HliD (Staleva et al. 2015), the HliAC- and HliBC-dimers were clearly in a quenching conformation, as shown by the absence of Chl fluorescence from the purified dimers (Fig. 1). This result further corroborates that constitutive quenching is a universal feature of Hlips. The absorption spectra of HliAC and HliBC exhibit a typical red-shift (> 520 nm) in Car absorbance, which appears to be characteristic for all LHC-like proteins able of thermal dissipation via Car S_1 state (Llansola-Portoles et al. 2017; Hontani et al. 2018; Skotnicová et al. 2021). As shown by Knoppová et al. (2014), the HliCD pair is able to dissipate excitation energy from the RCII complex. It is tempting to speculate that Hlips can also dissipate energy from the CP47 antenna. However, one has to keep in mind that the RCII complex contains only six Chl molecules, whereas the CP47m binds 16 Chls. Effectively quenching such a complicated pigment system would require a fast energy-transfer channel from Chls in CP47 to a Car in the associated Hlips. Whether CP47m can be photoprotected by Hlips, or HliAC and HliBC serve some different function (e.g., Chl delivery) needs to be addressed in future work.

The *Synechocystis* Hlip-interactome

HliA and HliB were previously found to co-elute after separation of thylakoid proteins by gel-filtration (He et al. 2001), which led to the proposition that these proteins form a complex. Based on 2D gel analysis of purified Hlips (Figs. 1 and 4) and MS analysis of His-HliA and His-HliB pull-downs (Fig. 5), we demonstrated that HliA and HliB form heterodimers specifically with HliC. HliC seems to be crucial for the accumulation of HliA/B (Fig. 3a) and for the correct localization of these proteins in thylakoids (Supplemental Fig. 2). These results imply a very limited stability of monomeric Hlips and we speculate that the only 'surviving' Hlips in Δ*hliC* mutant cells are those forming either homodimers or heterodimers with other Hlips. Indeed, only in the absence of HliC does HliA/B interact mutually or with HliD (Fig. 5c, d). It should be noted that in contrast to the aberrant interaction with HliD, which could be detected by immunoblotting (Fig. 7b), the formation of HliAB heterodimers was detectable only by the very sensitive MS approach (Fig. 5c, d) and thus must be extremely rare even in the Δ*hliC* mutant. Together, these results also explain the localization of HliA/B in Δ*hliC* thylakoids (Supplemental Fig. 2d, e): the unspecific pairing between HliA/B and HliD might lead to some HliA/B binding to HliD-associated complexes and vice versa.

The mechanism behind the strict selectivity of Hlip pairing is enigmatic. To clarify the dimerization 'rules', we mutated Lys35 of HliA into Glu (opposite charge) or Ala (small, neutral residue). Importantly, we found that the affinity of the K35E mutant protein to HliD and CP47 was significantly increased, while the K35A mutation also slightly increased the interactions (Fig. 7b). It seems plausible that K35 mutation strengthens the interaction with HliD. Additionally, it might facilitate the formation of homodimers, thereby increasing the stability of His-HliA in the Δ*hliC* background. As HliB contains a Glu residue in the '-3' position before the Chl-binding motif, these results are consistent

with the higher stability of this Hlip in the absence of HliC. It is also noteworthy that the N-terminal extensions of HliA and HliB are relatively long in comparison to HliC and HliD (Fig. 6a). Indeed, both HliC and HliD are able to accumulate as homodimers (Staleva et al. 2015; Shukla et al. 2018). Thus, it is possible that the long N-terminal extensions of HliA and HliB could further hinder their mutual dimerization. Based on these observations, we speculate that the very short stromal-exposed N-terminus and a non-polar residue in position '-3' are some of the key determinants for the ability of HliC to bind any other Hlip.

HliB was previously shown to bind near CP47 and PsbH (Promnares et al. 2006). Recently solved *Thermosynechococcus* RCCII structures revealed the presence of a novel Psb34 assembly factor next to PsbH and CP47 (Zabret et al. 2021; Xiao et al. 2021). Interestingly, the N-terminal sequence of this assembly factor shares significant similarity with HliA and HliB N-termini (Fig. 6b). The N-terminus of Psb34 forms a loop along the surface of CP47 with several hydrogen bonds with PsbH, PsbL, and CP47 stabilizing the interaction (Supplemental Fig. 3). As we did not observe Psb34 in our MS data (Supplemental Table 1), it is likely that both HliA and HliB compete with Psb34 for the same binding site of CP47. Furthermore, Hlips were not detected in FLAG-Psb34 affinity pull-downs even from high-light-treated cells (Rahimzadeh Karvansara et al. *accepted*). Thus, the N-terminal sequence of HliA/B most likely mediates the interaction between Hlip-dimers and CP47 in a manner similar to the Psb34 N-terminus. Because HliD interacts with Ycf39 even in the absence of HliC (Staleva et al. 2015), this interaction is also most probably mediated via the N-terminal sequence of HliD. Based on these data, we propose a model for Hlip-dimerization where HliC functions as a truncated 'generalist' helix that prevents aggregation of PSII assembly complexes, while the role of the other 'specialist' Hlip partner is to target Hlips to the desired complexes.

HliA and HliB in PSII biogenesis

All Chl-binding PSII core subunits as well as several known PSII assembly factors co-purified with His-HliA and His-HliB (Fig. 5, Supplemental Data 2), whereas no oxygen-evolving complex proteins were detected. The pattern of the eluted complexes on CN- and 2D-PAGE (Figs. 3b and 4) in combination with the MS data gave strong evidence that HliA and HliB associate with PSII assembly intermediates and not with the active complex. Based on the Hlip-interactome data presented in this publication (Figs. 4 and 5) and previous data describing the roles of HliCD-dimers during early steps of PSII biogenesis (Chidgey et al. 2014; Knoppová et al. 2014), we prepared a model depicting the participation of Hlips in PSII assembly/repair under stress conditions (Fig. 8). Hlips are involved in PSII biogenesis from the earliest steps: HliC and HliD form a complex with Chl synthase and Ycf39, which also associates with the YidC insertase (Chidgey et al. 2014). Together, this complex might assist Chl delivery to the newly formed D1 reaction center protein (Chidgey et al. 2014). The HliCD-Ycf39

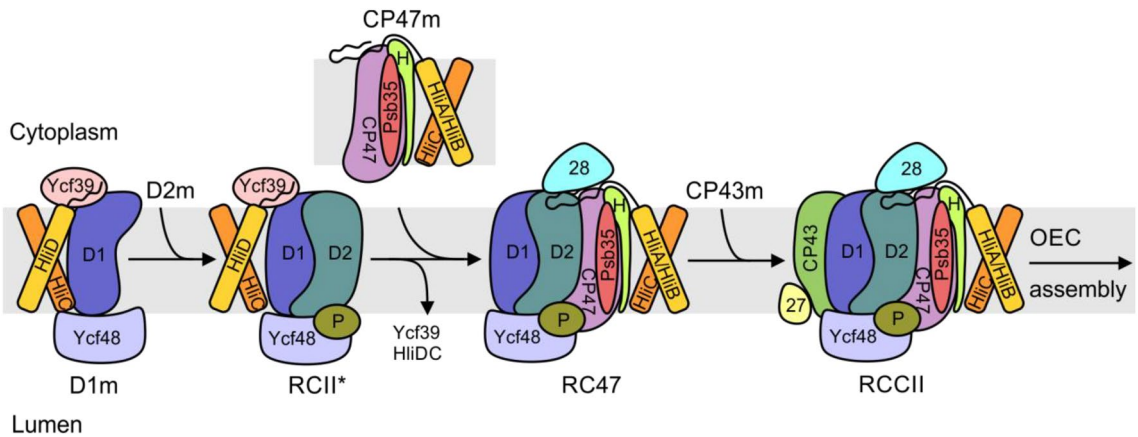

Fig. 8 Scheme of PSII assembly intermediates involving Hlips The PSII complex is assembled from four building blocks called modules (D1m, D2m, CP43m, CP47m), each of which is preloaded with Chl and Car cofactors before association to larger PSII assembly intermediates (Komenda et al. 2012b). During stress conditions, Hlips attach to distinct assembly/repair intermediates, potentially protecting the whole pathway. HliAC- and HliBC-dimers likely occupy the same binding site as the Psb34 assembly factor (Zabret et al. 2021; Xiao et al. 2021). Although both heterodimers bind to complexes containing CP47, HliBC appears to have a higher affinity to 'free' CP47m while HliAC might be more specific for later assembly steps. Small PSII subunits PsbE (Cyt b559 α), F (Cyt b559 *β*), I, K, L, M, T, X, Z and Ycf12 have been omitted for clarity. Known assembly factors Ycf48 (Komenda et al. 2008), CyanoP (Knoppová et al. 2016), Psb28 (Dobáková et al. 2009), Psb27 (Komenda et al. 2012a) and Psb35 (Pascual-Aznar et al. 2021) that were also identified in our His-HliA/B pull-downs are indicated. *D1m* D1 module, *CP47m* CP47 module, *CP43m* CP43 module, *P* CyanoP, *H* PsbH, *28* Psb28, *27* Psb27

complex remains attached to the D1 module and the RCII* complex, which they protect against photo-oxidative damage (Knoppová et al. 2014; Staleva et al. 2015). Upon CP47m binding, the HliCD-dimer and Ycf39 likely detach, as they are not seen in the RC47 complex (Boehm et al. 2012; this study Fig. 5a, b). HliAC- and HliBC-dimers pre-assemble to the CP47m under stress conditions, remain bound until formation of the monomeric PSII reaction center complex (RCCII), and detach before/during oxygen-evolving complex (OEC) assembly. We suggest that the protection of CP47m and later assembly steps against photo-oxidation is the main role of HliA/B proteins. As shown by Rahimzadeh Karvansara et al. (*accepted*), these Hlips have different dynamics after light stress, with HliB accumulating more transiently (maximal expression after 2 h of high light stress) and HliA showing more stable accumulation even after prolonged (24 h) high light stress. The different affinity of HliA and HliB to 'free' CP47m reported here supports the fine-tuning and specialized roles of these Hlips during stress conditions.

MS analysis of His-HliA and His-HliB pull-downs (Fig. 5a and b) revealed as yet unknown interactors for both Hlip isoforms. The discovery of SecD and SecF translocon proteins was especially interesting. In heterotrophic bacteria, the SecDF-dimer utilizes the transmembrane proton gradient to promote protein export across the plasma membrane (Gardel et al. 1990; Pogliano and Beckwith 1994; Arkowitz and Wickner 1994). Together with YidC, SecDF is also a part of the holo-translocon complex, which is required for efficient membrane insertion of polytopic membrane proteins (Komar et al. 2016; Botte et al. 2016). Our results suggest that the SecDF-dimer is also a component of the thylakoid holo-translocon and might participate in PSII biogenesis. The other identified Hlip-interactors, Sll1071 and Slr2105, are proteins of unknown function and thus candidates for novel (possibly high-light-specific) PSII assembly factors.

Materials and methods

Synechocystis strains

All mutant strains described in this work are constructed using the *Synechocystis* WT-P substrain (Tichý et al. 2016). To prepare a Δ*hliA* strain, we fully segregated the deletion construct described in (Xu et al. 2002) in WT-P; the Δ*hliB* and *his-hliB*/Δ*hliB* mutants were described in Promnares et al. (2006). To construct *his-hliA*/Δ*hliA*, we transformed the Δ*hliA* strain with the plasmid (pPD-his8-hliA) and segregated transformants on plates with increasing kanamycin concentration (starting with 10 µg ml^{-1} and doubling the amount until full segregation was achieved). To create the pPD-his8-hliA plasmid, the *hliA* gene was amplified from the *Synechocystis* chromosomal DNA using primers his8-hliA-fw and hliA-rev. The resulting insert was cloned into the pPD-FLAG plasmid (Hollingshead et al. 2012) using *NdeI* and *BglII* restriction sites. The *hliC* gene was deleted by chloramphenicol resistance cassette from the plasmid pACYC184. The deletion construct was created by overlap extension PCR (Lee et al. 2004) using the scpB1, scpB4, ScpBCm5, and scpBCm6 primers. The deletion construct was transformed into *Synechocystis* and segregated with increasing chloramphenicol concentration. Genomic DNA from this strain was used to transform the *his-hliA*/Δ*hliA* and *his-hliB*/ΔhliB strains to obtain *his-hliA*/Δ*hliA*/Δ*hliC* and *his-hliB*/Δ*hliB*/Δ*hliC*, respectively. The Δ*hliA*/Δ*hliC* strain was created by transforming genomic DNA isolated from Δ*hliA* into the Δ*hliC* strain and segregating transformants on plates with increasing erythromycin concentration (starting with 3 µg ml^{-1} and doubling the amount until full segregation was achieved). The Δ*hliB*/Δ*hliC* strain was created by transforming genomic DNA isolated from Δ*hliC* into the Δ*hliB* strain and segregating transformants on plates with increasing chloramphenicol concentration (starting with 10 µg ml^{-1} and doubling the amount until full segregation was achieved). His-HliA point mutants were constructed by mutating the pPD-his8-hliA plasmid using the QuikChange II XL kit (Agilent) with primers his-hliA(E22P), his-hliA(K35A), and his-hliA(K35E). The mutated plasmids were sequenced and transformed to the Δ*hliA*/Δ*hliC* background. All primer sequences are listed in Supplemental Table 1.

Growth conditions

Synechocystis cells were inoculated by suspending one loop of cells to 50 ml of BG11 medium in 250 ml Erlenmeyer flasks. Cells were grown under 40 µmol m^{-2} s^{-1} in a shaker at + 28 °C. The starting cultures were grown until $OD_{750} > 1.0$ (WPA S1200 Spectrawave, Biochrom) and used to inoculate experimental cultures at OD_{750} 0.1–0.2. For the expression analysis of the His-constructs, the cells were grown under the same conditions as above until logarithmic growth phase and then transferred to high light (500 µmol m^{-2} s^{-1}) for 1, 3, and 5 h; the control flask (0 h) was kept in 40 µmol m^{-2} s^{-1}. Cells were harvested at OD_{750} 0.8–1.0 by centrifuging at 10,000 rpm and + 4 °C for 10 min (Sigma 3K30, rotor 12,155) and resuspended to MES buffer [25 mM MES-NaOH (2-(*N*-morpholino) ethanesulfonic acid) pH 6.5, 10 mM $CaCl_2$, 10 mM $MgCl_2$, 25% glycerol] for storage. For localization of Hlips in thylakoid membranes, the cells were grown as above and treated with 3 h of high light before harvesting. For pull-down assays, cells were grown in 1 l cylinders with 600 ml of BG11, air bubbling and mixing by magnetic stirrer with 40 µmol m^{-2} s^{-1} illumination from the side at + 28 °C.

Cells were grown until OD_{750} 1.0–1.5 and treated with 500 µmol m^{-2} s^{-1} light for 3 h before harvesting. Cells were harvested by centrifuging at 6600 rpm and + 4 °C for 20 min (Sigma 8KS, rotor 12505-H) and resuspended either to phosphate buffer (25 mM Na-phosphate pH 7.8, 50 mM NaCl, 10% glycerol) or to MES buffer and pelleted again by centrifuging at 10,000 rpm and + 4 °C for 10 min (Sigma 3K30, rotor 12155). Cells were resuspended to the respective buffer for storage. Cells were frozen in $N_{2(l)}$ and stored in − 80 °C.

Thylakoid membrane extraction

Thylakoid membranes for expression analysis were extracted by breaking the cells in MES buffer. Pelleted cells were resuspended in 400 µl of MES buffer and mixed with 200 µl of glass beads (100–200 µm) and cOmplete™ protease inhibitor cocktail (Roche) in 2-ml lysis tubes. This suspension was vortexed 4 × 20 s and samples were cooled on ice for 3 min between each cycle. After breaking, the membranes were extracted by washing the glass beads with 200 µl MES buffer 4–5 times. The obtained suspension was pelleted by centrifuging at 36,000 g and + 4 °C for 20 min and resuspended to 100 µl of MES buffer. Thylakoids for localization studies were broken with Precellys® Evolution (Bertin Technologies) in 2-ml lysis tubes in MES buffer. Cells were pelleted in the lysis tubes and supplemented with 200 µl of buffer, 200 µl of glass beads (100–200 µm) and 10 µl of 50 × cOmplete™ protease inhibitor cocktail (Roche) (one tablet dissolved to 1 ml of H_2O). Lysis program was set to 3 × 20 s at 5 500 rpm with 120 s pause between the cycles; cooling was set to 0 °C. The glass beads were washed repeatedly with 200 µl of buffer and thylakoids collected in 2-ml eppendorf tubes. Thylakoids were pelleted by centrifuging at 18,000 rpm and + 4 °C for 30 min (Sigma 3K30, rotor 12131) and resuspended to ~ 100 µl of buffer for storage. For pull-down assays, the cells were broken in 7-ml lysis tubes either in phosphate or MES buffer. Cells were pelleted in the lysis tubes and supplemented with 1 ml of buffer, 2 ml of glass beads (100–200 µm) and 100 µl of 50× protease inhibitor. The same lysis program was used as above, but the program was run twice with 5 min incubation of samples on ice between the cycles. The glass beads were washed repeatedly with 1–2 ml of buffer and thylakoids collected in 30-ml centrifugation tubes. Thylakoids were pelleted by centrifuging at 20,000 rpm and + 4 °C for 30 min (Sigma 3K30, rotor 12158) and suspended in a few ml of buffer for storage. Membranes were frozen in $N_{2(l)}$ and stored in − 80 °C until use. After cell lysis, the samples were kept constantly cooled and protected from light. Thylakoid Chl concentration was determined in methanol according to Lichtenthaler and Wellburn 1983.

Pull-down assays

Thylakoid membranes were solubilized using 1% DDM (AppliChem). Thylakoid concentration was set to 0.5 µg $µl^{-1}$ Chl with phosphate or MES buffer and the membranes were incubated with the detergent and SIGMAFAST™ EDTA-free protease inhibitor (Sigma-Aldrich) for 10 min in + 10 °C with gentle rotation. Insoluble membrane debris was removed by centrifuging at 20,000 rpm and + 4 °C for 30 min (Sigma 3K30, rotor 12131). For MES buffer pull-downs, 1% glycodiosgenin (GDN, Anatrace) was added to the solubilized membranes to stabilize protein complexes (Chae et al. 2012). Solubilized membranes were mixed with ~ 100 µl of pre-equilibrated Protino® Ni-NTA agarose (Macherey–Nagel) per 1 mg of Chl in the starting material (typically 1.5 mg Chl was used). 500 mM NaCl and 10 mM imidazole were added to reduce unspecific binding. Proteins were bound to the Ni-NTA agarose by incubating for 1 h at + 10 °C with gentle rotation. All buffers used during the purification were supplemented with 0.04% DDM and MES buffer pull-downs with additional 0.04% GDN. Purification was performed in 10 ml Poly-Prep® chromatography columns (Bio-Rad). The nickel resin was washed with 20 column volumes (CV) of equilibration buffer (10 mM imidazole, 500 mM NaCl in phosphate or MES buffer) and 20 CV of washing buffer (20 mM imidazole in phosphate or MES buffer). Elution was performed with 5 or 10 CV of elution buffer (200 mM imidazole in phosphate or MES buffer, respectively). The final eluates were concentrated using 50 kDa cut-off centrifugal columns (Vivaspin® 6, Sartorius or Amicon® Ultra, Merck). All genotypes were purified in parallel for the MS analysis, and the experiment was replicated three times in total. First and second replicates were purified with new Ni-NTA resin and the second replicate with one-time-used and washed resin.

Electrophoretic methods

Clear native gel electrophoresis was performed as in (Komenda et al. 2019) with minor modifications. CN samples were prepared by solubilizing thylakoid membranes in 1% DDM + 1% GDN at 0.5 µg $µl^{-1}$ Chl concentration for 10 min on ice. We also omitted deoxycholate from the cathode running buffer and added 1% amphipol A8-35 (Tribet et al. 1996; Kameo et al. 2021) to the CN-PAGE samples before loading. CN-run was performed at constant current of 11 mA. 2D- and 1D-SDS-PAGE were performed on 16–20% acryl amide, 0–10% sucrose gradient gels prepared in 0.65 M Tris–HCl (pH8.6) (acryl amide:bis acryl amide 60:1). Proteins were transferred to PVDF membranes (Immobilon-P, Merck) in carbonate buffer (3 mM Na_2CO_3, 10 mM $NaHCO_3$) using Trans-Blot® Cell (Bio-Rad). Blotting was performed at 850 mA

for 3 h with water cooling at + 4 °C and mixing with magnetic stirrer. Antibodies against HliA/B (AS10 1603), HliD (AS10 1615), and CP47 (AS04 038) were purchased from Agrisera and used as 1:4000 dilutions. Antibody against HliC (Moravian Biotechnology) was generated against a synthetic N-terminal peptide (amino acids 1–17) in rabbit and used as 1:500 dilution. All antibodies were diluted in TTBS (10 mM Tris–HCl pH 7.6, 150 mM NaCl, 0.05% TWEEN® 20) and incubated on the membranes overnight at + 10 °C with gentle shaking. For detection, proteins were labeled with Peroxidase-conjugated goat anti-rabbit secondary antibody (A6154, Sigma-Aldrich, 1:10,000 dilution) for 1 h at room temperature and incubated for 1 min in Immobilon® Crescendo Western HRP Substrate (Merck). Chemiluminescence was detected with LAS-4000 (Fujifilm).

Pigment analysis

To identify pigments associated with purified His-Hlips, we cut a piece of CN gel (~ 3 × 2 mm) containing separated Hlips and cut it further into several smaller pieces. Gel pieces were incubated in 200 µl of MES with 0.04% DDM buffer overnight. After centrifugation, 150 µl of the supernatant was injected into the Agilent-1260 HPLC system equipped with a diode-array detector. Pigments were separated on a reverse-phase column (Zorbax Eclipse C18, 5 µm particle size, 3.9 × 150 mm; Agilent) with 35% (v/v) methanol and 15% (v/v) acetonitrile in 0.25 M pyridine (solvent A) and 20% (v/v) methanol, 20% (v/v) acetone, 60% (v/v) acetonitrile as solvent B. Pigments were eluted with a linear gradient of solvent B (30–95% (v/v) in 25 min) in solvent A followed by 95% of solvent B in solvent A at a flow rate of 0.8 ml min^{-1} at 40 °C. Chl *a* and Cars were detected at 440 nm; the obtained peaks were integrated and the molar stoichiometries calculated from calibration curves prepared using authentic standards.

Absorption spectra

Absorption spectra of purified Hlips were measured by cutting a piece from the CN gel containing the pigmented Hlip complexes and setting it on a plastic slip attached to a custom made adaptor to fit into a standard 1-ml cuvette slot in a spectrophotometer. Spectra were recorded from 750 to 350 nm in 0.5 nm intervals with a Shimadzu UV-3000 spectrophotometer (slit width 5 nm); an empty gel was used as blank. The spectra were normalized to the absorption maximum of the red region of Chl *a* (Q_Y band). Three independent pull-downs were analyzed per strain and the spectra averaged.

Mass spectrometry

Concentrated Ni-NTA eluates (5 µl) were diluted with 45 µl of 50 mM ammonium bicarbonate supplemented with 0.1% (v/v) Rapigest (Waters) surfactant and incubated at + 60 °C. After 45 min, proteomic grade trypsin (Sigma) was added to a final concentration of 10 ng $µl^{-1}$ and incubated at + 37 °C. After 12 h, samples were acidified and peptides were isolated by the StageTip procedure (Rappsilber et al. 2007) to produce 30 µl of sample. LC–MS/MS analysis was performed on an UltiMate 3000 UHPLC (Thermo Fisher Scientific) on-line coupled to a TimsTOF pro (Bruker) mass spectrometer. Samples (2 µl) were trapped for 1 min on a ThermoFisher trap (0.3 × 5 mm, C18, 5 µm) column, then separated by reverse phase liquid chromatography on a Acclaim PepMap RSLC column (75 µm × 15 cm, C18, 2 µm, 100 Å; Thermo Fisher Scientific). During 30 min, peptides were eluted by increasing ratio of acetonitrile (solvent B) in 0.1% formic acid (solvent A) from 3 to 50% directly into the CaptiveSpray nano ion source of the mass spectrometer. Spectra were acquired in PASEF (Parallel Accumulation/SErial Fragmentation) data dependent mode with an accuracy of 0.2 ppm for precursors and 0.5 ppm for peptides. Each sample was run twice (two technical repetitions). Raw data were processed by the MaxQuant/Andromeda software (Cox and Mann 2008; Cox et al. 2011; Tyanova et al. 2016a) and compared to a species specific *Synechocystis* protein database downloaded from Uniprot and Cyanobase.

Statistical analysis of protein groups obtained from MaxQuant was performed in Perseus 1.6.14.0 (Tyanova et al. 2016b). Proteins identified only by site or in the reverse dataset and potential contaminants were removed. Data were log_2-transformed and inspected by hierarchical clustering and one technical replicate was discarded due to low quality of the MS run (WT replicate 1.2). Other technical replicates were averaged with their respective pairs and data filtered to include only proteins that were detected in all three pull-downs at least in one genetic background. Missing data was imputed from normal distribution for statistical analysis. Data was inspected for significant background interactions (i.e., batch effect) by hierarchical clustering and checking the correlations between samples. A significant batch effect was detected between the different pull-down batches and subsequently removed using the Limma package (Ritchie et al. 2015) via the PerseusR-plugin (Rudolph and Cox 2019). Significant interactors were determined using the Hawaii plot function in Perseus, which uses a global permutation-based false-discovery rate (FDR) to detect significant hits (Rudolph and Cox 2019). High confidence (Class A) FDR rate was set to 0.1%, low-confidence (Class B) FDR rate was set to 1%, and s_0 was set to 2.

In silico analyses

Coding sequences of *Synechocystis* Hlips (*hliA*, *ssl2542*; *hliB*, *ssr2595*; *hliC*, *ssl1633* and *hliD*, *ssr1789*) and *psb34* (*ssl1498*) were obtained from the genomic sequence (GenBank assembly GCA_000009725.1) and translated. Sequences were aligned using the EMBL-EBI T-coffee multiple sequence alignment tool (Madeira et al. 2019).

Image manipulation

Histograms of gel images were adjusted with Photoshop CS2 (Adobe) to improve visual clarity. Volcano plots were exported from Perseus v. 1.6.15.0 (Tyanova et al. 2016b). Vector art was added and images were assembled in CorelDRAW X6.

Supplementary Information The online version contains supplementary material available at https://doi.org/10.1007/s11120-022-00904-z.

Acknowledgements European Research Council Synergy Award 854126 and the Czech Science Foundation, grant No. 19-29225X funded this work. RS also acknowledges institutional support RVO 61388971. PK acknowledges support from the Czech Ministry of Education, Youth and Sports project 'Mechanisms and dynamics of macromolecular complexes: from single molecules to cells', CZ.02.1 .01/0.0/0.0/15_003/0000441. Jan Pilný is thanked for HPLC analysis of pigments.

Author contributions MMK and RS designed the study; AW, MMK, and PK performed the experiments; MMK, PK, and RS analyzed the data; MMK and RS wrote the paper. All authors read and accepted the final manuscript.

Data Availabilty The raw MS data has been submitted to the MassIVE repository (CCMS, University of California, San Diego) and can be accessed via the link ftp://massive.ucsd.edu/MSV000088753/.

Declarations

Conflict of interest The authors declare no competing interests.

References

Arkowitz RA, Wickner W (1994) SecD and SecF are required for the proton electrochemical gradient stimulation of preprotein translocation. EMBO J 13:954–963. https://doi.org/10.1002/j.1460-2075.1994.tb06340.x

Bassi R, Croce R, Cugini D, Sandona D (1999) Mutational analysis of a higher plant antenna protein provides identification of chromophores bound into multiple sites. Proc Natl Acad Sci 96:10056–10061. https://doi.org/10.1073/pnas.96.18.10056

Becker K, Cormann KU, Nowaczyk MM (2011) Assembly of the water-oxidizing complex in photosystem II. J Photochem Photobiol B 104:204–211. https://doi.org/10.1016/j.jphotobiol.2011.02.005

Ben-Shem A, Frolow F, Nelson N (2003) Crystal structure of plant photosystem I. Nature 426:630–635. https://doi.org/10.1038/nature02200

Boehm M, Romero E, Reisinger V, Yu J, Komenda J, Eichacker LA, Dekker JP, Nixon PJ (2011) Investigating the early stages of photosystem II assembly in *Synechocystis* sp. PCC 6803. J Biol Chem 286:14812–14819. https://doi.org/10.1074/jbc.M110.207944

Boehm M, Yu J, Reisinger V, Bečková M, Eichacker LA, Schlodder E, Komenda J, Nixon PJ (2012) Subunit composition of CP43-less photosystem II complexes of *Synechocystis* sp. PCC 6803: implications for the assembly and repair of photosystem II. Philos Trans R Soc B 367:3444–3454. https://doi.org/10.1098/rstb.2012.0066

Botte M, Zaccai NR, Lycklama à J, Nijeholt JL, Martin R, Knoops K, Papai G, Zou J, Deniaud A, Karuppasamy M, Jiang Q, Roy AS, Schulten K, Schultz P, Rappsilber J, Zaccai G, Berger I, Collinson I, Schaffitzel C (2016) A central cavity within the holo-translocon suggests a mechanism for membrane protein insertion. Sci Rep 6:38399. https://doi.org/10.1038/srep38399

Chae PS, Rasmussen SGF, Rana RR, Gotfryd K, Kruse AC, Manglik A, Cho KH, Nurva S, Gether U, Guan L, Loland CJ, Byrne B, Kobilka BK, Gellman SH (2012) A new class of amphiphiles bearing rigid hydrophobic groups for solubilization and stabilization of membrane proteins. Chem Eur J 18:9485–9490. https://doi.org/10.1002/chem.201200069

Chidgey J, Linhartová M, Komenda J, Jackson PJ, Dickman MJ, Canniffe DP, Koník P, Pilný J, Hunter CN, Sobotka R (2014) A cyanobacterial chlorophyll synthase-HliD complex associates with the Ycf39 protein and the YidC/Alb3 insertase. Plant Cell 26:1267–1279. https://doi.org/10.1105/tpc.114.124495

Cox J, Mann M (2008) MaxQuant enables high peptide identification rates, individualized p.p.b.-range mass accuracies and proteome-wide protein quantification. Nat Biotechnol 26(12):1367–1372. https://doi.org/10.1038/NBT.1511

Cox J, Neuhauser N, Michalski A, Scheltema RA, Olsen JV, Mann M (2011) Andromeda: a peptide search engine integrated into the MaxQuant environment. J Proteome Res 10:1794–1805. https://doi.org/10.1021/pr101065j

Dobáková M, Sobotka R, Tichý M, Komenda J (2009) Psb28 protein is involved in the biogenesis of the photosystem II inner antenna CP47 (PsbB) in the cyanobacterium *Synechocystis* sp. PCC 6803. Plant Physiol 149:1076–1086. https://doi.org/10.1104/pp.108.130039

Dolganov NA, Bhayat D, Grossman AR (1995) Cyanobacterial protein with similarity to the chlorophyll *a*/*b* binding proteins of higher plants: Evolution and regulation. Proc Natl Acad Sci USA 92:636–640. https://doi.org/10.1073/pnas.92.2.636

Engelken J, Brinkmann H, Adamska I (2010) Taxonomic distribution and origins of the extended LHC (light-harvesting complex) antenna protein superfamily. BMC Evol Biol 10:233. https://doi.org/10.1186/1471-2148-10-233

Gardel C, Johnson K, Jacq A, Beckwith J (1990) The *secD* locus of *E. coli* codes for two membrane proteins required for protein export. EMBO J 9:3209–3216. https://doi.org/10.1002/j.1460-2075.1990.tb07519.x

Havaux M, Guedeney G, He Q, Grossman AR (2003) Elimination of high-light-inducible polypeptides related to eukaryotic chlorophyll *a*/*b*-binding proteins results in aberrant photoacclimation in *Synechocystis* PCC6803. Biochim Biophys Acta Bioenerget 1557:21–33. https://doi.org/10.1016/S0005-2728(02)00391-2

He Q, Dolganov N, Björkman O, Grossman AR (2001) The high light-inducible polypeptides in *Synechocystis* PCC6803. Expression and function in high light. J Biol Chem 276:306–314. https://doi.org/10.1074/jbc.M008686200

Hey D, Grimm B (2018) ONE-HELIX PROTEIN2 (OHP2) is required for the stability of OHP1 and assembly factor HCF244 and is functionally linked to PSII biogenesis. Plant Physiol 177:1453–1472. https://doi.org/10.1104/pp.18.00540

Hey D, Grimm B (2020) ONE-HELIX PROTEIN1 and 2 form heterodimers to bind chlorophyll in photosystem II biogenesis. Plant Physiol 183:179–193. https://doi.org/10.1104/pp.19.01304

Hollingshead S, Kopečná J, Jackson PJ, Canniffe DP, Davison PA, Dickman MJ, Sobotka R, Hunter CN (2012) Conserved chloroplast open-reading frame *ycf54* is required for activity of the magnesium protoporphyrin monomethylester oxidative cyclase in *Synechocystis* PCC 6803. J Biol Chem 287:27823–27833. https://doi.org/10.1074/jbc.M112.352526

Hontani Y, Kloz M, Polívka T, Shukla MK, Sobotka R, Kennis JTM (2018) Molecular origin of photoprotection in cyanobacteria probed by watermarked femtosecond stimulated Raman spectroscopy. J Phys Chem Lett 9:1788–1792. https://doi.org/10.1021/acs.jpclett.8b00663

Järvi S, Suorsa M, Aro EM (2015) Photosystem II repair in plant chloroplasts—regulation, assisting proteins and shared components with photosystem II biogenesis. Biochim Biophys Acta (BBA) - Bioenerg 1847:900–909. https://doi.org/10.1016/J.BBABIO.2015.01.006

Jordan P, Fromme P, Witt HT, Klukas O, Saenger W, Krauß N (2001) Three-dimensional structure of cyanobacterial photosystem I at 2.5 Å resolution. Nature 411:909–917. https://doi.org/10.1038/35082000

Kameo S, Aso M, Furukawa R, Matsumae R, Yokono M, Fujita T, Tanaka A, Tanaka R, Takabayashi A (2021) Substitution of deoxycholate with the amphiphilic polymer amphipol A8–35 improves the stability of large protein complexes during native electrophoresis. Plant Cell Physiol 62:348–355. https://doi.org/10.1093/pcp/pcaa165

Knoppová J, Sobotka R, Tichý M, Yu J, Konik P, Halada P, Nixon PJ, Komenda J (2014) Discovery of a chlorophyll binding protein complex involved in the early steps of photosystem II assembly in *Synechocystis*. Plant Cell 26:1200–1212. https://doi.org/10.1105/tpc.114.123919

Knoppová J, Yu J, Konik P, Nixon PJ, Komenda J (2016) CyanoP is involved in the early steps of photosystem II assembly in the cyanobacterium *Synechocystis* sp. PCC 6803. Plant Cell Physiol 57:1921–1931. https://doi.org/10.1093/pcp/pcw115

Komar J, Alvira S, Schulze RJ, Martin R, Nijeholt JL, Lee SC, Dafforn TR, Deckers-Hebestreit G, Berger I, Schaffitzel C, Collinson I (2016) Membrane protein insertion and assembly by the bacterial holo-translocon SecYEG–SecDF–YajC–YidC. Biochem J 473:3341–3354. https://doi.org/10.1042/BCJ20160545

Komenda J, Sobotka R (2016) Cyanobacterial high-light-inducible proteins - Protectors of chlorophyll-protein synthesis and assembly. Biochim Biophys Acta - Bioenerg 1857:288–295. https://doi.org/10.1016/j.bbabio.2015.08.011

Komenda J, Nickelsen J, Tichý M, Prášil O, Eichacker LA, Nixon PJ (2008) The cyanobacterial homologue of HCF136/YCF48 is a component of an early photosystem II assembly complex and is important for both the efficient assembly and repair of photosystem II in *Synechocystis* sp. PCC 6803. J Biol Chem 283:22390–22399. https://doi.org/10.1074/jbc.M801917200

Komenda J, Knoppová J, Kopečná J, Sobotka R, Halada P, Yu J, Nickelsen J, Boehm M, Nixon PJ (2012a) The Psb27 assembly factor binds to the CP43 complex of photosystem II in the cyanobacterium *Synechocystis* sp. PCC 6803. Plant Physiol 158:476–486. https://doi.org/10.1104/pp.111.184184

Komenda J, Sobotka R, Nixon PJ (2012b) Assembling and maintaining the photosystem II complex in chloroplasts and cyanobacteria. Curr Opin Plant Biol 15:245–251. https://doi.org/10.1016/j.pbi.2012.01.017

Komenda J, Krynická V, Zakar T (2019) Isolation of thylakoid membranes from the cyanobacterium *Synechocystis* sp. PCC 6803 and analysis of their photosynthetic pigment-protein complexes by clear native-PAGE. Bio-Protoc 9:3126. https://doi.org/10.21769/BIOPROTOC.3126

Kühlbrandt W, Wang DN, Fujiyoshi Y (1994) Atomic model of plant light-harvesting complex by electron crystallography. Nature 367:614–621. https://doi.org/10.1038/367614a0

Lee J, Lee HJ, Shin MK, Ryu WS (2004) Versatile PCR-mediated insertion or deletion mutagenesis. Biotechniques 36:398–400. https://doi.org/10.2144/04363BM04

Lichtenthaler HK, Wellburn AR (1983) Determinations of total carotenoids and chlorophylls *a* and *b* of leaf extracts in different solvents. Biochem Soc Trans 11:591–592

Liu Z, Yan H, Wang K, Kuang T, Gui L, An X, Chang W (2004) Crystal structure of spinach major light-harvesting complex at 2.72 Å resolution. Nature 428:287–292. https://doi.org/10.1038/nature02373

Li Y, Liu B, Zhang J, Kong F, Meng H, Li W, Rochaix JD, Li D, Peng L (2019) OHP1, OHP2, and HCF244 form a transient functional complex with the photosystem II reaction center. Plant Physiol 179:195–208. https://doi.org/10.1104/pp.18.01231

Llansola-Portoles MJ, Sobotka R, Kish E, Shukla MK, Pascal AA, Polívka T, Robert B (2017) Twisting a β-carotene, an adaptive trick from nature for dissipating energy during photoprotection. J Biol Chem 292:1396. https://doi.org/10.1074/JBC.M116.753723

Madeira F, Park YM, Lee J, Buso N, Gur T, Madhusoodanan N, Basutkar P, Tivey ARN, Potter SC, Finn RD, Lopez R (2019) The EMBL-EBI search and sequence analysis tools APIs in 2019. Nucleic Acids Res 47:W636–W641. https://doi.org/10.1093/nar/gkz268

Malavath T, Caspy I, Netzer-El SY, Klaiman D, Nelson N (2018) Structure and function of wild-type and subunit-depleted photosystem I in *Synechocystis*. Biochim Biophys Acta - Bioenerg 1859:645–654. https://doi.org/10.1016/j.bbabio.2018.02.002

Mazor Y, Borovikova A, Caspy I, Nelson N (2017) Structure of the plant photosystem I supercomplex at 2.6 Å resolution. Nat Plants 3:17014. https://doi.org/10.1038/nplants.2017.14

Myouga F, Takahashi K, Tanaka R, Nagata N, Kiss AS, Funk C, Nomura Y, Nakagami H, Jansson S, Shinozaki K (2018) Stable accumulation of photosystem II requires ONE-HELIX PROTEIN1 (OHP1) of the light harvesting-like family. Plant Physiol 176:2277–2291. https://doi.org/10.1104/pp.17.01782

Niedzwiedzki DM, Tronina T, Liu H, Staleva H, Komenda J, Sobotka R, Blankenship RE, Polívka T (2016) Carotenoid-induced non-photochemical quenching in the cyanobacterial chlorophyll synthase-HliC/D complex. Biochim Biophys Acta - Bioenerg 1857:1430–1439. https://doi.org/10.1016/j.bbabio.2016.04.280

Pascual-Aznar G, Konert G, Bečková M, Kotabová E, Gardian Z, Knoppová J, Bučinská L, Kaňa T, Sobotka R, Komenda J (2021) Psb35 protein stabilizes the CP47 assembly module and associated high-light inducible proteins during the biogenesis of photosystem ii in the cyanobacterium *Synechocystis* sp. PCC6803. Plant Cell Physiol 62:178–190. https://doi.org/10.1093/pcp/pcaa148

Pazderník M, Mareš J, Pilný J, Sobotka R (2019) The antenna-like domain of the cyanobacterial ferrochelatase can bind chlorophyll and carotenoids in an energy-dissipative configuration. J Biol Chem 294:11131–11143. https://doi.org/10.1074/jbc.ra119.008434

Pogliano JA, Beckwith J (1994) SecD and SecF facilitate protein export in *Escherichia coli*. EMBO J 13:554–561. https://doi.org/10.1002/j.1460-2075.1994.tb06293.x

Proctor MS, Pazderník M, Jackson PJ, Pilný J, Martin EC, Dickman MJ, Canniffe DP, Johnson MP, Hunter CN, Sobotka R, Hitckcock A (2020) Xanthophyll carotenoids stabilise the association

of cyanobacterial chlorophyll synthase with the LHC-like protein HliD. Biochem J 477:4021–4036. https://doi.org/10.1042/BCJ20200561

Promnares K, Komenda J, Bumba L, Nebesarova J, Vácha F, Tichý M (2006) Cyanobacterial small chlorophyll-binding protein ScpD (HliB) is located on the periphery of photosystem II in the vicinity of PsbH and CP47 subunits. J Biol Chem 281:32705–32713. https://doi.org/10.1074/jbc.M606360200

Rahimzadeh Karvansara P, Pascual Aznar G, Bečková M, Komenda J (2022) The Psb34 protein modulates binding of high-light-inducible proteins to CP47 containing photosystem II assembly intermediates in the cyanobacterium *Synechocystis sp.* PCC 6803. Photosynth Res, *accepted*

Rappsilber J, Mann M, Ishihama Y (2007) Protocol for micro-purification, enrichment, pre-fractionation and storage of peptides for proteomics using StageTips. Nat Protoc 2(8):1896–1906. https://doi.org/10.1038/NPROT.2007.261

Ritchie ME, Phipson B, Wu D, Hu Y, Law CW, Shi W, Smyth GK (2015) Limma powers differential expression analyses for RNA-sequencing and microarray studies. Nucleic Acids Res 43:e47. https://doi.org/10.1093/nar/gkv007

Rudolph JD, Cox J (2019) A network module for the Perseus software for computational proteomics facilitates proteome interaction graph analysis. J Proteome Res 18:2052–2064. https://doi.org/10.1021/acs.jproteome.8b00927

Shukla MK, Llansola-Portoles MJ, Tichý M, Pascal AA, Robert B, Sobotka R (2018) Binding of pigments to the cyanobacterial high-light-inducible protein HliC. Photosynth Res 137:29–39. https://doi.org/10.1007/s11120-017-0475-7

Skotnicová P, Staleva H, Kuznetsova V, Bína D, Konert M, Lu S, Polivka T, Sobotka R (2021) Plant LHC-like proteins show robust folding and static non-photochemical quenching. Nat Commun 12:6890. https://doi.org/10.1038/s41467-021-27155-1

Staleva H, Komenda J, Shukla MK, Šlouf V, Kaňa R, Polívka T, Sobotka R (2015) Mechanism of photoprotection in the cyanobacterial ancestor of plant antenna proteins. Nat Chem Biol 11:287–291. https://doi.org/10.1038/nchembio.1755

Tichý M, Bečková M, Kopečná J, Noda J, Sobotka R, Komenda J (2016) Strain of *Synechocystis* PCC 6803 with aberrant assembly of photosystem II contains tandem duplication of a large chromosomal region. Front Plant Sci 7:648. https://doi.org/10.3389/FPLS.2016.00648

Tribet C, Audebert R, Popot J-L (1996) Amphipols: polymers that keep membrane proteins soluble in aqueous solutions. Proc Natl Acad Sci 93:15047–15050. https://doi.org/10.1073/pnas.93.26.15047

Tyanova S, Temu T, Cox J (2016a) The MaxQuant computational platform for mass spectrometry-based shotgun proteomics. Nat Protoc 11:2301–2319. https://doi.org/10.1038/NPROT.2016.136

Tyanova S, Temu T, Sinitcyn P, Carlson A, Hein MY, Geiger T, Mann M, Cox J (2016b) The Perseus computational platform for comprehensive analysis of (prote)omics data. Nat Methods 13:731–740. https://doi.org/10.1038/nmeth.3901

Umena Y, Kawakami K, Shen JR, Kamiya N (2011) Crystal structure of oxygen-evolving photosystem II at a resolution of 1.9Å. Nature 473:55–60. https://doi.org/10.1038/nature09913

Vass I (2012) Molecular mechanisms of photodamage in the photosystem II complex. Biochim Biophys Acta (BBA) - Bioenerg 1817:209–217. https://doi.org/10.1016/J.BBABIO.2011.04.014

Wei X, Su X, Cao P, Liu X, Chang W, Li M, Zhang X, Liu Z (2016) Structure of spinach photosystem II-LHCII supercomplex at 3.2 Å resolution. Nature 534:69–74. https://doi.org/10.1038/nature18020

Xiao Y, Huang G, You X, Wang W, Kuang T, Han G, Sui SF, Shen JR (2021) Structural insights into cyanobacterial photosystem II intermediates associated with Psb28 and Tsl0063. Nat Plants 7:1132–1142. https://doi.org/10.1038/s41477-021-00961-7

Xu H, Vavilin D, Funk C, Vermaas WFJ (2002) Small Cab-like proteins regulating tetrapyrrole biosynthesis in the cyanobacterium *Synechocystis* sp. PCC 6803 Plant Mol Biol 49:149–160. https://doi.org/10.1023/A:1014900806905

Yao D, Kieselbach T, Komenda J, Promnares K, Hernández Prieto MA, Tichy M, Vermaas W, Funk C (2007) Localization of the small CAB-like proteins in photosystem II. J Biol Chem 282:267–276. https://doi.org/10.1074/jbc.M605463200

Zabret J, Bohn S, Schuller S, Arnolds O, Möller M, Meier-Credo J, Liauw P, Chan A, Tajkhorshid E, Langer J, Stoll R, Krieger-Liszkay A, Engel B, Rudack T, Schuller J, Nowaczyk M (2021) Structural insights into photosystem II assembly. Nat Plants 7:524–538. https://doi.org/10.1038/s41477-021-00895-0

BBA - Bioenergetics 1865 (2024) 149017

Contents lists available at ScienceDirect

BBA - Bioenergetics

journal homepage: www.elsevier.com/locate/bbabio

The cyanobacterial FtsH4 protease controls accumulation of protein factors involved in the biogenesis of photosystem I

Peter Koník [a,b], Petra Skotnicová [a], Sadanand Gupta [a,b], Martin Tichý [a], Surbhi Sharma [a,b], Josef Komenda [a], Roman Sobotka [a,b], Vendula Krynická [a,*]

[a] Institute of Microbiology of the Czech Academy of Sciences, Centre Algatech, Třeboň 379 01, Czech Republic
[b] Faculty of Science, University of South Bohemia, České Budějovice 370 05, Czech Republic

ARTICLE INFO

Keywords:
FtsH4 protease
Synechocystis
Photosystem I
Thylakoid membrane
Assembly factors

ABSTRACT

Membrane-bound FtsH proteases are universally present in prokaryotes and in mitochondria and chloroplasts of eukaryotic cells. These metalloproteases are often critical for viability and play both protease and chaperone roles to maintain cellular homeostasis. In contrast to most bacteria bearing a single *ftsH* gene, cyanobacteria typically possess four FtsH proteases (FtsH1–4) forming heteromeric (FtsH1/3 and FtsH2/3) and homomeric (FtsH4) complexes. The functions and substrate repertoire of each complex are however poorly understood. To identify substrates of the FtsH4 protease complex we established a trapping assay in the cyanobacterium *Synechocystis* PCC 6803 utilizing a proteolytically inactivated ^{trap}FtsH4-His. Around 40 proteins were specifically enriched in ^{trap}FtsH4 pulldown when compared with the active FtsH4. As the list of putative FtsH4 substrates contained Ycf4 and Ycf37 assembly factors of Photosystem I (PSI), its core PsaB subunit and the IsiA chlorophyll-binding protein that associates with PSI during iron stress, we focused on these PSI-related proteins. Therefore, we analysed their degradation by FtsH4 *in vivo* in *Synechocystis* mutants and *in vitro* using purified substrates. The data confirmed that FtsH4 degrades Ycf4, Ycf37, IsiA, and also the individual PsaA and PsaB subunits in the unassembled state but not when assembled within the PSI complexes. A possible role of FtsH4 in the PSI life-cycle is discussed.

1. Introduction

FtsHs are transmembrane metalloproteases universally conserved in bacteria, chloroplasts, and mitochondria. By modulating protein processing and turnover, the activity of FtsH proteases is essential for a broad spectrum of biological processes. In most bacteria, these enzymes are so crucial for maintaining cellular homeostasis that cannot be eliminated [1]. In cyanobacteria, algae and plants, FtsHs play an additional important role in the biogenesis of photosynthetic apparatus and the best-studied process involving FtsH in phototrophs is the quality control of the photosystem II complex (PSII) (reviewed in [2]). However, the contribution of FtsHs to photosystem I (PSI) biogenesis [3] and to plastid development [4] has also been proposed.

The molecular mechanisms, by which FtsHs control the biogenesis of photosynthetic complexes remain mostly unknown and only a few substrates of FtsHs related to photosystem biogenesis were identified in phototrophs [5–7]. Likewise the other cyanobacteria, the model species *Synechocystis* sp. PCC 6803 (hereafter *Synechocystis*) contains four FtsH homologues, FtsH1-FtsH4. Individual *Synechocystis* FtsHs form three oligomeric complexes *in vivo* — two heteromers FtsH1/3 and FtsH2/3, and homomeric FtsH4. The FtsH2/3 and FtsH4 complexes have been localized in the thylakoid membrane (TM) and levels of these complexes are comparable [7,8]. Similarly to its *Arabidopsis thaliana* orthologs FtsH2/8 and FtsH1/5 [9], the *Synechocystis* FtsH2/3 complex plays a pivotal role in the selective degradation of PSII subunits during PSII repair [10,11] and controlling the level of unassembled PSII subunits [12]. The deletion of *ftsH2* gene causes light sensitivity and photoinhibition of PSII [10]. Nonetheless, the role of FtsH2/3 is clearly not restricted to maintaining active PSII complexes. The inactivation of FtsH2 protease leads to other phenotypic changes such as a reduced level of PSI and a significant decrease in the cellular level of chlorophyll (Chl) [13].

The less abundant, but essential FtsH1/3 complex is located in the plasma membrane [14,15] and is more specifically involved in the

* Corresponding author at: Institute of Microbiology of the Czech Academy of Sciences, Centre Algatech, Třeboň 379 01, Czech Republic.
E-mail address: krynicka@alga.cz (V. Krynická).

https://doi.org/10.1016/j.bbabio.2023.149017
Received 30 May 2023; Received in revised form 18 September 2023; Accepted 4 October 2023
Available online 11 October 2023

acclimation of cells to nutrient deficiency. Several transcription factors, regulating mostly nutrient starvation genes, have been identified as potential substrates of FtsH1/3 [16]. In contrast to the essential role of FtsH1 and FtsH3 and poor viability of the FtsH2-less strain, the elimination of FtsH4 had no obvious negative impact on the *Synechocystis* growth under normal growth conditions (40 μmol of photons m^{-2} s^{-1}, 28 °C [13]) apart from a statistically significant higher level of Chl per cell compared with wild type (WT) [7]. This excess of Chl was incorporated into the PSI trimer (PSI [3]), the level of which was elevated in Δ*ftsH4* cells compared with WT [7].

This subtle phenotype of the *Synechocystis* Δ*ftsH4* strain, observed under moderate light intensities, contrasts to strongly retarded growth of this mutant under high light (HL) [7]. Interestingly, even more severe growth defects have been described for the Δ*ftsH4* mutant cells that were first grown to stationary phase and then diluted and shifted to HL [7]. Our recent results exclude that the *Synechocystis* FtsH4 structurally or functionally substitutes for FtsH2 and hence the FtsH2/3 complex in the repair of PSII. Instead, the FtsH4 acts in the photoprotection of PSII by dual regulation of high light-inducible proteins (Hlips). These small, single-helix proteins bind Chl and carotenoids and are crucial for the biogenesis of PSII under stress conditions [17,18]. FtsH4 positively regulates the expression of *hli* genes coding for Hlips, shortly after HL exposure but is also responsible for the post-stress removal of Hlips once they are no longer needed. In *Synechocystis*, FtsH4 complexes are concentrated in well-defined membrane regions at the inner and outer periphery of the thylakoid system. As the FtsH4 has been co-purified with a similar set of protein factors as the PSII assembly intermediates [19], it is likely that the observed FtsH4-rich membrane spots co-localize with compartments where the biogenesis of photosystems takes place.

In this work, we screened for substrates of the *Synechocystis* FtsH4 using a proteolytically inactive FtsH4 variant as a trap. Putative substrate proteins, co-isolated with inactive protease, were verified *in vivo* by employing *Synechocystis* FtsH4 mutants and *in vitro* using a proteolytic essay. We can conclude that the FtsH4 controls the level of at least two PSI assembly factors (Ycf37 and Ycf4), the unassembled PSI core subunits and the PSI-binding IsiA protein. Other potential substrates are also discussed.

2. Material and methods

2.1. Construction of Synechocystis strains

The *Synechocystis* glucose tolerant substrain GT-P [20] was used as WT for all experiments described in this study. The Δ*ftsH4* mutant and *Synechocystis* strains expressing C-terminally 3xFLAG-tagged FtsH4 under *psbA2* promoter (F4CF strain) and C-terminally 6xHis-tagged FtsH4 (*ftsH4-his*) under the native *ftsH4* promoter are described in [7]. To construct the ^{trap}*ftsH4-his* strain, the E439Q mutation was introduced into the *ftsH4-his* plasmid [7] using the QuikChange II XL site-directed mutagenesis kit (Agilent Technologies). The resulting plasmid was transformed into *Synechocystis* and transformants were fully segregated using an increasing concentration of chloramphenicol. The presence of ^{trap}*ftsH4-his* gene was confirmed by sequencing. The A3 strain, lacking *psbAI* and *psbAII* genes [21] was used as a control for the F4CF strain.

To construct *Synechocystis* strains expressing N-terminally 1xFLAG-tagged PsaA (f.PsaA) or PsaB (f.PsaB) from the native *psaAB* promoter, a set of DNA constructs was prepared by the NEBuilder HiFI DNA assembly kit, each containing the gentamycin or chloramphenicol resistance cassette downstream of the *psaAB* locus (see Fig. S1). These constructs were used to replace the whole *psaAB* operon to obtain strains expressing only f.PsaA or f.PsaB (*f.psaA*/Δ*psaB* or *f.psaB*/Δ*psaA* strains). The *f.psaA* strain, containing the assembled FLAG-PSI with tagged PsaA, was prepared by transforming the *f.psaA*/Δ*psaB* strain using the *psaB*-Gent construct and selecting for autotrophy (Fig. S1).

2.2. Cultivation of Synechocystis strains

Liquid cultures were grown in BG-11 medium in Erlenmeyer flasks at 28 °C on a rotary shaker (120 rpm) at a normal irradiance of 40 μmol photons m^{-2} s^{-1} (normal light, NL) or a high irradiance of 500 μmol photons m^{-2} s^{-1} (HL) provided by white fluorescence tubes. For FtsH4-His pulldown assays, *Synechocystis* strains were grown in 1 L cylinders bubbled with air at irradiance of 100 μmol photons m^{-2} s^{-1} which was increased to 300 μmol photons m^{-2} s^{-1} for 16 h before harvesting. PSI strains for FLAG-specific pulldowns were cultivated in a 10 L flask (culture volume 4 L) bubbled with air at 5 μmol photons m^{-2} s^{-1}.

For the cold stress experiment, strains were cultivated at 20 °C at irradiance of 150 μmol photons m^{-2} s^{-1}.

To inhibit the protein synthesis, the liquid cultures were supplemented with lincomycin at a concentration of 100 μg ml^{-1} of culture.

To remove iron, the cells were transferred to an iron-depleted medium (residual concentration of iron about 5 μM) supplemented with 10 μM deferoxamine B (DFB), an iron chelator. Cells were cultivated for another 72 h. For recovery from iron depletion, the cells were washed three times, resuspended in standard BG11 and grown for another 48 h.

2.3. Whole cell absorption spectroscopy and Chl determination

Absorption spectra of whole cells resuspended to the same OD_{750nm}, were acquired at room temperature using a UV-3000 spectrophotometer (Shimadzu, Japan). For routine Chl determination, methanol extracts of cell pellets or membranes were analysed spectroscopically according to Porra et al. [22].

2.4. Low temperature fluorescence spectroscopy

Low temperature Chl fluorescence emission spectra were measured at 77 K in cultures with the identical OD_{750nm} using an SM 9000 spectrophotometer (Photon Systems Instruments, Czech Republic) at an excitation wavelength of 470 nm.

2.5. Isolation of thylakoid membranes

Approximately 100 ml of cells at an OD_{750nm} of ~0.8 were harvested by centrifugation at 6000 ×*g* for 10 min and resuspended in buffer A (25 mM MES, pH 6.5, 10 mM $CaCl_2$, 10 mM $MgCl_2$, 25 % glycerol) for protein analysis and FLAG-tag specific pulldowns or buffer B (25 mM Na phosphate buffer, pH 8, 50 mM NaCl, 10 % glycerol) for His-tag specific pulldowns. Cells were mixed with 100–200 μm diameter glass beads in 1:1 ratio (1 volume of dense cell solution with 1 volume of glass beads) and broken (6 × 20 s) using a mini-bead beater. To separate soluble and membrane fractions, samples were centrifuged at 30,000 ×*g* for 20 min at 4 °C. Pelleted membranes were washed once with an excess of buffer and then resuspended in 150 μl of buffer A or B for later use.

2.6. Electrophoresis and immunoblotting

For 1D SDS-PAGE, membrane proteins were denatured with 2 % SDS (w/v) and 1 % (w/v) dithiothreitol for 30 min at room temperature and analysed by SDS-PAGE in a denaturing 12–20 % polyacrylamide gel containing 7 M urea or in 4–15 % TGX precast gels (Bio-Rad). For the clear native (CN) electrophoresis, the proteins were separated on 4–14 % (w/v) polyacrylamide gel as described in Komenda et al. [23] or 4–15 % TGX precast gel (Bio-Rad). The protein gels were scanned and the Chl fluorescence image was taken by LAS-4000 camera (Fuji). Individual components of protein complexes were resolved by incubating the gel strip from the first dimension in 2 % (w/v) SDS and 1 % (w/v) dithiothreitol for 30 min at room temperature and then proteins were separated in the second dimension by a 12–20 % linear gradient SDS-PAGE gel containing 7 M urea. Proteins in gels were stained by SYPRO Orange (Sigma-Aldrich) or Coomassie Blue (Bio-Rad).

For immunodetection, proteins were transferred from the SDS gel to a polyvinylidene difluoride (PVDF) membrane (Immobilon-P, Merck Millipore). Membrane was incubated with the primary antibody and subsequently with an anti-rabbit secondary antibody conjugated with horseradish peroxidase (Sigma-Aldrich). Chemiluminescence obtained using an Immobilon Crescendo substrate (Millipore) was imaged using the LAS-4000 camera (Fuji). These primary antibodies, specific for the following proteins and tags, were used in this study: FtsH4 [24], PsaA (Agrisera, cat. no. AS06 172), PsaB (Agrisera, cat. no. AS10 695), PsaD [25], Ycf4 (Agrisera, cat. no. AS07274), Ycf37 [26], 6xHis (Abcam, cat. no. ab9108), and FLAG (Abgent, cat. no. AP1013A).

2.7. Pulldown of tagged proteins

For the purification of His-tagged FtsH4 variants, 3.5 L of *Synechocystis* cells were broken using glass beads as described above in buffer B with EDTA-free protease inhibitor (Sigma). The pelleted membrane fraction, prepared essentially as described in Koskela et al. [27], was resuspended in buffer B (~0.5 mg Chl/ml) and solubilized for 60 min at 10 °C with 1 % 4-trans-propylcyclohexyl α-maltoside. Finally, insoluble contaminants were removed by centrifugation (47,000 ×*g*, 20 min). Pulldown was performed as described in Krynická et al. [7]; F.PsaA and F.PsaB were purified in buffer A as described in Koskela et al. [27].

2.8. FtsH in vitro assay

Proteolytically active FtsH4-His was isolated from *Synechocystis* membrane fraction as described above. The FtsH protease assay was carried out essentially according to Tomoyasu et al. [28] and Krynická et al. [7] using 0.3 μg of total FtsH4 and 0.2 μg of the substrate. For the inhibition of FtsH activity, the reaction was supplemented with cOmplete Protease Inhibitor Cocktail (Roche) containing EDTA. The reaction was carried out in 20 μl. Composition of the reaction buffer: 25 mM MES pH 6.5, 5 % glycerol, 2 mM Mg^{2+}, 2 mM Ca^{2+}, 0.4 μM Zn^{2+}, 3 mM ATP, and 0.04 % 4-trans-propylcyclohexyl α-maltoside. All samples were incubated for 3 h at 37 °C. After incubation, the samples were denatured by 1 % SDS, separated by 1D SDS-PAGE, and the presence of F.PsaA, F.PsaB, Ycf37, and FtsH4 was detected by specific antibodies, protoporphyrinogen IX oxidase (HemJ) was detected by FLAG-specific antibody. Quantification of the detected bands was performed by AzureSpot Pro software v. 2.2.167 (Azure Biosystems). The substrate amount is expressed as a percentage of the initial substrate level (100 %) and numbers represent means of 3 independent reactions ± standard deviation.

2.9. Analysis of His-tagged FtsH4 pulldowns by protein MS

For the eluates of His-tagged proteins, 5 μl were diluted in 45 μl of 0.1 % (v/v) Rapigest (Waters) surfactant in 50 mM ammonium bicarbonate. The final mixture was incubated for 45 min at 60 °C, cooled briefly and proteomic grade trypsin (Sigma) was added to a final concentration of 10 ng/μl and incubated at 37 °C. After 12 h, samples were acidified by adding formic acid to a final concentration of 0.5 % (v/v). The sample was desalted and peptides were isolated by the StageTip procedure [29]. LC-MS/MS analysis was performed on an UltiMate 3000 UHPLC (Thermo Fisher Scientific) on-line coupled to a TimsTOF pro (Bruker) mass spectrometer. 2 μl of the sample were trapped for 1 min on a ThermoFisher trap (0.3 × 5 mm, C18, 5 μm) column, then separated by reverse phase liquid chromatography on an Acclaim PepMap RSLC column (75 μm × 15 cm, C18, 2 μm, 100 Å; Thermo Fisher Scientific) column. Peptides were eluted by a linear water: acetonitrile gradient, where acetonitrile increased from 3 to 50 % over 30 min and the eluted fluid was fed directly into the CaptiveSpray nano ion source of the mass spectrometer. Both mobile phases contained 0.1 % of formic acid. Spectra were acquired in a data-dependent PASEF (Parallel Accumulation/SErial Fragmentation) regime with an accuracy of 0.2 ppm for precursors and 0.5 ppm for fragments. 3 technical replicates were acquired for each of the 3 biological replicates for each sample. Raw data were processed by the MaxQuant/Andromeda software [30,31] and matched to species-specific *Synechocystis* protein databases downloaded from Uniprot and Cyanobase. Statistical analysis of protein groups obtained from MaxQuant was performed in Perseus 1.6.14.0 [32]. After removing hits identified only by modified peptides, reverse database hits and most common contaminants, IBAQ intensities were log_2-transformed and missing data was imputed from normal distribution. Interactors were identified by comparing FtsH4-His with ^{trap}FtsH4-His samples using the volcano plot function, and non-specific reactions were identified by subtracting proteins identified in the non-his control sample. The MS proteomics data were deposited to the MassIVE, ID: MSV000092109.

3. Results

3.1. Pulldown assay using His-tagged FtsH4 as a bait

To establish a sensitive trap assay for the identification of FtsH4 substrates, we constructed *Synechocystis* strains expressing the active 6xHis-tagged FtsH4 variant and its proteolytically inactive derivative (^{trap}FtsH4-His) from the native *ftsH4* promoter. The inactive enzyme contains a point mutation E439Q abolishing the binding of the catalytic zinc ion [33]. The FtsH trap is still able to unfold and translocate substrates into the proteolytic chamber allowing to isolate stable FtsH-substrate complexes [34]. As confirmed by immunodetection, the levels of FtsH4-His and ^{trap}FtsH4-His were comparable with the level of native FtsH4 protease (Fig. S2). In order to find the optimal conditions for the purification of both active and inactive FtsH4 proteins we analysed the level of FtsH4 during different phases of growth. Notably, the highest accumulation of this protease was observed in the linear growth phase, followed by lag and stationary phase while the lowest level was found in the exponential growth phase (Fig. S3A).

To distinguish between potential FtsH4 substrates and proteins interacting in the cell with the FtsH4 enzyme for other reasons, we first performed a pulldown assay with the FtsH4-His as a control for ^{trap}FtsH-His. Both strains were cultivated in three independent parallels in 1 L cylinders under NL conditions till the linear growth phase (OD_{750nm} ~ 2.5) to ensure a high cellular accumulation of FtsH4 (see Fig. S3A, B). After cell disruption, FtsH4 protease was purified on a nickel column and subjected to nanoLC-MS/MS protein identification (Fig. 1). Raw data were processed using MaxQuant and the obtained IBAQ intensities were used to determine statistically enriched proteins [7,35]. Solubilized membrane proteins from WT were used as a negative control for the detection of non-specific interactors with the resin.

This analysis revealed 256 proteins that were significantly enriched compared to the WT TM control when the false discovery rate cut-off was 1 % (FDR = 0.01). Applying more stringent significance criteria: log2 FC (FtsH4 — WT) ≥ 3, which means 8 (2^3) times higher iBAQ intensity than the WT control (Fig. 1A, blue area), and corresponding to at least 1 % of the FtsH4 content, we selected the 51 hits (Fig. 1A, red square, Supplementary Dataset 1). The eight most abundant proteins (above 10 % of FtsH4 content) are listed in Table 1. Sll1106 protein is known to interact tightly with FtsH4 [7] and, indeed, Sll1106 was among the most abundant hits in our FtsH4 pulldown (36 % of the FtsH4 content). Apart from Sll1106, FtsH4 was co-isolated with GlgB and GlgA2 enzymes functioning in glycogen synthesis (75 % and 11 % of the FtsH4 iBAQ content) and Slr0374 protein (69 % of the FtsH4 content) that is involved in CO_2 uptake and utilization [36]. Glutamine synthetase was an additional enzyme among the most abundantly purified proteins with FtsH4 (47 % of the FtsH4 content). Finally, the set of top eight co-purified proteins comprised two transcriptional repressors including Fur that regulates gene expression in response to iron depletion (Table 1).

In agreement with our previous FLAG-FtsH4 pulldown (see

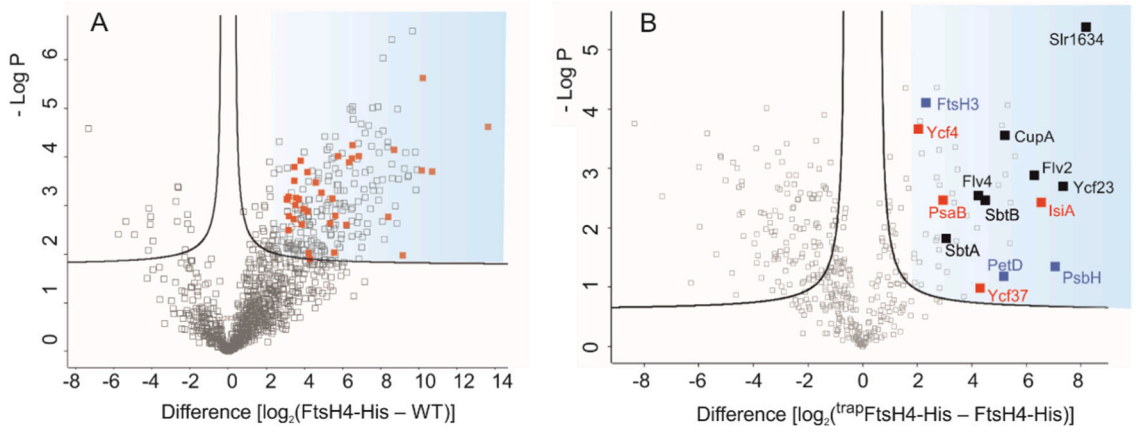

Fig. 1. Identification of candidate proteins for FtsH4-His substrates using ^{trap}FtsH4-His assay and protein MS. A) Volcano plot representing the difference in Log_2-transformed iBAQ intensities between FtsH4-His pulldown and the control WT TM elution. Three independent biological triplicates were carried out for both pulldowns; identified protein hits are indicated by grey squares. The FDR cut-off, represented by black line, was set to 1 % and proteins highlighted in red are the most significantly enriched with the highest abundance in comparison with the bait (Supplementary Dataset 1). B) Volcano plot representing the difference in Log_2-transformed iBAQ intensities between FtsH4-His and ^{trap}FtsH4-His pulldowns. Three independent biological triplicates were carried out for both pulldowns. Proteins (potential substrates) significantly enriched in the trap elution compared to FtsH4-His elution are inside the blue background rectangle. Proteins related to PSI are highlighted in red and proteins involved in CO_2 uptake are in black; other photosynthetic proteins are in blue. (For interpretation of the references to colour in this figure legend, the reader is referred to the web version of this article.)

Discussion section), we also identified CurT protein that is important for the organization of TM, RubA protein that is important for the PSII assembly [37], and several subunits of ATP synthase (Supplementary Dataset 1). However, all these proteins were represented only in units of percent relative to the FtsH4 iBAQ intensity and these are more likely only co-localized with FtsH4 or bind this protease transiently/very weakly.

After clarifying what proteins co-isolate with the active FtsH4-His, we purified the ^{trap}FtsH4-His protease and searched for specific hits that are absent or significantly less abundant in controls (FtsH4-His and WT TM). Using FDR = 0.05, we identified 64 proteins significantly enriched in trap pulldown (Fig. 1B). To narrow down the list of potential FtsH4 substrates, we defined more stringent criteria for significance: log_2 FC (^{trap}FtsH4-His – FtsH4-His) $\geq$ 2, which means 4 times more than in the FtsH4-His control. With this setting, 42 proteins were identified in total (Fig. 1B, blue area, Table S2). Most of these putative FtsH4 substrates were transmembrane and membrane-associated proteins and, quite specifically, proteins involved in photosynthesis.

Table 1
A list of proteins that were most abundantly represented in the His-tagged FtsH4 pulldown. Raw iBAQ intensities of proteins, co-eluted with FtsH4-His, were compared with their iBAQ intensities in the control elution. Log_2FC (FtsH4-His — WT) shows the Log_2 difference (enrichment) in the FtsH4-His sample compared to the control. The column labelled % of FtsH4 shows the calculated percentage of iBAQ intensities of the co-eluted proteins in respect to the bait protein (FtsH4-His). Only proteins with Log_2FC $\geq$ 3 and a percentage above 10 % are shown (see the Supplementary Dataset 1 for the full list of proteins). Experiments were performed in triplicates; averaged values are shown.

Number	Protein	iBAQ intensity FtsH4-His	WT	Log2FC (FtsH4-His − WT)	−log *P* value	% of FtsH4
	FtsH4 (Sll1463)	20,455,700	1908	14	5	100
1	GlgB (Sll0158)	13,336,700	1,229,830	3	4	75
2	Slr0374	11,833,400	146,968	6	4	69
3	GuaA (Slr0213)	8,556,310	1,043,050	3	2	47
4	Sll1106	6,887,130	99,608	6	4	36
5	Fur (Sll0567)	5,232,910	226,268	5	3	29
6	Slr1617	3,054,720	89,864	5	3	18
7	NrdR (Sll1780)	2,551,290	75,893	5	3	14
8	GlgA2	2,507,480	180,845	4	3	11

3.2. Identification of putative substrates using a protease trap assay

Interestingly, several proteins enriched in the ^{trap}FtsH4-His preparation were related to PSI and its biogenesis, namely IsiA, PsaB, Ycf4, and Ycf37. IsiA is the iron stress-induced Chl-binding protein that forms an oligomeric ring around the PSI under iron limitation [38,39]. PsaB is the core subunit of the PSI complex [40,41] and Ycf4 and Ycf37 are PSI assembly factors involved in the early stage of the PSI biogenesis [42,43]. PsaA was also enriched in the trap pulldown compared to active FtsH4, however since its level was relatively high in the WT control, the specific occurrence of PsaA in the pulldown was questionable. Notably, the amount of PsaA was 2.5 times lower than PsaB in the trap indicating that FtsH4 prefers PsaB to PsaA.

Apart from the PSI-related proteins, PsbH and PetD were also enriched in the ^{trap}FtsH4-His elution. PsbH is a small PSII subunit associated with the CP47 antenna protein and PetD (Slr0343) is a component of the cytochrome b_6f complex that mediates the electron transfer between PSII and PSI as well as the cyclic electron flow around PSI. In addition, we found prohibitin Phb1 and FtsH3 but not FtsH1 and FtsH2, as potential substrates of FtsH4. It is also worth noting that 8 of 44 selected proteins are involved in acclimation to low carbon and their expression increases during the CO_2 limitation, namely flavoproteins Sll0217, Sll0219, SbtA, SbtB, CupA and several proteins of unknown function like Ycf23 and Slr1634 [44]. However, as in the case of IsiA, our cell cultures were not stressed by CO_2 limitation, which is evident from low levels of bicarbonate or CO_2 transporters such as SbtA or CupA in the membrane fraction (Fig. S4). Finally, two heat shock proteins were found among the putative substrates of FtsH4.

3.3. FtsH4-less cells contain aberrant levels of PSI subunits and PSI assembly factors under stress conditions

The FtsH trap approach revealed two PSI assembly factors (Ycf37, Ycf4) and PsaB, the core subunit of the PSI complex, as putative substrates of FtsH4. Our previous study demonstrated that the deletion of *ftsH4* results in a surplus of PSI trimer under NL conditions (Fig. S5) [7].

Interestingly, after 5 days at 20 °C (cold-stress conditions), in the Δ*ftsH4* strain, we identified two additional PSI complexes migrating between the PSI monomer and the dimer in CN gel (Fig. 2A, blue and red arrow). These are presumably intermediates of PSI assembly since complexes of the same size were observed in 2D autoradiogram that is indicative of newly synthesized PsaA/PsaB proteins (Fig. 2B).

Since the presence of these PSI assembly intermediates could be related to the overaccumulation of Ycf37 and Ycf4 PSI assembly factors in Δ*ftsH4*, we tested it using the 2D blots of membranes from cells grown in cold-stress which were probed with antibodies specific for each assembly factor. Indeed, the content of Ycf37 was significantly increased in Δ*ftsH4* compared with WT (Fig. 2A) and a smearing signal of Ycf37 starting in the region of these complexes indicated their possible association with this assembly factor. We could not immunochemically detect Ycf4 on the 2D gel but it was possible on 1D gel and the analysis confirmed the overaccumulation of both, Ycf37 and Ycf4 in cold stress-treated Δ*ftsH4* cells (Fig. 2C). In contrast to cold stress, amounts of Ycf37 and Ycf4 were comparable in WT and Δ*ftsH4* under NL (Fig. 3A). Nonetheless, after the transfer of cells to HL conditions, effectively blocking the synthesis of PSI [45,46], the amount of Ycf4 and partly also Ycf37 assembly factor decreased in WT while it remained stable in Δ*ftsH4* after 72 h (Fig. 3A). 2D gel analysis of WT and Δ*ftsH4* cells after 24 h of HL supported these results (Fig. 3B) and a distinct band of Ycf37 in the region of the red-designated PSI complex of Δ*ftsH4* supports its identity as a PSI monomer with bound Ycf37. Notably, quite the opposite effect was observed in the F4CF strain overexpressing the FLAG-tagged FtsH4 [7]. The level of the Ycf37 protein was lower when compared with the control *psbAII* deletion strain A3 [21] after 24 h of HL (Fig. 3B).

As Ycf37 and Ycf4 accumulate in the mutant lacking FtsH4 and conversely, their levels are lower in the mutant overexpressing F4FC, these results strongly support the conclusion that these PSI assembly factors are substrates of FtsH4. To further confirm this hypothesis, we performed an FtsH4 *in vivo* degradation assay. In WT and Δ*ftsH4*, we monitored a decrease in Ycf37 and Ycf4, and for control also D1, after exposure to HL and inhibition of new protein synthesis by the addition of Lincomycin. While in WT we observed a reduction in the amount of all proteins during 6 h of HL exposure, in Δ*ftsH4* the amount of only D1 protein decreased comparably to WT while the amount of Ycf37 and Ycf4 did not decline (Fig. 3C).

3.4. *FtsH4 protease is involved in IsiA degradation during the recovery from iron depletion*

IsiA belonged to the most enriched proteins in the ^{trap}FtsH4-His pulldown (Fig. 1B, Table S2). Although the function of this protein is not completely clarified, IsiA has been proposed to serve as a Chl storage protein or an energy sink under stress conditions, most prominently

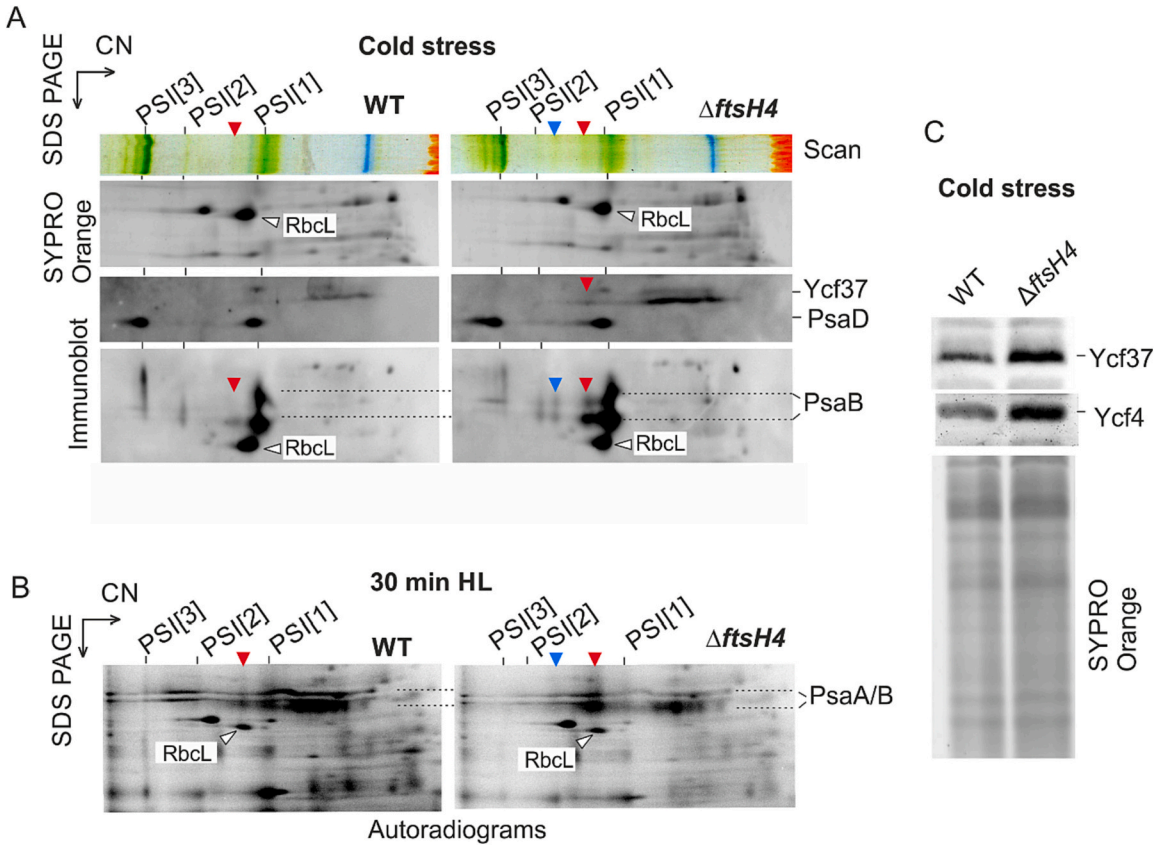

Fig. 2. Accumulation of PSI and PSI assembly complexes in the Δ*ftsH4* mutant grown in stress conditions. A) TM were isolated from WT and Δ*ftsH4* cells grown for 5 days under cold stress (20 °C/150 μmol of photons m^{-2} s^{-1}) and analysed by 2D CN/SDS-PAGE. The CN gel was scanned (Scan). The 2D SDS gels were stained by SYPRO Orange, electroblotted to PVDF membrane and the blot probed with antibodies specific for PsaB, Ycf37, and PsaD. PsaB migrates in the SDS gel in two forms differing in the degree of denaturation (marked with dash-line). The SYPRO Orange stained gels document equal loading. Designation of complexes: PSI[1], PSI[2], and PSI[3]: PSI monomer, dimer and trimer, respectively; and large subunit of RUBISCO (RbcL) is also indicated. Red and blue arrows in 2D blot indicate PSI assembly complexes; 2.5 μg of Chl of each sample was loaded on the 2D gel and 1 μg of Chl for the 1D SDS gel. B) The position of PSI assembly complexes indicated on immunoblot by red asterisks (A) were compared with 2D autoradiogram of membranes isolated from cells grown under standard conditions, radio-labelled and treated with HL (500 μmol of photons m^{-2} s^{-1}) for 30 min before the membrane isolation. The radio-labelled gels were exposed in a phosphoimager overnight. C) The same samples as in (A) were separated by SDS-PAGE, blotted and probed by antibodies against Ycf37 and Ycf4. (For interpretation of the references to colour in this figure legend, the reader is referred to the web version of this article.)

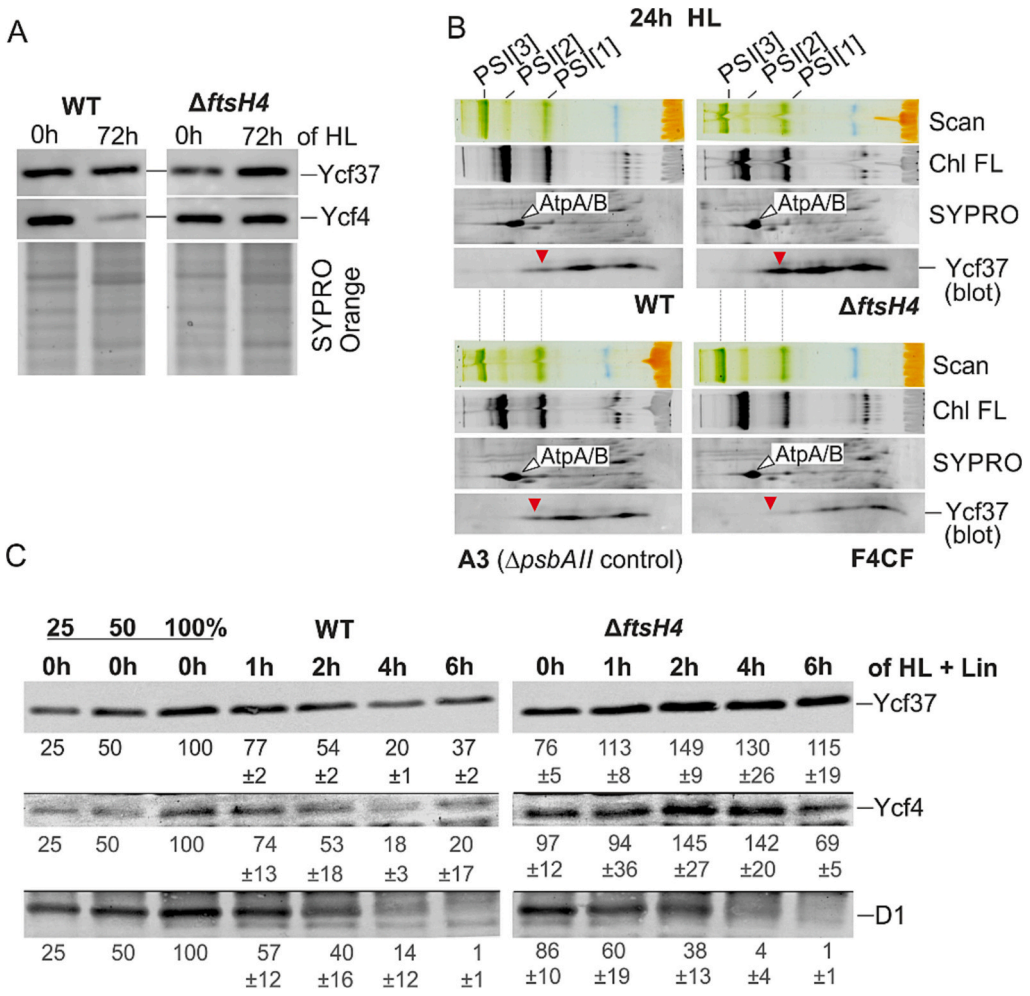

Fig. 3. Effects of the *ftsH4* deletion or overexpression on the amount of PSI assembly factors under HL conditions. A) SDS-PAGE analysis of TM isolated from WT and Δ*ftsH4* strains exposed to HL for 72 h (28 °C/500 μmol photons m^{-2} s^{-1}). The SDS gels were stained by SYPRO Orange, electroblotted to PVDF membrane and the blot probed with antibodies specific for Ycf37 and Ycf4. *Loaded samples were* normalized *per* number of cells. B) 2D CN/SDS-PAGE and immunoblot of TM proteins prepared from WT, Δ*ftsH4*, A3, and F4CF cells grown for 24 h under HL (28 °C/500 μmol photons m^{-2} s^{-1}). The CN gel was scanned (Scan) and Chl autofluorescence was detected (Chl FL); 2.5 μg of Chl was loaded per each sample. The SYPRO Orange stained gels are shown as a loading control. Designation of complexes: PSI[1], PSI[2] and PSI[3]: PSI monomer, dimer and trimer, respectively; AtpA/B: α/β subunits of ATP synthase. C) SDS-PAGE analysis of TM isolated from WT and Δ*ftsH4* strains supplemented with lincomycin and exposed to HL for 6 h. The SDS gels were electroblotted to PVDF membrane and the blot was probed with antibodies specific for Ycf37, Ycf4 and D1. *Loaded samples were* normalized *per* number of cells. The obtained protein signals were quantified by AzureSpot Pro software v. 2.2.107 (Azure Biosystems). A ratio (percentage) of each analysed substrate in comparison to 100 % in calibration is shown, values are means of 3 independent measurements ± standard deviation.

under iron depletion [39,47]. To test whether the IsiA is degraded by the FtsH4 protease *in vivo*, we monitored the level of IsiA in WT and Δ*ftsH4* cells during recovery from iron depletion. Initially, we exposed both strains to iron stress to induce the expression of *isiA* gene; iron-depleted conditions were induced by transferring the cells grown in BG11 to the BG11 lacking iron ($-Fe^{2+}$) and supplemented by Deferoxamine B chelator to remove iron traces.

After 72 h of the low-iron stress, we observed no difference in the level of IsiA in WT and Δ*ftsH4* strains (Fig. 4). However, when we replaced the medium with normal BG11 supplemented with iron, the degradation of IsiA in the mutant was clearly retarded. The difference was most prominent after 24 h of the recovery when the WT contained 40 % of the initial IsiA level while Δ*ftsH4* values remained twice as high (Fig. 4). Because FtsH4 was purified with Fur, which functions as a repressor of IsiA expression, we wanted to exclude the possibility that the accumulation of IsiA in ΔftsH4 is due to lower levels of Fur protein. Therefore, we also monitored the level of Fur during recovery from iron depletion. Nevertheless, in agreement with [15] the Fur levels increased during the course of recovery in both WT and ΔftsH4. Thus, we concluded that slower decrease in the IsiA level during recovery from iron depletion in the ΔftsH4 is not related to the lower accumulation of Fur and that the data support involvement of FtsH4 in the degradation of IsiA.

3.5. Validation of putative FtsH4 substrates using an in vitro FtsH assay

Results of the FtsH4 trap approach as well as the analysis of protein content in FtsH4 mutant strains indicated that PSI assembly factors, the PsaB PSI subunit and IsiA are potential substrates. To confirm that the FtsH4 can recognize and degrade these proteins, we performed an *in vitro* assay of FtsH4 proteolytic activity using the purified FtsH4-His as an active enzyme (see Material and Methods). For negative control, the protease activity was inhibited with EDTA. We tested first purified FLAG-PSI complexes, isolated from the strain expressing FLAG-tagged *psaA* instead of *psaA* (*f.psaA* strain), as a substrate (Fig. 5A; Fig. S1). During incubation with the active purified protease we did not detect any decrease in the level of FLAG-tagged PsaA (F.PsaA) and only a small decrease in PsaB (−EDTA) when compared with the negative control

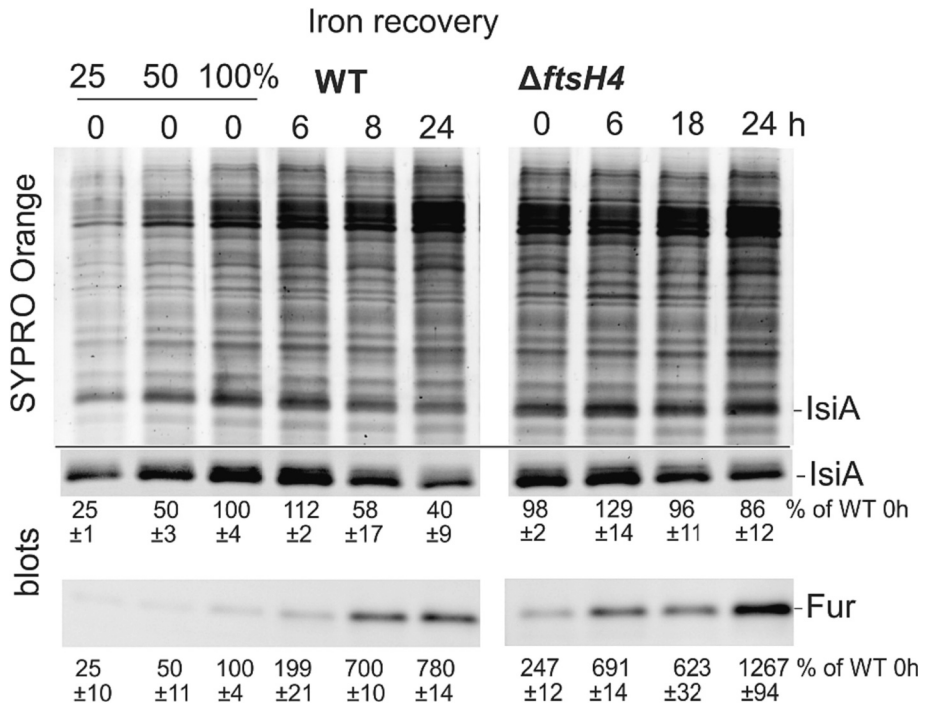

Fig. 4. Levels of IsiA in WT and Δ*ftsH4* cells after iron depletion and during the recovery from iron stress. Membrane proteins were isolated from WT and Δ*ftsH4* mutant exposed to iron depletion for 72 h and then were harvested at 0 h, 6 h, 18 h, and 24 h after the shift from iron depletion to normal BG11 medium (+Fe^{2+}). Membrane proteins were separated by SDS-PAGE and stained by SYPRO Orange, electroblotted to PVDF membrane and the blot probed with antibodies specific for IsiA and Fur. Samples were loaded per the same $OD_{750\ nm}$ of 0.3. The obtained protein signals were quantified by AzureSpot Pro software v. 2.2.107 (Azure Biosystems). A ratio (percentage) of each analysed substrate in comparison to 100 % in calibration is shown, values are means of 3 independent measurements ± standard deviation.

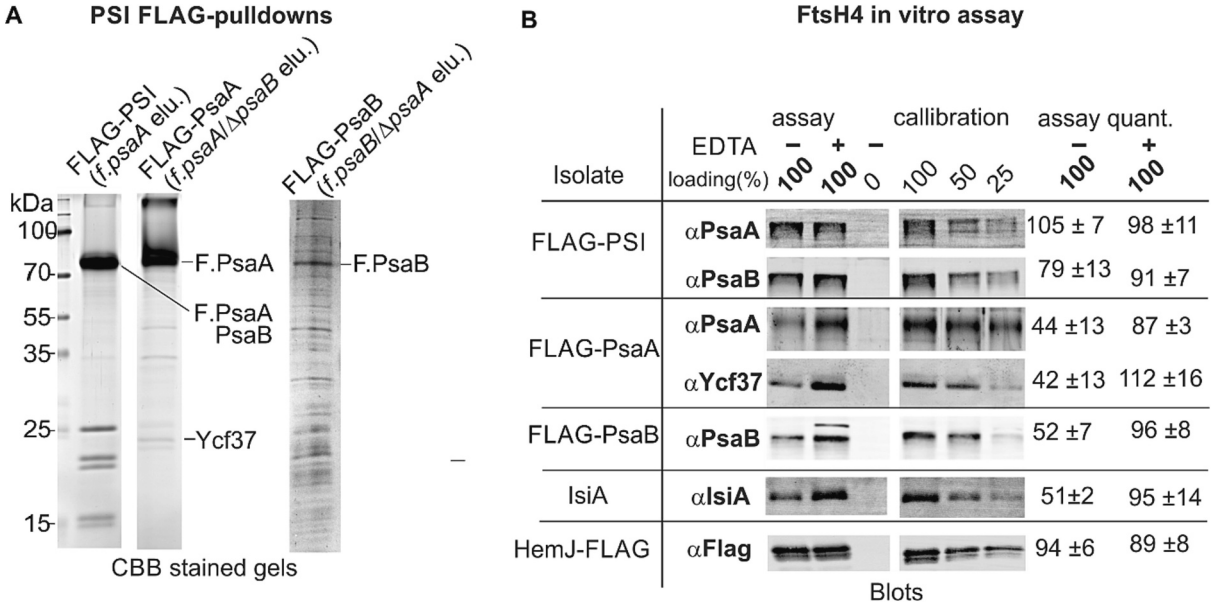

Fig. 5. Isolation of PSI, unassembled FLAG-PsaA/FLAG-PsaB subunits, IsiA and their digestion by FtsH4 *in vitro*. A) Analysis of PSI FLAG pulldowns. FLAG-PSI is an intact PSI complex isolated using F.PsaA protein produced in WT background (*f.psaA* strain) while the FLAG-PsaA (*f.psaA/ΔpsaB strain*) and FLAG-PsaB (*f.psaB/ΔpsaA strain*) elutions contained unassembled PSI core proteins. 10 µl of 10 times concentrated pulldowns were loaded onto the gel, which was then stained with Coomassie Blue. The identity of Ycf37 was verified by MS and immunodetection (Fig. S6B). B) FLAG-PSI, FLAG-PsaA, FLAG-PsaB and HemJ-FLAG pulldowns and IsiA gel extract were used as substrates for the FtsH4 activity assay. Adding 5 mM EDTA (+) inhibits the protease activity. At the start of the reaction, samples contained 0.3 µg of FtsH4 protein and 0.2 µg of the substrate in total, corresponding to 100 % in calibration; a control sample with no substrate added (0 %) is also shown. All samples were incubated for 3 h at 37 °C (see Material and Methods for details). After incubation, the samples were separated by SDS-PAGE, electroblotted to PVDF membrane and the presence of substrates and FtsH4 was detected by antibodies. According to substrate calibration, the obtained protein signals (in B) were quantified by AzureSpot Pro software v. 2.2.107 (Azure Biosystems). A ratio (percentage) of each analysed substrate in comparison to 100 % in calibration is shown, values are means of 3 independent reactions ± standard deviation. (For interpretation of the references to colour in this figure legend, the reader is referred to the web version of this article.)

(+EDTA) or with 100 % of a substrate in a calibration line (Fig. 5B). It indicates that the core proteins assembled in the PSI complex are not easily degraded by the FtsH4 protease.

To obtain unassembled PSI core subunits for the FtsH4 assay, we constructed *Synechocystis* strains producing either F.PsaA or FLAG-PsaB (F.PsaB) only, each in a genetic background lacking the second PSI core subunits (*f.psaA/ΔpsaB* and *f.psaB/ΔpsaA* strains — see Fig. S1). The resulting mutants showed a typical ΔPSI phenotype with a very low Chl level [48]. Importantly, F.PsaA and F.PsaB proteins could be detected by anti-FLAG antibody (Fig. S6A) and isolated, albeit the accumulation of FLAG-PsaB in TM is much lower than of FLAG-PsaA (Fig. S6A) and the amount of the purified F.PsaB is also low (Fig. 5A). Notably, the Ycf37 factor was co-eluted with F.PsaA (Fig. S6B) allowing us to test the Ycf37 as a substrate for FtsH4.

Fig. 5B shows that after 3 h in the assay, the amount of the Ycf37 decreased by >60 %. As expected, the substrate levels were not reduced in a control sample containing 5 mM EDTA. Importantly, by utilizing the unassembled F.PsaA and F.PsaB subunits as substrates, about half of this protein content was degraded.

To isolate IsiA as a substrate for *in vitro* FtsH4 assay, we separated membranes from WT grown under 72 h of iron depletion on the CN gel and extracted IsiA complexes from the CN gel. We focused on the monomeric IsiA not assembled with the PSI complex, (see Fig. S6C). The amount of IsiA decreased by 50 % after 3 h of the reaction with active FtsH4 protease while IsiA levels were only slightly reduced in a control sample containing 5 mM EDTA (Fig. 5B). These results also suggest that FtsH4 can degrade IsiA *in vitro*. We checked also the potential degradation of protoporphyrinogen IX oxidase enzyme (HemJ, Slr1790) involved in tetrapyrrole biosynthesis. This enzyme was identified among the 44 putative substrates of FtsH4 by MS and the purified FLAG-tagged HemJ protein (HemJ.f) is available in our laboratory [49]. However, we did not observe any significant decrease, which implies that this protein was not degraded by FtsH4 *in vitro*.

4. Discussion

The cyanobacterial FtsH4 and its plastid orthologs (*e.g. A. thaliana* AtFtsH7 and AtFtsH9) form a distinct phylogenetic subgroup of FtsH proteases [50]. These homo-oligomeric FtsHs differ structurally from hetero-oligomeric FtsH1/3 and FtsH2/3 and corresponding chloroplast FtsH2/FtsH8 complexes and seem to have little or no functional overlap with them. The unique function of FtsH4 is documented by a different regulation of this protease complex in *Synechocystis* (Fig. S3). While the level of FtsH1/2 and FtsH2/3 complexes decreased in the stationary phase and increased after shift to HL, the level of FtsH4 increased during the transition to stationary phase with its peak in linear growth phase and decreased after long-term exposition to HL. Different regulation was also observed at the transcript level (Fig. S2 [51]).

Recently, we have shown that the FtsH4 complex is not involved in the repair of PSII damaged by high irradiance or oxidative stress [7]. However, it is required for efficient acclimation of cell to sudden changes in light intensity. It controls the biogenesis of PSII by dual regulation of the level of Hlips [17]. Firstly, FtsH4 promotes the expression of Hlips after shift to high irradiance, most likely by modulation of the Hik33/RpaB regulon [7]. This role seems to be particularly crucial for cells exposed to HL after reaching the stationary phase; under these conditions the lack of FtsH4 is lethal. At another regulatory level, the FtsH4 controls the turnover of Hlips and degrades these proteins once stress conditions relieve [7].

In this work, we applied the substrate trapping approach to identify additional putative FtsH4 substrates. The identified candidates for substrate were predominantly membrane proteins related to photosynthesis (Table S2). We did not detect Hlips HliA, HliB, and HliC as (already known) substrates of FtsH4 [7], however, the cell cultures used for pulldowns were grown under conditions that do not induce a high expression of the *hliA-C* genes. The constitutively produced HliD protein [52] was 3.5-fold more abundant in our trap pulldown compared with the active FtsH4 form but did not meet our strict criteria for significance. Although the HliD is most likely the 'true' substrate of FtsH4, the detection of very small hydrophobic proteins by MS is problematic, especially when they are present in lower amounts. It is possible that other small membrane proteins were not detected as statistically significant substrate candidates due to the limits in their MS detectability.

On the other hand, the identification of Ycf4 and Ycf37 assembly factors as FtsH4 substrates looks quite convincing. In WT, the expression of *ycf4* and *ycf37* genes remains stable after shift of cells to HL [51], but the level of these proteins is significantly reduced (Fig. 3). We found lower content of Ycf37 in the F4CF mutant overexpressing FtsH4 in comparison with WT (Fig. 3B) but there was no HL-induced degradation of Ycf37 and Ycf4 in the FtsH4 deletion mutant (Fig. 3C). In addition, the digestion of Ycf37 by FtsH4 protease was confirmed *in vitro* (Fig. 5). Our results also suggest that FtsH4 can regulate the level of both PsaB and PsaA PSI core proteins. Nevertheless, *in vivo* and *in vitro* analyses suggest that the FtsH4 protease is involved in degradation of unassembled PsaA or PsaB core subunits rather than the intact PSI complex (Figs. 4 and 5). The *in vitro* digestion was however not so efficient as in the case of small proteins such are Hlips or Ycf37, which might be due to the large mass of PsaA/B (~ 80 kDa). Since the FtsH4 exhibits strong auto-proteolytic activity [7], the protease itself might be simply degraded faster than the large substrate. Notably, the level of PSI in FtsH4-less cells is aberrantly high [7] (Fig. S5) and this mutant also accumulates PSI assembly intermediates (Fig. 2) when exposed to cold stress. We therefore propose that the FtsH4 degrades the Ycf4 and Ycf37 factors under conditions when the PSI biogenesis needs to be rapidly arrested; typically, after shifting *Synechocystis* cells from NL to HL. As shown previously in [53], in the first hours at HL, *Synechocystis* strongly reduces the synthesis of PSI to 'dilute' the cellular concentration of this complex, thereby adjusting the PSI to PSII stoichiometry for HL. This new ratio is then stabilized in HL-acclimated cells [53].

Both Ycf37 and Ycf4 are involved in the early steps of PSI assembly [26,54] and we therefore speculate that the FtsH4 limits the biogenesis of new PSI by lowering the level of assembly factors. The remaining free PSI core subunits and partially assembled PSI complexes can also be degraded by FtsH4 (Fig. 5). Because Chl biosynthesis is almost completely blocked for 2–3 h after shift to HL (Sobotka, R, unpublished data), Chl molecules, released from PSI assembly complexes, might be important for the maintenance of active PSII complexes during the early stage of acclimation to HL. This hypothesis is in line with the patchy localization of FtsH4 at the periphery of TM where the biogenesis of photosynthetic apparatus is expected to occur [7,54]. The current study confirmed that the FtsH4 co-localizes with YidC and rubredoxin A proteins involved in the biosynthesis and assembly of photosystem proteins [19,37] (Supplementary Dataset 1). As it is speculated that the PSII and PSI biogenesis proceeds in a coordinated way [54], it is likely that FtsH4 modulates the biogenesis of both photosystems.

Another PSI-related protein identified as a putative substrate of FtsH4 is IsiA. This protein is homologous to PSII core antenna protein CP43 and it is massively produced in cyanobacteria under iron deficiency — it can bind up to 50 % of Chl in iron-starved cyanobacteria [55]. During the recovery from iron limitation, this large Chl deposit is probably released from degraded IsiA to support building of new photosystems [55]. The expression of the *isiA* gene is also induced, but to a lesser extent, under oxidative or HL stress and in the stationary phase, while it is subdued under optimal conditions. We did not observe any accumulation of IsiA in membranes isolated from *ftsH4-his* and ^{trap}*ftsH4-his* cells (Fig. S4), the level of this protein was apparently very low and the interaction between IsiA and FtsH4 thus must be very specific. The control of IsiA level by FtsH4 is supported by delayed IsiA degradation in Δ*ftsH4* mutant during the recovery from iron depletion (Fig. 4). It should be noted that IsiA was still degraded in Δ*ftsH4* (Fig. 4) and it is thus quite likely that other proteases participate in the IsiA digestion.

Although we focused on validation of substrates that are related to

the PSI complex, it is worth mentioning other proteins identified by our FtsH4 trap assay. One of the most prominent hits was the PetD subunit of the cytochrome b_6f complex. PetD binds the Chl molecule in cytochrome b_6f [56] and therefore exhibits the highest probability of the oxidative damage induced by this excited Chl. In line with its higher turnover, PetD is the only subunit of the complex which shows a clear radioactive labelling in *Synechocystis* (Fig. S6). Notably, components of cytochrome b_6f have already been considered a potential FtsH substrate in *Chlamydomonas* [6].

Remarkable is also the enrichment of proteins connected with CO_2 concentrating mechanism such as SbtA, SbtB, and CupA. Since their accumulation together with flavoproteins, Slr1634, Ycf23, and Sll1514 increases in response to low CO_2 and is controlled by NdhR regulon [57], we do not assume that all these hits are FtsH4 substrates. In fact, the level of these proteins might be just high in ^{trap}*ftsH4-his* strain due to the lack of FtsH4 (regulatory) activity. Alternatively, some of these proteins are real substrates but others are pulled out due to interaction with the substrate. For instance, SbtB, Flv2, and Flv4 were present only in the trap pulldown while other CCM proteins were co-isolated with active protease. Hypothetically, SbtB or Flv2/4 specifically trapped in inactive FtsH4 might serve as FtsH4 substrates associated with other proteins. These results, together with the fact that the FtsH4-His is copurified with Slr0374, another protein important for CO_2 uptake, suggest that the FtsH4 plays an important role in the acquisition of inorganic carbon.

Supplementary data to this article can be found online at https://doi.org/10.1016/j.bbabio.2023.149017.

CRediT authorship contribution statement

V.K., R.S., J.K. and P.K. designed the study, P.K., V.K., M.T., P.S. and S.D. performed research and obtained all results; V.K., R.S., J.K. and P.K. analysed data and wrote the paper. All authors discussed and critically read the manuscript.

Declaration of competing interest

The authors declare that they have no known competing financial interests or personal relationships that could have appeared to influence the work reported in this paper.

Data availability

The MS proteomics data were deposited in the MassIVE. The link to the MS Data will be shared in Manuscript in Method section

Acknowledgements

This work was supported by the Czech Science Foundation (19-08900Y to V.K., 19-29225X to J.K. and R.S.). P.K. acknowledges support from the Czech Ministry of Education, Youth and Sport (CZ.02.1.01/0.0/0.0/15_003/0000441).

References

[1] K. Ito, Y. Akiyama, Cellular functions, mechanism of action, and regulation of FtsH protease, Annu. Rev. Microbiol. 59 (2005) 211–231.
[2] Z. Adam, A. Zaltsman, G. Sinvany-Villalobo, W. Sakamoto, FtsH proteases in chloroplasts and cyanobacteria, Physiol. Plant. 123 (2005) 386–390.
[3] S. Jarvi, M. Suorsa, L. Tadini, A. Ivanauskaite, S. Rantala, Y. Allahverdiyeva, D. Leister, E.M. Aro, Thylakoid-bound FtsH proteins facilitate proper biosynthesis of photosystem I, Plant Physiol. 171 (2016) 1333–1343.
[4] Y. Kato, E. Miura, R. Matsushima, W. Sakamoto, White leaf sectors in yellow variegated2 are formed by viable cells with undifferentiated plastids, Plant Physiol. 144 (2007) 952–960.
[5] M. Yoshioka, S. Uchida, H. Mori, K. Komayama, S. Ohira, N. Morita, T. Nakanishi, Y. Yamamoto, Quality control of photosystem II — cleavage of reaction center D1 protein in spinach thylakoids by FtsH protease under moderate heat stress, J. Biol. Chem. 281 (2006) 21660–21669.
[6] A. Malnoe, F. Wang, J. Girard-Bascou, F.-A. Wollman, C. de Vitry, Thylakoid FtsH protease contributes to photosystem II and cytochrome b_6f remodeling in *Chlamydomonas reinhardtii* under stress conditions, Plant Cell 26 (2014) 373–390.
[7] V. Krynická, P. Skotnicová, P.J. Jackson, S. Barnett, J. Yu, A. Wysocka, R. Kaňa, M. J. Dickman, P.J. Nixon, C.N. Hunter, J. Komenda, FtsH4 protease controls biogenesis of the PSII complex by dual regulation of high light-inducible proteins, Plant Commun. 4 (2023), 100502.
[8] P.J. Jackson, A. Hitchcock, A.A. Brindley, M.J. Dickman, C.N. Hunter, Absolute quantification of cellular levels of photosynthesis-related proteins in *Synechocystis* sp. PCC 6803, Photosynth. Res. 155 (2023) 219–245.
[9] F. Yu, S. Park, S.R. Rodermel, The *Arabidopsis* FtsH metalloprotease gene family: interchangeability of subunits in chloroplast oligomeric complexes, Plant J. 37 (2004) 864–876.
[10] P. Silva, E. Thompson, S. Bailey, O. Kruse, C.W. Mullineaux, C. Robinson, N. H. Mann, P.J. Nixon, FtsH is involved in the early stages of repair of photosystem II in *Synechocystis* sp PCC 6803, Plant Cell 15 (2003) 2152–2164.
[11] V. Krynická, S. Shao, P.J. Nixon, J. Komenda, Accessibility controls selective degradation of photosystem II subunits by FtsH protease, Nat. Plants 1 (2015).
[12] J. Komenda, M. Barker, S. Kuviková, R. de Vries, C.W. Mullineaux, M. Tichý, P. J. Nixon, The FtsH protease *slr0228* is important for quality control of photosystem II in the thylakoid membrane of *Synechocystis* sp PCC 6803, J. Biol. Chem. 281 (2006) 1145–1151.
[13] N.H. Mann, N. Novac, C.W. Mullineaux, J. Newman, S. Bailey, C. Robinson, Involvement of an FtsH homologue in the assembly of functional photosystem I in the cyanobacterium *Synechocystis* sp PCC 6803, FEBS Lett. 479 (2000) 72–77.
[14] J. Sacharz, S.J. Bryan, J. Yu, N.J. Burroughs, E.M. Spence, P.J. Nixon, C. W. Mullineaux, Sub-cellular location of FtsH proteases in the cyanobacterium *Synechocystis* sp PCC 6803 suggests localised PSII repair zones in the thylakoid membranes, Mol. Microbiol. 96 (2015) 448–462.
[15] V. Krynická, M. Tichý, J. Krafl, J. Yu, R. Kana, M. Boehm, P.J. Nixon, J. Komenda, Two essential FtsH proteases control the level of the Fur repressor during iron deficiency in the cyanobacterium *Synechocystis* sp PCC 6803, Mol. Microbiol. 94 (2014) 609–624.
[16] V. Krynická, J. Georg, P.J. Jackson, M.J. Dickman, C.N. Hunter, M.E. Futschik, W. R. Hess, J. Komenda, Depletion of the FtsH1/3 proteolytic complex suppresses the nutrient stress response in the cyanobacterium *Synechocystis* sp strain PCC 6803, Plant Cell 31 (2019) 2912–2928.
[17] J. Komenda, R. Sobotka, Cyanobacterial high-light-inducible proteins—protectors of chlorophyll-protein synthesis and assembly, Biochim. Biophys. Acta 1857 (2016) 288–295.
[18] M.M. Konert, A. Wysocka, P. Koník, R. Sobotka, High-light-inducible proteins HliA and HliB: pigment binding and protein-protein interactions, Photosynth. Res. 152 (2022) 317–332.
[19] J. Knoppová, R. Sobotka, J. Yu, M. Bečková, J. Pilný, J.P. Trinugroho, L. Csefalvay, D. Bína, P.J. Nixon, J. Komenda, Assembly of D1/D2 complexes of photosystem II: binding of pigments and a network of auxiliary proteins, Plant Physiol. 187 (2022) 790–804.
[20] M. Tichý, B. Martina, J. Kopečná, J. Noda, R. Sobotka, J. Komenda, Strain of *Synechocystis* PCC 6803 with aberrant assembly of photosystem II contains tandem duplication of a large chromosomal region, Front. Plant Sci. 7 (2016).
[21] J.G. Metz, P.J. Nixon, M. Rögner, G.W. Brudvig, B.A. Diner, Directed alteration of the D1 polypeptide of photosystem II: evidence that tyrosine-161 is the redox component, Z, connecting the oxygen-evolving complex to the primary electron donor, P680, Biochemistry 28 (1989) 6960–6969.
[22] R.J. Porra, W.A. Thompson, P.E. Kriedemann, Determination of accurate extinction coefficients and simultaneous equations for assaying chlorophylls a and b extracted with four different solvents: verification of the concentration of chlorophyll standards by atomic absorption spectroscopy, Biochim. Biophys. Acta Bioenerg. 975 (1989) 384–394.
[23] J. Komenda, V. Krynická, T. Zakar, Isolation of thylakoid membranes from the cyanobacterium *Synechocystis* sp. PCC 6803 and analysis of their photosynthetic pigment-protein complexes by Clear Native-PAGE, Bio Protoc. 9 (2019).
[24] M. Boehm, J. Yu, V. Krynická, M. Barker, M. Tichý, J. Komenda, P.J. Nixon, J. Nield, Subunit organization of a *Synechocystis* hetero-oligomeric thylakoid FtsH complex involved in photosystem II repair, Plant Cell 24 (2012) 3669–3683.
[25] Q. Xu, Y.S. Jung, V.P. Chitnis, J.A. Guikema, J.H. Golbeck, P.R. Chitnis, Mutational analysis of photosystem I polypeptides in *Synechocystis* sp. PCC 6803. Subunit requirements for reduction of NADP+ mediated by ferredoxin and flavodoxin, J. Biol. Chem. 269 (1994) 21512–21518.
[26] U. Dühring, K.D. Irrgang, K. Lünser, J. Kehr, A. Wilde, Analysis of photosynthetic complexes from a cyanobacterial ycf37 mutant, Biochim. Biophys. Acta 1757 (2006) 3–11.
[27] M. Koskela, P. Skotnicová, E. Kiss, R. Sobotka, Purification of protein-complexes from the cyanobacterium *Synechocystis* sp. PCC 6803 using FLAG-affinity chromatography, Bio Protoc. 10 (2020).
[28] T. Tomoyasu, J. Gamer, B. Bukau, M. Kanemori, H. Mori, A.J. Rutman, A. B. Oppenheim, T. Yura, K. Yamanaka, H. Niki, S. Hiraga, T. Ogura, *Escherichia coli* FtsH is a membrane-bound, ATP-dependent protease which degrades the heat-shock transcription factor sigma 32, EMBO J. 14 (1995) 2551–2560.
[29] J. Rappsilber, M. Mann, Y. Ishihama, Protocol for micro-purification, enrichment, pre-fractionation and storage of peptides for proteomics using StageTips, Nat. Protoc. 2 (2007) 1896–1906.
[30] J. Cox, M. Mann, MaxQuant enables high peptide identification rates, individualized p.p.b.-range mass accuracies and proteome-wide protein quantification, Nat. Biotechnol. 26 (2008) 1367–1372.

[31] S. Tyanova, T. Temu, J. Cox, The MaxQuant computational platform for mass 0spectrometry-based shotgun proteomics, Nat. Protoc. 11 (2016) 2301–2319.
[32] S. Tyanova, T. Temu, P. Sinitcyn, A. Carlson, M.Y. Hein, T. Geiger, M. Mann, J. Cox, The Perseus computational platform for comprehensive analysis of (prote) omics data, Nat. Methods 13 (2016) 731–740.
[33] L. Atorino, L. Silvestri, M. Koppen, L. Cassina, A. Ballabio, R. Marconi, T. Langer, G. Casari, Loss of m-AAA protease in mitochondria causes complex I deficiency and increased sensitivity to oxidative stress in hereditary spastic paraplegia, J. Cell Biol. 163 (2003) 777–787.
[34] K. Westphal, S. Langklotz, N. Thomanek, F. Narberhaus, A trapping approach reveals novel substrates and physiological functions of the essential protease FtsH in *Escherichia coli*, J. Biol. Chem. 287 (2012) 42962–42971.
[35] B. Schwanhausser, D. Busse, N. Li, G. Dittmar, J. Schuchhardt, J. Wolf, W. Chen, M. Selbach, Global quantification of mammalian gene expression control, Nature 473 (2011) 337–342.
[36] H.B. Jiang, W.Y. Song, H.M. Cheng, B.S. Qiu, The hypothetical protein Ycf46 is involved in regulation of CO_2 utilization in the cyanobacterium *Synechocystis* sp. PCC 6803, Planta 241 (2015) 145–155.
[37] É. Kiss, J. Knoppová, G.P. Aznar, J. Pilný, J. Yu, P. Halada, P.J. Nixon, R. Sobotka, J. Komenda, A photosynthesis-specific Rubredoxin-like protein is required for efficient association of the D1 and D2 proteins during the initial steps of photosystem II assembly, Plant Cell 31 (2019) 2241–2258.
[38] E.J. Boekema, A. Hifney, A.E. Yakushevska, M. Piotrowski, W. Keegstra, S. Berry, K.P. Michel, E.K. Pistorius, J. Kruip, A giant chlorophyll-protein complex induced by iron deficiency in cyanobacteria, Nature 412 (2001) 745–748.
[39] T.S. Bibby, J. Nield, J. Barber, Iron deficiency induces the formation of an antenna ring around trimeric photosystem I in cyanobacteria, Nature 412 (2001) 743–745.
[40] C.E. Lubner, R. Grimme, D.A. Bryant, J.H. Golbeck, Wiring photosystem I for direct solar hydrogen production, Biochemistry 49 (2010) 404–414.
[41] J.H. Golbeck, D.A. Bryant, Photosystem I, in: C.P. Lee (Ed.), Current Topics in Bioenergetics, Academic Press, 1991, pp. 83–177.
[42] J.-D. Rochaix, Chloroplast reverse genetics: new insights into the function of plastid genes, Trends Plant Sci. 2 (1997) 419–425.
[43] A. Wilde, K. Lünser, F. Ossenbühl, J. Nickelsen, T. Börner, Characterization of the cyanobacterial ycf37: mutation decreases the photosystem I content, Biochem. J. 357 (2001) 211–216.
[44] I. Orf, D. Schwarz, A. Kaplan, J. Kopka, W.R. Hess, M. Hagemann, S. Klähn, CyAbrB2 contributes to the transcriptional regulation of low CO_2 acclimation in *Synechocystis* sp. PCC 6803, Plant Cell. Physiol. 57 (2016) 2232–2243.
[45] Y. Hihara, K. Sonoike, Regulation, inhibition and protection of photosystem I, in: E.-M. Aro, B. Andersson (Eds.), Regulation of Photosynthesis, Springer, Netherlands, Dordrecht, 2001, pp. 507–531.
[46] Regulation of Photosynthesis, 1st ed., Springer Netherlands, 2001. Imprint: Springer, Dordrecht, 2001.
[47] A.K. Singh, L.A. Sherman, Iron-independent dynamics of IsiA production during the transition to stationary phase in the cyanobacterium *Synechocystis* sp PCC 6803, FEMS Microbiol. Lett. 256 (2006) 159–164.
[48] G. Shen, W.F. Vermaas, Chlorophyll in a *Synechocystis* sp. PCC 6803 mutant without photosystem I and photosystem II core complexes. Evidence for peripheral antenna chlorophylls in cyanobacteria, J. Biol. Chem. 269 (1994) 13904–13910.
[49] P. Skotnicová, R. Sobotka, M. Shepherd, J. Hájek, P. Hrouzek, M. Tichý, The cyanobacterial protoporphyrinogen oxidase HemJ is a new b-type heme protein functionally coupled with coproporphyrinogen III oxidase, J. Biol. Chem. 293 (2018) 12394–12404.
[50] T. Cardona, S. Shao, P.J. Nixon, Early emergence of the FtsH proteases involved in photosystem II repair, Photosynthetica 56 (2018) 163–177.
[51] M. Kopf, S. Klaehn, I. Scholz, J.K.F. Matthiessen, W.R. Hess, B. Voss, Comparative analysis of the primary transcriptome of *Synechocystis* sp PCC 6803, DNA Res. 21 (2014) 527–539.
[52] Q. He, N. Dolganov, O. Bjorkman, A.R. Grossman, The high light-inducible polypeptides in *Synechocystis* PCC6803. Expression and function in high light, J. Biol. Chem. 276 (2001) 306–314.
[53] J. Kopečná, J. Komenda, L. Bučinská, R. Sobotka, Long-term acclimation of the cyanobacterium *Synechocystis* sp PCC 6803 to high light is accompanied by an enhanced production of chlorophyll that is preferentially channeled to trimeric photosystem I, Plant Physiol. 160 (2012) 2239–2250.
[54] J. Komenda, R. Sobotka, Chlorophyll-binding subunits of photosystem I and II: biosynthesis, chlorophyll incorporation and assembly, Adv. Bot. Res. 91 (2019) 195–223.
[55] A. Jia, Y. Zheng, H. Chen, Q. Wang, Regulation and functional complexity of the chlorophyll-binding protein IsiA, Front. Microbiol. 12 (2021), 774107.
[56] W.A. Cramer, Structure-function of the cytochrome b(6)f lipoprotein complex: a scientific odyssey and personal perspective, Photosynth. Res. 139 (2019) 53–65.
[57] S. Klähn, I. Orf, D. Schwarz, J.K.F. Matthiessen, J. Kopka, W.R. Hess, M. Hagemann, Integrated transcriptomic and metabolomic characterization of the low-carbon response using an ndhR mutant of *Synechocystis* sp PCC 6803, Plant Physiol. 169 (2015) 1540–1556.

Cell Reports

Report

Chlorophyll biosynthesis under the control of arginine metabolism

Graphical abstract

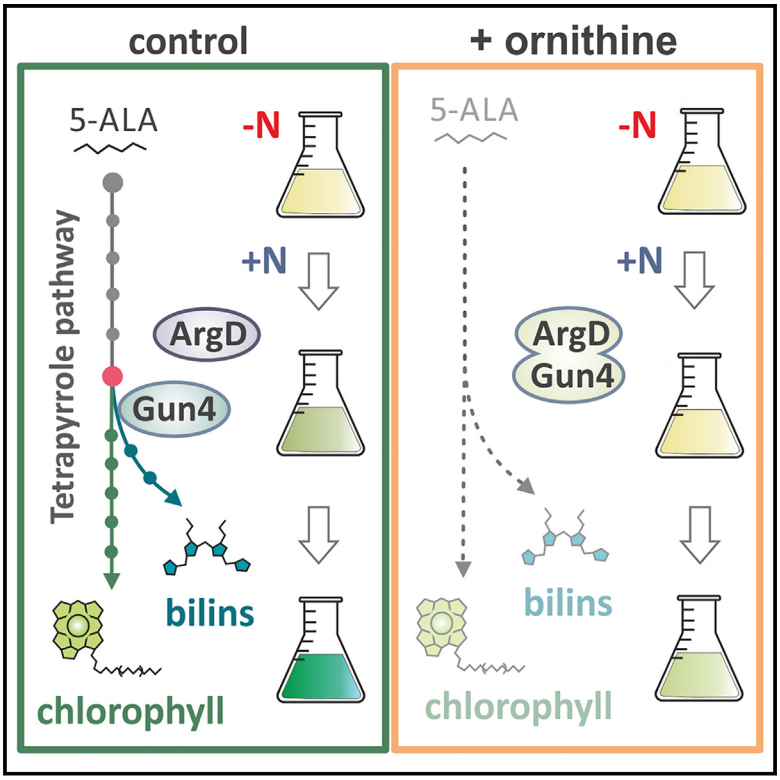

Highlights

- ArgD of arginine pathway interacts with the Gun4 protein of chlorophyll biosynthesis
- Ornithine stimulates the ArgD-Gun4 interaction and inhibits tetrapyrrole synthesis
- The inhibition by ornithine is released in a strain lacking the ArgD-Gun4 complex

Authors

Éva Kiss, Jana Talbot, Nathan B.P. Adams, ..., Peter Koník, Petr Šimek, Roman Sobotka

Correspondence

sobotka@alga.cz

In brief

Kiss et al. demonstrate that the synthesis of the main photosynthetic pigment, chlorophyll, and the metabolism of arginine (managing N-stockpile) are functionally coupled via protein-protein interactions in cyanobacteria.

Kiss et al., 2023, Cell Reports *42*, 113265
November 28, 2023
https://doi.org/10.1016/j.celrep.2023.113265

CellPress

Cell Reports

CellPress
OPEN ACCESS

Report

Chlorophyll biosynthesis under the control of arginine metabolism

Éva Kiss,[1] Jana Talbot,[1,6] Nathan B.P. Adams,[2,3] Stanislav Opekar,[4] Martin Moos,[4] Jan Pilný,[1] Tatjana Kvasov,[2] Emilia Schneider,[2] Peter Koník,[1,5] Petr Šimek,[4] and Roman Sobotka[1,5,7,*]

[1]Laboratory of Photosynthesis, Centre Algatech, Institute of Microbiology, The Czech Academy of Sciences, 37901 Třeboň, Czech Republic
[2]NanoTemper Technologies, Floessegasse 4, 81369 Munich, Germany
[3]Department of Molecular Biology and Biotechnology, University of Sheffield, Sheffield S10 2TN, UK
[4]Biology Centre of the Czech Academy of Sciences, Branišovská 1160/31, 370 05 České Budějovice, Czech Republic
[5]Faculty of Science, University of South Bohemia, 37005 České Budějovice, Czech Republic
[6]Present address: Wicking Dementia Research and Education Center, University of Tasmania, Hobart, TAS, Australia
[7]Lead contact
*Correspondence: sobotka@alga.cz
https://doi.org/10.1016/j.celrep.2023.113265

SUMMARY

In natural environments, photosynthetic organisms adjust their metabolism to cope with the fluctuating availability of combined nitrogen sources, a growth-limiting factor. For acclimation, the dynamic degradation/synthesis of tetrapyrrolic pigments, as well as of the amino acid arginine, is pivotal; however, there has been no evidence that these processes could be functionally coupled. Using co-immunopurification and spectral shift assays, we found that in the cyanobacterium *Synechocystis* sp. PCC 6803, the arginine metabolism-related ArgD and CphB enzymes form protein complexes with Gun4, an essential protein for chlorophyll biosynthesis. Gun4 binds ArgD with high affinity, and the Gun4-ArgD complex accumulates in cells supplemented with ornithine, a key intermediate of the arginine pathway. Elevated ornithine levels restricted *de novo* synthesis of tetrapyrroles, which arrested the recovery from nitrogen deficiency. Our data reveal a direct crosstalk between tetrapyrrole biosynthesis and arginine metabolism that highlights the importance of balancing photosynthetic pigment synthesis with nitrogen homeostasis.

INTRODUCTION

In natural environments, the fluctuating combined nitrogen (N) source is a growth-limiting factor. To cope with this constraint, photosynthetic organisms have to adjust their metabolism to the availability of N. For acclimation, the dynamic degradation/synthesis of tetrapyrrolic pigments (chlorophyll [Chl], bilins, hemes) as well as of the amino acid arginine (Arg) are evidently pivotal. Arg metabolism is in aid of balancing N availability for anabolic processes in a fluctuating environment.[1] The surplus N is primarily used for the synthesis of Arg that can be stockpiled in storage material, such as cyanophycin, which can be metabolized during N deficiency.[2] At the same time, N fluctuation causes extensive changes in the metabolism of tetrapyrroles. At low N, the accumulation of Chl and bilins is predominantly downregulated in a process called chlorosis or bleaching.[3,4] Since these tetrapyrroles are essential co-factors for photosynthetic apparatus, bleached cyanobacterial cells stop their photosynthetic activity.[5] When N becomes available, pigment synthesis is reactivated (regreening) for the biogenesis of photosynthetic machinery to allow photoautotrophic growth.[5]

Oxygenic phototrophs synthesize the main photosynthetic pigment, Chl, together with other tetrapyrroles via a common, branched pathway.[6] The tetrapyrrole pathway must be tightly regulated in virtually any type of organism since protoporphyrins and other pyrrolic intermediates are highly phototoxic.[7] In oxygenic phototrophs, the regulation of the tetrapyrrole pathway appears to be a particularly complicated task, as the pathway is branched and high quantities of end products (Chl, heme, bilins) are required for photosynthesis.[6] A sophisticated control mechanism(s) must evolve to counterbalance the pathway with other processes in the cell. In this way, the amounts of tetrapyrrole end products can vary depending on developmental stage and/or environmental conditions, and the accumulation of the phototoxic biosynthetic intermediates can be tightly coordinated.[6] How this regulation is accomplished remains mostly unclear. However, the main regulatory mechanisms appear linked to the formation of the rate-limiting precursor 5-aminolevulinc acid (5-ALA) and the branching between Chl and heme pathways.[8,9] At this branchpoint, the magnesium chelatase (MgCh) and ferrochelatase enzymes compete for the same protoporphyrin IX (P_{IX}) substrate.

The Gun4 protein has been recognized as a critical factor for the synthesis of Chl in cyanobacteria, as well as in algae and plants, and has been extensively studied by various biochemical and physiological approaches.[10–17] It is functionally linked to MgCh; however, *in vivo* characterization of Gun4 mutants revealed complex changes in tetrapyrrole metabolism far beyond

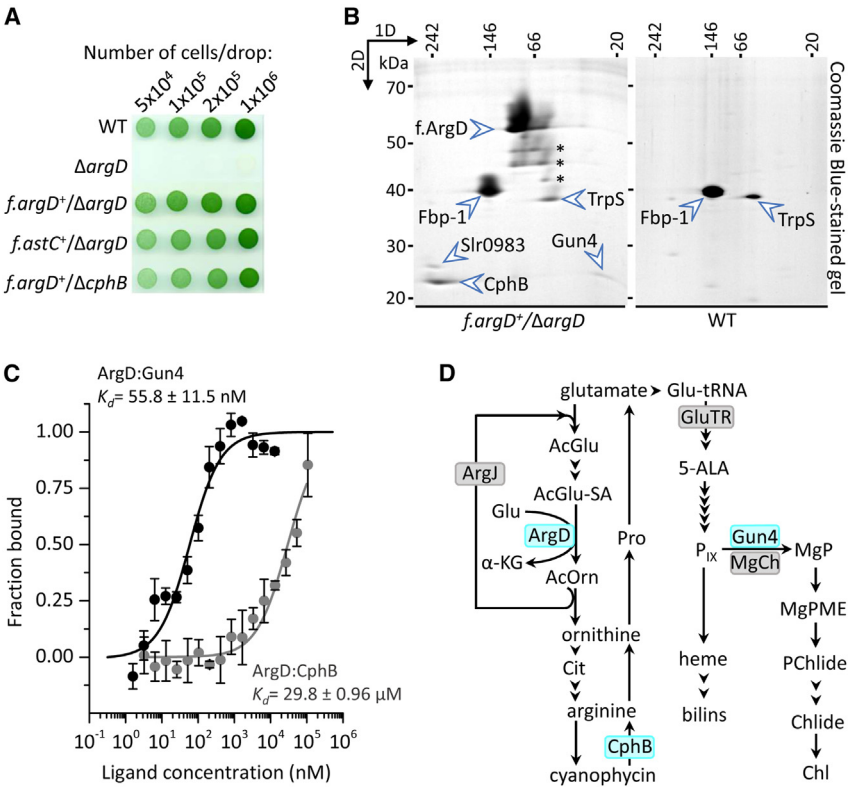

Figure 1. The Gun4 protein interacts with enzymes involved in Arg metabolism

(A) Photoautotrophic growth of *Synechocystis* strains constructed for anti-FLAG pull-downs.

(B) 2D BN/SDS-PAGE separation of *f.argD*$^+$/Δ*argD* and control (WT) pull-downs. The indicated protein dots were identified by MS (Table S2). Protein spots indicated by stars were identified as f.ArgD and most likely represent partially degraded fragments of f.ArgD.

(C) Quantitative analysis of the binding affinities of ArgD to CphB and Gun4. Recombinant proteins were analyzed with a spectral shift binding assay, where 5 nM labeled ArgD was titrated with CphB (gray symbols) or Gun4 (black symbols). Symbols and error bars represent the average data of three independent experiments and their standard deviation; the determined K_d values are indicated.

(D) The main steps of Arg metabolism and the biosynthesis of tetrapyrroles according to Flores et al.[29] and Sobotka[30] and references therein. The interacting protein partners found in this study are designated by blue boxes. AcGlu, N-acetylglutamate; AcGlu-SA, AcGlu semialdehyde; α-KG, α-ketoglutarate; AcOrn, N-acetylornithine; Cit, citrulline; Pro, proline; Glu-tRNA, glutamyl-tRNA; GluTR, Glu-tRNA reductase; MgPME, Mg protoporphyrin IX monomethyl ester; PChlide, divinyl protochlorophyllide *a*; Chlide, monovinyl chlorophyllide *a*.

what is expected from the altered MgCh activity.[16–23] These results imply that Gun4 can regulate tetrapyrrole biosynthesis in multiple ways.

Gun4 binds tightly to the ChlH subunit of MgCh, forming a membrane-localized complex, which is expected to be the site of Mg-P_{IX} (MgP) synthesis.[12,24,25] However, a fraction of Gun4 is localized in the cytosol/stroma.[12,24,25] Here, we show that in the cyanobacterium *Synechocystis* sp. PCC 6803 (hereafter *Synechocystis*), the soluble N-acetylornithine aminotransferase (ArgD) and cyanophycinase (CphB) enzymes interact with Gun4. CphB is a peptidase that breaks down the cyanophycin biopolymer into β-Asp-Arg dipeptides.[26] It is categorically found in cyanophycin-containing bacteria and is apparently dispensable in *Synechocystis*.[27] On the other hand, ArgD is an essential enzyme in Arg biosynthesis from bacteria to plants. Our study shows that ArgD binds Gun4 with high affinity and that the accumulation of the Gun4-ArgD complex is modulated by the cellular level of ornithine (Orn), a central intermediate of Arg biosynthesis. High levels of Orn inhibit Chl biosynthesis via an ArgD-dependent mechanism, supporting the role of the Gun4-ArgD complex in a cross-talk between the Arg and tetrapyrrole pathways.

RESULTS

The Gun4 protein interacts with enzymes involved in Arg metabolism

To better understand the metabolism of N in *Synechocystis*, we focused on the Arg metabolic pathway playing a central role in N homeostasis. Specifically, we used anti-FLAG pull-downs to identify protein interactors of enzymes involved in Arg biosynthesis. We constructed a strain expressing 3×FLAG-tagged ArgD (f.ArgD) from the constitutive *psbAII* promoter while lacking the native enzyme (*f.argD*$^+$/Δ*argD* strain; see Table S1). Unlike the Δ*argD* mutant, which is an Orn auxotroph,[28] the *f.argD*$^+$/Δ*argD* mutant proliferated without Orn supplement, showing growth and pigmentation comparable with the wild-type (WT) strain (Figure 1A).

The f.ArgD enzyme was isolated from the soluble fraction according to Koskela et al.,[31] and the obtained eluate was separated on a 2D blue native (BN)/SDS-PAGE together with a WT control. The resulting gel was stained, and the visible protein spots were identified by mass spectrometry (MS) (Figure 1B; Table S2). Tryptophanyl t-RNA synthetase (TrpS) and fructose-1,6-biphosphatase (Fbp-1) were evident contaminants, eluted from the FLAG resin also when using the WT control. On the other hand, despite their detachment from f.ArgD during the separation by BN, Slr0983 (hypothetical glucose-1-phosphate cytidylyltransferase homolog), CphB, and Gun4 were identified as specific co-eluates of f.ArgD (Figure 1B). CphB (29.4 kDa) migrated like a large oligomer (>200 kDa), which was more intensely stained than the spot of the apparently monomeric Gun4 (26.6 kDa). The mass of f.ArgD (49.8 kDa) on the BN gel appeared at about 100 kDa, indicating a dimer consistent with other studies.[32] Given the well-established and critical role of Gun4 in Chl biosynthesis,[24] we focused on the interaction of Gun4 with enzymes involved in Arg metabolism (ArgD and CphB).

To assess the *in vitro* affinities of *Synechocystis* ArgD to CphB and Gun4, we expressed these proteins in *Escherichia coli* (*E. coli*) as 6×His-tagged variants. After purification on a nickel column, recombinant proteins were subjected to isothermal spectral shift assays, in which a standard concentration of labeled ArgD was titrated with CphB or with Gun4. Fitting of the resultant binding isotherms revealed K_d values of 29.8 ± 0.96 μM and 55.8 ± 11.5 nM for the titration of ArgD with CphB and Gun4, respectively (Figure 1C). These results indicate that even though CphB and ArgD both participate in Arg metabolism (see Figure 1D), the *in vitro* binding affinity of ArgD to Gun4 is much stronger than to CphB.

Although Gun4 was recognized in a membrane-localized complex,[24,25] herein, it was shown to interact with the strictly soluble ArgD protein.[33] To confirm the presence of Gun4 in a cytosolic enzyme complex, the co-purification assay was repeated using a cytosolic extract of a *Synechocystis* strain expressing 3× FLAG-tagged Gun4 (f.Gun4). *In vivo* activity of Gun4 has been shown previously to be unaffected by the addition of FLAG tag.[25] The obtained f.Gun4 and control WT eluates were separated by SDS-PAGE and stained, and the most intense protein bands were analyzed by proteomic MS. Pyruvate kinase 1 (Pyk-1), ArgD, and CphB were the most abundant, specific co-eluates of f.Gun4 (Figure 2A; Table S3). The interaction of Gun4 with CphB was analyzed by *in vitro* spectral shift assays, revealing a K_d of 2.16 ± 0.64 μM (Figure 2B). This value indicates a ∼40 times weaker binding affinity of Gun4 to CphB compared with ArgD (Figure 1C).

ArgD strongly binds Gun4 *in vitro* (Figure 1C). Nevertheless, the relatively high level of CphB in the f.ArgD and f.Gun4 pull-downs (Figures 1B, 2A, 2C, and 2D) raises the question of whether CphB is important for the Gun4-ArgD interaction *in vivo*. To address this, we purified f.ArgD from the *cphB*-deletion background (Δ*cphB*) that shows no phenotypic changes during photoautotrophic growth[27] (see also Figure 1A). Since co-purification of Gun4 with f.ArgD was apparently not affected by the absence of CphB (Figures 2C and 2D), we concluded that CphB is not required for the accumulation of the Gun4-ArgD complex *in vivo*.

While Gun4 is specific for oxygenic phototrophs, ArgD is a housekeeping enzyme in virtually any organism. To investigate the role of the Gun4-ArgD complex in *Synechocystis*, we replaced the ArgD enzyme with its FLAG-tagged homolog (AstC) from *E. coli.* The resulting strain (*f.astC*$^+$/Δ*argD*) expressed the f.AstC enzyme to a level comparable to f.ArgD (Figure S1A) while showing no alteration in the accumulation of amino acids including Orn and Arg (Figures S1B and S1C). The purified f.AstC, however, did not co-elute with either Gun4 or CphB (Figures 2C and 2D), implying that the *E. coli* enzyme does not bind these proteins *in vivo*. The *f.astC*$^+$/Δ*argD* strain showed photoautotrophic growth similar to *f.argD*$^+$/Δ*argD* (Figure 1A) and exhibited no apparent phenotype under the various physiological conditions tested (Figures S2A–S2E).

Orn triggers the formation of the Gun4-ArgD complex and reduces the steady states of Chl precursors

Although the interaction of Gun4 with enzymes participating in Arg metabolism was not detectable in *f.astC*$^+$/Δ*argD*, no apparent growth defect was caused by the absence of these protein assemblages (Figures 1A and S2A–S2E). However, it is possible that Gun4-ArgD is important for regulation during severe or prolonged shifts in Arg metabolism, and such conditions are difficult to mimic in laboratory. As an alternative, we monitored the phenotype of studied strains after feeding with biosynthetic intermediates of Arg. Using metabolic profiling, we checked first the ability of *Synechocystis* to uptake N-acetylornithine (AcOrn), the enzymatic product of ArgD. The treatment of WT with 100 μM AcOrn for 40 min did not, however, increase the concentration of this compound in cells above the detection limit, suggesting an inefficient uptake (Figure S3A; Table S4). On the other hand, the same treatment with 100 μM Orn, which is the center intermediate metabolite for both Arg biosynthesis and degradation (see Figure 1D), elevated the concentration of intracellular Orn by three magnitudes. Orn also caused severe changes in the accumulation of other metabolites, including an increase of AcOrn (Figure S3A; Table S4). In line with previous studies,[29,34] Orn effectively redirected metabolic fluxes in the Arg pathway and likely blocked the initial steps of Arg synthesis.[35,36]

Given the well-established role of Gun4 in Chl biosynthesis,[24] we then compared the levels of biosynthetic intermediates of Chl in cells grown with $NaNO_3$ supplement with or without 1 mM Orn. We employed as a negative control the *f.astC*$^+$/Δ*argD* strain, in which the ArgD-Gun4 complex was undetectable (Figures 2C and 2D). While Orn apparently did not affect the pool of Chl precursors in *f.astC*$^+$/Δ*argD*, the *f.argD*$^+$/Δ*argD* and WT strains accumulated significantly ($p < 0.05$) lower relative amounts of the monitored tetrapyrroles (Figures 3A and S3B). Further cultivation in the Orn-containing BG-11 media resulted in decreased amount of bilins and Chl (Figure S3C). Consequently, all the strains used in the study had impaired photoautotrophy in the presence of Orn except for those that did not contain the ArgD enzyme (Δ*argD*, f.*astC*/Δ*argD*; Figure 3B). Orn was converted also to Arg (Figure S3A); however, the direct addition of Arg had a milder or no effect on the photoautotrophic growth (Figure S3D).

To test whether the lower accumulation of Chl precursors in the Orn-fed *f.argD*$^+$/Δ*argD* cells can be related to Gun4-ArgD, we compared the *in vivo* abundance of the complex in cells that were fed with nitrate supplement only or also with Orn before FLAG-affinity purification. Analysis of the obtained f.ArgD pull-downs revealed six times more Gun4 co-purified with f.ArgD from cells pre-treated with 1 mM Orn for 24 h (Figure 3C). It is notable that CphB was also more enriched in the eluate after Orn feeding. In our standard purification protocol, FLAG-tagged proteins are released from the resin under native conditions using FLAG-tag peptide.[31] To exclude the possibility that a fraction of the specifically bound proteins remained attached to the resin after elution, we performed another preparation in which proteins were released from the FLAG resin using SDS instead of FLAG peptide. Using this approach and subsequent immunodetection, we detected an even stronger Orn-stimulated enrichment of Gun4 (>12×) in the pull-down (Figure 3D). In this experiment, we monitored the effect of short-term (1 h) feeding with 100 μM Orn that also substantially increased the amount of f.ArgD-co-purified Gun4 (∼6 times; Figure 3D).

To see the extent of Gun4 sequestered from the membranes to the soluble ArgD-Gun4 complex, we performed western blot

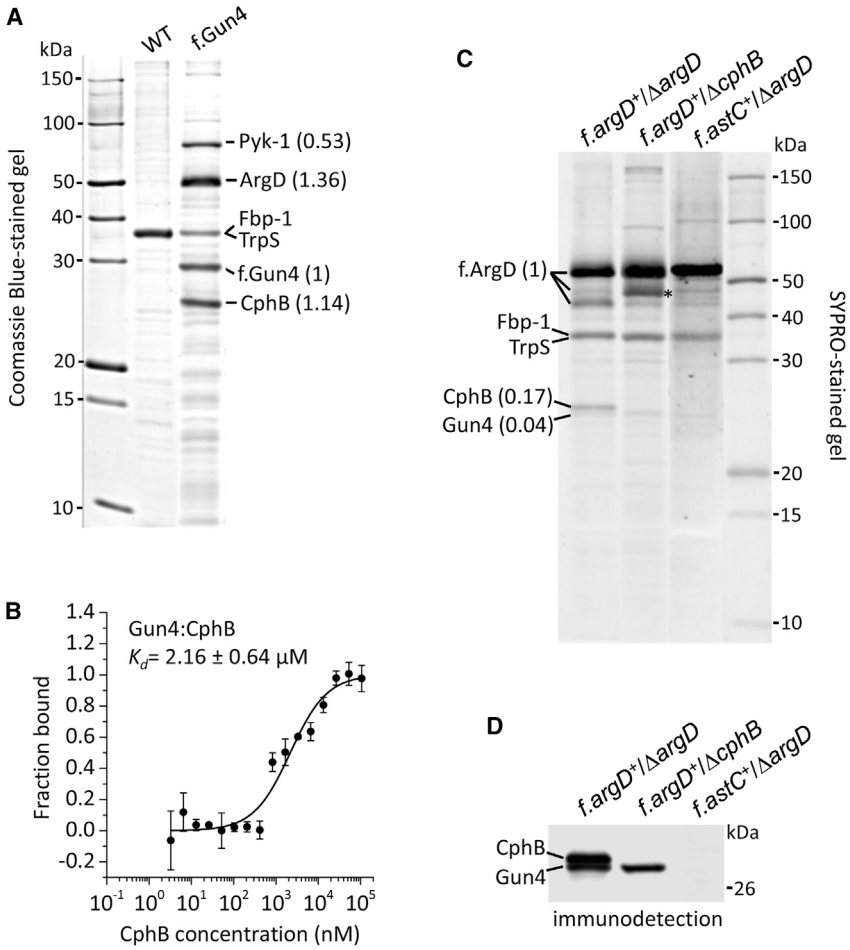

Figure 2. Gun4 is co-isolated with ArgD and CphB but not with the heterologously expressed *E. coli* AstC

(A) SDS-PAGE separation of the f.Gun4 and control (WT) pull-downs. The indicated proteins were identified by MS (Table S3). The molar ratios of co-eluted proteins, calculated from raw band intensities normalized to the molecular weights, are shown in brackets.

(B) Recombinant Gun4 and CphB proteins were subjected to a spectral shift assay, in which 20 nM labeled Gun4 was titrated with CphB. Symbols and error bars represent the average data of three independent experiments and their standard deviation; the obtained K_d value is shown.

(C) Protein pull-downs prepared from indicated strains were separated on SDS-PAGE and stained. Asterisk indicates the native ArgD that was present in the Δ*cphB* background. The molar ratios of co-eluted proteins are also indicated (see A).

(D) The SDS-PAGE gel shown in (C) was blotted to a polyvinylidene fluoride (PVDF) membrane and probed with specific antibodies against Gun4 and CphB.

analysis of the soluble (cytoplasm [C]) and insoluble (membrane [M]) fractions of cells with or without Orn treatment. In fact, a higher portion of Gun4 could be detected from the soluble fraction of the Orn-treated compared with the untreated *f.argD*$^+$/-Δ*argD* and WT but not of the *f.astC*$^+$/Δ*argD* cells (Figure 3E). On the other hand, Orn had the opposite effect on the relative distribution of CphB, as it could be detected from the insoluble fraction dependent on Orn treatment.

Orn inhibits *de novo* biosynthesis of tetrapyrroles and postpones recovery from nitrogen deprivation

To clarify whether the lower accumulation of Chl precursors in the presence of additional Orn was due to inhibition of *de novo* tetrapyrrole synthesis, we tested the effect of Orn on regreening cells, in which *de novo* pigment synthesis is cardinal.[37] Bleaching of the cultures was achieved by 20 h of N starvation, and the recovery was induced by the addition of 1 mM $NaNO_3$ alternatively combined with 100 μM Orn. When Orn was omitted from the N supply of the N-starved cultures, Chl precursors were synthetized within 40 min, and after an hour of N upshift, their relative amounts substantially increased in all strains studied (Figures 4A and S4A). However, unlike in the *f.astC*$^+$/Δ*argD* strains, in which Orn did not affect tetrapyrrole synthesis, in the control WT as well as in the *f.argD*$^+$/Δ*argD* strains, the accumulation of Chl precursors (including P_{IX}) was arrested for at least 3 h (Figures 4A and S4A). Consequently, in the Orn-fed WT and *f.argD*$^+$/Δ*argD*, the overall accumulation of Chl was inhibited (Figures 4B and S4B), and in the first 14 h of N upshift, the cell absorption remained comparable to that of the N-starved cultures (Figures 4C and S4C). On the other hand, 14 h of N upshift increased the tetrapyrrole pigment-binding complexes in *f.astC*$^+$/Δ*argD* regardless of the presence of Orn (Figure 4C), while in the Orn-fed WT as well as *f.argD*$^+$/Δ*argD*, the cell absorption peaks at 625 and 682 nm started to increase only after 30 h (Figures 4C and S4C), indicating accumulation of the phycobilin- (625 nm) and Chl-binding (682 nm) photosynthetic proteins that eventually allowed photoautotrophic growth (Figures 4D and S4E). The recovery of the N-starved, bleached WT cultures in the presence of Orn was thus much slower compared with the strain possessing the *E. coli* AstC enzyme (Figure 4E), while it was comparable with the Orn-fed *f.argD*$^+$/Δ*argD* cultures (Figure S4).

DISCUSSION

The Gun4 protein is specific and ubiquitous to oxygenic phototrophs, where it is essential for efficient Chl production. Consistent with the model of active, membrane-bound MgCh,[19] Gun4 was co-isolated with ChlH from thylakoids[24] or total cell extracts[25] but not from the cytosolic fraction (Figure 2A). Prior to this work, the only known protein partner of Gun4 was the ChlH subunit of MgCh. Herein, we identified *Synechocystis* Gun4 in a soluble protein complex(es) consisting of the Arg metabolism-related ArgD and CphB, as well as the Pyk-1

CellPress
OPEN ACCESS

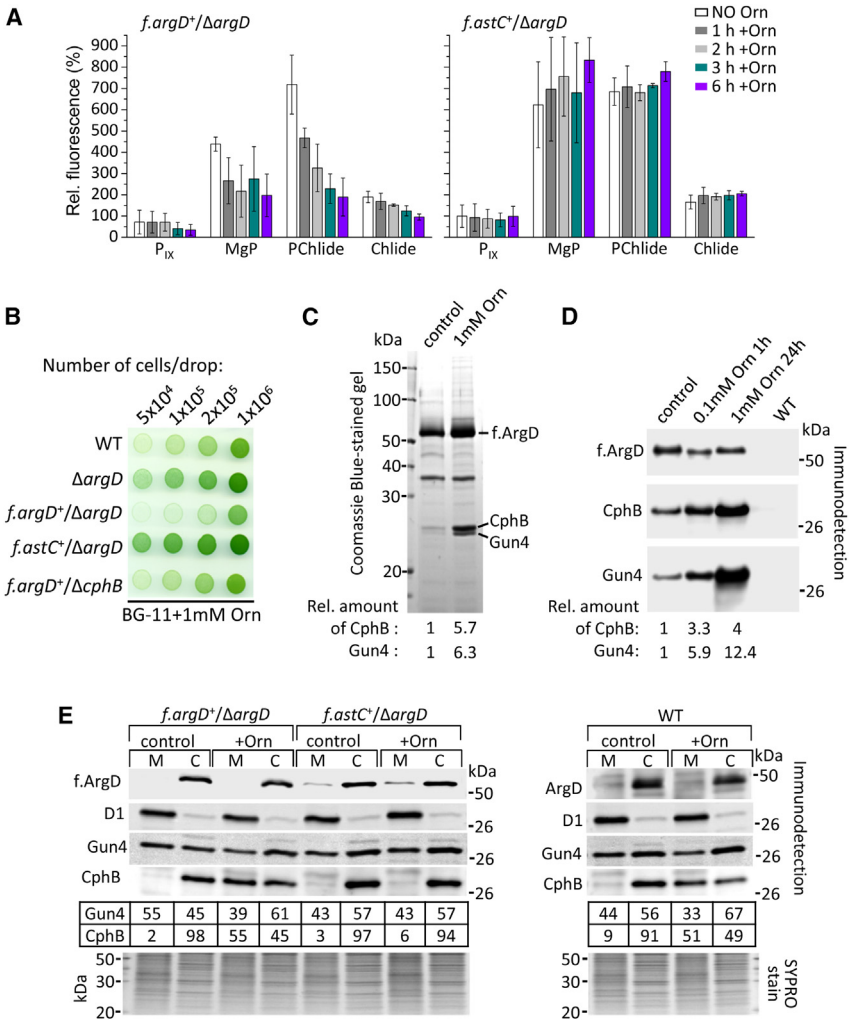

Figure 3. Orn triggers the *in vivo* formation of the Gun4-ArgD complex and reduces the steady states of Chl precursors

(A) The effect of Orn on the steady states of Chl precursors. The columns and error bars represent the averaged data and standard deviation derived from three independent experiments, respectively. The samples were taken before (no Orn) and 1, 2, 3, and 6 h after the addition of 1 mM Orn.

(B) The effect of additional Orn on the photoautotrophic growth of the *Synechocystis* strains used in the study.

(C) Co-immunopurification of Gun4 and CphB with f.ArgD from *Synechocystis* cells that were grown with 18 mM nitrate without (control) or with 24 h treatment with 1 mM Orn. Eluted proteins were separated by SDS-PAGE and stained by Coomassie blue.

(D) Co-immunoprecipitation of the f.ArgD and Gun4 proteins from cells that were grown with 18 mM nitrate without (control) or with Orn supplement. The WT strain was used as control for the specificity of the assay. Proteins were eluted from the anti-FLAG column by 1% SDS and analyzed by western blot.

(C and D) The abundance of CphB and Gun4 relative to ArgD is indicated below each lane (Gun4:ArgD or CphB:ArgD in controls was taken as 1).

(E) Immunoblot analysis of soluble (cytoplasmic [C]) and insoluble (membrane [M]) fractions of the *f.argD*$^+$/Δ*argD*, *f.astC*$^+$/Δ*argD* and WT cells grown in BG-11 without (control) or with 24 h treatment with 1 mM Orn (+Orn). The indicated proteins were detected by antibodies against the whole protein (D1, Gun4, CphB, ArgD) or against the FLAG tag (f.ArgD, f.AstC). Below the immunoblots, the abundance (in percentage) of Gun4 and CphB in the C and M fractions are indicated (total amount in C + M was taken as 100%). The signal of the D1 subunit of photosystem II is shown as a control for the purity of soluble fraction, and the SYPRO Orange stain serves as a loading control.

enzymes (Figure 2A). Apart from Pyk-1, this protein set can be isolated by using both f.ArgD (Figures 1B and 2C) and f.Gun4 (Figure 2A) as bait. The putative interaction of Gun4 with Pyk-1 needs further confirmation and studies. Herein, we confirmed and evaluated the interactions between Gun4-ArgD and ArgD-CphB, as well as Gun4-CphB; however, it is not definite whether we isolate these separate protein-protein interactions or one ternary complex (ArgD-Gun4-CphB). The absence of CphB does not cause obvious phenotypic changes under the photoautotrophic conditions used in our and in previous studies.[27] However, it was previously noted that the Δ*cphB* strain accumulates slightly more bilin-containing light-harvesting complexes.[27] The herein identified interaction of CphB with Gun4 implies that CphB can directly modulate the distribution of Chl and bilin pigments via its interaction with Gun4.

The interaction of ArgD with CphB is likely connected to the regulation of the Arg levels in the cell since both these enzymes contribute to the accumulation of Arg. Additional Orn intensified the interaction of these soluble enzymes; however, at the same time, approximately half of the total amount of CphB could be isolated from the insoluble fraction of the cells. These results are difficult to interpret since the physiological importance of CphB in *Synechocystis* remains enigmatic.

On the other hand, the importance of ArgD as an AcOrn aminotransferase in Arg biosynthesis has been established.[28] Although it was proposed to function also as Orn[38] or gamma aminobutyric acid[39] aminotransferases, these activities are negligible compared to its AcOrn aminotransferase activity.[32] These results imply that ArgD-Gun4 participates in an Arg biosynthesis-dependent regulation of the tetrapyrrole pathway. ArgD bound Gun4 with a K_d of 55.8 ± 11.5 nM (Figure 1C), which is close to the binding constant obtained by a fluorescence quenching measurement for the Gun4-ChlH complex (K_d ~10 nM).[40] These data indicate that the binding affinities of Gun4 to ArgD and ChlH are comparable. We demonstrated that additional Orn, which can also boost the interaction of f.ArgD with Gun4 and CphB (Figures 3C and 3D), halted *de novo* Chl production in the presence, but not in the absence, of *Synechocystis* ArgD (Figure 4A). These results imply an Orn-dependent downregulation of tetrapyrrole biosynthesis that is likely related to the formation of the ArgD-Gun4 complex. ChlH was absent in the herein isolated soluble complexes of Gun4 (Figures 1B, 2A, and 2C). The

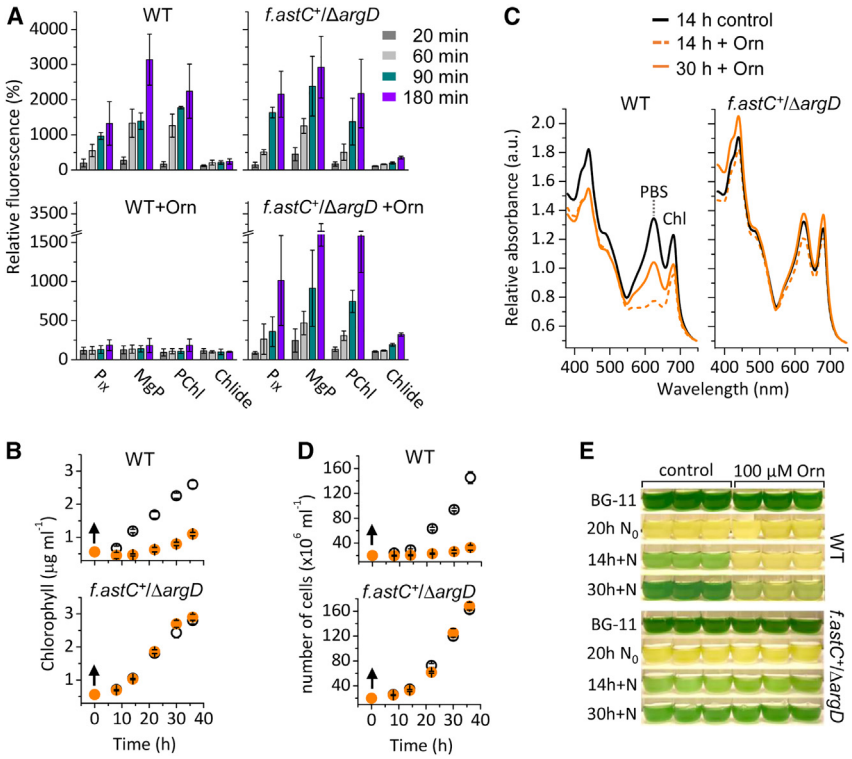

Figure 4. Orn inhibits *de novo* biosynthesis of tetrapyrroles and postpones the recovery of *Synechocystis* WT cells from nitrogen deprivation

(A) The relative amounts of Chl precursors were measured during N repletion of 20 h N-starved cells. The amounts before the addition of 1 mM $NaNO_3$ were taken as 100%.

(B) Changes in Chl content of the cultures after N repletion (indicated by arrows) in the absence (open symbol) or presence (orange symbol) of 100 μM Orn.

(C) *In vivo* cell spectra 14 h after the addition of 1 mM $NaNO_3$ (black line) compared with the spectra measured at 14 (dotted orange line) and 30 h (solid orange line) of N repletion in the presence of 100 μM Orn.

(D) Cell content of the cultures was assessed after the N upshift (indicated by arrows) in the absence (open symbol) or presence (orange symbol) of 100 μM Orn.

(A, B, and D) The averaged data are shown with the error bars representing standard deviation of three independent experiments.

(E) The examined cultures were photographed before (BG-11) and after 20 h of N starvation (N_0) and at indicated times during N repletion (+N) in the absence (control) or presence of 100 μM Orn.

concentration of Gun4 in *Synechocystis* (~1,000 copies per cell) is about half that of ChlH (~2,000 copies per cell).[41] Since this ratio is optimal for the MgCh activity *in vitro*,[20] sequestration of a fraction of Gun4 into soluble complexes could restrict MgP synthesis. In the presence of Orn, we could indeed observe a portion of the total Gun4 redirected from the membrane to the cytoplasm of *f.argD*$^+$/Δ*argD* and WT (Figure 3E). Dependent on the intensity of Chl production in chloroplast, Gun4 was reported to dynamically bind to the ChlH subunit in the membrane or dissociate from it to the soluble fraction.[12,19] We hypothesize that when ArgD *in vivo* binds Gun4 with higher affinity (directly or indirectly triggered by Orn), a population of Gun4, which would move to MgCh, binds ArgD and remains in the cytoplasm. This way, the rate of Chl and bilin production can be modulated by Arg metabolism. *Synechocystis* stores the majority of excess N in its bilin-containing light-harvesting antennae.[32] On the other hand, a considerable amount of the synthesized Arg is directed toward the cyanophycin N stockpile.[1] It is likely that the excess N has to be synchronously biased; therefore, it is conceivable to tune the production of bilins in an Arg biosynthesis-dependent manner via Gun4 acting at the branchpoint of the Chl and heme (bilin) pathways (see Figure 1D). Although not only the product but also the P_{IX} substrate of MgCh were affected (Figures 3A, 4A, and S4A), feedback downregulation of the entire tetrapyrrole biosynthetic pathway has been repeatedly observed for MgCh and Gun4 mutants in plants.[42,43] Also, a number of studies suggest that Gun4 is not merely a protein factor enhancing the activity of MgCh but that it can also directly or indirectly modulate the synthesis of 5-ALA.[44–46]

ArgD is an essential enzyme for the biosynthesis of Orn that is conserved from bacteria to plants. In consequence, an ArgD homolog from *E. coli* (AstC) functionally replaced the *Synechocystis* ArgD in the biosynthesis of Arg (Figures 1A and S1B), but its *in vivo* interaction with Gun4 and CphB was not detectable (Figures 2C and 2D). However, the absence of the Gun4-ArgD interaction did not affect the viability of cells even under severe stress conditions such as fluctuating and/or high light intensities combined with cold stress (Figure S2A), unstable availability of N supply (Figure S2B), or recovery from dormancy (Figures S2C–S2E). These results imply that the presence of this complex is not critical under the tested conditions. Alternatively, Gun4-ArgD might function in the fine regulation of tetrapyrrole biosynthesis, which is difficult to track down unless the intracellular levels of Arg metabolites are intensely altered by Orn supplement (Figure S3A; Table S4). Also, our recent data suggest that there are other sites of cross-talk besides Gun4-ArgD, where the tetrapyrrole and Arg pathways are intertwined in *Synechocystis* (Sobotka, R., unpublished data). Using a similar approach as described here, we discovered a stable protein complex between the bifunctional ArgJ, which catalyzes the first and fifth steps of the Arg biosynthesis (see Figure 1D), and GluTR, a rate-limiting enzyme of 5-ALA formation.[9] Multiple regulatory checkpoints (protein complexes) between these two metabolic pathways can indeed mitigate the absence of a single point, which could explain why the *f.astC*$^+$/-Δ*argD* strain showed no defects in viability under the stress conditions tested (Figure S2). Nevertheless, the co-existence of multiple protein-protein interactions further supports the

importance of the co-regulation of Arg metabolism with the biosynthesis of tetrapyrroles.

Limitations of the study

Our working model postulates that at elevated Orn levels, Gun4 preferentially associates with ArgD in the cytoplasm and that its availability for membrane-localized Chl synthesis becomes limited. We observed Gun4 relocalization in Orn-treated cells using immunodetection from fractionated cells (Figure 3E). However, the weakly membrane-bound Gun4[25] could partially dissociate during the preparation of cellular fractions. A better approach would be to monitor the Orn-driven relocalization of Gun4 in intact cells. However, the fluorescent-tagged Gun4 was unstable and prone to degradation. The current study also lacks the identification of a physiological condition in which the discovered ArgD-Gun4 complex plays an important role. This is most likely due to the gap in our knowledge on the eco-physiology of our model strain, which was isolated 52 years ago.[47] Since then, *Synechocystis* has been widely cultivated under optimal laboratory conditions in growth media containing waste amount of nutrients, including N, which particularly undermines studies related to N homeostasis. Consequently, there are no information available on Orn signaling or on the physiological significance of the CphB enzyme in our organism. It conceivably deflects the interpretation of the herein described effect of Orn on the regulation of tetrapyrrole synthesis. Similarly, without knowing the physiological relevance of CphB, it is too early to make conclusion about the importance of its interactions with other proteins in a metabolic network. Therefore, the current report inspires further studies in these directions.

STAR★METHODS

Detailed methods are provided in the online version of this paper and include the following:

- KEY RESOURCES TABLE
- RESOURCE AVAILABILITY
  - Lead contact
  - Materials availability
  - Data and code availability
- EXPERIMENTAL MODEL AND SUBJECT DETAILS
- METHOD DETAILS
  - Construction of the Synechocystis model strains
  - Isolation of Synechocystis soluble and membrane proteins
  - Isolation of protein complexes from Synechocystis
  - Protein electrophoresis, immunoblotting and mass spectrometry
  - Quantification of selected metabolites
  - Purification of recombinant Gun4, CphB and ArgD proteins from Escherichia coli
  - Spectral shift assays
- QUANTIFICATION AND STATISTICAL ANALYSIS

SUPPLEMENTAL INFORMATION

Supplemental information can be found online at https://doi.org/10.1016/j.celrep.2023.113265.

ACKNOWLEDGMENTS

This work was supported by European Research Council Synergy Award 854126.

AUTHOR CONTRIBUTIONS

E.K., J.T., and R.S. designed the study and constructed the strains; E.K., N.B.P.A., S.O., M.M., J.P., T.K., E.S., and P.K. performed the experiments; E.K., M.M., N.B.P.A., P.S., and R.S. analyzed the data; and E.K. and R.S. wrote the paper. All authors read and accepted the final manuscript.

DECLARATION OF INTERESTS

The authors declare no competing interests.

Received: February 14, 2023
Revised: August 11, 2023
Accepted: September 29, 2023

REFERENCES

1. Zhang, H., Liu, Y., Nie, X., Liu, L., Hua, Q., Zhao, G.P., and Yang, C. (2018). The cyanobacterial ornithine-ammonia cycle involves an arginine dihydrolase. Nat. Chem. Biol. *14*, 575–581. https://doi.org/10.1038/s41589-018-0038-z.
2. Watzer, B., and Forchhammer, K. (2018). Cyanophycin synthesis optimizes nitrogen utilization in the unicellular cyanobacterium *Synechocystis* sp. strain PCC 6803. Appl. Environ. Microbiol. *84*, e01298-18–e01218. https://doi.org/10.1128/AEM.01298-18.
3. Görl, M., Sauer, J., Baier, T., and Forchhammer, K. (1998). Nitrogen-starvation-induced chlorosis in *Synechococcus* PCC 7942: adaptation to long-term survival. Microbiology *144*, 2449–2458, (Pt 9). https://doi.org/10.1099/00221287-144-9-2449.
4. Wase, N., Black, P.N., Stanley, B.A., and DiRusso, C.C. (2014). Integrated quantitative analysis of nitrogen stress response in *Chlamydomonas reinhardtii* using metabolite and protein profiling. J. Proteome Res. *13*, 1373–1396. https://doi.org/10.1021/pr400952z.
5. Klotz, A., Georg, J., Bučinská, L., Watanabe, S., Reimann, V., Januszewski, W., Sobotka, R., Jendrossek, D., Hess, W.R., and Forchhammer, K. (2016). Awakening of a dormant cyanobacterium from nitrogen chlorosis reveals a genetically determined program. Curr. Biol. *26*, 2862–2872. https://doi.org/10.1016/j.cub.2016.08.054.
6. Brzezowski, P., Richter, A.S., and Grimm, B. (2015). Regulation and function of tetrapyrrole biosynthesis in plants and algae. Biochim. Biophys. Acta *1847*, 968–985. https://doi.org/10.1016/j.bbabio.2015.05.007.
7. Papenbrock, J., Mishra, S., Mock, H.P., Kruse, E., Schmidt, E.K., Petersmann, A., Braun, H.P., and Grimm, B. (2001). Impaired expression of the plastidic ferrochelatase by antisense RNA synthesis leads to a necrotic phenotype of transformed tobacco plants. Plant J. *28*, 41–50. https://doi.org/10.1046/j.1365-313x.2001.01126.x.
8. Vavilin, D., Brune, D.C., and Vermaas, W. (2005). N-15-labeling to determine chlorophyll synthesis and degradation in *Synechocystis* sp. PCC 6803 strains lacking one or both photosystems. Biochim. Biophys. Acta *1708*, 91–101. https://doi.org/10.1016/j.bbabio.2004.12.011.
9. Wang, P., Ji, S., and Grimm, B. (2022). Post-translational regulation of metabolic checkpoints in plant tetrapyrrole biosynthesis. J. Exp. Bot. *73*, 4624–4636, 10.1093/jxb/erac203. https://doi.org/10.1093/jxb/erac1203.
10. Davison, P.A., Schubert, H.L., Reid, J.D., Iorg, C.D., Heroux, A., Hill, C.P., and Hunter, C.N. (2005). Structural and biochemical characterization of Gun4 suggests a mechanism for its role in chlorophyll biosynthesis. Biochemistry *44*, 7603–7612. https://doi.org/10.1021/bi050240x.
11. Verdecia, M.A., Larkin, R.M., Ferrer, J.L., Riek, R., Chory, J., and Noel, J.P. (2005). Structure of the Mg-chelatase cofactor GUN4 reveals a novel

hand-shaped fold for porphyrin binding. PLoS Biol. *3*, e151. https://doi.org/10.1371/journal.pbio.0030151.

12. Adhikari, N.D., Orler, R., Chory, J., Froehlich, J.E., and Larkin, R.M. (2009). Porphyrins promote the association of GENOMES UNCOUPLED 4 and a Mg-chelatase subunit with chloroplast membranes. J. Biol. Chem. *284*, 24783–24796. https://doi.org/10.1074/jbc.M109.025205.
13. Chen, X., Pu, H., Wang, X., Long, W., Lin, R., and Liu, L. (2015). Crystal Structures of GUN4 in Complex with Porphyrins. Mol. Plant *8*, 1125–1127. https://doi.org/10.1016/j.molp.2015.04.013.
14. Adams, N.B.P., Brindley, A.A., Hunter, C.N., and Reid, J.D. (2016). The catalytic power of magnesium chelatase: a benchmark for the AAA+ ATPases. FEBS Lett. *590*, 1687–1693. https://doi.org/10.1002/1873-3468.12214.
15. Hu, J.H., Chang, J.W., Xu, T., Wang, J., Wang, X., Lin, R., Duanmu, D., and Liu, L. (2021). Structural basis of bilin binding by the chlorophyll biosynthesis regulator GUN4. Protein Sci. *30*, 2083–2091. https://doi.org/10.1002/pro.4164.
16. Zhang, W., Willows, R.D., Deng, R., Li, Z., Li, M., Wang, Y., Guo, Y., Shi, W., Fan, Q., Martin, S.S., et al. (2021). Bilin-dependent regulation of chlorophyll biosynthesis by GUN4. Proc. Natl. Acad. Sci. USA *118*, e2104443118. https://doi.org/10.1073/pnas.2104443118.
17. Fölsche, V., Großmann, C., and Richter, A.S. (2022). Impact of porphyrin binding to GENOMES UNCOUPLED 4 on tetrapyrrole biosynthesis in planta. Front. Plant Sci. *13*, 850504. https://doi.org/10.3389/fpls.2022.850504.
18. Wilde, A., Mikolajczyk, S., Alawady, A., Lokstein, H., and Grimm, B. (2004). The *gun4* gene is essential for cyanobacterial porphyrin metabolism. FEBS Lett. *571*, 119–123. https://doi.org/10.1016/j.febslet.2004.06.063.
19. Adhikari, N.D., Froehlich, J.E., Strand, D.D., Buck, S.M., Kramer, D.M., and Larkin, R.M. (2011). GUN4-porphyrin complexes bind the ChlH/GUN5 subunit of Mg-chelatase and promote chlorophyll biosynthesis in Arabidopsis. Plant Cell *23*, 1449–1467. https://doi.org/10.1105/tpc.110.082503.
20. Kopečná, J., Cabeza de Vaca, I., Adams, N.B.P., Davison, P.A., Brindley, A.A., Hunter, C.N., Guallar, V., and Sobotka, R. (2015). Porphyrin binding to Gun4 protein, facilitated by a flexible loop, controls metabolite flow through the chlorophyll biosynthetic pathway. J. Biol. Chem. *290*, 28477–28488. https://doi.org/10.1074/jbc.M115.664987.
21. Formighieri, C., Ceol, M., Bonente, G., Rochaix, J.D., and Bassi, R. (2012). Retrograde signaling and photoprotection in a *gun4* mutant of *Chlamydomonas reinhardtii*. Mol. Plant *5*, 1242–1262. https://doi.org/10.1093/mp/sss051.
22. Li, R.-Q., Jiang, M., Liu, Y.-H., Zheng, Y.-C., Huang, J.-Z., Wu, J.-M., and Shu, Q.-Y. (2017). The xantha marker trait is associated with altered tetrapyrrole biosynthesis and deregulated transcription of PhANGs in rice. Front. Plant Sci. *8*, 901. https://doi.org/10.3389/fpls.2017.00901.
23. Mochizuki, N., Tanaka, R., Tanaka, A., Masuda, T., and Nagatani, A. (2008). The steady-state level of Mg-protoporphyrin IX is not a determinant of plastid-to-nucleus signaling in Arabidopsis. Proc. Natl. Acad. Sci. USA *105*, 15184–15189. https://doi.org/10.1073/pnas.0803245105.
24. Larkin, R.M., Alonso, J.M., Ecker, J.R., and Chory, J. (2003). GUN4, a regulator of chlorophyll synthesis and intracellular signaling. Science *299*, 902–906. https://doi.org/10.1126/science.1079978.
25. Sobotka, R., Dühring, U., Komenda, J., Peter, E., Gardian, Z., Tichý, M., Grimm, B., and Wilde, A. (2008). Importance of the cyanobacterial GUN4 protein for chlorophyll metabolism and assembly of photosynthetic complexes. J. Biol. Chem. *283*, 25794–25802. https://doi.org/10.1074/jbc.M803787200.
26. Richter, R., Hejazi, M., Kraft, R., Ziegler, K., and Lockau, W. (1999). Cyanophycinase, a peptidase degrading the cyanobacterial reserve material multi-L-arginyl-poly-L-aspartic acid (cyanophycin): molecular cloning of the gene of *Synechocystis* sp. PCC 6803, expression in *Escherichia coli*, and biochemical characterization of the purified enzyme. Eur. J. Biochem. *263*, 163–169. https://doi.org/10.1046/j.1432-1327.1999.00479.x.
27. Li, H., Sherman, D.M., Bao, S., and Sherman, L.A. (2001). Pattern of cyanophycin accumulation in nitrogen-fixing and non-nitrogen-fixing cyanobacteria. Arch. Microbiol. *176*, 9–18. https://doi.org/10.1007/s002030100281.
28. Quintero, M.J., Muro-Pastor, A.M., Herrero, A., and Flores, E. (2000). Arginine catabolism in the cyanobacterium *Synechocystis* sp. strain PCC 6803 involves the urea cycle and arginase pathway. J. Bacteriol. *182*, 1008–1015. https://doi.org/10.1128/jb.182.4.1008-1015.2000.
29. Flores, E., Arévalo, S., and Burnat, M. (2019). Cyanophycin and arginine metabolism in cyanobacteria. Algal Res. *42*, 101577. https://doi.org/10.1016/j.algal.2019.101577.
30. Sobotka, R. (2014). Making proteins green; biosynthesis of chlorophyll-binding proteins in cyanobacteria. Photosynth. Res. *119*, 223–232. https://doi.org/10.1007/s11120-013-9797-2.
31. Koskela, M.M., Skotnicová, P., Kiss, É., and Sobotka, R. (2020). Purification of protein-complexes from the cyanobacterium *Synechocystis* sp. PCC 6803 using FLAG-affinity chromatography. Bio. Protoc. *10*, e3616. https://doi.org/10.21769/BioProtoc.3616.
32. Li, Z.-M., Bai, F., Wang, X., Xie, C., Wan, Y., Li, Y., Liu, J., and Li, Z. (2023). Kinetic characterization and catalytic mechanism of N-acetylornithine aminotransferase encoded by *slr1022* gene from *Synechocystis* sp. PCC 6803. Int. J. Mol. Sci. *24*, 5853. https://doi.org/10.3390/ijms24065853.
33. Baers, L.L., Breckels, L.M., Mills, L.A., Gatto, L., Deery, M.J., Stevens, T.J., Howe, C.J., Lilley, K.S., and Lea-Smith, D.J. (2019). Proteome mapping of a cyanobacterium reveals distinct compartment organization and cell-dispersed metabolism. Plant Physiol. *181*, 1721–1738. https://doi.org/10.1104/pp.19.00897.
34. Quintero, M.J., Montesinos, M.L., Herrero, A., and Flores, E. (2001). Identification of genes encoding amino acid permeases by inactivation of selected ORFs from the Synechocystis genomic sequence. Genome Res. *11*, 2034–2040. https://doi.org/10.1101/gr.196301.
35. Cunin, R., Glansdorff, N., Piérard, A., and Stalon, V. (1986). Biosynthesis and metabolism of arginine in bacteria. Microbiol. Rev. *50*, 314–352. https://doi.org/10.1128/mr.50.3.314-352.1986.
36. Abadjieva, A., Pauwels, K., Hilven, P., and Crabeel, M. (2001). A new yeast metabolon involving at least the two first enzymes of arginine biosynthesis: acetylglutamate synthase activity requires complex formation with acetylglutamate kinase. J. Biol. Chem. *276*, 42869–42880. https://doi.org/10.1074/jbc.M103732200.
37. Chen, G.E., Hitchcock, A., Mareš, J., Gong, Y., Tichý, M., Pilný, J., Kovářová, L., Zdvihalová, B., Xu, J., Hunter, C.N., and Sobotka, R. (2021). Evolution of Ycf54-independent chlorophyll biosynthesis in cyanobacteria. Proc. Natl. Acad. Sci. USA *118*, e2024633118. https://doi.org/10.1073/pnas.2024633118.
38. Schriek, S., Rückert, C., Staiger, D., Pistorius, E.K., and Michel, K.-P. (2007). Bioinformatic evaluation of L-arginine catabolic pathways in 24 cyanobacteria and transcriptional analysis of genes encoding enzymes of L-arginine catabolism in the cyanobacterium *Synechocystis* sp. PCC 6803. BMC Genom. *8*, 437. https://doi.org/10.1186/1471-2164-8-437.
39. Xiong, W., Brune, D., and Vermaas, W.F.J. (2014). The γ-aminobutyric acid shunt contributes to closing the tricarboxylic acid cycle in *Synechocystis* sp. PCC 6803. Mol. Microbiol. *93*, 786–796. https://doi.org/10.1111/mmi.12699.
40. Adams, N.B.P., Marklew, C.J., Qian, P., Brindley, A.A., Davison, P.A., Bullough, P.A., and Hunter, C.N. (2014). Structural and functional consequences of removing the N-terminal domain from the magnesium chelatase ChlH subunit of *Thermosynechococcus elongatus*. Biochem. J. *464*, 315–322. https://doi.org/10.1042/bj20140463.
41. Jackson, P.J., Hitchcock, A., Brindley, A.A., Dickman, M.J., and Hunter, C.N. (2023). Absolute quantification of cellular levels of photosynthesis-related proteins in *Synechocystis* sp. PCC 6803. Photosynth. Res. *155*, 219–245. https://doi.org/10.1007/s11120-022-00990-z.

42. Papenbrock, J., Mock, H.P., Tanaka, R., Kruse, E., and Grimm, B. (2000). Role of magnesium chelatase activity in the early steps of the tetrapyrrole biosynthetic pathway. Plant Physiol. *122*, 1161–1169. https://doi.org/10.1104/pp.122.4.1161.

43. Richter, A.S., Hochheuser, C., Fufezan, C., Heinze, L., Kuhnert, F., and Grimm, B. (2016). Phosphorylation of GENOMES UNCOUPLED 4 alters stimulation of Mg chelatase activity in angiosperms. Plant Physiol. *172*, 1578–1595. https://doi.org/10.1104/pp.16.01036.

44. Peter, E., and Grimm, B. (2009). GUN4 is required for posttranslational control of plant tetrapyrrole biosynthesis. Mol. Plant *2*, 1198–1210. https://doi.org/10.1093/mp/ssp072.

45. Brzezowski, P., Schlicke, H., Richter, A., Dent, R.M., Niyogi, K.K., and Grimm, B. (2014). The GUN4 protein plays a regulatory role in tetrapyrrole biosynthesis and chloroplast-to-nucleus signalling in *Chlamydomonas reinhardtii*. Plant J. *79*, 285–298. https://doi.org/10.1111/tpj.12560.

46. Wang, P., Richter, A.S., Kleeberg, J.R.W., Geimer, S., and Grimm, B. (2020). Post-translational coordination of chlorophyll biosynthesis and breakdown by BCMs maintains chlorophyll homeostasis during leaf development. Nat. Commun. *11*, 1254. https://doi.org/10.1038/s41467-020-14992-9.

47. Stanier, R.Y., Kunisawa, R., Mandel, M., and Cohen-Bazire, G. (1971). Purification and properties of unicellular blue-green algae (order Chroococcales). Bacteriol. Rev. *35*, 171–205. https://doi.org/10.1128/br.35.2.171-205.1971.

48. Tichý, M., Bečková, M., Kopečná, J., Noda, J., Sobotka, R., and Komenda, J. (2016). Strain of *Synechocystis* PCC 6803 with aberrant assembly of photosystem II contains tandem duplication of a large chromosomal region. Front. Plant Sci. *7*, 648. https://doi.org/10.3389/fpls.2016.00648.

49. Chidgey, J.W., Linhartová, M., Komenda, J., Jackson, P.J., Dickman, M.J., Canniffe, D.P., Koník, P., Pilný, J., Hunter, C.N., and Sobotka, R. (2014). A cyanobacterial chlorophyll synthase-HliD complex associates with the Ycf39 protein and the YidC/Alb3 insertase. Plant Cell *26*, 1267–1279. https://doi.org/10.1105/tpc.114.124495.

50. Schneider, C.A., Rasband, W.S., and Eliceiri, K.W. (2012). NIH Image to ImageJ: 25 years of image analysis. Nat Meth *9*, 671–675. https://doi.org/10.1038/nmeth.2089.

51. Spät, P., Klotz, A., Rexroth, S., Maček, B., and Forchhammer, K. (2018). Chlorosis as a developmental program in cyanobacteria: the proteomic fundament for survival and awakening. Mol. Cell. Proteomics *17*, 1650–1669. https://doi.org/10.1074/mcp.RA118.000699.

52. Hollingshead, S., Kopecná, J., Jackson, P.J., Canniffe, D.P., Davison, P.A., Dickman, M.J., Sobotka, R., and Hunter, C.N. (2012). Conserved chloroplast open-reading frame ycf54 is required for activity of the magnesium protoporphyrin monomethylester oxidative cyclase in *Synechocystis* PCC 6803. J. Biol. Chem. *287*, 27823–27833. https://doi.org/10.1074/jbc.M112.352526.

53. Kiss, É., Knoppová, J., Aznar, G.P., Pilný, J., Yu, J., Halada, P., Nixon, P.J., Sobotka, R., and Komenda, J. (2019). A photosynthesis-specific rubredoxin-like protein is required for efficient association of the D1 and D2 proteins during the initial steps of photosystem II assembly. Plant Cell *31*, 2241–2258. https://doi.org/10.1105/tpc.19.00155.

54. Komenda, J. (2005). Autotrophic cells of the Synechocystis *psbH* deletion mutant are deficient in synthesis of CP47 and accumulate inactive PSII core complexes. Photosynth. Res. *85*, 161–167. https://doi.org/10.1007/s11120-005-1294-9.

55. Bučinská, L., Kiss, É., Konik, P., Knoppová, J., Komenda, J., and Sobotka, R. (2018). The ribosome-bound protein Pam68 promotes insertion of chlorophyll into the CP47 subunit of Photosystem II. Plant Physiol *4*, 2931–2942. https://doi.org/10.1104/pp.18.00061.

56. Pilný, J., Kopečná, J., Noda, J., and Sobotka, R. (2015). Detection and quantification of heme and chlorophyll precursors using a High Performance Liquid Chromatography (HPLC) system equipped with two fluorescence detectors. Bio-protocol *5*, e1390. https://doi.org/10.21769/BioProtoc.1390.

57. Ritchie, R.J. (2006). Consistent sets of spectrophotometric chlorophyll equations for acetone, methanol and ethanol solvents. Photosynth. Res. *89*, 27–41. https://doi.org/10.1007/s11120-006-9065-9.

58. Opekar, S., Kvíčala, J., Moos, M., Pejchal, V., and Šimek, P. (2021). Mechanism of alkyl chloroformate-mediated esterification of carboxylic acids in aqueous media. J. Org. Chem. *86*, 16293–16299. https://doi.org/10.1021/acs.joc.1c01546.

59. Langer, A., Bartoschik, T., Cehlar, O., Duhr, S., Baaske, P., and Streicher, W. (2022). A new spectral shift-based method to characterize molecular interactions. Assay Drug Dev. Technol. *20*, 83–94. https://doi.org/10.1089/adt.2021.133.

STAR★METHODS

KEY RESOURCES TABLE

REAGENT or RESOURCE	SOURCE	IDENTIFIER
Antibodies		
anti-FLAG	Sigma-Aldrich	Cat# F7425, RRID:AB_439687
anti-Gun4	Raised in rabbit against the recombinant *Synechocystis* Gun4 (Sobotka et al.[25])	N/A
anti-CphB	Raised in rabbit against the recombinant *Synechocystis* CphB (this study).	N/A
anti-ArgD	Raised in rabbit against the recombinant *Synechocystis* ArgD (this study).	N/A
anti-rabbit IgG-peroxidase antibody produced in goat	Sigma-Aldrich	Cat# A6154, RRID:AB_11125345
goat-*anti*-rabbit IgG IR800	Azure Biosystems	Cat# AC2134
Bacterial strains		
WT-P substrain of *Synechocystis* sp. PCC 6803 (used as a background for all other strains of this study).	Tichý et al.[48]	N/A
Δ*argD Synechocystis* sp. PCC 6803	This study	N/A
f.argD^{+}/Δ*argD Synechocystis* sp. PCC 6803	This study	N/A
f.astC^{+}/Δ*argD Synechocystis* sp. PCC 6803	This study	N/A
Δ*cphB Synechocystis* sp. PCC 6803	This study	N/A
f.argD^{+}/Δ*cphB Synechocystis* sp. PCC 6803	This study	N/A
f.gun4^{+}/*Δgun4 Synechocystis* sp. PCC 6803	Sobotka et al.[25]	N/A
pET21a-gun4 Escherichia coli	This study	N/A
pET21a-argD Escherichia coli	This study	N/A
pET21a-cphB Escherichia coli	This study	N/A
Chemicals, peptides, and recombinant proteins		
anti-FLAG M2 affinity gel	Sigma-Aldrich	Cat# A2220
3xFLAG peptide	Sigma-Aldrich	Cat# A4799
Gun4-6xHis	This study	N/A
ArgD-6xHis	This study	N/A
CphB-6xHis	This study	N/A
Deposited data		
Proteomics data (identification of protein gel bands)	MassIVE: https://massive.ucsd.edu/ProteoSAFe/static/massive.jsp	MassIVE: MSV000091280
Metabolomics data	figshare: https://figshare.com/	figshare: https://doi.org/10.6084/m9.figshare.24205368.v1
Oligonucleotides		
For list of primers see Supplementary Table S5	This study	N/A
Recombinant DNA		
pPD-*N*FLAG (Km)	Chidgey et al.[49]	N/A
Software and algorithms		
Thermo Xcalibur	Thermo Fisher Scientific	RRID:SCR_014593
MassHunter Quantitative Analysis software	Agilent	RRID:SCR_015040
ImageJ	Schneider et al.[50]	RRID:SCR_003070

RESOURCE AVAILABILITY

Lead contact

Further information and requests for resources and reagents should be directed to and will be fulfilled by the lead contact, Roman Sobotka (sobotka@alga.cz).

Materials availability

The *E. coli* and *Synechocystis* strains generated in this study will be sent after request from the lead contact.

Data and code availability

- Proteomics data have been deposited at MassIVE: MSV000091280 and are publicly available as of the date of publication. Accession numbers are listed in the key resources table. Metabolomics data have been deposited at figshare (https://doi.org/10.6084/m9.figshare.24205368.v1) and are publicly available as of the date of publication.
- Further data reported in this paper, and any additional information required to reanalyze the data reported in this paper will be shared by the lead contact upon request.
- This paper does not report original code.

EXPERIMENTAL MODEL AND SUBJECT DETAILS

Synechocystis sp. PCC 6803 substrain GT-P[48] was used as the wild type (WT) and as a genetic background for all prepared strains listed in Table S1. Unless stated otherwise, the *Synechocystis* strains were grown photoautotrophically in liquid BG-11 medium on a rotary shaker at 28°C, under continuous, moderate irradiance of 40 μmol photons m^{-2} s^{-1} given by white fluorescence tubes. The plate-drop experiments were performed by pipetting liquid cultures on a BG-11 agar plate. The drops were photographed after three days of photoautotrophic growth at 30°C, under constant illumination with 30 μmol photons m^{-2} s^{-1}. Alternatively, the plates were exposed to 500 μmol photons m^{-2} s^{-1} (high light) at 28 or 22°C; or to repeated periods of 5 min illumination with high light and 5 min dark (fluctuating light). The fluctuating nitrogen (N) stress was mimicked by repeated cycles of washing the cells to nitrate-less BG-11 (N_0) for 8 h; followed by the addition of 18 mM $NaNO_3$ supplement to the liquid cultures for another 8 h; while agitated with 240 rpm at 28°C, illuminated by 200 μmol m^{-2} s^{-1}. Dormancy and recovery were induced by 25 d of N-starvation[51] and the addition of 1 mM $NaNO_3$, respectively. When amino acids were included to the media the stable pH was ensured by 10 mM TES. The absorption spectra of cells were measured by a UV-3000 spectrophotometer (Shimadzu). The number and average size of cells were assessed by coulter counter (Multisizer 4, Beckman Coulter).

METHOD DETAILS

Construction of the Synechocystis model strains

The Δ*argD* and Δ*cphB* strains were constructed by replacing the *slr1022* and *slr2001* genes by erythromycin or spectinomycin resistance cassettes, respectively. The primers in the megaprimer PCR method used for mutagenesis are listed in Table S5. The segregation of Δ*argD* locus was achieved in the presence of 5 mM Orn. For the construction of strains expressing the N-terminally 3xFLAG-tagged ArgD protein (f.ArgD) we purchased a synthetic *Synechocystis argD* gene (GenScript, USA) with an optimized codon usage to remove the common restriction binding sites. To express the AstC enzyme from *Escherichia coli* (*E. coli*) in *Synechocystis*, the *astC* gene of *E. coli* was amplified by PCR from the genomic DNA. The *argD* and *astC* genes were cloned to the pPD-*N*FLAG plasmid[52,49] (for all primers used see Table S5). The obtained constructs were transformed into *Synechocystis* Δ*argD* and/or Δ*cphB* cells. All transformed *Synechocystis* cells were fully segregated on BG-11 plates with increasing concentrations of relevant antibiotics (see Table S1).

Isolation of Synechocystis soluble and membrane proteins

Synechocystis cells (5 x 10^9) from exponential growth phase were pelleted, washed, and re-suspended in buffer A containing 20 mM HEPES pH 7.4, 5 mM $CaCl_2$, 10 mM $MgCl_2$, 25% glycerol, protease inhibitor (cOmplete; Roche). The cells were broken mechanically in a Precellys Evolution tissue homogenizer (Bertin Instruments) using balotina beads (100–200 μm). The breaking was performed in three cycles of shaking at 7500 rpm at 0°C; the sample was chilled for 2 min between the cycles. After removing the beads by repeated washing and sedimentation steps, the insoluble and soluble fractions were separated by three series of centrifugation at high speed (4°C, 65000 *x* ***g***, 20 min).

Isolation of protein complexes from Synechocystis

Cells from 4 L of *Synechocystis* cultures (*c*. 2x10^8 mL^{-1} cell content) were centrifuged, washed with buffer A and broken as described in the 'Isolation of *Synechocystis* soluble proteins' section. The soluble fraction was applied to anti-FLAG M2 affinity gel chromatography (Sigma-Aldrich) essentially as described in.[31] Proteins bound to the column were washed with 15 column volumes of buffer A. FLAG-tagged protein complexes were eluted with synthetic 3xFLAG peptide (150 μg/mL) in buffer A. Alternatively, the proteins were eluted form the column with 1% SDS in buffer A.

Protein electrophoresis, immunoblotting and mass spectrometry

The isolated proteins and protein complexes were solubilized and separated on SDS-PAGE essentially as described in[53]; and subsequently stained by Coomassie Blue. In case of immunoblot, the gel was stained by SYPRO Orange (Sigma-Aldrich) and

transferred onto a PVDF membrane that was subsequently incubated with specific primary antibody and then with secondary antibody conjugated with horseradish peroxidase (Sigma-Aldrich). The following primary antibodies were used in the study: anti-Gun4,[25] anti-D1[54]; anti-FLAG (Sigma-Aldrich Cat# F7425, RRID:AB_439687); the polyclonal anti-CphB and anti-ArgD antibodies were generated in rabbit, against the full-length *Synechocystis* recombinant proteins produced in *E. coli* (Moravia Biotech). The primary antibodies were probed with anti-rabbit IgG-peroxidase antibody produced in goat (Sigma-Aldrich Cat# A6154, RRID:AB_11125345) and visualized using Immobilon Crescendo Western HRP substrate (Millipore, Cat# WBLUR0500, RRID:AB_439687) and luminescence image analyzer (ImageQuant, LAS-4000). Alternatively, we used goat-*anti*-rabbit IgG IR800 antibody (Cat# AC2134) and visualize the signal using Azure Biosystems. For the identification of proteins by liquid chromatography (LC) coupled tandem mass spectrometry (MS/MS), the Coomassie Blue-stained bands were cut from the gel, digested and analyzed as described here.[55] For protein identification, MS/MS spectra were searched against *Synechocystis* species-specific protein bases (UNIPROT Universal Protein Resource, (RRID:SCR_002380) and CyanoBase (RRID:SCR_007615)) using the PLGS3.0 (Waters) software package.

Quantification of selected metabolites

The biosynthetic precursors of Chl/heme were extracted from equal number of cells and quantified by HPLC, essentially as described in.[56] The Chl content per cell was determined for three independent cultures after methanol extraction of pigments according to.[57] For the quantification of selected metabolites by combined GC-MS and LC-MS analysis[58] $3x10^9$ cells were collected by centrifugation and frozen in liquid N. Cell pellets were dried and immediately extracted with 400 μL of a cold extraction medium methanol:ACN:H2O (2:2:1 v/v/v) containing an internal standard 4-fluorophenylalanine (80 nmol). The sample was then homogenized using a Tissue Lyser II (Qiagen) at 50 Hz, 0°C for 5 min. The mixture was then centrifuged at (8000 ***g***, 10 min, 5°C). The supernatant was removed, and the extraction step was repeated under the same conditions but without the internal standard. The supernatants were combined and the obtained sample extract stored (−80°C). A 100 μL aliquot of each extract was mixed with ^{13}C-labeled internal standards ($^{13}C_3$-Serine, $^{13}C_3$-Alanine, $^{13}C_6$-Tyrosine, $^{13}C_2$-Glutamic acid, $^{13}C_6$-Arginine, $^{13}C_6$-Lysine, $^{13}C_6$-Phenylalanine, $^{13}C_4$-Asparagine, $^{13}C_5$-Methionine, $^{13}C_2$-Threonine, $^{13}C_4$-2-Oxoglutarate, $^{13}C_5$-Glutamine, $^{13}C_5$-Proline, $^{13}C_6$-Arginine) (absolute 2 nmol each) were concentrated in a vacuum concentrator (RVC 2–25 CD Plus combined with ALPHA 1–2 LD Plus, Thermo-Fischer Scientific). Each dried extract sample was then subjected to derivatization with ethanol (EtOH) - ethyl chloroformate (ECF) reaction medium under pyridine catalysis and simultaneous liquid-liquid microextraction into a lower chloroform layer as described earlier.[58] Briefly, the following five sequential steps were used for the addition of a corresponding medium to the evaporated sample extract: (1) 50 μL of the mixture EtOH: water (2:1; v/v), (2) 50 μL of the mixture EtOH: pyridine (2:1; v/v), (3) 50 μL of the mixture ECF: chloroform (1:7; v/v), (4) 50 μL 1 M NaOH, (5) 50 μL of the mixture ECF: chloroform (1:7; v/v). The reaction mixture was stirred before addition of the particular medium. Finally, 30 μL of the lower chloroform layer was evaporated by a gentle stream of nitrogen and redissolved in 100 μL methanol: water (3:7; v/v) for LC-MS analysis. 50 μL of 1 M HCl was added to the remaining reaction mixture and stirred. The 50 μL of the lower chloroform phase was used for GC-MS analysis. An LTQ XL mass spectrometer coupled to a Accela 600 liquid chromatograph (LC) and a Accela autosampler (all Thermo Fisher Scientific) was used for quantitative analysis. Amino acids were separated on a 150 mm × 3 mm i.d., 2.6 μm, Kinetex C18 (Phenomenex) with a mobile phase flow rate of 400 μL/min, an injection volume of 5 μL, and a column temperature of 35°C. The mobile phase was A = 5 mmol/L ammonium format in methanol, B = 5 mmol/L aqueous ammonium format; gradient (A): 0.0 min, 30%; 10.0 min, 100%; 11.0 min, 100%; 11.1 min, 30%; 14.5 min, 30%. Full scan positive ion mass spectra were acquired in a mass range of 85–850 Da. LT-Q settings were as follows: 2.5 kV spray voltage ion source parameter, 300°C capillary temperature, sheath gas at 40 au, aux gas at 10 au, spare gas at 1 au, 300°C source temperature. Data were processed using Thermo Xcalibur software (Thermo Fisher Scientific, RRID:SCR_014593), version 4.0. GC-MS analyses of amino acids were performed using a VF-17ms capillary column (30 m, 250 mm, 250 μm) and a gas chromatograph 5977B coupled to a quadrupole mass spectrometer 5977B MSD (Agilent) equipped with an electron ionization source (EI) and operated in full-scan mode (40–500 Da). The instrument settings were: Helium flow rate, 1.2 mL/min; inlet temperature, 280°C; injection mode, splitless; split flow, 40 mL/min; splitless time, 1.0 min; septum purge flow 3 mL/min; temperature program, 45°C, hold for 2 min, 16°C/min to 320°C, hold for 2 min; transfer line temperature, 280°C; and EI source temperature, 230°C; ionization energy, 70 eV. Data were processed using Agilent MassHunter WorkStation - Qualitative Analysis for GC/MS (Agilent, RRID:SCR_016657) and Agilent Masshunter Quantitative Analysis software (Agilent, RRID:SCR_015040) version 10.

Purification of recombinant Gun4, CphB and ArgD proteins from Escherichia coli

C-terminal His6-tagged Gun4, CphB and ArgD proteins were over-expressed in *E. coli* BL21 (DE3) using a pET21a plasmid (Novagen). The expression was induced with isopropyl-β-D-thiogalactopyranoside (0.4 mM) and shaken for additional 20 h at 18°C. Cells were harvested by centrifugation (10 min, 4°C, 10000 × ***g***), resuspended in lysis buffer (25 mM Tris/HCl pH 7.8, 150 mM NaCl, 10 mg L^{-1} of DNase I, 10 mg L^{-1} of lysozyme, protease inhibitor (cOmplete; Roche), and incubated for 30 min at 37°C. After incubation, cells were disrupted by sonication and the lysate was clarified by centrifugation (4°C, 30 min, 10000 × ***g***). Soluble His-tagged proteins were purified by metal-affinity chromatography (Protino Ni-NTA agarose, Macherey-Nagel; buffer: 25 mM Tris/HCl pH 8.0, 150 mM NaCl); their purity and concentration were checked by SDS-PAGE.

Spectral shift assays

Recombinant Gun4 and ArgD proteins were labeled with 2nd Generation Red NHS dye using standard protocols (NanoTemper Technologies GmbH, Munich, Germany) and used for isothermal spectral shift assays.[59] 5 or 20 nM labeled ArgD or Gun4 was titrated with a serial dilution of CphB or Gun4, respectively. Binding experiment were performed in triplicate, in 25 mM Tris, 0.1% Pluronic F-127, pH 8 at 25°C. Samples were loaded into Monolith Premium capillaries (NanoTemper Technologies) and loaded into a Monolith X instrument (NanoTemper Technologies) and excited at 590 nm (100% LED power), using software version Mo.Control 2.4.1. The ratio of fluorescence emission at 670 : 650 nm was collected; and the data were exported to CSV files, where custom Python scripts were used to determine the dissociation constant (K_d) using the equations in.[59]

QUANTIFICATION AND STATISTICAL ANALYSIS

The ratios of the co-purified f.ArgD and Gun4 proteins indicated on Figures 3B and 3C were assessed from the intensity of the stained protein bands or antibody signals using the ImageJ software (RRID:SCR_003070).[50] The average (arithmetic mean) and standard deviation of the data (shown on Figures 3A and 4A, 4B and 4D; S4B and S4E) were determined from measurements of n = 3 samples. Significance of the data (where indicated) was tested with one-tailed *t* test, with a significance level set to $p < 0.05$.